THE SEARCH FOR VH $\rightarrow$ VWW STANDARD MODEL HIGGS PRODUCTION IN THE TRILEPTON SIGNATURE WITH 5.9fb^{-1} OF DATA FROM $p\bar{p}$ COLLISIONS AT $\sqrt{S} = 1.96$ GEV

by

Jason Michael Nett

A dissertation submitted in partial fulfillment of
the requirements for the degree of

Doctor of Philosophy

(Department of Physics)

at the

UNIVERSITY OF WISCONSIN–MADISON

2010

ACKNOWLEDGMENTS

Thanks Matt and Jen

DISCARD THIS PAGE

TABLE OF CONTENTS

Page

Appendix

Page

Appendix

Page

DISCARD THIS PAGE

LIST OF TABLES

Appendix
Table Page

Appendix
Table Page

Appendix
Table

DISCARD THIS PAGE

LIST OF FIGURES

Appendix
Figure Page

Appendix
Figure

Appendix
Figure Page

DISCARD THIS PAGE

NOMENCLATURE

TEX	a typesetting system by Donald Knuth [**?**]. It also refers to the "plain" format. The proper pronounciation rhymes with "heck" and "peck" and does not sound like "hex" or "Rex."
LATEX	a set of TEX macros originally written by Leslie Lamport [**?**]. The proper pronunciation is `lā·tek'` and not `lā'·teks` (see above).
BIBTEX	a bibliography generation program by Oren Patashnik [**?**] that can be used with either plain TEX or LATEX.
C_1	Constant 1
V	Voltage
$	US Dollars

THE SEARCH FOR VH $\rightarrow$ VWW STANDARD MODEL HIGGS PRODUCTION IN THE TRILEPTON SIGNATURE WITH 5.9fb^{-1} OF DATA FROM $p\bar{p}$ COLLISIONS AT $\sqrt{S} = 1.96$ GEV

Jason Michael Nett

Under the supervision of Associate Professor Matthew Herndon

At the University of Wisconsin-Madison

We present here the first search for Standard Model $VH \rightarrow VWW \rightarrow l\nu l\nu l\nu$ production, where V is the W and Z weak vector bosons, using 5.9 fb^{-1} of integrated luminosity. This analysis adds to the existing CDF HWW group's dilepton analysis two new regions characterized by a **tri**-lepton signature, which are chosen to isolate the $WH \rightarrow WWW$ and $ZH \rightarrow ZWW$ associated production signals in the three-lepton bin. As such, we define two new regions denoted trilepton-*NoZPeak* (for the WH-centered analysis) and trilepton-*InZPeak* (for the ZH-centered analysis) with which we expect to contribute an additional $\sim 5.8\%$ (for $m_H = 160$ GeV) acceptance to the current $H \rightarrow WW$ dilepton analysis. The trilepton-*InZPeak* region is defined by events having at least one lepton pairing (among three possible pairings) with opposite-sign, same flavor, and a dilepton invariant mass within $[91.0, 101.0]$ GeV–a 10 GeV window around the Z-boson mass. The trilepton-*NoZPeak* region is then defined by those trilepton events which do not match the *InZPeak* definition. In this note, we shall refer to the study of the trilepton-*NoZPeak* region as the WH analysis and the study of the trilepton-*InZPeak* region as the ZH analysis, though note that both regions do contain at least some of both signals.

These two new regions are poised to make a substantial contribution to the $H \rightarrow WW$ group result. At $m_H = 165$ GeV, the WH analysis expected limits reach 8.9 times the standard model cross section; the ZH analysis is set at 12.6 times the expected standard model cross section; and the combined trilepton analysis is set at 6.3 times the expected standard model cross section. Finally, for the combined $H \rightarrow WW$ analysis result, in the 165 GeV bin the expected limit

drops from 1.21 for the dilepton analyses alone to 1.15 while the observed limit drops from 1.23 to 1.08.[15] As such, we are poised to begin excluding the standard model Higgs boson at 95% confidence level with CDF-only analyses in short order.[16]

Matthew Herndon

ABSTRACT

We present here the first search for Standard Model $VH \rightarrow VWW \rightarrow l\nu l\nu l\nu$ production, where V is the W and Z weak vector bosons, using 5.9 fb^{-1} of integrated luminosity. This analysis adds to the existing CDF HWW group's dilepton analysis two new regions characterized by a **tri**-lepton signature, which are chosen to isolate the $WH \rightarrow WWW$ and $ZH \rightarrow ZWW$ associated production signals in the three-lepton bin. As such, we define two new regions denoted trilepton-*NoZPeak* (for the WH-centered analysis) and trilepton-*InZPeak* (for the ZH-centered analysis) with which we expect to contribute an additional $\sim 5.8\%$ (for $m_H = 160$ GeV) acceptance to the current $H \rightarrow WW$ dilepton analysis. The trilepton-*InZPeak* region is defined by events having at least one lepton pairing (among three possible pairings) with opposite-sign, same flavor, and a dilepton invariant mass within $[91.0, 101.0]$ GeV–a 10 GeV window around the Z-boson mass. The trilepton-*NoZPeak* region is then defined by those trilepton events which do not match the *InZPeak* definition. In this note, we shall refer to the study of the trilepton-*NoZPeak* region as the WH analysis and the study of the trilepton-*InZPeak* region as the ZH analysis, though note that both regions do contain at least some of both signals.

These two new regions are poised to make a substantial contribution to the $H \rightarrow WW$ group result. At $m_H = 165$ GeV, the WH analysis expected limits reach 8.9 times the standard model cross section; the ZH analysis is set at 12.6 times the expected standard model cross section; and the combined trilepton analysis is set at 6.3 times the expected standard model cross section. Finally, for the combined $H \rightarrow WW$ analysis result, in the 165 GeV bin the expected limit drops from 1.21 for the dilepton analyses alone to 1.15 while the observed limit drops from 1.23 to 1.08.[15] As such, we are poised to begin excluding the standard model Higgs boson at 95% confidence level with CDF-only analyses in short order.[16]

Chapter 1

Introduction

The Standard Model of particle physics describes the known fundamental constituents of matter (categorized as "quarks" and "leptons") and the particles that carry the forces by which they interact. That is, the electromagnetic force is arises from the exchange of a "photon" (γ); the weak force arises from the exchange of a "weak vector boson" (W^+, W^-, Z); and the strong force arises from the exchange of a "gluon" (g). The final piece of the Standard Model is the Higgs boson, which remains the sole particle whose existence or non-existence has yet to be confirmed experimentally. If the Higgs boson does exist as postulated in the Standard Model, it is a key consequence of our understanding of the origin of mass in the universe.

The Higgs boson was postulated in 1964 by Peter Higgs as a consequence of a mathematical mechanism that rectified an apparent contradiction in the fledgling quantum field theories being formulated at that time. With Schrodinger equation-based quantum mechanics describing the physics of very small particles and special relativity describing the physics of high energy motion, physicists were naturally attempting to formulate a theory consistent with both realms–effectively, the physics of high energy fundamental particles. Before the Higgs mechanism was postulated, there was an inherent contradiction. Particles are known to have nonzero mass from experience and experiment, but introducing mass terms directly into the Lagrangian breaks certain symmetry requirements. The Higgs mechanism resolved the problem and lead to the formulation of a coherent quantum field theory that allows for massive fundamental particles.

The first serious experimental search for the Higgs boson was conducted by the Large Electron-Positron Collider (LEP) at the European Organization for Nuclear Research (CERN "*Organisation Europenne pour la Recherche Nucléaire*") which operated from 1989 to 2000. The Higgs sector

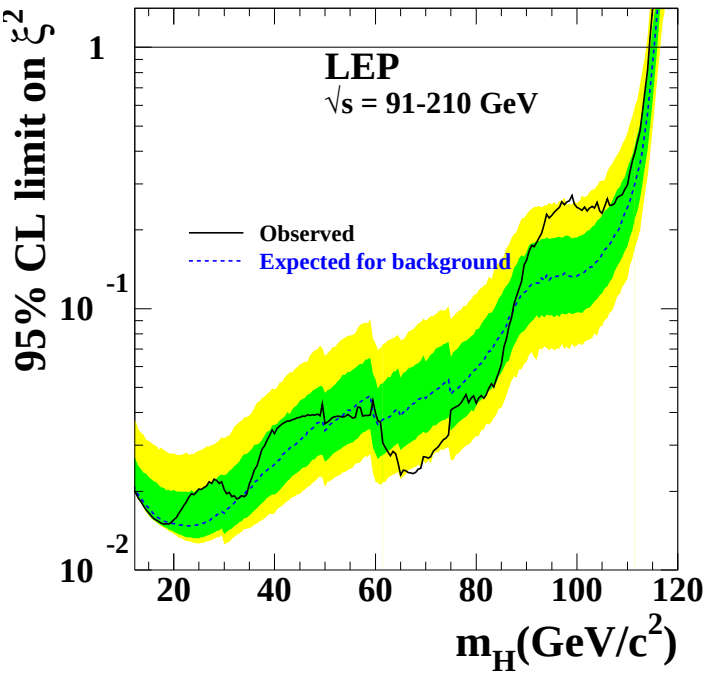

Figure 1.1 Experimental exclusion limits at 95% confidence level from the LEP collider at CERN.

of the Standard Model does not directly postulate or predict the mass of the Higgs boson, so a wide range of possible masses must be explored. LEP experimentally ruled out the existence of a Standard Model Higgs boson for masses $m_H < 114\mathrm{GeV/c^2}$. The LEP exclusion limits are shown in figure 1.1.

The Tevatron, a proton-antiproton ($p\bar{p}$) collider at the Fermi National Accelerator Laboratory, has carried the torch since LEP was dismantled in 2000 to construct the Large Hadron Collider (LHC) in its place. In $p\bar{p}$ interactions, the search for the Higgs boson is divided between a "high mass" region ($114 < m_H < 135\mathrm{GeV/c^2}$) and a "low mass" region ($135 < m_H < 200\mathrm{GeV/c^2}$). Observe in figure 1.2 that this low mass region corresponds to masses of the Higgs boson where it decays primarily to b-quark pairs and the high mass region corresponds to masses where it decays primarily to vector boson (W^+, W^-, Z) pairs. This thesis contributes a new search for the Standard Model Higgs boson in the high mass region ($H \to WW$), orthogonal to and augmenting the search that preceded it.

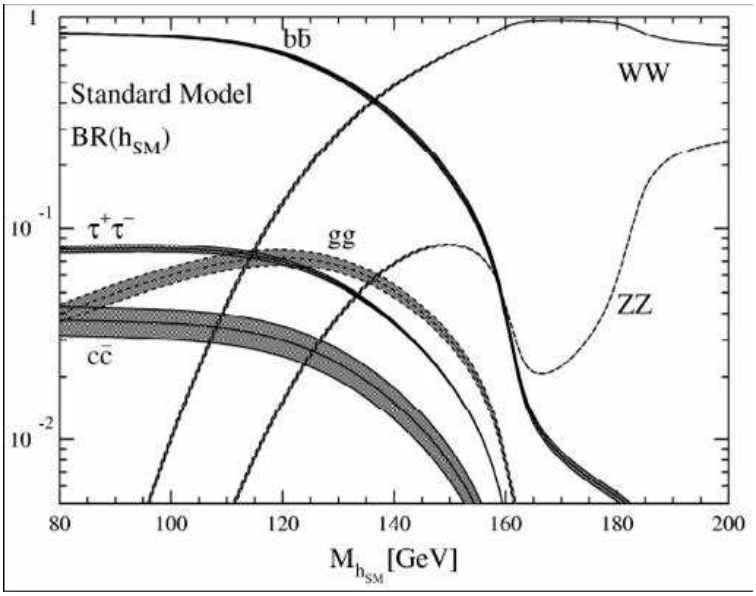

Figure 1.2 Standard Model branching ratios for the Higgs boson at the Tevatron.

Until recently, the high mass Higgs search exclusively studied $H \rightarrow WW$ interactions that result in a two-lepton signature [16]. The reason is that the dominant production of a high mass Higgs boson is via gluon fusion, which is then best studied in the case where both Higgs-W-bosons decay leptonically. The cases of having one or both Higgs-W-bosons decay hadronically is severely limited by large backgrounds. This thesis presents for the first time a search for a high mass Higgs boson in the three-lepton signature, shifting focus to the associated production channels $WH \rightarrow WWW \rightarrow l\nu, l\nu, l\nu$ and $ZH \rightarrow ZWW \rightarrow ll, l\nu,$ jet, where the jet is the result of a W-boson decaying hadronically.

This dissertation focuses on two new regions chosen specifically to isolate the $WH \rightarrow WWW$ and $ZH \rightarrow ZWW$ associated production processes because of their unique characteristics. The signal of WH associated production in the three lepton bin requires the W-boson to radiate a standard model Higgs boson that decays to two more W-bosons. Subsequently, all three W-bosons decay leptonically to produce a trilepton signature. Similarly, the ZH associated production signal requires a Z-boson to radiate a standard model Higgs boson that decays to two W-bosons. The Z-boson then decays to two leptons and we need one of the Higgs-W-bosons to decay leptonically and the other hadronically to produce an exact three-lepton signature (four-lepton events are rejected from this analysis). Correspondingly, the two new regions we introduce for trileptons in $H \rightarrow WW$ are denoted trilepton-*NoZPeak* (for the WH-centered analysis) and trilepton-*InZPeak* (for the ZH-centered analysis) to be defined in section 9.2.

The three lepton + $\not\!\!E_T$ signature with an unspecified number of jets is a relatively complex event topology that introduces a correspondingly large number of variables that describe the event. This is a fortuitous circumstance as it allows the formulation of many complex variables that powerfully discriminate the signals from backgrounds in both of these new trilepton-*NoZPeak* (WH analysis) and trilepton-*InZPeak* (ZH analysis) regions. Together, they represent a strong addition to the search for the standard model Higgs boson.

We will see in the Results section (section 9.6) that, at $m_H = 160$ GeV, the WH analysis expected limits reach 8.9 times the standard model cross section; the ZH analysis is set at 12.6 times the expected standard model cross section; and the combined trilepton analysis is set at 6.3

times the expected standard model cross section. Finally, for the combined $H \rightarrow WW$ analysis result, in the 165 GeV bin the expected limit drops from 1.21[15] to 1.15 while the observed limit drops from 1.23 to 1.08. As such, we are poised to begin excluding the standard model Higgs boson at 95% confidence level with CDF-only analyses in short order.

Chapter 2

The Higgs Mechanism and the Standard Model of Particle Physics

2.1 Intro. to the Standard Model of Particle Physics

The "Standard Model" of particle physics is a collection of gauge "quantum field theories," reformulations of Schroedinger-based quantum mechanics that are consistent with Einstein's special theory of relativity. Of the four known forces in nature (gravity, electromagnetism, weak force, and strong force), the Standard Model incorporates and establishes a quantum theory for all but gravity. Although hypothesized models exist, there is not yet a quantum theory of gravity, which is instead described macroscopically by Einstein's general theory of relativity.

The standard model is based on the gauge group formed from the product space of three special unitary gauge groups: $SU(3)_C \times SU(2)_L \times U(1)_Y$. The $SU(3)_C$ component represents the symmetry group describing the strong force interaction, with the C subscript referring to "color charge" of quantum chromodynamics. The rest of the gauge group is the "electroweak" portion of the Standard Model, represented by the $SU(2)_L \times U(1)_Y$ group. The "L" refers to the $SU(2)$ group's containing particularly *left-handed* weak doublets and the "Y" (a conserved quantum number) refers to the $U(1)$ group's *right-handed* weak hypercharge singlets.

The Standard Model also contains known particles that interact via these forces. The known particles are categorized as "fermions" (see section 2.2.1) and "bosons" (see section 2.2.2). The fermions of the Standard Model are then divided among "quarks" and "leptons," which are the known fundamental constituents of matter. The forces by which they interact manifest from the exchange of gauge bosons that exist as a consequence of various symmetries in the Standard Model's

$SU(3)_C \times SU(2)_L \times U(1)_Y$ gauge group. The existence of all the quarks, leptons, and gauge bosons described so far have been verified experimentally.

There does remain one last constituent of the Standard Model has not yet been experimentally verified: the Higgs boson. Unlike the other bosons that are related to the forces of nature, the Higgs boson is postulated as a consequence of a spontaneously broken symmetry in the electroweak sector ($SU(2)_L \times U(1)_Y$) which is hypothesized to be the property of the universe that results in fundamental particles and weak gauge bosons with non-zero mass. The rest of this chapter will describe the function of the Higgs boson in the Standard Model and the focus of this thesis is on a new contribution to the experimental search for the Higgs boson at the CDFII experiment.

2.2 Elementary Particles in the Standard Model

Particle physics is the study of the most fundamental known constituents of matter in the universe and the forces by which they interact. The "Standard Model" of particle physics is composed of all known fundamental particles, plus the postulated Higgs boson and the forces by which they interact.

We separate the known fundamental particles of the Standard Model into two categories: fermions and bosons.

2.2.1 Fermions

$u^{\pm\frac{2}{3}}$ "up"	$c^{\pm\frac{2}{3}}$ "charm"	$t^{\pm\frac{2}{3}}$ "top"
$d^{\mp\frac{1}{3}}$ "down"	$s^{\mp\frac{1}{3}}$ "strange"	$b^{\mp\frac{1}{3}}$ "bottom"

Table 2.1 Quarks of the Standard Model. The superscript indicates the particles' electric charges (the top charge refers to the "particles" while the bottom charge refers to the "anti-particles"). As fermions, all quarks have spin of $1/2$.

Fundamental particles are known from experiment to have intrinsic angular momentum denoted colloquially as "spin." In quantum mechanical systems, particles are capable of assuming only discrete spin states, just as they are also capable of only discrete energy states. Fermions are

$e^{\mp 1}$ "electron"	$\mu^{\mp 1}$ "muon"	$\tau^{\mp 1}$ "tau"
ν_e "electron neutrino"	ν_μ "muon neutrino"	ν_τ "tau neutrino"

Table 2.2 Leptons of the Standard Model. The particles in the top row exist as both "matter" (electric charge of -1) and "anti-matter" (electric charge of $+1$). The bottom row consists of the associated "neutrinos" which have no electric charge. As fermions, all particles listed here have spin $1/2$.

defined as particles with half-integer spin magnitudes: $1/2, 3/2, 5/2, \ldots$, where the spin is given in units of the Plank constant $\hbar = 6.582 \times 10^{-16}(\text{eV}\cdot\text{s})$[34]. Physically, $\hbar$ relates cycles (in radians because $\hbar = h/2\pi$) to energy as $E = \hbar\omega$. All the fundamental particles listed in tables 2.1 and 2.2 have spin magnitude $1/2$.

2.2.2 Bosons

Bosons are defined as particles with integer spin magnitudes: $0, 1, 2, \ldots$. The three forces of nature described by the Standard Model manifest from an exchange of a boson among the quarks and leptons. These force-carrying bosons arise from symmetries in the Standard Model's $SU(3)_C \times SU(2)_L \times U(1)_Y$ gauge group. They are:

- *photons (γ)*: The gauge boson of the $SU(2)_L \times U(1)_Y$ group which manifests as the electromagnetic force.
- W^+, W^-, Z^0: The gauge bosons of the $SU(2)_L \times U(1)_Y$ group which manifest as the weak force.
- *gluons (g)*: The gauge bosons of the $SU(3)_C$ group which manifest as the strong force.

The Standard Model Higgs boson is unique in that it is not associated with a force of nature and that it arises as a consequence of a broken symmetry referred to as "electroweak symmetry breaking." We will look at this electroweak symmetry breaking in section 2.3. Then in section 2.4, we will see how the fermion masses are consequences of the Higgs field. Section 2.5 will briefly discuss the role the Higgs boson plays in quark mixing and the CKM matrix. Finally, sections 2.6

and 2.7 will discuss phenomenological calculations of Higgs production and decay, respectively, involved in the experimental search covered by this thesis.

2.3 Electroweak Interactions in the Standard Model: Spontaneously Broken Local $SU(2)_L \times U(1)_Y$ Symmetry

The forces of nature appear to manifest from inherent symmetries. The logical foundation of a physical system is a postulated "lagrangian," from which the interactions of nature can then be derived. When the fields in a lagrangian can be transformed by an arbitrary element of a particular algebraic "group" and the lagrangian (and therefore the consequential physics) is left unchanged, then we say the lagrangian is "symmetric" to tranformations under that particular group.

Definition 2.1 A *group* is a set G along with any binary operation $\star$ on G that satisfies the following three axioms[21]:

- Associativity: $(a \star b) \star c = a \star (b \star c),\ \forall a, b, c \in G$
- Identity: $\exists e \in G$, denoted the *identity*, such that $\forall a \in G$ we have $a \star e = e \star a = e$.
- Inverse: $\forall a \in G,\ \exists a^{-1} \in G$, denoted the *inverse* of a, such that $a \star a^{-1} = a^{-1} \star a = e$.

For electroweak physics, we will be concerned with just two groups: $U(1)$ and $SU(2)$. Both of these groups are "unitary," which is critical to establishing such symmetries in the lagrangian.

Definition 2.2 A *unitary matrix* is an $n \times n$ complex matrix M that satisfies $M^\dagger M = M M^\dagger = I_n$, where I_n is the n-dimensional identity matrix and $\dagger$ denotes the Hermitian conjugate (complex conjugate and transpose).

2.3.1 Global $U(1)$ Symmetry

Definition 2.3 The *unitary group* $U(n)$ is a group of unitary $n \times n$ matrices with the binary operation of matrix multiplication. The $U(1)$ unitary group is then the group of complex numbers that equal 1 when multiplied by their complex conjugate, effectively becoming the group of rotations in the complex plane via Euler's relation: $\cos x + i \sin x = e^{ix}$.

Let's begin by assuming a scalar, complex particle $\phi = \frac{1}{\sqrt{2}}(\phi_1 + i\phi_2)$ and the corresponding Klein-Gordon lagrangian:

$$\mathcal{L} = (\partial_\mu \phi)^\dagger (\partial^\mu \phi) - m_0^2 \phi^\dagger \phi - \frac{1}{4}\lambda \left(\phi^\dagger \phi\right)^2 \tag{2.1}$$

This lagrangian is invariant to a $U(1)$ "global" (not dependent on spacetime coordinate) transformation $\phi \rightarrow \phi' = e^{i\alpha}\phi$ because of the unitary nature of $U(1)$[25]. Lagrangians have the structure of kinetic energy minus potential energy, so the potential described here is $V(\phi) = m_0^2 \phi^\dagger \phi + \frac{1}{4}\lambda \left(\phi^\dagger \phi\right)^2$. This potential is symmetric in the complex plane and has an extremum at the origin. If $m_0^2 > 0$, then the extremum is a minimum and we determine the particle spectrum by calculating perturbative oscillations about the minimum. The system describes a complex scalar particle of mass m_0.

However, Higgs phyics in the Standard Model is based on *broken* symmetry, so assume $m_0^2 < 0$. Now the extremum at the origin is unstable and we instead have a minima circle of radius v. To find the particle spectrum in this case, express the field ϕ in polar coordinates

$$\phi(x) = \underbrace{\frac{\rho(x)}{\sqrt{2}}}_{\text{Radial Perturbation}} \cdot \underbrace{e^{\frac{i}{v}\theta(x)}}_{\text{Angular Perturbation}} \tag{2.2}$$

$$\rho(x) \equiv v + h(x) \tag{2.3}$$

and expand about any arbitrary point in the minima manifold. Substituting this form back into the lagrangian yields

$$\mathcal{L} = \frac{1}{2}(\partial_\mu h)^2 + v(\partial_\mu h) + \frac{1}{2}v^2 + \left(\frac{1}{2v^2}h^2 + \frac{1}{v^2}hv + \frac{1}{2v^2}v^2\right)(\partial_\mu \theta)^2 \tag{2.4}$$

$$- \frac{1}{2}m_0^2 h^2 - m_0^2 vh - \frac{1}{2}m_0^2 v^2 - \frac{1}{16}\lambda(h+v)^4 \tag{2.5}$$

$$= \frac{1}{2}(\partial_\mu h)^2 + \frac{1}{2}(\partial_\mu \theta)^2 - \frac{1}{2}m_0^2 h^2 + \cdots \tag{2.6}$$

$$\tag{2.7}$$

Hence, we find that the field perturbation in the radial direction h acquires a mass (note: the direction that climbs the potential) while the angular field perturbation θ (note: directed within

the minima manifold) does not acquire a mass. So field perturbations that climb the potential represent particle states that acquire mass, while not climbing away from the minima manifold of the potential keeps the particle massless. Also, given this parametrization of $\phi(x)$, the vacuum expectation value is

$$\langle 0 \mid \phi \mid 0 \rangle = \frac{v}{\sqrt{2}} \tag{2.8}$$

See appendix C for a detailed calculation of these results.

This is a situation where a symmetric field potential is spontaneously broken in nature and this breaking manifests in a physical system different from the situation of the origin being a stable extremum, in which case the symmetry would not spontaneously break in nature.

2.3.2 Local $U(1)$ Symmetry

The global $U(1)$ symmetry of section 2.3.1 is a special case of "local" (the transformation *does* depend on spacetime coordinate) $U(1)$ symmetry. Now, let the angle of rotation in the complex plane α depend on coordinate: $\phi \to \phi' = e^{i\alpha(x)}\phi$. The lagrangian (eqn. 2.1) of the previous section is not invariant to local $U(1)$ transformations.

To have a lagrangian that is invariant to $U(1)$ local transformations, we must replace the derivative with a "covariant derivative"

$$\partial_\mu \to D_\mu = \partial_\mu + iqA_\mu \tag{2.9}$$

Thus, to keep the lagrangian invariant, we are postulating the existence of a "gauge field" A_μ and must introduce kinetic terms $F^{\mu\nu} = \partial^\mu A^\nu - \partial^\nu A^\mu$ for it. So the new postulated $U(1)$ locally invariant lagrangian is

$$\mathcal{L} = [(\partial^\mu + iqA^\mu)\phi]^\dagger \, [(\partial_\mu + iqA_\mu)\phi] - \frac{1}{4}F_{\mu\nu}F^{\mu\nu} - \frac{1}{4}\lambda(\phi^\dagger\phi)^2 - m_0^2(\phi^\dagger\phi) \tag{2.10}$$

$$\tag{2.11}$$

where the gauge field itself transforms as

$$A^\mu(x) \to A'^\mu(x) = A^\mu(x) + \frac{1}{q}\partial^\mu\alpha(x) \tag{2.12}$$

(see appendix D). If we then use the field parametrization as in the $U(1)$ global case (eqn. 2.2) we find that the field equation is

$$\Box A^\nu - \partial^\nu(\partial_\mu A^\mu) = -v^2 q^2 \left(A^\nu - \frac{\partial^\nu \theta}{vq} \right) \tag{2.13}$$

where on the right hand side we see the angular field perturbation θ in a term that looks just like the form of the gauge field transformation. As such, define

$$A'^\nu = A^\nu - \frac{\partial^\nu \theta}{vq} \tag{2.14}$$

Then the field equation becomes

$$\left(\Box + v^2 q^2\right) A'^\nu - \partial^\nu \partial_\mu A'^\mu = 0 \tag{2.15}$$

Thus, because of $U(1)$ local gauge symmetry, we have two physical consequences: first, we must postulate the existence of a gauge field A_μ; second, the symmetry allows us to choose a particular $U(1)$ transformation that causes the gauge field A_μ to absorb the θ term and become massive. This technique will be critical for computing the weak vector bosons and the photon. See appendix D for a detailed calculation of these results.

2.3.3 Global $SU(2)$ Symmetry

Definition 2.4 The *special unitary groups* $SU(n)$ are groups of $n \times n$ matrices with determinant 1 that have the binary operation matrix multiplication. The particular case of $n = 2$ is critical to electroweak physics.

Consider a doublet of complex scalar particles

$$\phi = \begin{bmatrix} \phi^+ \\ \phi^0 \end{bmatrix} = \begin{bmatrix} \frac{1}{\sqrt{2}}(\phi_1 + i\phi_2) \\ \frac{1}{\sqrt{2}}(\phi_3 + i\phi_4) \end{bmatrix} \tag{2.16}$$

where ϕ^+ destroys positively charged particles and creates negatively charged particles, and ϕ^0 destroys neutral particles and creates neutral antiparticles.

Postulate the form of the lagrangian as a direct generalization of section 2.3.1.

$$\mathcal{L} = (\partial_\mu \phi)^\dagger (\partial^\mu \phi) - m_0^2 \phi^\dagger \phi - \frac{\lambda}{4}(\phi^\dagger \phi)^2 \tag{2.17}$$

where $m_0^2 < 0$. This lagrangian is not only invariant to global $SU(2)$ transformations, but also to the global $U(1)$ transformations of section 2.3.1 (and appendix C). We treat the global $SU(2)$ case here, so α is not dependent on spacetime coordinate. The $SU(2)$ transformation takes a form similar to the $U(1)$ case:

$$\phi \to \phi' = e^{-\frac{i}{2}\vec{\alpha}\cdot\vec{\tau}}\phi \tag{2.18}$$

where the $\vec{\tau}$ are the Pauli spin matrices.

To determine the particle spectrum, we again want to find the minima manifold of the potential and compute oscillations from a point in it. The minimum is found at

$$\frac{\partial \mathcal{L}}{\partial(\phi^\dagger \phi)} = -m_0^2 - \frac{\lambda}{2}(\phi^\dagger \phi)_{\text{min}} = 0 \tag{2.19}$$

$$(\phi^\dagger \phi)_{\text{min}} = \frac{-2m_0^2}{\lambda} \equiv \frac{v^2}{2} \tag{2.20}$$

As before, we take the minimum to be the vacuum.

$$\langle 0 \mid \phi^\dagger \phi \mid 0 \rangle = \frac{v^2}{2} = \langle 0 \mid \phi_1^2 + \phi_2^2 + \phi_3^2 + \phi_4^2 \mid 0 \rangle \tag{2.21}$$

To obtain the particle spectrum we expand the fields ϕ about the choice of vacuum. Again, rather than a single point, we have a whole space of minima to choose from. Let,

$$\langle 0 \mid \phi \mid 0 \rangle = \begin{bmatrix} 0 \\ \frac{v}{\sqrt{2}} \end{bmatrix} \tag{2.22}$$

Oscillations about this vacuum choice are parametrized by

$$\phi = e^{-\frac{i}{2}(\vec{\theta}(x)\cdot\vec{\tau})v} \begin{bmatrix} 0 \\ \frac{1}{\sqrt{2}}(v + H(x)) \end{bmatrix} \tag{2.23}$$

We now have three "angular" field oscillations $\vec{\theta}$ and one radial $H(x)$. Just as in the $U(1)$ case, the angular oscillations are massless particles while $H(x)$ is massive. The lagrangian becomes:

$$\mathcal{L} = \frac{1}{8v^2}(\partial^\mu \vec{\theta}\cdot\vec{\tau})(\partial_\mu \vec{\theta}\cdot\vec{\tau})(v+H)^2 + \frac{1}{2}(\partial^\mu H)(\partial_\mu H) - \frac{m_0^2}{2}v^2 - \frac{m_0^2}{2}vH - \frac{m_0^2}{2}H^2 - \frac{\lambda}{4}(v+H)^4 \tag{2.24}$$

where we see mass terms for $H(x)$ and no mass terms for the $\vec{\theta}$ fields. We will again exploit the symmetry to gauge the $\vec{\theta}$ fields away. See appendix E for a detailed calculation of these results.

2.3.4 Local $SU(2)$ Symmetry

To generalize to local $SU(2)$ symmetry, we again must assume $\vec{\alpha}$ to be spacetime coordinate dependent.

$$\phi(x) \to \phi'(x) = e^{\frac{ig}{2}\vec{\tau}\cdot\vec{\alpha}(x)}\phi(x) \tag{2.25}$$

where the factor g is inserted to represent the coupling strength.

Just as in the local $U(1)$ case, our particles are not covariant under this transformation unless we replace the derivatives with suitable covariant derivatives.[12] Our $SU(2)$ covariant derivative is

$$D^\mu \equiv \partial^\mu + \frac{ig}{2}\vec{\tau}\cdot\vec{W}^\mu \tag{2.26}$$

where $\vec{W}^\mu \equiv (W_1^\mu, W_2^\mu, W_3^\mu)$, a slight precursor to the weak vector bosons. These three gauge fields transform as (see appendix F for this derivation)

$$\vec{W'}^\mu = \vec{W}^\mu - \partial^\mu\vec{\epsilon}(x) - g\left[\vec{\epsilon}(x)\times\vec{W}^\mu\right] \tag{2.27}$$

Now that we know how the gauge field and the covariant derivative transform with an $SU(2)$ gauge transformation, we can compute the consequences from our basic postulated lagrangian, which can now be repostulated in $SU(2)$ invariant form

$$\mathcal{L} = (D_\mu\phi)^\dagger(D^\mu\phi) - m_0^2\phi^\dagger\phi - \frac{\lambda}{4}\left(\phi^\dagger\phi\right)^2 - \frac{1}{4}\vec{W}_{\mu\nu}\cdot\vec{W}^{\mu\nu} \tag{2.28}$$

where $\vec{W}_{\mu\nu} \equiv \partial_\mu \vec{W}_\nu - \partial_\nu \vec{W}_\mu - g\vec{W}_\mu \times \vec{W}_\nu$, where the last term is necessary because of the non-Abelian nature of the $SU(2)$ group.

Note that if $m_0^2 > 0$, then we just have a system of four scalar particles of mass m_0. However, we are interested in the $m_0^2 < 0$ symmetry breaking case. Just as for the $U(1)$ case, we want to find the minima manifold.

$$\frac{\partial \mathcal{L}}{\partial(\phi^\dagger \phi)} = 0 \tag{2.29}$$

$$(\phi^\dagger \phi)_{\text{min}} = -\frac{2m_0^2}{\lambda} = \frac{1}{2}\left(\phi_1^2 + \phi_2^2 + \phi_3^2 + \phi_4^2\right) \tag{2.30}$$

We must choose some particular point on the minima manifold upon which to expand and calculate the particle spectrum, so choose $\phi_1 = \phi_2 = \phi_4 = 0$ and then we are left with

$$\frac{1}{2}\phi_3^2 = \frac{-2m_0^2}{\lambda} \tag{2.31}$$

$$\phi_3 = 2\sqrt{\frac{-m_0^2}{\lambda}} \equiv v \tag{2.32}$$

Then our complex field doublet at this minimum becomes

$$\phi_{\text{min}} = \frac{1}{\sqrt{2}}\begin{bmatrix}\phi_1 + i\phi_2 \\ \phi_3 + i\phi_4\end{bmatrix} = \frac{1}{\sqrt{2}}\begin{bmatrix}0 \\ v\end{bmatrix} \tag{2.33}$$

Again, completely analogous to the $U(1)$ case, we can parametrize perturbations about this minimum as

$$\phi(x) = \frac{\rho(x)}{\sqrt{2}} e^{\frac{i}{v}\vec{\tau}\cdot\vec{\theta(x)}} \quad \text{, where} \tag{2.34}$$

$$\rho(x) = \begin{bmatrix}0 \\ v + h(x)\end{bmatrix} \tag{2.35}$$

and analogous to the $U(1)$ case again, we can choose particular $SU(2)$ transformations to gauge away the $\vec{\theta}$ fields to be left with massive gauge bosons $\vec{W}$ and $H(x)$. This is another example of the Higgs mechanism.

See appendix F for a detailed calculation of these results.

2.3.5 Isospin, Weak Hypercharge, and $SU(2) \times U(1)$ Symmetry

We have now discussed the two basic symmetries, invariance to $U(1)$ and $SU(2)$ transformations that are fundamental to understanding electroweak physics. Just as translational symmetry implied conservation of momentum and temporal symmetry implies conservation of energy in classical physics, for example, these symmetries also imply conserved quantities or "quantum numbers." From $U(1)$ symmetry, we have conserved quantum number Y ("weak hypercharge"); and from $SU(2)$ symmetry, we have conserved quantum number t_3 ("weak isospin"). In this section, we explore the physics implied by symmetries under the product group $SU(2) \times U(1)$ and see that our choice of location on the minima manifold to expand on will leave the vacuum invariant to a transformation of the form '$U(1) + 3^{\text{rd}}$ component of $SU(2)$.' Y and t_3 will together define the electric charge of the fundamental particles according to

$$Q = t_3 + \frac{Y}{2} \tag{2.36}$$

Examples of values for the first generation of quarks and leptons are given in tables 2.3 and 2.4.

Leptons	Q	t_3	Y
ν_e	0	$\frac{1}{2}$	-1
e_L^-	-1	$-\frac{1}{2}$	-1
e_R^-	-1	0	-2

Table 2.3 Weak isospin and hypercharge quantum numbers for the first generation of leptons. Left and right handed electrons are listed separately.[25]

For a theory that is invariant to local transformations, we must introduce three $SU(2)$ gauge fields (see appendix F) and one $U(1)$ gauge field (see appendix D). Denote them here as $W_i^\mu(x)$ for $i = 1, 2, 3$ and $B^\mu(x)$, respectively. Also, the derivatives must be replaced with a covariant derivative for both $U(1)$ and $SU(2)$.

$$D^\mu \phi = \left(\partial^\mu + \underbrace{\frac{ig}{2} \vec{\tau} \cdot \vec{W}^\mu}_{SU(2)\text{piece}} + \underbrace{\frac{ig'Y}{2} B^\mu}_{U(1)\text{piece}} \right) \phi \tag{2.37}$$

Quarks	Q	t_3	Y
u_L	$\frac{2}{3}$	$\frac{1}{2}$	$\frac{1}{3}$
d_L	-$\frac{1}{3}$	-$\frac{1}{2}$	$\frac{1}{3}$
u_R	$\frac{2}{3}$	0	$\frac{4}{3}$
d_R	-$\frac{1}{3}$	0	-$\frac{2}{3}$

Table 2.4 Weak isospin and hypercharge quantum numbers for the first generation of quarks. Left and right handed quarks are listed separately.[25]

Kinetic terms for the new gauge fields must also be included.

$$\vec{F}^{\mu\nu} = \partial^\mu \vec{W}^\nu - \partial^\nu \vec{W}^\mu - g\vec{W}^\mu \times \vec{W}^\nu \tag{2.38}$$

$$G^{\mu\nu} = \partial^\mu B^\nu - \partial^\nu B^\mu \tag{2.39}$$

So the new full lagrangian is

$$\mathcal{L} = (D_\mu \phi)^\dagger (D^\mu \phi) + m_0^2 \phi^\dagger \phi - \frac{\lambda}{4}\left(\phi^\dagger \phi\right)^2 - \frac{1}{4}\vec{F}_{\mu\nu} \cdot \vec{F}^{\mu\nu} - \frac{1}{4} G_{\mu\nu} G^{\mu\nu} \tag{2.40}$$

$$\tag{2.41}$$

For electroweak theory, we should be left with three massive gauge bosons ($W^\pm, Z$) and one massless gauge boson (photon). Being massless, the photon corresponds to some symmetry that is left unbroken. Weinberg suggested [12]

$$\langle 0 \mid \phi \mid 0 \rangle = \begin{bmatrix} 0 \\ \frac{\sqrt{2}m_0}{\sqrt{\lambda}} \end{bmatrix} \equiv \begin{bmatrix} 0 \\ \frac{v}{\sqrt{2}} \end{bmatrix} \tag{2.42}$$

This choice leaves the vacuum invariant to a transformation of $U(1)+$ third component of $SU(2)$. That is,

$$(1+\tau_3)\langle 0 \mid \phi \mid 0 \rangle = (1+\tau_3) \begin{bmatrix} 0 \\ \frac{v}{\sqrt{2}} \end{bmatrix} = \begin{bmatrix} 2 & 0 \\ 0 & 0 \end{bmatrix} \begin{bmatrix} 0 \\ \frac{2}{\sqrt{2}} \end{bmatrix} = \begin{bmatrix} 0 \\ 0 \end{bmatrix} \tag{2.43}$$

where the $\vec{\tau}$ are the Pauli matrices. This is also why we eventually find the electric charge to be expressed in terms of weak hypercharge Y and third component of isospin t_3 [25]. We are about to

see that this interplay between the $U(1)$ symmetry (corresponding to Y) and the third component of $SU(2)$ symmetry (corresponding to t_3) manifests as a mixing of the W_3^μ and B^μ gauge fields to yield the photon field A^μ and the neutral weak vector boson Z.

To consider oscillations about the vacuum, parametrize the degrees of freedom by

$$\phi = e^{-\frac{i}{2v}\vec{\theta}(x)\cdot\vec{\tau}} \begin{bmatrix} 0 \\ \frac{1}{\sqrt{2}}(v + H(x)) \end{bmatrix} \tag{2.44}$$

However, recall that the three $\vec{\theta}$ field perturbations, which would become Goldstone bosons, disappear if we make the appropriate gauge transformation. So we effectively use

$$\phi = \begin{bmatrix} 0 \\ \frac{1}{\sqrt{2}}(v + H(x)) \end{bmatrix} \tag{2.45}$$

The consequences for the lagrangian are (details of how the following form of the lagrangian are calculated are in appendix J)

$$\mathcal{L} = \frac{1}{2}(\partial_\mu H)(\partial^\mu H) + \frac{m_0^2}{2}(v+H)^2 - \frac{\lambda}{16}(v+H)^4 - \frac{1}{4}\vec{F}_{\mu\nu}\cdot\vec{F}^{\mu\nu} - \frac{1}{4}G_{\mu\nu}G^{\mu\nu} \tag{2.46}$$

$$\begin{aligned}
\mathcal{L} = {} & \frac{1}{2}(\partial_\mu H)(\partial^\mu H) + \frac{m_0^2}{2}(v+H)^2 - \frac{\lambda}{16}(v+H)^4 && (2.47)\\
& - \frac{1}{4}(\partial_\mu W_{1\nu} - \partial_\nu W_{1\mu})(\partial^\mu W_1^\nu - \partial^\nu W_1^\mu) + \frac{1}{8}g^2v^2 W_{1\nu}W_1^\nu && (2.48)\\
& - \frac{1}{4}(\partial_\mu W_{2\nu} - \partial_\nu W_{2\mu})(\partial^\mu W_2^\nu - \partial^\nu W_2^\mu) + \frac{1}{8}g^2v^2 W_{2\nu}W_2^\nu && (2.49)\\
& - \frac{1}{4}(\partial_\mu W_{3\nu} - \partial_\nu W_{3\mu})(\partial^\mu W_3^\nu - \partial^\nu W_3^\mu) - \frac{1}{4}G_{\mu\nu}G^{\mu\nu} && (2.50)\\
& + \frac{1}{8}v^2(gW_{3\mu} - g'YB_\mu)(gW_3^\mu - g'YB^\mu) + \text{Higgs interactions} && (2.51)
\end{aligned}$$

The second and third lines show that the W_1 and W_2 gauge fields are massive and have the same mass $m_W = \frac{gv}{2}$. These are the W^+, W^- vector gauge bosons in electroweak theory. The Higgs interaction terms are being ignored here because we are focusing on the generation of the Standard Model gauge bosons in this section. In appendix J, I go through the details of deriving the full version of this and discuss the interactions between the Higgs and gauge bosons that are produced.

The Higgs boson decaying to gauge bosons is precisely the kind of interaction that this dissertation explores experimentally.

The last two lines show that the gauge fields W_3 and B are mixed. The key clue is to notice in the last line it is the combination $(gW_3^\mu - g'YB^\mu)$ that has a mass. Introduce the linear combinations

$$Z^\mu \equiv W_3^\mu \cos\theta_W - B^\mu \sin\theta_W \tag{2.52}$$

$$A^\mu \equiv W_3^\mu \sin\theta_W + B^\mu \cos\theta_W \tag{2.53}$$

where

$$\cos\theta_W = \frac{g}{\sqrt{g^2 + g'Y^2}} \tag{2.54}$$

$$\sin\theta_W = \frac{g'Y}{\sqrt{g^2 + g'Y^2}} \tag{2.55}$$

Using this, we can write the last two lines of the lagrangian in terms of A^μ and Z^μ, instead of B^μ and W_3^μ. They become:

$$-\frac{1}{4}\left(Z_{\mu\nu}Z^{\mu\nu} + \mathcal{F}_{\mu\nu}\mathcal{F}^{\mu\nu}\right) + \frac{1}{8}v^2 Z_\mu Z^\mu (g^2 + g'Y^2) \tag{2.56}$$

for $\mathcal{F}_{\mu\nu} \equiv \partial_\mu A_\nu - \partial_\nu A_\mu$ and $Z_{\mu\nu} \equiv \partial_\mu Z_\nu - \partial_\nu Z_\mu$.

Hence, we have unmixed the two fields. They become the Z boson and the photon.

$$m_Z = \frac{1}{2}v^2\sqrt{g^2 + g'Y^2} = \frac{m_W}{\cos\theta_W} \tag{2.57}$$

$$m_A = 0 \tag{2.58}$$

where $Y = 1$ and $t_3 = -1/2$ breaks both $SU(2)$ and $U(1)_Y$ symmetries, but leaves the $U(1)_{em}$ symmetry unbroken ($Q = t_3 + Y/2 = -1/2 + 1/2 = 0$).[25]

See appendix G for a detailed calculation of these results.

2.4 The Higgs Mechanism and Fermion Masses

Section 2.3 explored $SU(2) \times U(1)$ spontaneous symmetry breaking and the Higgs mechanism for scalar particles, with Klein-Gordon lagrangians. However, leptons and quarks are fermions. We

will first explore spontaneous $SU(2)_L \times U(1)_Y$ symmetry breaking for a massless fermion doublet, then focus on how the Higgs mechanism generates the fermion masses. We will also see that the same covariant derivatives used for scalar particles will be applicable here and produce the gauge bosons.

For more extensive computational details pertinent to this section, please refer to the appendices H and I.

2.4.1 $SU(2) \times U(1)$ Symmetry For Massless Fermions

We know now from section 2.3 what our postulated lagrangian should look like in order to be both $U(1)$ and $SU(2)$ invariant, which necessarily involved the weak vector bosons and the photon. Let's look at $SU(2) \times U(1)$ gauge invariance for the first generation of quarks; the calcuation is identical for the higher generations. The calculation for the lepton generations is also very similar and so not repeated in this dissertation.

The Higgs mechanism is *not* included here so the quarks will still be massless; that will be dealt with in section 2.4.2. Instead, we will deal with fermions that appear as a left-handed doublet and right-handed singlets for both particles.

Suppose we have the (fermion) quark doublet

$$q = \begin{bmatrix} u \\ d \end{bmatrix} \tag{2.59}$$

and recall that

$$\psi_L = \left(\frac{1 - \gamma_5}{2} \right) \psi \tag{2.60}$$

$$\psi_R = \left(\frac{1 + \gamma_5}{2} \right) \psi \tag{2.61}$$

are relations distinguishing the left and right handed components.

As always, we must postulate a lagrangian. In the sections exploring $U(1)$ and $SU(2)$ symmetries, we used generalizations of the Klein-Gordon equation's lagrangian for scalar particles. Now we want to look at spin-$1/2$ fermions, so we must use the Dirac lagrangian in our gauge invariant form.

Recall the Dirac lagrangian

$$\mathcal{L} = i\bar{\psi}\gamma_\mu\partial^\mu\psi - m\bar{\psi}\psi \tag{2.62}$$

Now we want a massless version for a fermion doublet:

$$\mathcal{L} = \bar{q}i\not{D}q \tag{2.63}$$

$$\mathcal{L} = \bar{q}_L i\not{D}_L q_L + \bar{u}_R i\not{D}_R u_R + \bar{d}_R i\not{D}_R d_R \tag{2.64}$$

where the covariant derivative for the doublet $\not{D}_L$ is $SU(2) \times U(1)$ invariant, and $\not{D}_R$ is only $U(1)$ invariant for the singlet:

$$D_L^\rho = \partial^\rho + \frac{ig}{2}\vec{\tau}\cdot\vec{W}^\rho + \frac{ig'Y}{2}B^\rho \tag{2.65}$$

$$D_R^\rho = \partial^\rho + \frac{ig'Y}{2}B^\rho \tag{2.66}$$

After exhaustive computation reminiscent of previous sections (and found in appendix H) we arrive at

$$\mathcal{L} = i\bar{u}\gamma_\rho\left(\frac{1+\gamma_5}{2}\right)(\partial^\rho u) + i\bar{d}\gamma_\rho\left(\frac{1+\gamma_5}{2}\right)(\partial^\rho d) + i\bar{u}\gamma_\rho\left(\frac{1-\gamma_5}{2}\right)(\partial^\rho u) + i\bar{d}\gamma_\rho\left(\frac{1-\gamma_5}{2}\right)(\partial^\rho d) \tag{2.67}$$

$$+ \frac{1}{\sqrt{2}}g\bar{u}\gamma_\rho W^\rho\left(\frac{1-\gamma_5}{2}\right)d + \frac{1}{\sqrt{2}}g\bar{d}\gamma_\rho W^{\rho\dagger}\left(\frac{1-\gamma_5}{2}\right)u \tag{2.68}$$

$$+ \frac{g}{2\cos\theta_W}Z^\rho\left[\bar{u}\gamma_\rho\left(\frac{1+\gamma_5}{2}\right)u\left(\frac{4}{3}\sin^2\theta_W\right) - \bar{d}\gamma_\rho\left(\frac{1+\gamma_5}{2}\right)d\left(\frac{2}{3}\sin^2\theta_W\right)\right. \tag{2.69}$$

$$\left. + \bar{u}\gamma_\rho\left(\frac{1-\gamma_5}{2}\right)u\left(-1+\frac{4}{3}\sin^2\theta_W\right) - \bar{d}\gamma_\rho\left(\frac{1-\gamma_5}{2}\right)d\left(-1+\frac{2}{3}\sin^2\theta_W\right)\right] \tag{2.70}$$

$$- \frac{2e_0}{3}\bar{u}\gamma_\rho u A^\rho + \frac{e_0}{3}\bar{d}\gamma_\rho d A^\rho \tag{2.71}$$

where the electric charge isdefined as $e_0 = g\sin\theta_W$. This form illustrates the interactions among the quarks in the fermion doublet and the gauge bosons.

2.4.2 The Higgs Mechanism in Fermion Mass Generation

The kinetic part of a free Dirac fermion does not mix the left and right components of the field:

$$\bar{\psi}\gamma_\mu\partial^\mu\psi = \bar{\psi}_R\gamma_\mu\partial^\mu\psi_R + \bar{\psi}_L\gamma_\mu\partial^\mu\psi_L \tag{2.72}$$

Because of this, we can gauge the left and right handed components differently. Weak interactions are parity violating in the Standard Model and the $SU(2)_L$ covariant derivative acts only on the left-handed term. However, a Dirac mass term has the form

$$-m\left(\bar{\psi}_L\psi_R + \bar{\psi}_R\psi_L\right) \tag{2.73}$$

when we write the left and right handed components separately. So the components are coupled, meaning any such mass term breaks $SU(2)_L$ gauge invariance.

In a theory with spontaneous symmetry breaking, there is a way of giving mass to fermions without explicitly introducing gauge invariance breaking mass terms in the lagrangian. Consider the electron $SU(2)_L$ doublet

$$l = \begin{bmatrix} \nu \\ e \end{bmatrix}_L \tag{2.74}$$

the Higgs doublet

$$\phi = \begin{bmatrix} \phi^+ \\ \phi^0 \end{bmatrix} \tag{2.75}$$

$$\phi^+ = \frac{1}{\sqrt{2}}(\phi_1 - i\phi_2) \tag{2.76}$$

$$\phi^0 = \frac{1}{\sqrt{2}}(\phi_3 - i\phi_4) \tag{2.77}$$

and the right handed electron singlet in a Yukawa model.

$$\mathcal{L}_e = -g_e\bar{l}_L\phi e_R - g_e\bar{e}_R\phi^\dagger l_L \tag{2.78}$$

Recall from section 2.3.5 that the vacuum expectation value of the Higgs doublet assumes the value

$$\langle 0 \mid \phi \mid 0\rangle = \begin{bmatrix} 0 \\ \frac{v}{\sqrt{2}} \end{bmatrix} \tag{2.79}$$

The consequence for a fermion doublet in this lagrangian is

$$\mathcal{L}_e = -g_e \bar{l}_L \phi e_R - g_e \bar{e}_R \phi^\dagger l_L \tag{2.80}$$

$$= -\frac{g_e v}{\sqrt{2}} \left[\bar{e}_L e_R + \bar{e}_R e_L\right] \tag{2.81}$$

This is exactly a Dirac mass with $m_e = \frac{g_e v}{\sqrt{2}}$. That was precisely the vacuum. Now let's see that if we consider also oscillations about the vacuum we generate a coupling between the electron and the Higgs field. In the last line, use $v + H$ instead of just v.

$$\langle 0 \mid \mathcal{L}_e \mid 0 \rangle = -\frac{g_e v}{\sqrt{2}} \left[\bar{e}_L (v + H) e_R + \bar{e}_R (v + H) e_L\right] \tag{2.82}$$

$$= -\frac{g_e v}{\sqrt{2}} \Bigg[\underbrace{v \bar{e} e}_{\text{Dirac electron mass}} + \underbrace{\bar{e} H e}_{\text{electron-Higgs coupling}} \Bigg] \tag{2.83}$$

Notice for the coupling term

$$\left(\frac{-g_e}{\sqrt{2}}\right) \bar{e} H e = \left(-\frac{m_e}{v}\right) \bar{e} H e = \left(-\frac{g m_e}{2 m_W}\right) \bar{e} H e \tag{2.84}$$

So in addition to interations of the form $f \bar{f} \to (\gamma \text{ or } Z^0) \to W^+ W^-$ we also have the possibility $f \bar{f} \to H \to W^+ W^-$–precisely the interaction this dissertation conducts an experimental search for. The presence of the fermion mass in the coupling to the Higgs is significant.

Summarily, to give the electron-neutrino $SU(2)$ doublet mass (as well as the other lepton and quark doublets), we are adding more terms to the lagrangian derived at the end of section H of the form:

$$\mathcal{L}_{f,\text{Higgs}} = \sum_{l=e,\mu,\tau} \left[-\frac{g_l}{\sqrt{2}} \left[v \bar{l} l + \bar{l} H l \right] - \frac{g_{\nu_l}}{\sqrt{2}} \left[v \bar{\nu}_l \nu_l + \bar{\nu}_l H \nu_l \right] \right] \tag{2.85}$$

for the three lepton generations and similar terms for the three quark doublets. Because of the Higgs mechanism, we now have sensible masses for Standard Model particles; however, it should be noted that this does not quite give the final form of the quark mass terms. A similar treatment for all three generations of quarks yields a results that includes "quark mixing," the ability of quarks to change flavor via charged weak interations in which the Higgs boson plays a central role. This treatment is outlined in section 2.5. (See appendix I for more details).

2.5 The Higgs Field, Quark Mixing, and the CKM Matrix

Generating the masses of quarks and leptons is not the only function the Higgs boson serves in the Standard Model. It also plays a central role in "quark mixing," the ability of quarks to change flavor via weak charge changing interactions.

Consider three doublets of left-handed quark fields:

$$q_{L1} = \begin{bmatrix} u_{L1} \\ d_{L1} \end{bmatrix}; \qquad q_{L2} = \begin{bmatrix} u_{L2} \\ d_{L2} \end{bmatrix}; \qquad q_{L3} = \begin{bmatrix} u_{L3} \\ d_{L3} \end{bmatrix} \tag{2.86}$$

and the six corresponding right-handed singlets: $u_{R1}, d_{R1}, u_{R2}, d_{R2}, u_{R3}, d_{R3}$. The lagrangian is then similar to the case for leptons already considered. The difference is that there are three quark families and each $SU(2)_L$ scalar (such as $\bar{q}_{Li}\phi_c$) can be paired with any of the three u_{Rj}, for $i, j \in \{1, 2, 3\}$. So allowing "mixing" of the families results in nine pairings. The nine couplings form the 3×3 CKM matrix.

We begin with the lagrangian

$$\mathcal{L} = \sum_{\{i,j\}=1,2,3} \left[a_{ij}\bar{q}_{Li}\phi_c u_{Rj} + a^{\dagger}_{ij}\bar{u}_{Rj}\phi^{\dagger}_c q_{Li} + b_{ij}\bar{q}_{Li}\phi d_{Rj} + b^{\dagger}_{ij}\bar{d}_{Rj}\phi^{\dagger} q_{Li} \right] \tag{2.87}$$

So far, a_{ij} and b_{ij} may be any complex value and are included as values to gauge the coupling strength. After much working over, the lagrangian becomes[12]

$$\mathcal{L} = \sum_k \left[m_{a,k} \left(\bar{u}_{Lk} u_{Rk} \left(1 + \frac{H}{v} \right) + \bar{u}_{Rk} u_{Lk} \left(1 + \frac{H}{v} \right) \right) \right. \tag{2.88}$$

$$\left. + m_{b,k} \left(\bar{d}_{Lk} d_{Rk} \left(1 + \frac{H}{v} \right) + \bar{d}_{Rk} d_{Lk} \left(1 + \frac{H}{v} \right) \right] \right. \tag{2.89}$$

where v appears again from the parametrization of the potential minimum in the Higgs mechanism, and $m_{a,k} = a_{kk}v/\sqrt{2}$, $m_{b,k} = b_{kk}v/\sqrt{2}$ are the quark masses. Notice also that quark couplings to the Higgs boson are another consequence.

It is important to note that the mass and Higgs interaction terms are not the only places that quark field appear in the Standard Model lagrangian. There were certain variable transformations performed to get this result– whose details are not pertinent to this disseratation–that must be

propagated in the terms of line 2.68, above. Beginning with that line for all three generations of quarks:

$$\sum_{k=1,2,3} \frac{1}{\sqrt{2}} g \bar{u}_k \gamma_\rho W^\rho \left(\frac{1-\gamma_5}{2} \right) d_k + \frac{1}{\sqrt{2}} g \bar{d}_k \gamma_\rho W^{\rho\dagger} \left(\frac{1-\gamma_5}{2} \right) u_k \tag{2.90}$$

We now perform a change of variables on the u and d quarks with unitary matrices S and T:

$$u_k = U_{ki} u_i \tag{2.91}$$

$$d_k = S_{kj} d_j \tag{2.92}$$

to get the following:

$$= \frac{g}{\sqrt{2}} \sum_{i,j,k} \left[(U_{ki} u_i)^\dagger \gamma_0 \not{W} (S_{kj} d_j) \left(\frac{1-\gamma_5}{2} \right) + (S_{kj} d_j)^\dagger \gamma_0 \not{W}^\dagger (U_{ki} u_i) \left(\frac{1-\gamma_5}{2} \right) \right] \tag{2.93}$$

$$= \frac{g}{\sqrt{2}} \sum_{i,j,k} \left[u_i^\dagger U_{ik}^* \gamma_0 \not{W} S_{kj} d_j \left(\frac{1-\gamma_5}{2} \right) + d_j^\dagger S_{jk}^* \gamma_0 \not{W}^\dagger U_{ki} u_i \left(\frac{1-\gamma_5}{2} \right) \right] \tag{2.94}$$

$$= \frac{g}{\sqrt{2}} \sum_{i,j,k} \left[\bar{u}_i \not{W} d_j (U_{ik}^* S_{kj}) \left(\frac{1-\gamma_5}{2} \right) + \bar{d}_j \not{W}^\dagger u_i (S_{jk}^* U_{ki}) \left(\frac{1-\gamma_5}{2} \right) \right] \tag{2.95}$$

$$\tag{2.96}$$

That is, the charge changing weak interactions link the three u_i quarks with a unitary rotation of the triplet of d_i quarks, with this rotation given by the unitary matrix $V \equiv U^\dagger S$,

$$V = \begin{bmatrix} V_{ud} & V_{us} & V_{ub} \\ V_{cd} & V_{cs} & V_{cb} \\ V_{td} & V_{ts} & V_{tb} \end{bmatrix} \tag{2.97}$$

2.6 Higgs Boson Associated Production with a Vector Boson

There are four major way to produce a Standard Model Higgs boson in the mass range relevant to the high mass search: gluon fusion, vector boson fusion, associated production with a W-boson, and associated production with a Z-boson. In the $H \to WW$ trilepton channel, only the two associated production processes contribute a non-negligible amount of signal.

The Tevatron consists of a proton beam and an anti-proton beam that collide within the heart of the CDF detector. Protons are composite particles of two up quarks and one down quark while anti-protons are composed of one up quark and two down quarks, so the specific interactions involved are:

- $u^{+\frac{2}{3}} + \bar{d}^{+\frac{1}{3}} \to W^+ \to HW^+$
- $\bar{u}^{-\frac{2}{3}} + d^{-\frac{1}{3}} \to W^- \to HW^-$
- $\bar{q} + q \to Z \to HZ$

To calculate the cross section for one of these interactions, we begin with the fundamental postulate of experimentally verified physics (except, of course, for the Higgs boson itself): the Standard Model Lagrangian. The relevant terms for the first interaction listed above, for example, are:

$$\mathcal{L} = \underbrace{\frac{1}{2}\left(\partial_\mu H\right)\left(\partial^\mu H\right) + \frac{1}{2}\mu^2 H^2 + \frac{g^2 v^2}{4} W_\mu^\dagger W^\mu + \frac{g^2 v}{2} W_\mu^\dagger W^\mu H}_{\text{Higgs Sector}} \tag{2.98}$$

$$\underbrace{-\frac{1}{4}\sum_{i=1,2}\left(\partial_\mu W_{i\nu} - \partial_\nu W_{i\mu}\right)\left(\partial^\mu W_i^\nu - \partial^\nu W_i^\mu\right)}_{\text{W boson kinetic terms}} \tag{2.99}$$

$$\underbrace{+i\overline{u}\gamma_\rho\left(\frac{1-\gamma_5}{2}\right)\partial^\rho u + i\overline{d}\gamma_\rho\left(\frac{1-\gamma_5}{2}\right)\partial^\rho d + \frac{gV_{ud}}{\sqrt{2}}\overline{d}\gamma_\rho W^{\dagger\rho}\left(\frac{1-\gamma_5}{2}\right)u}_{\text{Quark Doublet}} \tag{2.100}$$

We see in the first line the "Higgs Sector" which contains the kinetic term for the Higgs boson, the self-energy of the Higgs boson and W boson, and the term allowing interactions between the W-boson and the Higgs boson. The second line contains the W-boson kinetic terms and the third line yields the left-handed quark doublet (the $\left(\frac{1-\gamma_5}{2}\right)$ factor ensures left-handedness) and their interaction with the W-boson. Following the computations of appendix K, we arrive at the invariant amplitude.

$$\boxed{i\mathcal{M} = \left[-i\frac{\alpha m_W V_{ud}}{\sqrt{2}\sin^2\theta_W}\right]\epsilon_\mu^{s\,*}(k')\left[\frac{-g^{\mu\rho} + \frac{q^\mu q^\rho}{m_W^2}}{q^2 - m_W^2 + i\varepsilon}\right]\bar{d}^{r_1}(p')\gamma_\rho\left(\frac{1-\gamma_5}{2}\right)u^{r_2}(p)} \tag{2.101}$$

The next step in finding the differential cross section is to compute $|\mathcal{M}|^2$, for which we first need $\mathcal{M}^*$.

$$\mathcal{M}^* = -\frac{\alpha m_W V_{ud}}{\sqrt{2}\sin^2\theta_W}\left[\epsilon_\mu^{s\,*}(k')\left[\frac{-g^{\mu\rho}+\frac{q^\mu q^\rho}{m_W^2}}{q^2-m_W^2+i\varepsilon}\right]\bar{d}^{r_1}(p')\gamma_\rho\left(\frac{1-\gamma_5}{2}\right)u^{r_2}(p)\right]^* \tag{2.102}$$

$$= -\frac{\alpha m_W V_{ud}}{\sqrt{2}\sin^2\theta_W}\bar{u}\gamma_\rho\left(\frac{1-\gamma_5}{2}\right)d\left[\frac{-g^{\mu\rho}+\frac{q^\mu q^\rho}{m_W^2}}{q^2-m_W^2+i\varepsilon}\right]\epsilon_\mu^s(k') \tag{2.103}$$

The beam at the Tevatron is unpolarized, so average over spins r_1, r_2 of the quarks. The polarization of the end states is not measured, so the cross section is a sum of the possible polarization states of the W. As such, we want to compute

$$\frac{1}{2}\sum_{r_1}\frac{1}{2}\sum_{r_2}\sum_s|\mathcal{M}|^2 \tag{2.104}$$

To do this, we use the spin sums (see eqns. (3.66), (3.67) of Peskin and Schroeder [33])

$$\sum_s u^s(p)\bar{u}^s(p) = \gamma\cdot p + m \tag{2.105}$$

$$\sum_s v^s(p)\bar{v}^s(p) = \gamma\cdot p - m \tag{2.106}$$

$$\sum_s \epsilon_\sigma^s(k')\epsilon_\mu^{s\,*}(k') = -g_{\sigma\mu}+\frac{k'_\sigma k'_\mu}{m_W^2} \tag{2.107}$$

to get

$$\frac{1}{4}\sum_{r_1,r_2,s}|\mathcal{M}|^2 = \frac{1}{4}\left(\frac{\alpha m_W V_{ud}}{\sqrt{2}\sin^2\theta_W}\right)^2\sum_{r_1,r_2,s}\left[\epsilon_\mu^{s\,*}(k')\left[\frac{-g^{\mu\rho}+\frac{q^\mu q^\rho}{m_W^2}}{q^2-m_W^2+i\varepsilon}\right]\bar{d}^{r_1}(p')\gamma_\rho\right. \tag{2.108}$$

$$\left.\left(\frac{1-\gamma_5}{2}\right)u^{r_2}(p)\bar{u}^{r_2}(p)\gamma_\nu\left(\frac{1-\gamma_5}{2}\right)d^{r_1}(p')\left[\frac{-g^{\sigma\nu}+\frac{q^\sigma q^\nu}{m_W^2}}{q^2-m_W^2+i\varepsilon}\right]\epsilon_\mu^s(k')\right] \tag{2.109}$$

$$= \frac{1}{4}\left(\frac{\alpha m_W V_{ud}}{\sqrt{2}\sin^2\theta_W}\right)^2\left[\left(-g_{\sigma\mu}+\frac{k'_\sigma k'_\mu}{m_W^2}\right)\left(\frac{-g^{\mu\rho}+\frac{q^\mu q^\rho}{m_W^2}}{q^2-m_W^2+i\varepsilon}\right)\left(\frac{-g^{\sigma\nu}+\frac{q^\sigma q^\nu}{m_W^2}}{q^2-m_W^2+i\varepsilon}\right)\right. \tag{2.110}$$

$$\left.\mathrm{Tr}\left[\gamma_\rho\left(\frac{1-\gamma_5}{2}\right)(\not{p}+m_u)\gamma_\nu\left(\frac{1-\gamma_5}{2}\right)(\not{p}\,'-m_d)\right]\right] \tag{2.111}$$

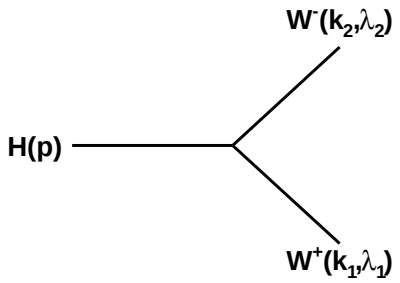

It remains to evaluate the trace and simplify the terms, then use the invariant amplitude squared to compute the cross section with general form [33]

$$d\sigma = \frac{1}{2E_A \cdot 2E_B |v_A - v_B|} \left[\frac{d^3k}{2E_k(2\pi)^3} \frac{d^3k'}{2E'_k(2\pi)^3} \right] \frac{1}{4} \sum_{r_1, r_2, s} |\mathcal{M}|^2 (2\pi)^4 \delta^4(k + k' - p - p') \tag{2.112}$$

where $|v_A - v_B| \cong 2c$ is the relative velocity difference in the lab frame.

Finally, the cross section for Higgs boson associated production with a W boson is (in terms of the Mandelstam variables) [13]

$$\boxed{\sigma(u\bar{d} \to WH) = \frac{\pi\alpha^2 |V_{ud}|^2}{36 \sin^4\theta_W} \frac{2k}{\sqrt{s}} \frac{k^2 + 3m_W^3}{(s - m_W^2)^2}} \tag{2.113}$$

Similarly, the cross section for associated production with a Z boson is[13]

$$\boxed{\sigma(q\bar{q} \to ZH) = \frac{2\pi\alpha^2 (l^2 + r^2)}{144 \sin^4\theta_W \cos^4\theta_W} \frac{2k}{\sqrt{s}} \frac{k^2 + 3m_Z^3}{(s - m_Z^2)^2}} \tag{2.114}$$

where $l \equiv 2(t_3 - Q\sin^2\theta_W),\ r \equiv -2Q\sin^2\theta_W$, Q is the electric charge, and t_3 is the weak isospin quantum number.

2.7 Higgs Boson Decay ($H \to WW$)

Now that we have a physical model with a Higgs boson and have computed the cross sections of its production channels pertinent to our experimental search, let's see how it decays.

Consider the decay in figure 2.7. The lagrangian density for a Standard Model Higgs boson decaying to two W-bosons comes from the Higgs sector of the Standard Model lagrangian.

$$\mathcal{L} = \underbrace{\frac{1}{2}\left(\partial_\mu H\right)\left(\partial^\mu H\right) + \frac{1}{2}\mu^2 H^2 + \frac{g^2 v^2}{4} W_\mu^\dagger W^\mu + \frac{g^2 v}{2} W_\mu^\dagger W^\mu H}_{\text{Higgs Sector}} \tag{2.115}$$

$$\underbrace{-\frac{1}{4}\sum_{i=1,2}\left(\partial_\mu W_{i\nu} - \partial_\nu W_{i\mu}\right)\left(\partial^\mu W_i^\mu - \partial^\nu W_i^\mu\right)}_{\text{W boson kinetic terms}} \tag{2.116}$$

$$\tag{2.117}$$

The decay rate derived from this lagrangian is (see appendix L for details):

$$\Gamma = \frac{G_F m_H^3}{8\sqrt{2}\pi}\left(1 - \frac{4m_W^2}{m_H^2} + \frac{12 m_W^4}{m_H^4}\right)\sqrt{1 - \frac{4m_W^2}{m_H^2}} \tag{2.118}$$

$$\tag{2.119}$$

Chapter 3

The Tevatron

This contribution to the search for the Standard Model Higgs boson is conducted at the Fermi National Accelerator Laboratory with the "Tevatron," a roughly four mile circular track around which protons and antiprotons are accelerated and collided with a center of mass energy of 1.96 TeV. These collisions occur at the "Collider Detector at Fermilab" experiment (CDF) where the data is recorded for future analysis. The collection, manipulation, and collision of protons and antiprotons is a formidible task. This chapter oulines process that leads to the colliding beams of the Tevatron while the CDF collider experiment is detailed in chapter 4

Figure 3.1 illustrates the stages of producing the colliding beams, beginning with the Cockcroft-Walton site and ending with the Tevatron collisions in the CDF and D0 experiments.

3.1 Beginning of the Beam: Cockcroft-Walton

The beams begin simply as hydrogen gas. The gas is injected into an electric field that is strong enough to strip the electrons from the hydrogen nuclei, leaving positively charged hydrogen ions (H^+). In the electric field, these ions are then directed towards a cesium anode where they acquire two electrons, become *negatively* charged H^- ions now. With a newly acquired negative net charge, these H^- ions are repelled from the anode and accelerated to 750 KeV by a Cockcroft-Walton accelerator–a type of Van de Graaf accelerator–towards a linear accelerator.

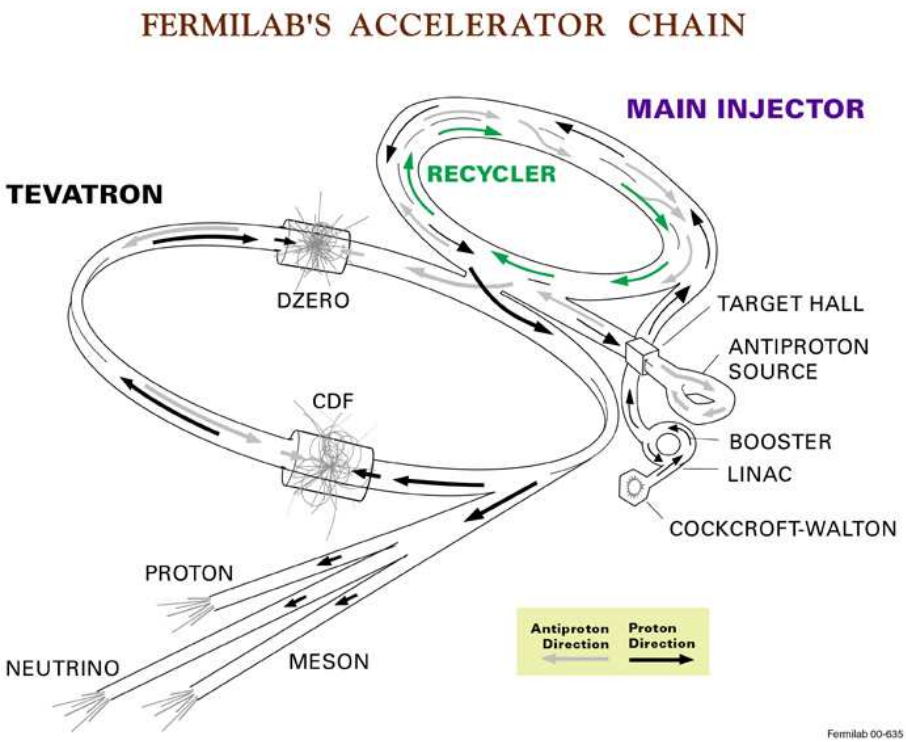

Figure 3.1 The Tevatron Accelerator Chain [10]

3.2 LINAC: The Linear Accelerator

The 750 KeV hydrogen ions enter a linear accelerator that operates with a succession of drift tubes generating an electric field oscillating with a radio frequency. H^- ions arriving at the linac in phase with the field oscillation are accelerated to 400 MeV over a distance of 130 meters, while those arriving out of phase with the linac's field are lost. This creates a beam of discrete bunches of ions rather than a steady stream. At the end of the linac, the bunched beam of ions impigns on a carbon barrier that strips the electrons from the hydrogen nuclei which are now just protons that pass.

3.3 Booster

Observe in figure 3.1 that the linac tangentially intersects the circular "booster." Sequentially, this is the first synchrotron–a circular accelerator with carefully synchronized electric and magnetic field to direct the beam of ions–that the protons encounter on their path to the colliders. The booster accelerates the protons from 400 MeV to 8 GeV.

3.4 Main Injector

After being ramped to an energy of 8 GeV in the Booster, the protons are redirected towards the "main injector"–another larger synchrotron that accelerates the proton bunches to 150 GeV for injection into the Tevatron. The main injector also plays a central role in the production of the antiprotons. Some protons from the main injector are used to produce antiprotons, which are accumulated separately. They are then also directed into the main injector which will inject the antiprotons into the tevatron. [2]

3.5 Anti-protons

Protons in the main injector are accelerated to 150 GeV if they are to be injected into the Tevatron, but are accelerated to 120 GeV if they are to be used for antiproton production. These 120 GeV protons are directed to impact a nickel-based target every 1.5 seconds causing a variety

of interactions. For every one million protons that hit the nickel target, only ~ 20 antiprotons are produced with enough energy to enter the "accumulator."

After passing the nickel target, the products pass through a "lithium lens" that focuses them into a beam that passes through a magnet. This magnet then filters the antiprotons by redirecting them on a unique path that leads them to the "debuncher." Because of the radio-frequency used to accelerate the 120 GeV protons in the main injector, the antiprotons are still in a beam of discrete bunches. These antiprotons also have a large spread in energy, so the debuncher is tuned in a way that decelerates higher energy antiprotons and accelerates lower energy antiprotons.

After the debuncher is finished with the antiprotons, they are successively stored in the "accumulator" at 8 GeV over many hours (or even up to a few days) while waiting to be transferred to the Tevatron for a fresh beam. When the Tevatron is ready for new colliding beams, the antiprotons are transferred from the accumulator to the "recycler" (also an 8 GeV ring) before moving on to the main injector and the Tevatron. [1]

3.6 The Tevatron

The first version of the tevatron became operational in 1983. It was the world's first superconducting synchrotron, containing about 1000 superconducting magnets. Because superconducting wires provide no resistance to the flow of charge, stronger magnetic fields are achievable and operational costs are reduced because electricity is not lost to dissipation.

The collider physics program at the Tevatron is separated between a *Run I* (1992-1996, 1.8 TeV) and *Run II* (2001-present, 1.96 TeV). As the Tevatron approaches the last years of *Run II* operation, the CDF and D0 experiments are quickly closing in on achieving Standard Model sensitivity for the Higgs boson search. [9]

The Tevatron receives the proton and antiproton beams from the main injector, both at 150 GeV. Both beams are injected in 36 discrete bunches, though not in equal densities since antiprotons are far more difficult to collect than protons. Each bunch contains on the order of 10^{11} protons or 10^{10} antiprotons.

Once all 36 bunches of each beam have been injected into the Tevatron, the beam is ramped from the 150 GeV to its colliding energy of 980 GeV. They are then focused, or "squeezed," and collimaters are used to absorb extraneous particles orbiting the beam. This is sometimes denoted the "beam halo."

The instantaneous luminosity for the collisions is given by:

$$L_{\text{inst.}} = \frac{36 f N_p N_{\bar{p}}}{4\sigma_x \sigma_y} \tag{3.1}$$

where the 36 denotes the number of bunches in each beam, f is the frequency of the revolutions, N_p is the number of protons in the bunch, $N_{\bar{p}}$ is the number of antiprotons in a bunch, and $\sigma_x,\ \sigma_y$ are Gaussian profiles of a transverse cross section of the beams. Integrated (over time) luminosities are typically given in units of inverse barns, which can then be easily multiplied by the cross section for a particular process (units in barns) to obtain the expected number of occurances for that physical interaction. [3]

3.7 The Performance of the Tevatron in Run II

As of March 30, 2010, the Tevatron is no longer the world's most powerful particle collider. The LHC produced collisions at 7 TeV. However, the Tevatron continues to produce impressive results. During the same calender month, the Tevatron broke two of its own records: it delivered 272.7pb^{-1} of integrated luminosity and saw an initial instantaneous luminosity record of $371 \times 10^{30}\text{cm}^{-2}\text{s}^{-1}$. It has also been consistently seeing initial instantaneous luminosities of $\sim 350 \times 10^{30}\text{cm}^{-2}\text{s}^{-1}$. Further, figure 3.1 illustrates consistent and accelerating progress in data delivery.

As such, the Tevatron will still retain a leading role in particle physics research for at least the next few years as of this writing (spring 2010).

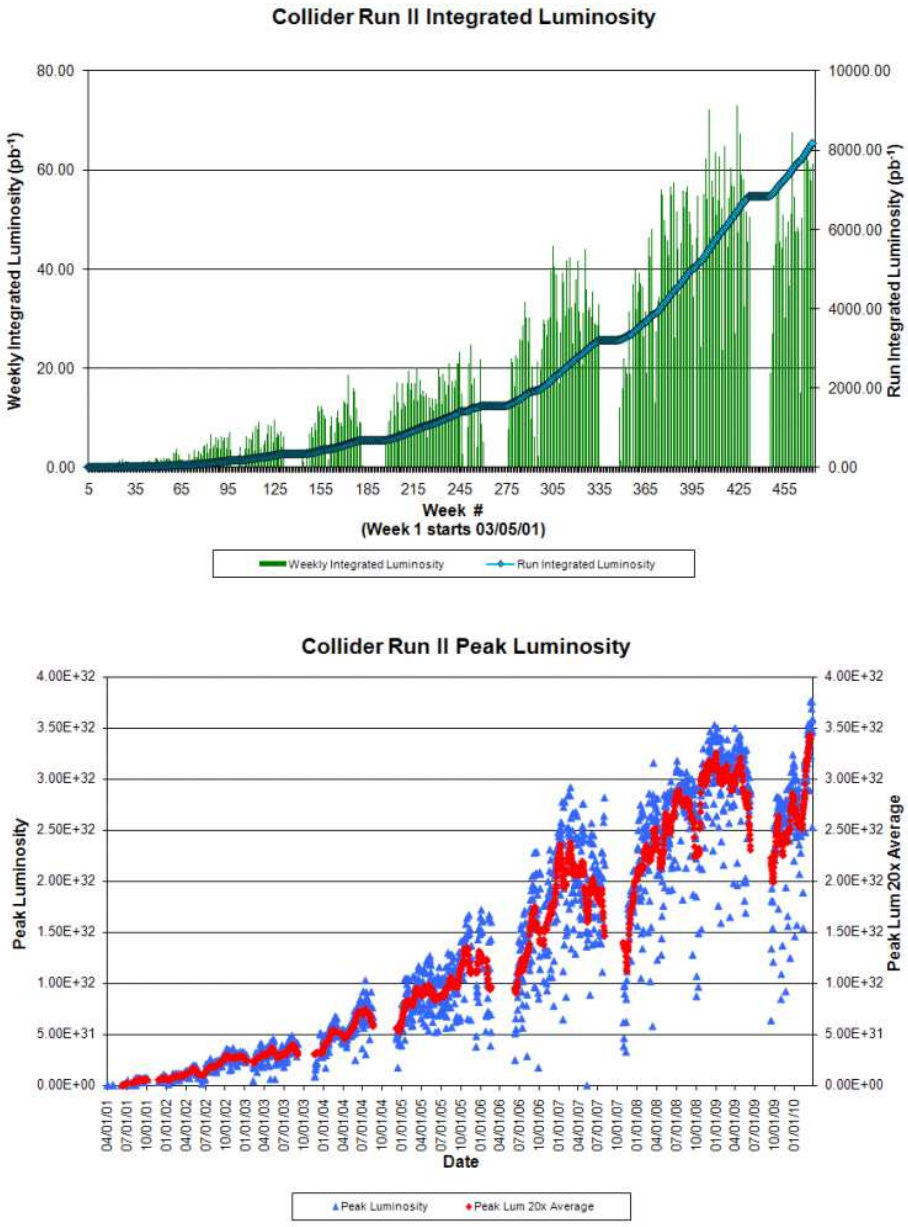

Figure 3.2 The Tevatron Run II luminosity performance [7]

Chapter 4

The CDF II Detector

The CDF experiment resides at the B0 site of the Tevatron and is one of two experimental detectors that collide the proton-antiproton beams to record the consequences of the collisions. The present incarnation of the CDF detector ("Run II") has been operational since 2001. It was originally designed with several specific purposes in mind: [20]

- Study the properties of the top quark
- Obtain more precise measurements of important quantities in electroweak physics
- Test perturbative Quantum Chromodynamics
- Constrain the CKM matrix with measurements of B decays
- Directly search for new physics

Since the Higgs boson has not been experimentally verified, the study presented in this dissertation falls into the "search for new physics" category, though is certainly related to electoweak measurements as well.

An overview of the experimental apparatus can be seen in figure 4.1. It contains a variety of different detection systems designed to collectively distinguish a variety of objects that may result from the $p\bar{p}$ collisions. Closest to the beamline is the silicon detector, which records the tracks of charged particles like leptons and charged hadrons. The silicon is encased in the "Central Outer Tracker" (COT), which also provides tracking information (see section 4.2). The next layer outward is the electromagnetic calorimeter, which is designed to absorb and measure the energy

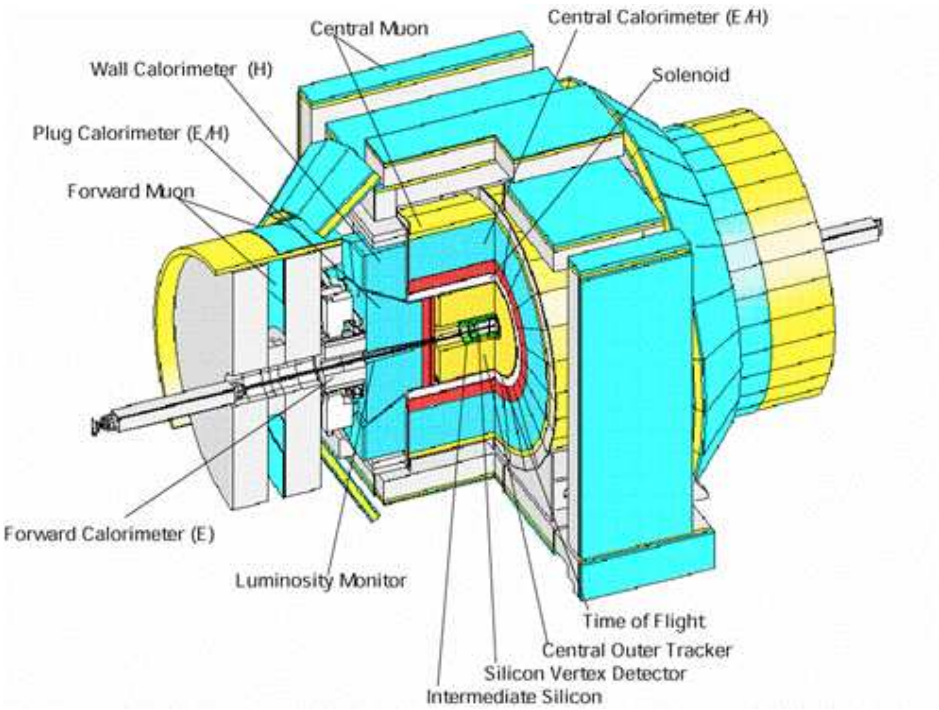

Figure 4.1 The CDF II Detector

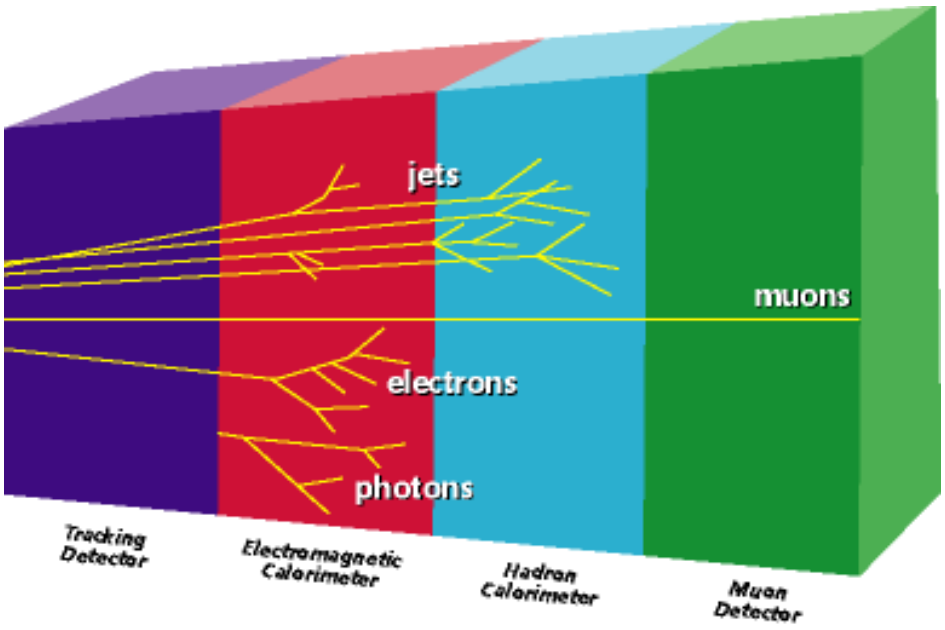

Figure 4.2 Diagram showing the types of objects various layers are constructed to detect.

of photons and electrons as indicated by figure 4.2. Hadrons tend to be more massive and are measured in the subsequent "hadronic calorimeter" (see section 4.3). Though charged, muons tend to punch through the calorimeter system and are then detected by one of several muon detection systems (see section 4.4).

The various systems are used interactively to detect any particular kind of object. Electrons are tracked through the silicon and COT, then these tracks are matched to energy deposits in the electromagnetic calorimeter, for example. Muons are also tracked through the silicon and COT, then matched to signals left in the muon system. Jets are collections of particles that deposit energy in both the electromagnetic and hadronic calorimeter systems. All together, the CDF detector is designed to record the presence of any kind of electron, muon, photon, or jet produced in $p\bar{p}$ collisions.

4.1 CDF Coordinates

Tracking the paths of various detector quantities requires a common coordinate system and CDF places the origin at the center of the experiment, on the beamline, where collisions are most

likely to occur. The positive x coordinate points radially away from the center of the Tevatron, y points vertically upward, and z is directed tangent to the path of the proton beam.

The azimuthal angle is denoted ϕ and given by

$$\phi = \arctan\left(\frac{y}{x}\right) \tag{4.1}$$

The polar angle is denoted θ and given by

$$\theta = \arctan\left(\frac{y}{z}\right) \tag{4.2}$$

The angle θ, however, is not often used. Instead, we use "pseudorapidity," where "rapidity" is defined as

$$\text{rapidity} = \frac{1}{2}\ln\frac{E + p_z}{E - p_z} \tag{4.3}$$

and in its massless approximation ($p >> m$) becomes pseudorapidity:

$$\eta = -\ln\tan\left(\frac{\theta}{2}\right) \tag{4.4}$$

4.2 Trackers

The CDF II tracking system is composed of three major components: a silicon microstrip system that provides precise tracking of charged particles close to the beamline; the "Central Outer Tracker" (COT) that envelops the silicon system; and finally a solenoid magnet generating a 1.4 T field along the $\hat{z}$ direction. The two tracking systems trace the paths of charged particles while the solenoid's field causes those paths to follow a helical pattern. Positive and negative charges can then be distinguished by the direction the helical path curves, while the particle's momentum can be calculated by the magnitude of the curvature.

4.2.1 The Silicon Detectors

The CDF II silicon detector is composed of three components: L00, SVXII, and ISL. Layer zero-zero (L00) is a single sided, radiation tolerant silicon strip detector, which is closest to the

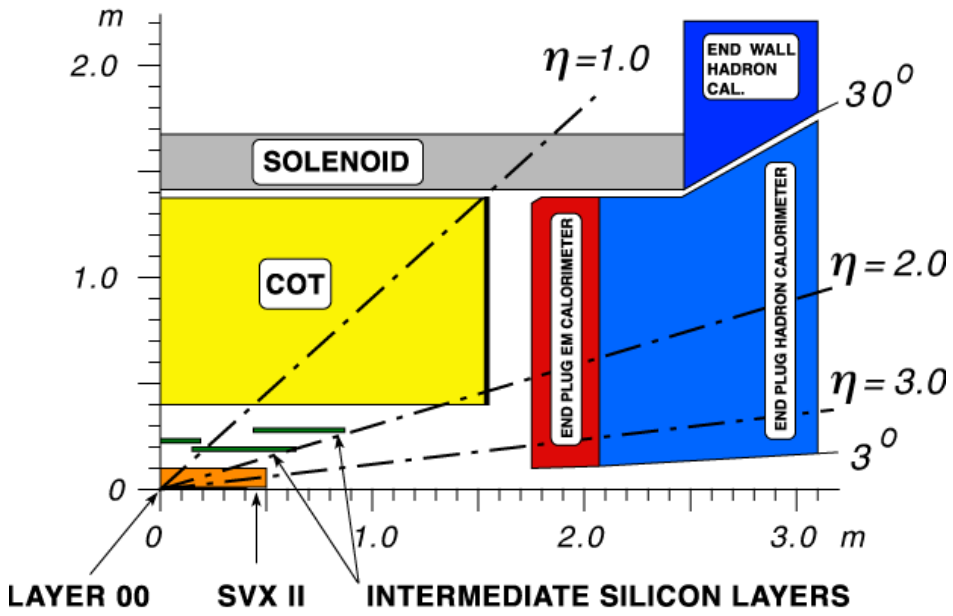

Figure 4.3 Diagram showing a side view of the tracking, solenoid, and forward calorimeter systems. The horizontal axis is the $\hat{z}$-direction from the interaction vertex and the vertical axis is the radial direction from the beamline.

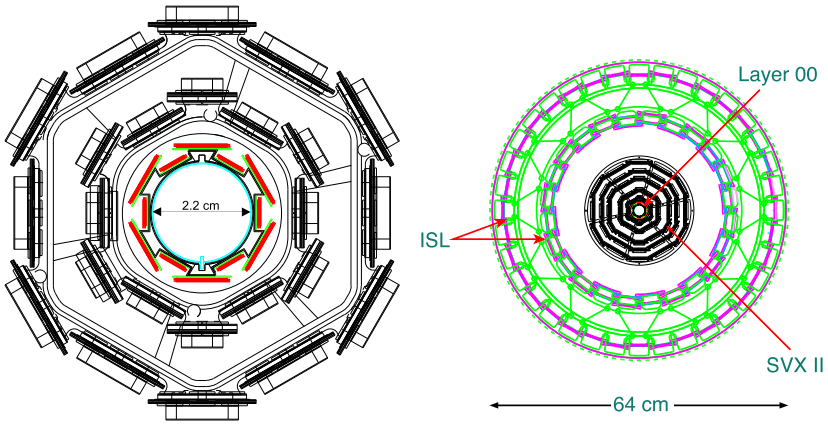

Figure 4.4 End view of L00 (left) and the full silicon system (right)[4],[5]

beamline. It is 87 cm long, centered on $z = 0$, and has a radius of just 1.1 cm (see figure 4.4). L00 is constructed in six segments in both z and ϕ. Each ϕ segment contains 128 channel of narrow, inner sensors and 256 channels of wider, outer sensors. Each z segment is composed of two long sensors. In total, L00 contains 13,824 channels. [4]

The SVX II silicon detector encapsulates L00. It is composed of three barrels, positioned end-to-end to achieve a length of 81 cm and full coverage in ϕ. Each barrel contains five layers of silicon microstrip detectors ranging from 2.4 cm to 10.6 cm from the beamline. In all, the SVX contains 405,504 detection channels and covers $|\eta| < 2.0$.[5],[20]

The "intermediate silicon layers" (ISL) are the outermost section of the silicon detector system, between the SVX and the COT (see figure 4.3). The ISL are an important compliment to the SVX and COT (see section 4.2.2) in that they provide extra tracking information in $1.0 < |\eta| < 2.0$, where COT coverage is partial. In this forward region, there are two silicon layers placed at 20 cm and 28 cm from the beamline. there is also an additional ISL layer in the central region at 22 cm from the beamline. [6],[20]

4.2.2 Central Outer Tracker

The CDF Central Outer Tracker (COT) compliments the silicon tracking system to provide additional tracking information. It covers the comparatively larger range of 40 cm to 130 cm from the beamline and is approximately three meters long. Instead of the wafers of silicon, the COT operates as a 96-layered drift chamber. The 96 layers are partitioned into 8 "superlayers" alternating between axial and stereo. "Axial" layers provide hit coordinates in the transverse plane (radial and azimuthal angle) while "stereo" layers supply the z coordinate, together yielding hit information in three dimensions.

The COT is filled with an equal mixture of argon and ethane in an electric field. When a charged particle enters the COT apparatus, it ionizes the gas by creating e^+e^- pairs. Electrons then drift under the influence of the electric field toward anode wires and signals are induced from the flow of charge.[8],[19]

Use of these tracking systems–in conjuction with the calorimeters and muon systems– is critical to the detection of leptons emanating from the $p\bar{p}$ collisions. This dissertation is devoted to the rare events that contain three recognized leptons, so a clear understanding of how physical leptons produced in $p\bar{p}$ interactions translate into detected leptons used for analysis is critical. This dissertation devotes chapter 6 to a detailed understanding of how the CDF subsystems are collectively used to identify leptons from charged tracks and other detector information.

4.3 Calorimeters

The calorimeter systems are located outside the solenoid and record the energies of particles resulting from $p\bar{p}$ interactions. They are composed of scintillators with layers of heavy metal to induce electromagnetic or hadronic showers.

Electromagnetic showers are induced for high energy photons and electrons via a combination of bremsstrahlung and pair production. When impigning on the heavy metal layer, a high energy electron will radiate high energy photons, which then converts to $e\bar{e}$ pairs, which go on to emit more photons, etc. This cycle continues until the individual photons and electrons no longer have enough energy to pair-produce and the ionization loss prevents further radiation. The physical depth acheived by this "shower" is then an indicator of how much energy the original electron or photon posessed. [32]

Hadronic showers occur when a high energy hadron experiences an inelastic nuclear collision with the heavy metal layer, producing secondary hadrons that go onto have their own collisions. This cycle continues until the individual hadrons no long have enough energy to break up nuclei. Hadrons tend to be much more massive than electrons and a relatively large amount of energy is released from nuclear interactions, so the depth that a hadronic shower penetrates is largers and such calorimeters must be physically larger than the electromagnetic calorimeters.[32]

4.3.1 CDF Central Electromagnetic Calorimeter (CEM)

CDF's central electromagnetic calorimeter (CEM) is composed of 48 wedges that each cover 15° in azimuth and 0.11 in pseudorapidity (η). Each 15° wedge has alternating lead and scintillator

layers. The energy resolution (in GeV) of the EM calorimeter is

$$\frac{\delta E}{E} = 13.5\%/\sqrt{E_T} + 1.7\% \tag{4.5}$$

[20]

4.3.2 CDF Hadronic Calorimeters (CHA,WHA)

The central hadronic calorimeter (CHA) and the endwall hadronic calorimeter (WHA) wedges are composed of alternating layers of iron and scintillator. Both the CHA and WHA are an array of 48 wedges, with the CHA covering $|\eta| < 0.9$ and the WHA covering $0.7 < |\eta| < 1.3$. The energy resolution of the CHA and WHA detectors are

$$\frac{\delta E}{E_T} = \frac{50\%}{\sqrt{E_T}} \tag{4.6}$$

and

$$\frac{\delta E}{E_T} = \frac{75\%}{\sqrt{E_T}} \tag{4.7}$$

repsectively.

4.3.3 CDF Forward Calorimeters (PEM, PHA)

The forward calorimeters are also divided between a “plug electromagnetic calorimeter” (PEM) and a “plug hadronic calorimeter” (PHA), covering $1.1 < |\eta| < 3.6$ and $1.2 < |\eta| < 3.6$, respectively. The design and function is similar to the central calorimeters. The energy resolution of the PEM is

$$\frac{\delta E}{E} = 16\%/\sqrt{E_T} + 1\% \tag{4.8}$$

and the energy resolution of the PHA is

$$\frac{\delta E}{E} = 80\%/\sqrt{E_T} + 5\% \tag{4.9}$$

[20]

4.4 Muon Detectors

The first thing to know about muon detectors is that there is no such thing as a muon detector, just a charged particle detector located behind so much material that only muons tend to reach it. Given that, the CDF muon detectors are located outside the calorimeter system from the beam-line. This way, any high energy photons will have already been absorbed by the EM calorimeter and any high energy hadrons will have already been absorbed by the hadronic calorimeter–aside from the occasional "punch through" hadron. The three muon detectors used for this analysis are the "Central MUon chambers" (CMU), "Central Muon uPgrade" (CMP), and the "Central Muon eXtension" (CMX). Not used is the "Intermediate MUon" (IMU) system in the forward region of the detector ($|\eta| > 1.0$), which contains the "Barrel MUon" chamber (BMU) and BSU/TSU scintillators (see table 4.1 for a summary).

The CMP and CMX muon detectors contain two systems: a stack of four single-cell drift chambers that provide a short track called a "stub" and a scintillation counter. The CMU has only a drift chamber. These muons detectors are used in tandem with the silicon and COT trackers to establish muon tracks from which the transverse momentum p_T is gauged by the track curvature. Since this analysis focuses on a signal with a leptonic signature, the detection of muon (along with electrons) is critical to finding, excluding, or setting limits on a signal. Also, we shall see in chapter 9 that distinguishing muons from electrons will be a useful tool in using a neural net (see chapter 7) to distinguish signal from particular backgrounds.

Chambers/Counters	$\Delta\eta$	$\Delta\phi$	$T_{\text{max drift}}$	# channels
CMU	[0.0, 0.6]	360°	800 ns	2304
CMP/CSP	[0.0, 0.6]	360°	1500 ns	1076/274
CMX/CSX	[0.6, 1.0]	360°	1600 ns	2208/324
BMU/BSU,TSU	[1.0/(1.0,1.3),1.5/(1.5,1.5)]	$270^\circ/270^\circ, 360^\circ$	800 ns	1728/432,144

Table 4.1 Basic Summary of CDF Muon Detectors [35]

4.5 CDF Detector Summary for $VH \rightarrow VWW \rightarrow$ Trileptons

This chapter explored the basic structure and design of the CDF II detector. At the broadest level, the CDF detector is composed of trackers, calorimeters, and the muon detectors (very similar to the trackers). The trackers trace the paths of the charged particles while the calorimeters absorb and record their energies.

This analysis searches for a $VH \rightarrow VWW \rightarrow$ Trilepton $+ \not\!\!E_T$ signature, so understanding how physical leptons (electrons and muons) translate into detector quantities is critical for matching the Standard Model physics of chapter 2 to experimental observation.

The Tevatron generates collisions very quickly and most will produce interactions that are not of interest to the experimentalist. Therefore, collider detectors have "trigger systems" that can quickly use tracker and calorimeter information to make decisions in real time about whether or not a particular event ($p\bar{p}$ interaction) has generated products that are interesting for some reason. Because the $VH \rightarrow VWW$ signature of interest to this analysis contains leptons and $\not\!\!E_T$, triggers that are programmed to record specifically these events are of particular interest. We shall subsequently explore the idea of triggers and the particular triggers used in this analysis in chapter 5. Once the triggers have recorded datasets that *may* have the signature of interest, offline algorithms perform more computationally intensive calculations to more accurately decide if a collection of detector quantities does constitute a reconstructed lepton. Such reconstructed lepton identification will be explored in more detail in chapter 6. Although jet identification will be useful for distinguishing signal from backgrounds (ZH tends to have ~ 2 jets while it's background tend to have 0 jets, for example), jet-based triggers will not be an item of interest to this analysis.

Chapter 5

Triggers, Datasets, and Event Selection

The Tevatron $p\bar{p}$ collisions happens every 396 ns; or equivalently, with a frequency of 2.5 MHz. The CDF detector cannot–and would not want to–record the products of every single collision that occurs. Instead, it has a three level "trigger" system that can decide whether or not to record an event using basic detector information. Ultimately, CDF is capable of recording at a rate only up to 100 Hz, so the trigger system is designed to filter the events to those of interest for current analyses. This is done with hardware systems at level 1 and 2, then a computer farm at level 3. Each particular "trigger" refers to a collection of decisions at all three levels.

5.1 Level 1

The level 1 trigger has ~ 5.5 μs to make a decision and a maximum accept rate of ~ 20 kHz. This hardware system is composed of three parallel processing streams. One stream finds calorimeter based objects (L1CAL), one looks for primitive muon signals (MUON PRIM-L1MUON), and the last finds tracks in the COT with the "eXtremely Fast Tracker" (XFT). Up to 64 level 1 triggers can be formed from the objects in these streams using simple boolean logic (AND & OR operators). [20]

5.2 Level 2

After a level 1 acceptance, the information of an event proceeds to level 2 for a more detailed decision. The level 2 trigger has ~ 20 μs to make a decision and a maximum accept rate of ~ 300 kHz. There are four buffers for processing an event coming from level 1, when a particular one of

these buffers is busy processing an event it is not available for futher use. When all four buffers are in use, further events coming from level 1 are lost. The time that level 2 is busy processing and incapable of accepting more events from level 1 is denoted as "deadtime."

Level 2 is capable of using silicon, shower max, and calorimeter information in addition to the level 1 information to perform further reconstruction of an event. Once the event data is loaded into the level 2 processors, a decision can be made about whether the event satisfies any of the level 2 triggers. [20]

5.3 Level 3

The level 3 trigger has a maximum accept rate of ~ 20 kHz. It is divided between an event builder that stores raw detector data and a linux PC farm that makes a decision on whether to store an event using higher level event objects. Level 3 is designed to make a decision on an event using data that approximates full reconstruction.

5.4 Trigger Paths ("Datasets") of the $H \rightarrow WW$ Group

"Trigger" tends to be a bit of an overloaded term; it may refer colloquially to a variety of objects. Any particular criteria within any of the three levels are often denoted as triggers, collections of criteria within one of the three levels are denoted as "LX triggers" (X$= 1, 2, 3$), as well as sets of criteria from all three levels. For the purposes of this disseratation, "trigger bits" will refer to particular criteria that exist within any one of the three "trigger levels" just discussed. There will be "LX triggers" (X$= 1, 2, 3$) for collective decision at a particular level. "Trigger paths" will be the broadest categories of collections of trigger bits that are chosen by analyses interested in data with particular features. For instance, the $H \rightarrow WW$ group is interested in leptonic decays from the weak vector bosons, so it chooses to use data from "trigger paths" that record high p_T lepton events during online operations.

The following are the triggers paths, or "datasets," used for the CDF high mass Higgs boson group and this analysis. Trigger design may evolve over time, so note that these trigger paths refer

to their incarnations in trigger table PHYSICS_5_04_v-3. This trigger table can be referenced for a more detailed breakdown of the trigger bits within each trigger level. [11]

5.4.1 ELECTRON_CENTRAL_18

The ELECTRON_CENTRAL_18 trigger path is designed to select data with high p_T electrons absorbed by the central calorimeter.

- Level 1 (L1_CEM8_PT8_v-5): This trigger requires a cluster of energy in the central EM calorimeter with at least 8 GeV, the ratio of $E_{\text{Had}}/E_{\text{EM}} < 0.125$ to distinguish the EM energy deposit from charged hadrons that may deposit some of its energy in the EM calorimeter, and an XFT track with $p_T > 8.34$.

- Level 2 (L2_CEM18_PT8_v-1): Additional requirements of an EM cluster with at least 18 GeV and $|\eta| < 1.317$ are imposed here.

- Level 3 (L3_ELECTRON_CENTRAL_18_v-6):

  - $L_{shr} < 0.4$, a variable that compares lateral shower profile in towers next to the seed tower to some expected profile.

  - Δz between the COT track and the central EM calorimeter shower to match within 8 cm.

  - a COT track with p_T at least 9 GeV

5.4.2 MUON_CMUP18

The MUON_CMUP18 trigger path is designed to identify high p_T muons with tracks in both the CMU and CMP muon detectors.

- Level 1 (L1_CMUP6_PT4_v-2): This trigger requires an XFT track with $p_T > 4.09$ GeV and fiducial to a CMU stub with $pt > 6$ GeV, and a CMP stub.

- Level 2 (L2_CMUP6_PT15_3DMATCH_v-1): This trigger tightens the XFT criteria by requiring a four layer track with $p_T > 14.77$ GeV.

- Level 3 (L3_MUON_CMUP_18_v-3): This trigger raises the p_T cut to 18 GeV and continues the requirement of matching the track to stubs in the CMU and CMP.

5.4.3 MUON_CMX18

The MUON_CMX18 trigger path is designed to identify high p_T muons with tracks that lead to the CMX muon detector.

- Level 1 (L1_CMX6_PT8_CSX_v-2): This trigger requires an XFT track with $p_T > 8.34$ GeV and fiducial to a CMX stub with $p_T > 6$ GeV, as well a a hit in the CSX scintillator.

- Level 2 (L2_CMX6_PT15_3DMATCH_HTDC_v-1): This trigger tightens the XFT criteria by requiring a four layer track with $p_T > 14.77$ GeV.

- Level 3 (L3_MUON_CMX18_v-2): This trigger raises the p_T cut to 18 GeV and continues the requirement of of matching the track to a CMX stub.

5.4.4 MET_PEM

The leptonic decays studied by the $H \to WW$ group, and especially the associated production leptonic decay of $WH \to WWW \to l\nu l\nu l\nu$, also tend to exhibit high values of missing transverse energy ($\not\!\!E_T$). So we are also interested in the dataset pertaining to the MET_PEM trigger path that is designed to accept events with energy clusters in the plug electomagnetic calorimeter in association with $\not\!\!E_T$. Note that this online version of $\not\!\!E_T$–denoted here as $\not\!\!E_T{}^{\text{raw}}$– simply uses the sum of transverse energies over the calorimeter towers and does not employ the muon or jet corrections described later in chapter 6.

- Level 1 (L1_EM8_&_MET15_v-11): At this level, the trigger requires either a central or plug EM cluster with $E_T > 8$ GeV, with $E_{\text{Had}}/E_{\text{EM}} < 0.125$ for a central cluster and $E_{\text{Had}}/E_{\text{EM}} < 0.0625$ for a plug cluster. The L1_MET15 trigger bit is also employed for a $\not\!\!E_T{}^{\text{raw}} > 15$ GeV cut.

- Level 2 (L2_PEM20_MET15_v-1): This trigger continues to require a $\not\!\!E_T^{\text{raw}} > 15$ GeV cut, requires a plug EM object with $E_T > 20$ GeV, and $1.1 < |\eta| < 3.6$.

- Level 3 (L3_PEM20_MET15_v-8): This level imposes a plug calorimeter requirement of 3 towers with $E_T > 20$ GeV, $E_{\text{Had}}/E_{\text{EM}} < 0.125$ for the plug cluster, and a $\not\!\!E_T^{\text{raw}} > 15$ GeV cut again.

5.4.5 MUON_CMP18_PHI_GAP

This trigger path has been working properly only since period 21 data-taking [14]. The MUON_CMP18_PH trigger path is designed to account for gaps in ϕ coverage between the calorimeter wedges. This puts a 2.25 degree gap in the CMU ϕ coverage every 15 degrees. The basic idea of this trigger is to require tracks that point towards a gap to be coincidence with a CMP stub and a CSP hit. Previous incarnations of this trigger had problems keeping the rate under reasonable levels at high instantaneous luminosities, so it does employ a dynamic prescale up to a factor of 60. [17]

- Level 1 (L1_CMP3_PT15_3D_PHIGAP_DPS_v-2): This trigger requires an XFT track with $p_T > 14.77$ GeV.

- Level 2 (L2_CMP3_PT15_3D_PHIGAP_CSP_v-1): This level goes on to require a CSP hit.

- Level 3 (L3_MUON_CMP18_v-1): At level 3, this trigger requires

  - cmpDx=20

  - $p_T > 18$ GeV

  - CMP stub

Chapter 6

High p_T Object Identification

Datasets from any given trigger path begin as little more than collections of detector signals: hits in the silicon and COT, showers in the calorimeters with some measured energy, etc. Translating these signals into objects the experimentalist is looking for (leptons, jets, photons, etc.) is a formidible and detailed task. This chapter will first discuss the details of lepton identification (section 6.1), jet identification (section 6.2), and how missing energy is computed (section 6.3). Then other important details related to the shortcomings of object identification like "fake leptons" (section 6.4), as well as efficiencies and scale factors related to lepton ID (sections 6.5 and 6.6) will be discussed.

6.1 Lepton Identification

This analysis is mostly interested in the identification of electrons and muons, as well as missing energy ($\not\!\!E_T$). To determine what pattern of detector information should be called "electrons" and "muons," hits in the silicon and COT detectors must undergo essentially a high brow game of connect-the-dots to form "tracks." Such tracks must then be fiducial to energy deposits in the EM calorimeter to be identified as electrons, or fiducial to short tracks ("stubs") in one of the muons detectors to be identified as muons.

This analysis, along with the rest of the $H \rightarrow WW$ group, constructs from the trigger paths listed in section 5.4 these lepton categories:

- Electrons: Likelihood-based electrons, phoenix electrons (see section 6.1.2)

- Muons: CMUP, CMP, CMU, CMX, CMXMsKs, BMU, CMIOCES, CMIOPES (see section 6.1.3)

- Lepton of unspecified flavor: CrkTrk ("crack track")

All of these categories will require some collection of several cuts on detector quantities such as [14]:

- E_{HAD}/E_{EM} – the ratio of the hadronic calorimeter energy to the electromagnetic calorimeter energy associated with the candidate

- E/P – the ratio of the EM cluster transverse energy to the COT track transverse momentum

- L_{shr} – the lateral shower profile in the transverse plane to the electron direction

$$L_{\text{shr}} = 0.14 \frac{\sum_i (M_i - P_i)}{\sqrt{(0.14\sqrt{E_{\text{EM}}})^2 + \sum_i (\Delta P_i)^2}} \tag{6.1}$$

  where i is the sum over adjacent towers, M_i is the measured energy, and P_i is the predicted energy in the i^{th} tower [36].

- $CalIso$ – The energy E_T in a cone of radius $\Delta R = \sqrt{(\Delta\eta)^2 + (\Delta\phi)^2} \leq 0.4$ around the electron cluster excluding the electron cluster divided by the energy in the electron cluster:

$$CalIso = \frac{E_T^{cone} - E_T^{electron}}{E_T^{electron}}$$

- $TrkIso$ – the same variable as above $CalIso$ but measured using tracks instead of calorimeter

- $Q \times \Delta x_{CES}$ – The distance in the *r*-ϕ plane between the extrapolated, COT beam constrained track and the best matching CES cluster, times the charge Q of the track.

- Δz_{CES} – The distance in the *r*-*z* plane between the extrapolated, COT beam constrained track and the best matching CES cluster.

- $NCotHitsAx$ – number of COT hits on axial layers belonging to track associated to the candidate electron
- $NCotHitsSt$ – number of COT hits on stereo layers belonging to track associated to the candidate electron
- χ^2_{COT} – χ^2 associated with the COT hits belonging to track
- $NSvxHits$ – number of SVX hits belonging to track associated to the candidate electron
- Track p_T – Transverse momentum measured from the charged particle's track
- Track z_0 – Position along the longitudinal direction of the beamline.
- Axial and Stereo Superlayer – The number of axial and stereo superlayers in the COT having at least 5 hits associated to the track in question.
- CES ΔX – The difference in the $r - \phi$ plane between the best CES match and the COT beam-constrained track extrapolation to the CES.
- PEM 3x3 Fit – A χ^2 fit to electron test beam data of nine Plug EM towers.
- PES 5x9 U/V – The ratio of the central five tower energy to the total nine tower energy.
- χ^2 – This chi squared compares the fitted track to the actual hits in the trackers.
- Curvature Significance – The measured track curvature divided by the curvature error.

Section 6.1.1 will briefly discuss track formation from hits in the trackers, then sections 6.1.2, 6.1.3, and 6.1.4 will discuss how such tracks are combined with other detector information to be counted as lepton objects.

6.1.1 Track Formation

Recall from section 4.2 that the silicon and COT trackers are surrounded by a 1.4 T field along the $\hat{z}$ direction. This field causes charged particles to follow the path of a helix with its axis parallel

to the magnetic field, so the connect-the-dots game is a matter of constructing an algorithm that will recognize a collection of silicon and COT hits that follow the path of a helix that leads near the $p\bar{p}$ interaction on one end and to either a calorimeter energy deposit or muon stub on the other end.

The COT forms segments with hits in the axial layers, then links these segments together into tracks. To form these tracks, the algorithm begins with segments in the outermost superlayers, then uses the curvature of the segment and the beamline location to search for possible other segments that could form a helix to the primary vertex. Stereo segments are then also linked to form a three dimensional track [26].

Once a COT track is formed, the silicon tracking uses this track as a "seed," essentially a starting point, and then uses an "outside-in" tracking algorithm. This will start with the outermost layer and work inwards searching for hits that form the best possible helix back to the primary vertex [37].

Forward electrons may need a different strategy if their pseudorapidity is to large to make suitable COT seed tracks for the silicon. In this case, seed tracks are formed from "CdfEmObject" objects–energy deposits in the Plug EM calorimeter–which then drives the outside-in silicon pattern recognition [24].

6.1.2 Electron ID

Central electrons ($|\eta| < 1.0$) with high p_T are expected to traverse the silicon and COT detectors, leaving behind a track. Then they enter the EM calorimeter where they will cause an electromagnetic shower and deposit their energy. Until recently, these electrons has to pass a set of criteria called "tight central electron." These criteria were a set of hard cuts, so if an object that looked very electron-like still failed even one cut it would not pass selection. This category has since been replaced by the "likelihood-based electron" (LBE) category that creates a single function out of mostly the same set of criteria, but then imposed just a single cut on the end value of that function. LBE criteria are [14]

- having a track fiducial to the CEM

- Track $z_0 < 60$ cm
- the electron candidate object is not a photon conversion
- $E_{HAD}/E_{EM} < 0.125$, which satisfies trigger requirements and cuts out charged hadronic objects.
- CalIso < 0.3, calorimeter isolation requirement to cut out fakeable objects
- $p_T(track) > 10$ GeV ($p_T(track) > 5$ GeV if $E_T < 20$ GeV)
- Likelihood cut: $\mathcal{L} > 0.90$

Given these, the values used in the likelihood function are: E_{HAD}/E_{EM}, E/P, L_{shr}, $CalIso$, $TrkIso$, $Q \times \Delta x_{CES}$, Δz_{CES}, $NCotHitsAx$, $NCotHitsSt$, $\chi^2_{COT} - \chi^2$, and $NSvxHits$. Finally, the likelihood function itself is:

$$\mathcal{L}(\vec{x}) = \frac{L_{sig}}{L_{sig} + L_{bckg}} = \frac{\prod_{i=1}^{N} P_i^{sig}(x_i)}{\prod_{i=1}^{N} P_i^{sig}(x_i) + \prod_{i=1}^{N} P_i^{bckg}(x_i)} \tag{6.2}$$

Electrons in the pseudorapidity region $1.2 < |\eta| < 2.0$ would not be found by the LBE category because they are not fiducial to the CEM. They are instead found by the "phoenix" tracking algorithm which the more traditional path of making a collection of cuts (see table 6.1).

6.1.3 Muon ID

The muon categories are denoted by which muon detector a track is found in. Muons are "minimum ionizing particles," meaning that they deposit only a small fraction of their energy in the calorimeters and can traverse through the entire CDF detector. All muon object candidates must pass a basic set of cuts (see table 6.2), then have a that is fiducial to one of the muon detectors.

- CMUP: CMUP muons are required to have stubs in both the CMP and CMU detectors, covering a pseudorapidity range of $|\eta| < 0.68$.
- CMU: High p_T tracks with a CMU stub, but not a CMP stub

- CMP: High p_T tracks with a CMP stub, but not a CMU stub
- CMX: High p_T tracks with a CMX stub, covering a pseudorapidity range of $0.6 < |\eta| < 1.0$.
- BMU: High p_T track with a BMU stub, covering a pseudorapidity range of $1.0 < |\eta| < 1.5$
- CMIOCES: A minimum ionizing track that does not register as CMUP, CMU, CMP, or CMX, but is fiducial to the central calorimeter
- CMIOPES: A minimum ionizing track that does not register as BMU, but is fiducial to the plug calorimeter.
- CMXMsKs: A high p_T track that points to either the miniskirt or keystone detectors.

Two categories of muons used do not actually use muons stubs. CMIOCES and CMIOPES muons are tracks that do not have muon stubs, but rather rely on a muon's minimum ionizing nature in a calorimeter. A track whose curvature implies high p_T, but does not deposit energy in either the EM or hadronic calorimeters strongly tends to be a muon since muons are the only particles produced that have this signature and do not tend to decay before traversing the entire CDF detector. See tables 6.3, 6.4, 6.5, 6.6, 6.7, 6.8, and 6.9 for specific cuts on each muon category. [1]

6.1.4 Unspecified Track ID

The last category of leptons considered in this analysis are tracks that are considered sufficiently lepton-like, but their flavor cannot be specified. This "CrkTrk" category is defined to cover tracks that specifically point to cracks in calorimeter acceptance

[1] Based on the CDF $H \rightarrow WW$ group's Diboson_v17 framework

Forward Electrons (PHX)	
Region	Plug EM Cal.
η_{PES}	$1.2 < \lvert\eta\rvert < 2.0$
E_{HAD}/E_{EM}	< 0.05
PEM 3x3 Fit	true
χ^2_{PES}	10
PES 5x9 U	≥ 0.65
PES 5x9 V	≥ 0.65
Isolation$/E_T$	≤ 0.1
$\Delta R(PES, PEM)$	≤ 3.0
Track Matched	true
# of Silicon Hits	≥ 3
Track $\lvert z_0\rvert$	≤ 60 cm

Table 6.1 Phoenix (PHX) electron definition

Muon Base Cuts	
p_T	> 10 GeV
E_{EM}	2+max$(0, (p - 100) \cdot 0.0115)$
E_{HAD}	6+max$(0, (p - 100) \cdot 0.028)$
Isolation$/p_T$	≤ 0.1
# Axial SL	≥ 3
# Stereo SL	≥ 2
Track $\lvert z_0\rvert$	≤ 60 cm
Track $\lvert d_0\rvert$	0.2 cm (< 0.02 cm with silicon)
χ^2/deg. of freedom	< 4.0 (< 3.0 if Run # > 186598)

Table 6.2 Base muon identification criteria for all categories

CMUP Muons	
CMU Fiducial	$x_{\text{fid}} < 0,\ z_{\text{fid}} < 0$ cm
CMP Fiducial	$x_{\text{fid}} < 0,\ z_{\text{fid}} < -3$ cm
ΔX_{CMU}	7 cm
ΔX_{CMP}	max(6, 150/p_T) cm
CMU Stub	true
CMP Stub	true

Table 6.3 Cuts for CMUP muons beyond the base muon cuts

CMP Muons	
CMU Fiducial	$x_{\text{fid}} < 0,\ z_{\text{fid}} < 0$ cm
CMP Fiducial	$x_{\text{fid}} < 0,\ z_{\text{fid}} < -3$ cm
ΔX_{CMP}	max(6, 150/p_T) cm
Run Numbers	≥ 229764
CMP Stub	true

Table 6.4 Cuts for CMP muons beyond the base muon cuts

CMU Muons	
CMU Fiducial	$x_{\text{fid}} < 0,\ z_{\text{fid}} < 0$ cm
CMP Fiducial	$x_{\text{fid}} < 0,\ z_{\text{fid}} < -3$ cm
CMX Fiducial	$x_{\text{fid}} < 0,\ z_{\text{fid}} < -3$ cm
ΔX_{CMU}	7 cm
CMU Stub	true

Table 6.5 Cuts for CMU muons beyond the base muon cuts. [Note: the code comments state "Make them starting from run 270062" but the code itself has "if (RunNumber $<$ 999999) _BitSet.SetFalse(kBit_IsFiducial);" indicating that CMU may not be in use.]

CMX Muons	
CMX Fiducial	$x_{\text{fid}} < 0,\ z_{\text{fid}} < -3$ cm
Fiducial to CMX Arches	true
Fiducial to CMX Miniskirt	false
Fiducial to CMX Keystone	false
ΔX_{CMX}	max(6, 125/p_T) cm
COT Exit Radius	> 140 cm
CMX Stub	true

Table 6.6 Cuts for CMX muons beyond the base muon cuts

BMU Muons	
BMU Fiducial	true
BMU Stub	true
PES Fiducial	true
NSvxHits	≥ 3
Cal. Energy	> 0.1 GeV
COT Hit Fraction	> 0.6
Curvature Significance	> 12
Run Number	≥ 162312

Table 6.7 Cuts for BMU muons beyond the base muon cuts

CMIOCES Muons	
	Not CMUP or CMX
Cal. Energy	> 0.1 GeV
NCotStSeg	≥ 3
Fiduciality	CES
χ^2/deg. of freedom	< 3.0

Table 6.8 Cuts for CMIOCES muons beyond the base muon cuts

CMIOPES Muons	
	Not BMU
Cal. Energy	> 0.1 GeV
Fiduciality	PES
COT Hit Fraction	> 0.6
Curvature Significance	> 12

Table 6.9 Cuts for CMIOPES muons beyond the base muon cuts

CrkTrk Muons	
	Not CMUP or CMX
# Axial SL	≥ 3
# Stereo SL	≥ 3
Cal. Isolation	≤ 0.1 using CDF Muon or ≤ 0.1 using EM cluster
Fiduciality	Not CES or PES fiducial
Cal. Energy	> 0.1 GeV
Fiduciality	PES
χ^2/deg. of freedom	< 3.0

Table 6.10 Cuts for CrkTrk muons beyond the base muon cuts

6.2 Jet ID

Quarks are known to exist only in groups of two ("mesons") or three ("hadrons"). The $p\bar{p}$ interactions have high enough energy to tear the quarks of the proton and antiproton out of their hadronic configurations. When this happens, they will subsequently recombine or even create pairs out of the vacuum. This typically results in a spray of particles with a common general direction which are denoted "jets" in particle physics. As such, jets tend to deposit energy in both the EM and hadronic calorimeters assiciated with multiple tracks.

In the analysis, jets are defined as calorimeter cluster within $\Delta R < 0.4$ and at least $E_T > 15$ GeV. While jets are not a part of the signal this analysis select upon, the number of jets in a particular event will be an important variable for discriminating the WH and ZH signals from their backgrounds.

6.3 Missing Transverse Energy ($\not\!\!E_T$)

The $p\bar{p}$ beam is defined as the $\hat{z}$-direction in CDF coordinates. Hence, since the beginning state of the $p\bar{p}$ interaction has no momentum or energy directed in the plane transverse to the beamline, the energies of products after the $p\bar{p}$ interaction should sum to zero. Particles that do not interact with the detector do not have their energies included in the vector sum, so the result is "missing transverse energy" ($\not\!\!E_T$).

Neutrinos are the only known particles that will not interact with the detector and are inherent to the leptonic decays of W weak vector bosons. Therefore, $\not\!\!E_T$ is an important quantity in the signatures of $WH \to WWW$ and $ZH \to ZWW$ signals of the $H \to WW$ group.

There are, however, some caveats that must be accounted for first. The raw missing transverse energy is just the sum over the calorimeter towers.

$$\vec{\not\!\!E_T}^{\text{raw}} = -\sum_i \vec{E_T^i} \tag{6.3}$$

where $\vec{E_T^i}$ is the energy magnitude deposited in the i^{th} calorimeter tower with a unit vector pointing from the primary vertex to the center of the calorimeter tower artificially attached to make it a

vector quantity, then the transverse component is taken. It was discussed that muons are minimum ionizing particles, so they do not deposit much of their energy in the calorimeters. This also counts as missing energy in $\vec{\not\!\!E}_T^{\text{raw}}$ so the $\not\!\!E_T$ is corrected by having the muon's energy added back, minus the small amount of energy the muon did deposit. The same goes for CrkTrk leptons which do not deposit energy in the calorimeters by definition. Lastly, jets undergo some energy corrections in reconstruction which then affects the vector energy sum.

6.4 Fake Leptons

Some small, but significant, portion of jets will produce a signature that passes one of the lepton definitions. These objects are denoted "fake leptons" or just "fakes." Note that these are distinct from "photon converted leptons," which are photons that interact with the detector apparatus to become an electron-positron pair and then register as an electron.

Modeling of fakes has been unreliable, so this background is instead estimated from "jet samples" of data. Four such jet samples are used, based on trigger paths requiring a leading jet E_T of at least 20 GeV, 50 GeV, 70 GeV, and 100 GeV. In these data samples, the number of jet-like objects that pass a very loose selection of lepton cuts are counted. These loose lepton selections are called "denominator objects," and various denominator objects are defined for the different lepton categories. These are considered to be the collection of jet-objects that have any non-negligible chance at all of passing a full lepton definition. The "fake rate" is then the ratio of these denominator objects that actually do pass a full lepton definition to the full set that pass just a denominator definition. Note that the actually number of isolated, fully recognized leptons (i.e. "real" leptons) must be subtracted in the numerator and number of isolated lepton-objects passing the denominator definition must be subtracted from the denominator. Hence, for a generic lepton category i, the fake rate is [14]

$$f_i = \frac{N_I(\text{full leptons}) - \sum\limits_{j\in\{\text{EWK}\}} N_{ij}(\text{full leptons})}{N_I(\text{denom. objects}) - \sum\limits_{j\in\{\text{EWK}\}} N_{ij}(\text{denom. objects})} \tag{6.4}$$

The four data samples provide four independent estimates of the fake probability, the average of which are use as the fake probability in this analysis. The systematic uncertainty on the rate beyond the statistical error is estimated by adding a parameter α as $\sqrt{\text{stat.} + \alpha}$ large enough so that all four samples agree to within one standard deviation.

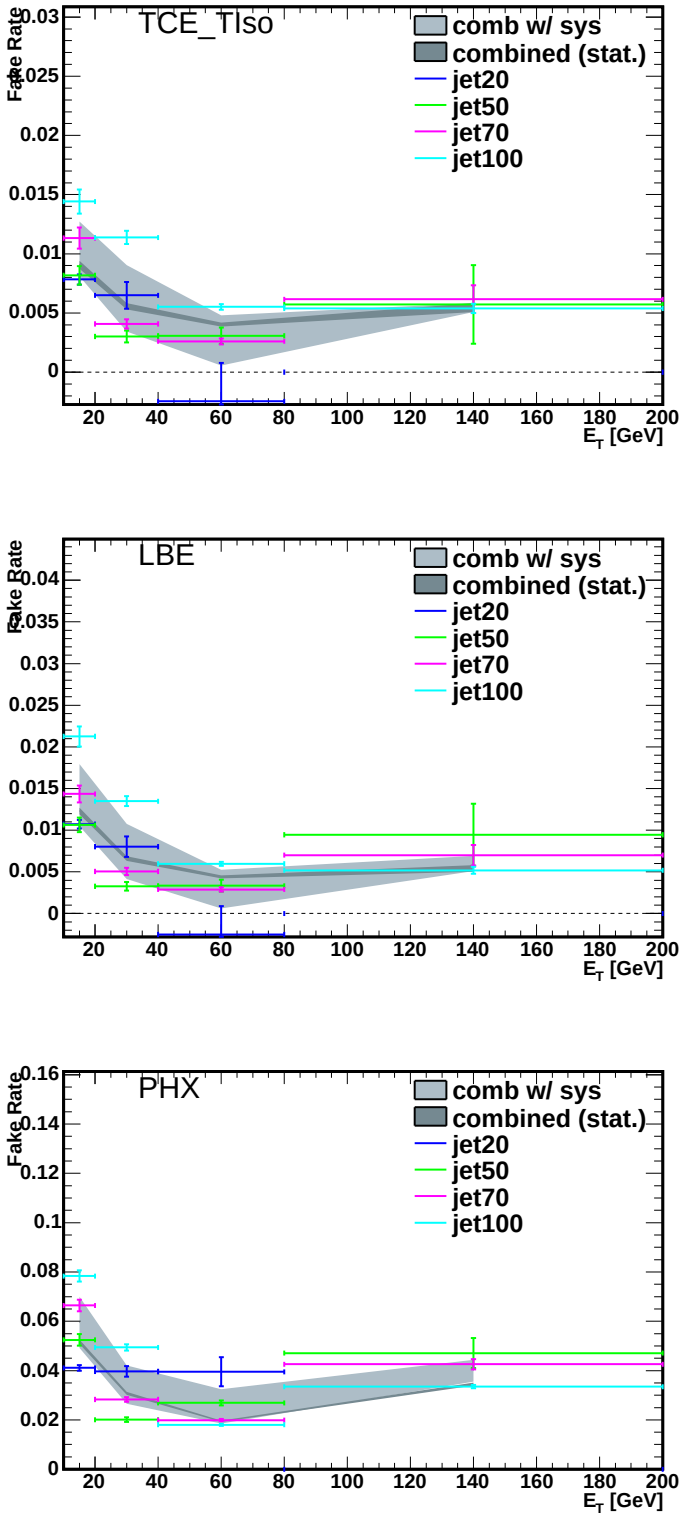

Figure 6.1 Fake rates for electrons. PHX and LBE have no track isolation requirement. TCE is include for comparison. [16]

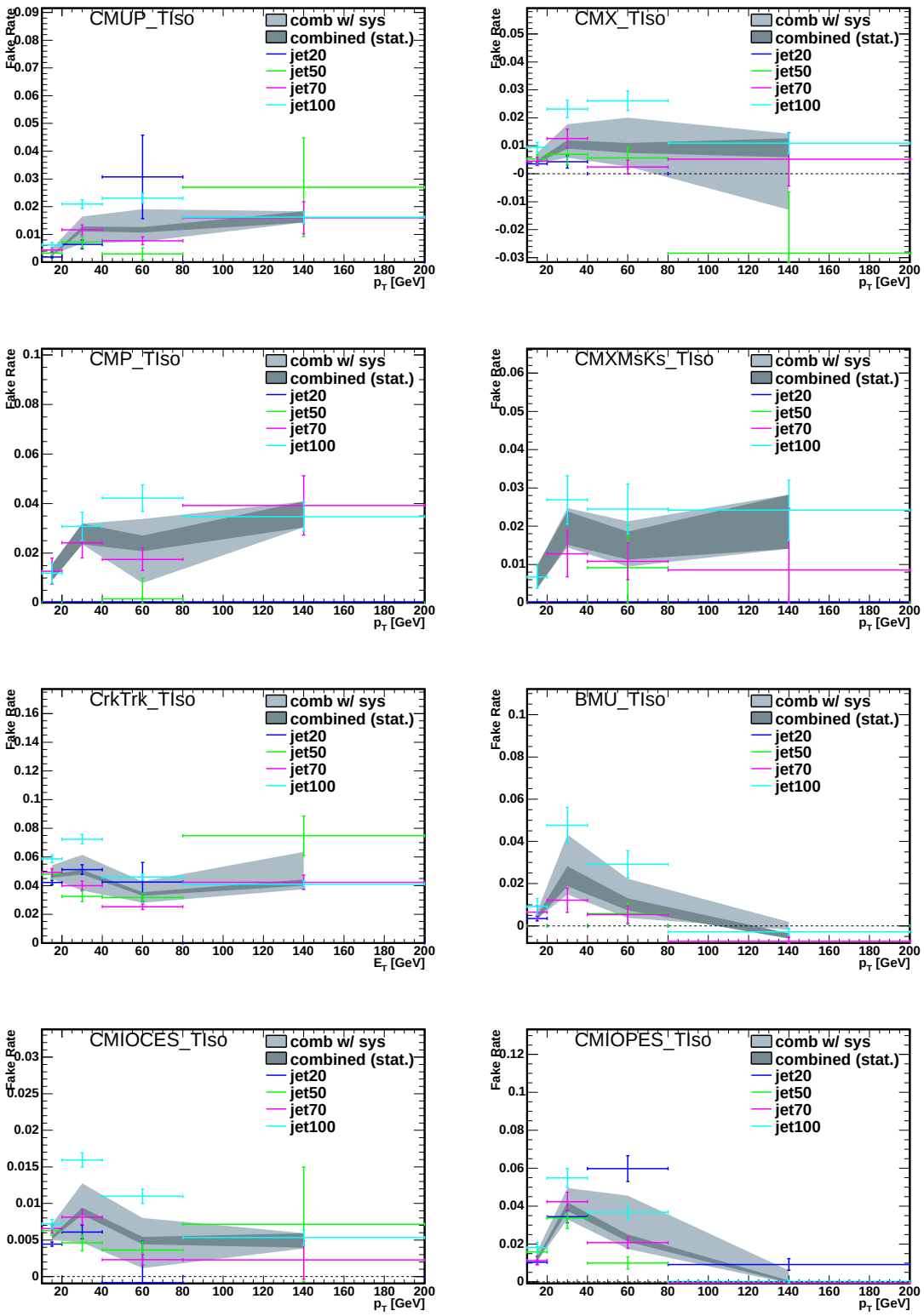

Figure 6.2 Fake rates for muons. [16]

6.5 Lepton Efficiencies

Monte carlo simulated backgrounds and signals must be appropriately calibrated to the data to be accurate. Lepton efficiencies are measured with Drell-Yan ($Z \rightarrow ll$) events in MC and data because of the relatively large sample size, then compared. Such corrections are then applied to all MC processes.

Lepton efficiency is defined as

$$\epsilon_{\text{ID}} = \frac{N_{TT}}{N_{TL}} \tag{6.5}$$

where N_{TT} is the count of tight-tight lepton pairs and N_{TL} is the count of tight-loose pairs ($\{N_{TT}\} \subset \{N_{TL}\}$) [31].

6.6 Lepton Scale Factors

The "lepton scale factor" is the ratio of lepton identification efficiencies in data to the monte carlo. This factor is used later in determining how to weight each event in an MC process. It is recalculated for different periods in data taking.

$$s = \frac{\epsilon_{\text{ID}}^{\text{data}}}{\epsilon_{\text{ID}}^{\text{MC}}} \tag{6.6}$$

Lepton Category	Period 0	Period 1-4	Period 5-7	Period 8-10
CMUP	0.973 ± 0.012	0.938 ± 0.009	0.932 ± 0.013	0.955 ± 0.009
CMU	0.000 ± 1.000	0.000 ± 0.500	0.000 ± 0.577	0.000 ± 0.577
CMP	0.000 ± 1.000	0.000 ± 0.500	0.000 ± 0.577	0.965 ± 0.032
CMX	1.027 ± 0.016	1.020 ± 0.017	1.026 ± 0.019	1.007 ± 0.014
CMXMsKs	0.000 ± 1.000	0.000 ± 0.500	0.000 ± 0.577	0.930 ± 0.036
BMU	1.127 ± 0.032	1.107 ± 0.025	1.076 ± 0.032	1.099 ± 0.021
CMIOCES	1.049 ± 0.019	1.060 ± 0.015	1.085 ± 0.018	1.086 ± 0.014
CMIOPES	1.000 ± 0.000	1.005 ± 0.020	1.029 ± 0.025	0.980 ± 0.018
CrkTrk μ	0.958 ± 0.015	0.978 ± 0.012	0.976 ± 0.015	0.973 ± 0.012

Table 6.11 Muon scale factors in Diboson_v17 data [14].

Lepton Category	Period 11-12	Period 13	Period 14-25
CMUP	0.924 ± 0.011	0.937 ± 0.011	0.884 ± 0.004
CMU	0.000 ± 0.707	0.000 ± 1.000	0.000 ± 1.000
CMP	0.893 ± 0.022	0.987 ± 0.022	0.876 ± 0.009
CMX	0.981 ± 0.018	0.986 ± 0.020	0.978 ± 0.008
CMXMsKs	0.935 ± 0.032	0.890 ± 0.033	0.912 ± 0.012
BMU	1.064 ± 0.028	1.142 ± 0.037	1.100 ± 0.013
CMIOCES	1.204 ± 0.019	1.186 ± 0.022	1.196 ± 0.011
CMIOPES	0.955 ± 0.023	0.998 ± 0.037	0.970 ± 0.010
CrkTrk μ	0.990 ± 0.020	0.952 ± 0.021	0.959 ± 0.008

Table 6.12 Muon scale factors in Diboson_v17 data [14].

Lepton Category	Period 0	Period 1-4	Period 5-7	Period 8-10
LBE($\mathcal{L} > 0.9$)	1.012 ± 0.004	1.001 ± 0.003	0.996 ± 0.004	0.992 ± 0.003
PHXTrk	0.998 ± 0.005	1.007 ± 0.004	1.018 ± 0.005	1.001 ± 0.004
PHXPEM	0.951 ± 0.006	0.953 ± 0.005	0.944 ± 0.006	0.931 ± 0.004
PEM	0.943 ± 0.011	0.916 ± 0.010	0.911 ± 0.015	0.875 ± 0.010
CrkTrk e	0.950 ± 0.016	0.989 ± 0.016	0.957 ± 0.019	0.948 ± 0.014
PESTrk	0.913 ± 0.013	0.949 ± 0.013	0.974 ± 0.017	0.947 ± 0.012

Table 6.13 Electron scale factors in Diboson_v17 data [14].

Lepton Category	Period 11-12	Period 13	Period 14-25
LBE($\mathcal{L} > 0.9$)	0.993 ± 0.004	0.994 ± 0.005	0.991 ± 0.001
PHXTrk	0.999 ± 0.004	1.004 ± 0.057	1.026 ± 0.002
PHXPEM	0.939 ± 0.005	0.936 ± 0.007	0.911 ± 0.002
PEM	0.870 ± 0.013	0.871 ± 0.013	0.829 ± 0.005
CrkTrk e	1.002 ± 0.021	0.966 ± 0.021	0.964 ± 0.007
PESTrk	0.966 ± 0.015	0.922 ± 0.021	0.907 ± 0.006

Table 6.14 Electron scale factors in Diboson_v17 data [14].

Chapter 7

Computations with Artificial Neural Networks

This analysis uses the NeuroBayes artificial neural network to discriminate the Higgs boson signal from its backgrounds. After all analysis cuts are made and we have a final event count for the monte carlo signals and backgrounds, as well as the experimental data, variables showing separation in the distributions of signals and backgrounds can be used as a collection of input variables for a neural network. This neural network then uses the N_{in} input variables to compute a single one-dimensional distribution–denoted the "neural network score" in this dissertation–for each signal and background. In the end, the distributions in the neural network score should show much better separation between signals and backgrounds than any one of the input variables since the information of distribution separation of all the input variables is included in the final neural net score.

The neural network itself is an information processing system that is characteristically nonlinear, nonalgorithmic, and parallel. The NeuroBayes version of a neural net begins with a set of N_{in} inputs $\{x\}$ of any value and a single output $z_{\text{net}} \in (-1, 1)$. The output z_{net} is computed from some function of the N_{in} input variables, as well as weights and thresholds that may be associated with the variables [23]:

$$z_{\text{net}} = F_{\text{net}}(\{x\}, \{w\}, \{T\}) \tag{7.1}$$

The most basic structure of a neural net is called a "neurode" (see figure 7.1), which has some N input variables, their weights, and some single threshold value. From these, the neurode outputs a single value a.

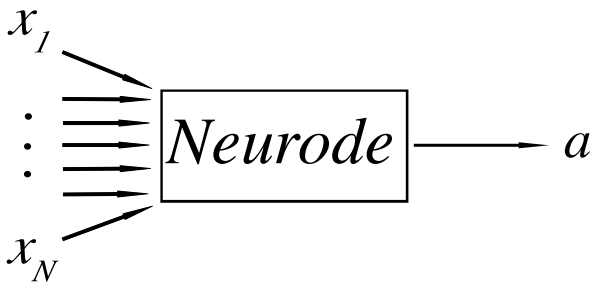

Figure 7.1 Neural Network “neurode”

Next, suppose we group together N_2 neurodes, each taking as input a set of N_1 variables. This structure is denoted a “network node” (see figure 7.2). With N_2 neurodes composing it, the network node has then a set $\{a_i\},\ i \in \{1, \ldots, N_2\}$ of outputs values–one output value for each neurode.

Finally, consider a network node with N_{in} input variables and N_1 output values. Then use these N_1 values as the input variables for another network node, which will output some N_2 values. Such a succession of network nodes using the output of the previous network node as the input for the next is called a “neural network” (see figure ????). The first network node is called the “first hidden layer,” the i^{th} network node is the “i^{th} hidden layer,” until the last network node–the “output layer”–is reached and outputs the single score value z_{net}.

Having a neural network and having it do something useful are two distinct tasks. The tricky part is finding a network that yields $z_{\text{net}} \simeq -1$ for backgrounds and $z_{\text{net}} \simeq +1$ for signals. This requires a properly “trained” neural network. To do this, an “error function” [23]–or sometimes called “quadratic loss function”– (χ^2_{net}) is defined on the N_{in} input variables so that small values for signals and a comparatively larger values for backgrounds are returned. NeuroBayes uses [22]:

$$\chi^2_{\text{net}} = \sum_j w_j \frac{1}{2} \sum_i (T_{ji} - z_{ji})^2 \tag{7.2}$$

where j runs over the outputs of a network node, i runs over the event list, and T_{ji} is the target value for the node.

By doing this, we have established an N_{in}-dimensional space whose minimum characterizes a signal-like signature and whose maximum characterizes a background-like signature. “Training”

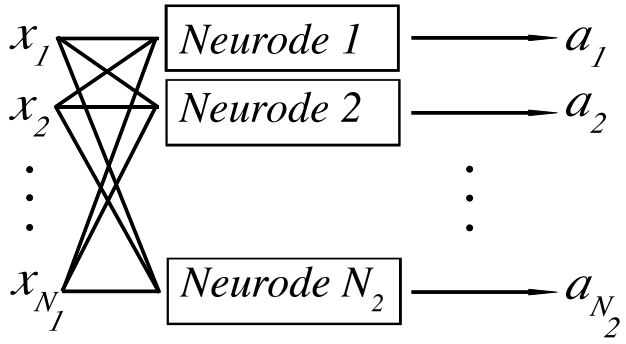

Figure 7.2 Neural Network "network node"

the neural net is synonomous with locating the minima of χ^2_{net} as closely as possible ($\frac{d\chi^2_{\text{net}}}{dz} = 0$). Note that one of the great dangers of training a neural net is having a quadradic loss function get stuck in a *local* minima inadvertantly. Though, the technical details of how the minimization is performed are designed with this in mind. Once this is done, the trained error function is used in the neural network to yield $z_{\text{net}} \simeq -1$ for background-like events and $z_{\text{net}} \simeq +1$ for signal-like events.

The usage and results of the neural network method in this particular analysis is expounded in section 9.3, where the inputs variables and neural network scores for the '$VH \to VWW \to$ trilepton' analysis is examined in detail.

Chapter 8

Statistics of Confidence Level Limits In the Search for New Physics

8.1 Poisson Statistics and Physical Processes

It is not presumptive to state that this analysis does not constitute a discovery of the Higgs boson. Rather, this analysis sets and updates an experimental limit excluding the Higgs boson of a particular mass range with a certain confidence level. As such, this chapter explains the method of how such a statistical exclusion is computed in general, while the experimental exclusion set for this analysis in particular is given in chapter 9.6.

Let's begin by explicitly identifying some basic assumptions inherent to particle interactions. These assumptions provide the logical foundation upon which the rest of the statistical aspects of the analysis are based:

1. The probability for a particular outcome of interest occuring more than once in a single event is negligible. This analysis searches for a higgs boson in the trilepton signature. The cross sections of Higgs production mechanisms explored–as well as all of the backgrounds–is so small that we can assume that none of the processes occure more than once in a single event.

2. Each $p\bar{p}$ interaction is an independent event.

3. The occurence of any particular outcome of interest (both backgrounds and signals) is independent of other occurences. In other words, a process occuring or not occuring in one event does not affect the probability that it will occur in another event.

This set of assumptions implies the processes studied will follow a Poisson distribution [28].

Definition 8.1 The *Poisson distribution* is the continuous distribution attained from the discrete binomial distribution when taking the limit of an infinite number of events ($n \to \infty$). Let n be the number of events, p be the probability of an occurence of interest happening, k is the number of events inwhich the occurence of interest is observed, and $\lambda \equiv np$ remain constant (this becomes the expected value). Then the *Poisson distribution* is [29]:

$$\lim_{n\to\infty} \binom{n}{k} p^k (1-p)^{n-k} = \frac{e^{-\lambda}\lambda^k}{k!}, \quad \forall\, k \in \{0 \bigcup \mathbb{Z}\}. \tag{8.1}$$

8.2 Gaussian Statistics and Systematic Errors

In any kind of experimental measurement, infinite precision is impossible. Knowing what we know always must include knowing what we don't know. Systematic errors of measurement must be set in order to not overstate the significance of a measurement.

Collider physics experiments inherently contain a plethora of systematic uncertainties. There are uncertainties of the beam intensity, acceptances, theoretical cross sections of the processes, etc. (see section 9.5 for the full list of systematic uncertainties inherent to this analysis). In statistics, these are sometimes called "nuissance parameters," but this analysis will use the term "systematic uncertainty."

Suppose, for the sake of argument, a particular quantity is to be measured and the measurement is performed many times on the exact same quantity, with the measurement performed in the same manner each time. Because infinite precision of measurement is impossible, there must be some distribution formed about the measurable value. The "Gaussian distribution" (or "Normal distribution" to statisticians) describes data that is clustered about some mean, so systematic errors in particle physics are assumed to have a Gaussian-like distribution.

Definition 8.2 [30] A random variable is *normally distributed*–or follows a *Gaussian distribution*–with mean μ and variance σ^2 if

$$f(y) = \frac{1}{\sigma\sqrt{2\pi}} e^{-\frac{1}{2}\left(\frac{y-\mu}{\sigma}\right)^2} \tag{8.2}$$

8.3 Likelihood and Confidence Level Computation

Without any a priori expectations about the outcome of the analysis, it either must compute the significance of a signal observed or set an exclusion if one is not observed. In either case, the data is compared to two hypotheses: one model using background processes only and one that include both the background and signal estimate. Confidence level computations in this analysis are performed by a program called `MCLimit`–written specifically for CDF analyses.

The benchmark for excluding a signal is set at 95% confidence level. This means that a 95% confidence level exclusion should be obtained no more than 5% of the time if a real signal is present. If the discovery of a signal is possible, then data surplus over background must be distinguished as being a signal rather than an upward statistical fluctuation of the background hypothesis. Therefore, the probability of an upward fluctuation of the background must be computed. A signal is "discovered" if the probability of an upward fluctuation of the background is no more than the integrated probability of the 5σ tails of the Gaussian distribution.

Let's proceeed by defining a "likelihood" and "likelihood rato," then move on to their use in computing "confidence levels." The starting point is the neural net score described in chapter 7. With the background and signal distributions separated as much as possible, a stronger confidence level can be computed in the end. The neural net score is divided into some number of bins; each bin will have it's own Poisson probability term in the likelihood.

Definition 8.3 The *likelihood* function $\mathbb{L}$ is a product of Poisson probabilities for each bin of the neural net score, in this analysis. Further, there is a separate product of Gaussian distributions for each systematic error.

$$\mathbb{L} = \left(\prod_i \frac{\mu_i^{n_i} e^{-\mu_i}}{n_i!} \right) \cdot \prod_c e^{\frac{S_c^2}{2}} \tag{8.3}$$

where μ_i is the total expectation in the i-th bin and n_i is the number of data events in the i-th bin. μ_i is given by

$$\mu_i = \sum_k \alpha_k \left[\prod_c (1 + f_k^c S_c) \right] (N_k^{Exp})_i \tag{8.4}$$

Here f_k^c is the fractional uncertainty associated with the systematic S_c and process k.

Now, μ_i is the total expectation of the i-th bin, but the expectation can differ depending on which hypothesis we use: the background-only hypothesis or the background-plus-signal hypothesis. Both shall be employed in the likelihood ratio.

Definition 8.4 A *test statistic* is a value X which discriminates signal-like outcomes from background-like outcomes. For the purposes of this analysis, the likelihood ratio is chosen to be the test statistic [27].

Definition 8.5 Ignoring systematic errors for now, the *likelihood ratio* is the ratio of the likelihood function for the background-plus-signal hypothesis to the likelihood function for the background-only hypothesis.

$$X = \prod_{i=1}^{n} \frac{\frac{e^{-(s_i+b_i)}(s_i+b_i)^{d_i}}{d_i!}}{\frac{e^{-b_i} b_i^{d_i}}{d_i!}} \tag{8.5}$$

where s_i is the signal expectation in the i-th bin of the neural net score, b_i is the background expectation, and d_i is the number of events observed in data.

Definition 8.6 The *confidence level* for exclusion of the signal-plus-background hypothesis is the probability of the test statistic X being less than or equal to the test statistic of the observed data $X_{\text{obs.}}$.

$$CL_{s+b} = P_{s+b}(X \leq X_{\text{obs.}}) \tag{8.6}$$

$$P_{s+b}(X \leq X_{\text{obs.}}) = \sum_{X(\{d_i'\}) \leq X(\{d_i\})} \prod_{i=1}^{n} \frac{e^{-(s_i+b_i)}(s_i+b_i)^{d_i'}}{d_i'!} \tag{8.7}$$

where $X(\{d_i\})$ is computed for the observed candidates for each channel $\{d_i\}$ and the sum is over final outcomes $\{d_i'\}$ with test statistic value less than or equal to the observed one [27].

An exclusion of at least 95% confidence level is achieved if $CL_{s+b} \leq 0.05$. The confidence level reported by this analysis will be normalized to the Standard Model background hypothesis $CL/CL_{\sigma_{\text{SM}}}$. Hence, $CL/CL_{\sigma_{\text{SM}}} = 1$ means that the background-plus-signal hypothesis has been excluded at 95% confidence level. This is then compared to the same confidence level normalized

to Standard Model computed with pseudoexperiments assuming the background hypothesis and normalized to the amount of data available to date. When an insufficient amount of data has been collected to distinguish the $s + b$ hypothesis from the b hypothesis, $CL/CL_{\sigma_{\text{SM}}} > 1$. As more data is collected, this value decreases. When these pseudoexperiments assuming the background hypothesis achieve $CL/CL_{\sigma_{\text{SM}}} = 1$, we say we have "achieved Standard Model sensitivity" at the 95% confidence level.

Chapter 9

The High Mass Higgs Boson Analysis in the Trilepton Signature

9.1 Motivation for Trileptons

The production cross sections for WH and ZH may be small relative to the gluon fusion cross section of the current $H \rightarrow WW$ analysis, but until now the trilepton signature has been completely unexplored, the uniqueness of the trilepton signature keeps background low, and every little bit counts as we push observed limits toward the standard model cross section.

Leptons decaying from a W-boson are physically detectable from an experimental point of view if the W decays to an electron, a muon, or a tau provided that the tau goes on to decay to an electron or muon. Given a generic W-boson, the probability of getting a lepton via any of these decays is : [1][13]

$$\begin{aligned} P(W \rightarrow l) &= P(W \rightarrow e) + P(W \rightarrow \mu) + P(W \rightarrow \tau)\,[P(\tau \rightarrow e) + P(\tau \rightarrow \mu)] \\ &= 0.2528 \end{aligned}$$

The relevant cross sections are (from tables 9.2, 9.3, and see [16])

- $\sigma_{\text{ggH160}} = 0.4607$ pb
- $\sigma_{\text{WH160}} = 0.0510$ pb
- $\sigma_{\text{ZH160}} = 0.0331$ pb

[1] Basic decay values are from PDG Particle Physics Booklet (July 2006), Institute of Physics

The dominant mode for the current $H \to WW$ group analysis is gluon fusion in the two-lepton bin, which has an expected yield of:

$$\sigma_{\text{ggH160}} \cdot \mathcal{BR}(H \to WW) \cdot P(W \to l)^2 = 0.02653\text{pb}$$

By comparision, the expected yield for WH associated production in the three-lepton bin is:

$$\sigma_{\text{WH160}} \cdot \mathcal{BR}(H \to WW) \cdot P(W \to l)^3 = 7.425 \times 10^{-4}\text{pb}$$

or 2.8% the yield of the dilepton analysis (for $m_H = 160$ GeV).

ZH associated production may have a smaller cross section than WH, but given one such event there is a higher probability of producing three leptons. In this case, the Z decays to two leptons so we need only one of the two Higgs-W-bosons to decay leptonically and there are two ways for this to happen:

$$P(W \to l, W \to l) = P(W \to l)^2 = 0.06391$$
$$P(W \to l, W \to \text{had.}) = P(W \to l)\left[1 - P(W \to l)\right] = 0.1889$$
$$P(W \to \text{had.}, W \to l) = P(W \to l)\left[1 - P(W \to l)\right] = 0.1889$$
$$P(W \to \text{had.}, W \to \text{had.}) = \left[1 - P(W \to l)\right]^2 = 0.5583$$

[2] So the expected ZH yield is

$$\sigma_{\text{ZH160}} \cdot \mathcal{BR}(H \to WW) \cdot P(Z \to ll) \cdot 2 \cdot P(W \to l, W \to \text{had.}) = 7.582 \times 10^{-4}\text{pb}$$

or 3.0% of the current $H \to WW$ dilepton analysis (for $m_H = 160$ GeV). Thus, based on cross sections and branching ratios alone we pursued this trilepton analysis expecting to contribute another $\sim 5.7\%$ compared to the gluon fusion process in the current $H \to WW$ dilepton analysis.

Incidentally, one of the future improvements to this analysis is to accept τ leptons directly. Noting that the above prediction assumes that vector boson decays to τ's result in a detectable lepton only if that τ decays to an electron or muon, if we repeat the prediction assuming we may accept one hadronically decaying tau into the trilepton analysis, then the 5.7% becomes 6.9% (for $m_H = 160$ GeV).

[2] Observe that 0.06391+0.1889+0.1889+0.5583=1.0

9.2 Event Summary and Signatures of the WH and ZH Trilepton Analyses

9.2.1 Lepton Selection

This trilepton analysis is a high mass ($m_H > 135$ GeV) standard model higgs boson search conducted by the $H \rightarrow WW$ group, so the lepton selection criteria of the $H \rightarrow WW$ group follow implicitly as well. The lepton categories used are [16]:

- Electrons: LBE, PHX (TCE has been replaced with the likelihood-based electron selection)
- Muons: CMUP, CMP, CMU, CMX, CMXMsKs, BMU, CMIOCES, CMIOPES, CrkTrk

The $H \rightarrow WW$ group also recently replaced the standard selection method of hard cuts with a likelihood-based selection for electrons. This new selection method is therefore also assumed in this trilepton analysis and detailed further in [16].

The datasets used are bhel0d/0h/0i/0j/0k/0m for electrons, bhmu0d/0h/0i/0j/0k/0m for muons, and bpel0d/0h/0i/0j/0k/0m for MET+PEM; with the following corresponding trigger paths:

- ELECTRON_CENTRAL_18
- MUON_CMUP18
- MUON_CMX18
- MUON_PEM
- MUON_CMP18_PHI_GAP

9.2.2 Trilepton Signal Regions Defined

The current $H \rightarrow WW$ group analysis is constrained only to the study of events with exactly two leptons, which focuses primarily on the gluon fusion Higgs boson signal because of its large cross section relative to associated production. The trilepton analysis, however, focuses virtually entirely on the two associated production channels because there are three vector bosons that allow for decays to more than two leptons, whereas the gluon fusion and vector boson fusion signals do

mode	Period	Stntuple	$\sigma \times \mathcal{B}$ (pb)	K-factor[a]	Filter Eff
WZ	0-23	we0s6d,we0scd,we0shd we0sld,we0sod,we0sbf we0shf	3.46×0.101	1.0	0.754
ZZ	0-23	we0s7d,we0sdd,we0sid we0smd, we0spd,we0scf we0sif	1.511	1.0	0.233
$t\bar{t}$	0-11	te0s2z	7.9×0.1027	1.0	1.0
$Z\gamma$	0-11	re0s33, re0s34, re0s37	14.05	1.36[b]	1.0

[a] If cross section is NLO, then K-factor is one.

[b] http://www-cdf.fnal.gov/tiki/tiki-index.php?page=EwkDatasets#_Drell_Yan_Z_gamma_Sample

Table 9.1 Monte Carlo samples used in this analysis

$M_H(GeV^2)$	Period	Stntuple	σ (pb)	BR ($H \to WW$)	Filter Efficiency
110	0-23	fhgs4a,fhgs6a	0.2075	0.0441	0.6880
120	0-23	fhgs4b,fhgs6b	0.1529	0.1320	0.6978
130	0-23	fhgs4c,fhgs6c	0.1141	0.2869	0.7032
140	0-23	fhgs4d,fhgs6d	0.0860	0.4833	0.7065
150	0-23	fhgs4e,fhgs6e	0.0654	0.6817	0.7085
160	0-23	fhgs4f,fhgs6f	0.0510	0.9011	0.7108
170	0-23	fhgs4g,fhgs6g	0.0389	0.9653	0.7125
180	0-23	fhgs4h,fhgs6h	0.0306	0.9345	0.7141
190	0-23	fhgs4i,fhgs6i	0.0243	0.7761	0.7151
200	0-23	fhgs4j,fhgs6j	0.0193	0.7347	0.7165
145	0-23	fhgs4o,fhgs6o	0.0749	0.5731	0.7075
155	0-23	fhgs4p,fhgs6p	0.0572	0.8007	0.7098
165	0-23	fhgs4q,fhgs6q	0.0441	0.9566	0.7114
175	0-23	fhgs4r,fhgs6r	0.0344	0.9505	0.7130

Table 9.2 Associated Higgs production with a W boson (from CDF Note 9863).

$M_H(GeV^2)$	Period	Stntuple	σ (pb)	BR ($H \to WW$)	Filter Efficiency
110	0-23	uhgs4a,uhgs6a	0.1236	0.0441	0.6930
120	0-23	uhgs4b,uhgs6b	0.0927	0.1320	0.7031
130	0-23	uhgs4c,uhgs6c	0.0705	0.2869	0.7087
140	0-23	uhgs4d,uhgs6d	0.0542	0.4833	0.7122
150	0-23	uhgs4e,uhgs6e	0.0421	0.6817	0.7151
160	0-23	uhgs4f,uhgs6f	0.0331	0.9011	0.7172
170	0-23	uhgs4g,uhgs6g	0.0261	0.9653	0.7184
180	0-23	uhgs4h,uhgs6h	0.0208	0.9345	0.7204
190	0-23	uhgs4i,uhgs6i	0.0166	0.7761	0.7220
200	0-23	uhgs4j,uhgs6j	0.0135	0.7347	0.7239
145	0-23	uhgs4o,uhgs6o	0.0477	0.5731	0.7135
155	0-23	uhgs4p,uhgs6p	0.0373	0.8007	0.7155
165	0-23	uhgs4q,uhgs6q	0.0294	0.9566	0.7183
175	0-23	uhgs4r,uhgs6r	0.0233	0.9505	0.7196

Table 9.3 Associated Higgs production with a Z boson (from CDF Note 9863).

not contribute a real third lepton. Monte Carlo signal simulation does indicate that gluon fusion and vector-boson fusion have negligible contribution to the three-lepton bin. Thus, we are left with two signals to study: a $WH \rightarrow WWW \rightarrow l\nu, l\nu, l\nu$ signal and a $ZH \rightarrow ZWW \rightarrow ll, l\nu,$ jet signal. With two signals we naturally define two new trilepton signal regions attempting to isolate each, ameliorating the effort to discriminate each from background based on their unique characteristics.

Consider the three leptons as ordered by their transverse momentum p_T (or transverse energy E_T for electrons) such that the highest p_T lepton is the 1^{st} and the lowest p_T lepton is the 3^{rd}. First, we filter trilepton events into an *InZPeak* category if any of the three possible dilepton pairings (that is, pairing the 1^{st} lepton with the 2^{nd} lepton; the 1^{st} lepton with the 3^{rd} lepton; or the 2^{nd} lepton with the 3^{rd} lepton) has an invariant mass value that falls within a 10 GeV window of the Z-boson mass at 91 GeV, have opposite signs, and have same flavor. This *InZPeak* region is chosen to isolate the ZH signal process. The rest of the trileptons events are directed toward the *NoZPeak* region, which focuses on the WH signal process. These regions are new to the $H \rightarrow WW$ analysis group.

Additionally, the WH analysis has a missing energy cut of $\not\!\!E_T > 20$ GeV. This cut drastically reduces the $Z\gamma$ background contribution and also provides a WH control region in $10.0GeV < \not\!\!E_T < 20.0$. Because the $WH \rightarrow WWW \rightarrow l\nu l\nu l\nu$ event topology has three $W \rightarrow l\nu$ decays, the missing energy is relatively large and a negligible amount of signal is lost from moving the $\not\!\!E_T$ cut up to 20.0 GeV from 10.0 GeV.

The $\not\!\!E_T$ distribution for the $ZH \rightarrow ZWW$ trilepton events is somewhat lower than that of the WH analysis because it produces fewer neutrinos ($WWW \rightarrow l\nu, l\nu, l\nu$ has three neutrinos while $ZWW \rightarrow ll, l\nu, jet$ has only one), so defining a control region by a higher $\not\!\!E_T$ cut is less appropriate. The ZH analysis also has somewhat larger backgrounds than the WH region and is topologically similar to the most significant background, WZ. However, for a $ZH \rightarrow ZWW$ event to produce a three-lepton signature we either have one of the W-leptons decaying hadronically or–less frequently–we have a $ZH \rightarrow ZWW \rightarrow llll$ physics event that loses one of it's leptons to an area of the detector that is incapable of reconstructing a track (detector holes or too far forward in pseudorapidity, for example) but is still recorded by the calorimeter system. Therefore, ZH trilepton events inherently have a higher number of jets than the backgrounds and very

little signal in the NJet$= 0$ bin. This characteristic of the ZH trilepton signal allows us to create a control region for the ZH analysis in the NJet$= 0$ bin with very little signal loss, and so NJet$= 0$ events are not included in the ZH analysis.

Observe in table 9.2.3 that $\sim 77\%$ of the signal in the *NoZPeak* region is WH, while $\sim 96\%$ of the signal in the *InZPeak* region is ZH. We will see in section 9.6 how this division allows us to focus on the unique characteristic of each signal for discrimination from the background in the NeuroBayes neural net treatment.

9.2.3 Backgrounds

Both regions of this trilepton analysis have five background categories considered: WZ, ZZ, $Z\gamma$ (replacing Drell-Yan), Fakes (data-based WW and Z+jets), and $t\bar{t}$. Each is summarized in table 9.2.3 along with the predicted signal for a $m_H = 160$ GeV standard model Higgs boson and the data.

CDF Run II Prebless $\int \mathcal{L} = 5.3\ \mathrm{fb}^{-1}$

($m_H = 165\ \mathrm{GeV}/c^2$)	**WH Signal Region**	**ZH Signal Region**
WZ	$7.01 \pm 0.96_{\mathrm{syst}}$	$9.01 \pm 1.74_{\mathrm{syst}}$
ZZ	$1.49 \pm 0.20_{\mathrm{syst}}$	$4.41 \pm 0.68_{\mathrm{syst}}$
$Z\gamma$	$2.47 \pm 0.42_{\mathrm{syst}}$	$3.00 \pm 0.63_{\mathrm{syst}}$
Fakes (WW,Z+Jets)	$3.22 \pm 0.97_{\mathrm{syst}}$	$7.74 \pm 2.32_{\mathrm{syst}}$
$t\bar{t}$	$0.18 \pm 0.07_{\mathrm{syst}}$	$0.03 \pm 0.01_{\mathrm{syst}}$
Total Background	$14.5 \pm 1.58_{\mathrm{syst}}$	$24.3 \pm 3.57_{\mathrm{syst}}$
WH	$0.58 \pm 0.08_{\mathrm{syst}}$	$0.02 \pm 0.004_{\mathrm{syst}}$
ZH	$0.18 \pm 0.02_{\mathrm{syst}}$	$0.58 \pm 0.08_{\mathrm{syst}}$
Total Signal	$0.76 \pm 0.10_{\mathrm{syst}}$	$0.60 \pm 0.08_{\mathrm{syst}}$
Data	14	33

- *Heavy Dibosons (WZ, ZZ):* The WZ and ZZ diboson contributions provide three physical leptons, with WZ being the dominant background in both trilepton signal regions. Both samples are Pythia-based, where the W is allowed to decay inclusively and the Z is forced to decay leptonically (electron, muon, or tau pairs)[16].

- $Z\gamma$*:* The $Z\gamma$ background in the trilepton analyses replaces the Drell Yan contribution of the dilepton analyses and is created by the Bauer generator. We acquire a third lepton from a Drell Yan process when either an initial or final state radiated photon undergoes a conversion and showers in the calorimeter for the third lepton. As such, the $Z\gamma$ is the restriction of Drell Yan to those events which do radiate a photon for the purpose of working with a larger statistical sample.

- *Fakes(WW, Z+Jets):* In the dilepton analysis, the Fakes category is measured from single high p_T lepton data (rather than MC) and assumed to have a W+jets event topology, where the one lepton is from the W-boson. From this data sample, events with one-lepton+denominator object are selected and then re-weighted based on the rates at which jets fake a lepton, measured from QCD samples–where "denominator-objects" are looser lepton objects that do not fully satisfy lepton ID, but considered candidates for a physical object that may fake a lepton.

  Similarly, for the trilepton analyses we are interested in processes that produce two physical leptons+ one denominator object from the jets. Two high p_T lepton data is dominated by WW and Z+jets. First note that we do not consider simulated WW background as the dilepton analyses do to avoid double counting the process. Second, because the rate at which a jet is expected to fake a lepton is on the order of $1-5\%$, the rate at which such an event is expected to fake two leptons is drastically lower: $0.01-0.25\%$. As such, we consider the contribution of W+jets with one real lepton and two faked lepton to be negligible for the trilepton analyses and so label this category WW,Z+Jets instead of W+Jets, but "W+Jets" is still accounted for.

The actual rates for which a light jet fakes a lepton used in this analysis are estimated from jet triggered data and expounded further in CDF note [16]. These rates were determined in the $H \rightarrow WW$ group's dilepton analysis and we adopt the same values here.

- $t\bar{t}$*:* The $t\bar{t}$ process is the smallest background, but arguably the most complex. This process decays to two pairs of a b-jet accompanied by a W boson. For the case of trileptons, we consider the case of the two W's decaying leptonically. The third lepton signature is then due to one of the b-jets, which is supposed to produce a lepton candidate with higher probability than a light jet, but this rate is not precisely known.

  Because of this, we cannot ignore the possible contribution of $t\bar{t}$ in our Fakes background category where the lepton decayed from the b-jet is the fake lepton (denominator object). However, any $t\bar{t}$ that might be included in the high p_T lepton data of the Fakes background is then scaled down by a fake rate determined for a sample of jets assumed to be mostly light– hence, the $t\bar{t}$ contribution to the Fakes background is scaled down further than it should be since it's jets are the heavy b-jets.

  The standard MC $t\bar{t}$ ntuple used by the $H \rightarrow WW$ group requires reconstructed leptons to pass a matching criteria to either a generator-level lepton or photon (for the case of photon conversion). For our purposes in the trilepton analysis, we are interested in a third lepton whose signature is the result of those b-jets, so we have our own MC $t\bar{t}$ sample that allows matching to b-jets as well as leptons and photons. The MC $t\bar{t}$ sample accounts for such events that result in three fully identified leptons, as opposed to the 2 leptons+1 fake lepton signature of the Fakes background.

  Lastly, there is inevitably some overlap between the $t\bar{t}$ that occurs implicitly in the Fakes data-based background and the MC sample. By measuring the difference between the 3-lepton bin of the default $t\bar{t}$ sample (lepton match only to generator-level leptons or photons) with another $t\bar{t}$ sample allowing matching to b-jets as well, we take half the percentage difference to be the systematic error (23%) accounting for overlap.

- *Correction to Simulation and Fake Rates:* To properly weight events from simulation and scale data-based backgrounds, we follow the same standard procedures that the rest of the $H \to WW$ group as described on page 41 in CDF Note 9863.

9.2.4 Signal Yields in the *NoZPeak* and *InZPeak* Regions

Although we have defined two trilepton signal regions to separately focus on the WH and ZH associated production channels, both regions do contain both signals and are summarized for all generated masses in table 9.4.

m_H GeV	*NoZPeak*			*InZPeak*		
	WH	ZH	Total	WH	ZH	Total
110	0.05	0.02	0.07	0.002	0.06	0.06
120	0.15	0.05	0.20	0.004	0.15	0.15
130	0.28	0.09	0.37	0.008	0.29	0.30
140	0.40	0.12	0.52	0.01	0.41	0.42
145	0.44	0.14	0.58	0.02	0.45	0.47
150	0.47	0.14	0.61	0.02	0.48	0.50
155	0.50	0.16	0.66	0.02	0.51	0.53
160	0.53	0.16	0.69	0.02	0.51	0.53
165	0.50	0.15	0.65	0.02	0.49	0.52
170	0.45	0.14	0.59	0.02	0.46	0.48
175	0.40	0.13	0.53	0.02	0.42	0.44
180	0.35	0.11	0.46	0.02	0.38	0.40
190	0.24	0.08	0.32	0.01	0.27	0.28
200	0.18	0.06	0.24	0.01	0.22	0.23

Table 9.4 Signal Summary

9.3 Neural Net

The trilepton $H \rightarrow WW$ analyses rely on the NeuroBayes neural network package to discriminate signal from background; we do not attempt the Matrix Element method in this study. We use 13 input variables for the WH analysis and 16 for the ZH analysis. The neural net results can be seen in figures 9.1, 9.2, 9.3, and 9.4.

Because the interaction topology under consideration involves three leptons and also because we do not separate the analyses by jet bin (aside from reserving the NJet=0 bin for the *InZPeak* control region of the ZH analysis), the signatures of the signal regions under consideration involve many potentially complex variables whose discriminatory power must be explored. As such, a larger than usual quantity of discriminating variables are used to train the NeuroBayes neural nets and we have found no reason yet to believe that fewer variables would be any benefit.

Recall that the standard model Higgs boson is postulated as a scalar particle and so decays to two W-bosons having $+1$ and -1 spin, respectively. Leptonic W-boson decays have a $V - A$ distribution, so one of the W bosons decays to a lepton projected forward along its momentum vector while the other decays its lepton backwards along its momentum vector. If the two Higgs-W-bosons decay close to back-to-back in the experimental rest frame–which is not a terrible assumption for a high mass Higgs–then the two decayed leptons will tend to have a relatively close proximity. Indeed, we find that this is the case (see figure A.1) for WH events since both Higgs-W-bosons must decay leptonically. Also, $\not\!\!E_T$ is an excellent discriminating variable for WH events since three leptonic decays of W's implies at least three neutrinos carrying away undetected energy.

Likewise, a trilepton signal in a ZH event implies a hadronic decay of one of the two Higgs-W-bosons while WZ and $Z\gamma$ events do not tend to have jets. As such, NJet is an excellent discriminating variable for the ZH signal (see figure A.7). Other variables that are excellent for discriminating ZH in the trilepton case are $\not\!\!E_T$ (ZH may have fewer neutrinos that WH, but the distribution still tends to be higher than the backgrounds), Lead Jet E_T (jets from vector bosons tend to have higher energy than other sources of jets), and ΔR between the W-lepton and the leading jet (that is, between the decay products of the two Higgs-W-bosons).

WH Variable Descriptions/Details:

- ΔR b/w Opp. Sign Close Leptons: With three leptons there are three possible pairings of leptons. Events with all three leptons having the same sign are rejected from this analysis, so every event has two possible pairings of opposite-signed leptons. Of those two pairings, this variable is the ΔR value of the pairing with lower ΔR value.
- $\not\!\!E_T$: Missing Transverse Energy
- H_T: Sum of the transverse energies of all three leptons, the $\not\!\!E_T$, and all jets.
- Dimass b/w Opp. Sign Close by ϕ: Dilepton invariant mass of the opposite-signed lepton pair that is closer in the ϕ coordinate.
- $\Delta\phi$(Lep2,$\not\!\!E_T$): The magnitude of the difference in ϕ between the 2^{nd} lepton by p_T and the $\not\!\!E_T$.
- Inv. Mass(Lep3,$\not\!\!E_T$,Jets): Invariant mass of the vector sum of the 3^{rd} lepton, $\not\!\!E_T$, and Jets.
- m_T(Leptons,$\not\!\!E_T$,Jets): Transverse mass of the vector sum of all three leptons, $\not\!\!E_T$, and all jets.
- p_T of the 2^{nd} lepton by p_T.
- ΔR Opp. Sign Far Leptons: With three leptons there are three possible pairings of leptons. Events with all three leptons having the same sign are rejected from this analysis, so every event has two possible pairings of opposite-signed leptons. Of those two pairings, this variable is the ΔR value of the pairing with higher ΔR value.
- m_T Trilepton Mass: Transverse mass of the vector sum of the three leptons.
- NJet: The number of jets in the event. For this use of NJet, all events with NJet ≥ 2 jets are thrown into the NJet = 2 bin.
- m_T (Lep3, $\not\!\!E_T$): Transverse mass of the vector sum of the 3^{rd} lepton and the $\not\!\!E_T$.

- Inv. Mass(Lep1,Lep2,$\not\!\!E_T$): Invariant mass of the vector sum of the 1^{st} lepton, 2^{nd} lepton, and $\not\!\!E_T$.

ZH Variable Descriptions/Details:

- NJet: The number of jets in the event.
- $\not\!\!E_T$: Missing Transverse Energy
- Lead Jet E_T: Transverse energy of the leading jet. Note that the control region for *InZPeak* is NJet = 0, so all events in the signal region must have at least one jet by definition. Also, for this use of NJet, all events with NJet $\geq$ 2 jets are thrown into the NJet = 2 bin.
- ΔR(W-Lep, Lead Jet): The *InZPeak* region is defined by having one lepton paring (opposite signed, same flavor) near the Z boson mass. Denote the one other lepton not in this pairing as the W-lepton. This variable is then the ΔR between the W-lepton and the leading jet.
- $\Delta\phi$(Leptons,$\not\!\!E_T$): $\Delta\phi$ between the vector sum of the three leptons and the $\not\!\!E_T$.
- H_T(Leptons,$\not\!\!E_T$,Jets): Sum of E_T of all three leptons, $\not\!\!E_T$, and all jets.
- m_T(Leptons,$\not\!\!E_T$,Jets): Transverse mass of the vector sum of all three leptons, $\not\!\!E_T$, and all jets.
- $\Delta\phi$(Lep2,$\not\!\!E_T$): The magnitude of the difference in ϕ between the 2^{nd} lepton by p_T and the $\not\!\!E_T$.
- ΔR b/w Opp. Sign Close Leptons: With three leptons there are three possible pairings of leptons. Events with all three leptons having the same sign are rejected from this analysis, so every event has two possible pairings of opposite-signed leptons. Of those two pairings, this variable is the ΔR value of the pairing with lower ΔR value.
- Trimass:The invariant mass of the vector sum of the three leptons.
- Inv. Mass(Lep3,$\not\!\!E_T$,Jets): Invariant mass of the vector sum of the 3^{rd} lepton, $\not\!\!E_T$, and Jets.

- Dimass(W-Lep,$\not\!\!E_T$): The *InZPeak* region is defined by having one lepton paring (opposite signed, same flavor) near the Z boson mass. Denote the one other lepton not in this pairing as the W-lepton. This variable is then the invariant mass of the vector sum of the W-lepton and the $\not\!\!E_T$.

- m_T Jets: Transverse mass of the vector sum of all jets. Note that the control region for *InZPeak* is NJet = 0, so all events in the signal region must have at least one jet by definition.

- m_T(W-Lep,$\not\!\!E_T$): Transverse mass of the vector sum of the W-lepton and the $\not\!\!E_T$.

- $\Delta\phi$(Z-Leptons,W-Lepton): ΔR between the vector sum of the two leptons whose dimass is near the Z-boson mass, and the other lepton.

- ΔR Opp. Sign Far Leptons: With three leptons there are three possible pairings of leptons. Events with all three leptons having the same sign are rejected from this analysis, so every event has two possible pairings of opposite-signed leptons. Of those two pairings, this variable is the ΔR value of the pairing with higher ΔR value.

Variable(WH)	110	120	130	140	145	150	155
ΔR b/w Opp. Sign Close Lept.	12.4	40.8	9.69	40.2	41.4	40.8	43.1
$\not\!\!E_T$	26.0	21.2	33.8	25.7	26.2	28.1	28.9
Dimass b/w Opp. Sign Close by ϕ	41.0	14.9	29.7	9.52	8.14	12.7	11.6
H_T	3.38	3.82	16.1	11.9	13.1	9.14	9.38
$\Delta\phi$(Lep2,$\not\!\!E_T$)	5.77	6.48	7.60	6.67	6.47	7.74	8.94
m_T(Leptons,$\not\!\!E_T$,Jets)	(0.38)	2.08	4.84	5.46	5.99	6.33	7.42
p_T2$^{\text{nd}}$ Lepton	2.77	5.06	3.26	5.12	3.08	4.57	6.88
Inv. Mass(Lep3,$\not\!\!E_T$,Jets)	2.05	2.46	4.34	4.51	4.57	7.84	6.64
ΔR Opp. Sign Far Lept.	9.24	11.0	12.6	9.93	10.9	6.31	6.67
NJet	7.24	7.30	3.64	3.16	3.27	3.04	3.11
m_T Trilepton Mass	(0.52)	2.62	3.78	3.85	6.62	6.67	4.44
m_T (Lep3, $\not\!\!E_T$)	3.38	2.13	(0.80)	(0.04)	(0.90)	2.32	3.17
Inv. Mass(Lep1,Lep2,$\not\!\!E_T$)	8.38	8.34	4.51	2.69	4.16	1.75	1.56
Variable(WH)	160	165	170	175	180	190	200
ΔR b/w Opp. Sign Close Lept.	45.7	47.1	31.5	29.0	27.3	19.5	17.3
$\not\!\!E_T$	29.8	11.3	45.9	46.4	47.0	48.0	21.6
Dimass b/w Opp. Sign Close by ϕ	12.4	10.9	8.61	8.11	7.31	6.78	5.14
H_T	10.5	11.3	6.05	13.4	16.4	22.7	49.7
$\Delta\phi$(Lep2,$\not\!\!E_T$)	9.49	8.81	9.19	9.41	7.70	7.37	6.58
m_T(Leptons,$\not\!\!E_T$,Jets)	8.08	8.57	9.93	8.35	8.67	9.54	10.7
p_T2$^{\text{nd}}$ Lepton	7.85	4.59	8.48	8.57	4.66	8.28	8.45
Inv. Mass(Lep3,$\not\!\!E_T$,Jets)	6.99	7.63	12.7	10.0	8.67	8.72	7.34
ΔR Opp. Sign Far Lept.	6.30	5.65	5.79	5.18	5.25	5.54	5.01
NJet	4.58	3.09	3.67	3.36	3.50	2.72	2.25
m_T Trilepton Mass	4.59	7.55	4.65	4.57	7.70	3.98	3.23
m_T (Lep3, $\not\!\!E_T$)	3.77	4.14	4.46	3.64	3.68	3.05	1.85
Inv. Mass(Lep1,Lep2,$\not\!\!E_T$)	3.15	1.98	1.52	(0.90)	(0.77)	(0.26)	1.67

Table 9.5 WH Significance: The variables are ordered by their significance as discriminating variables for the NeuroBayes neural net trained at the 160 GeV signal. Values in parentheses (*) indicate the input variable was not used for the given m_H.

Variable(ZH)	110	120	130	140	145	150	155
NJet	23.6	29.7	33.2	37.6	39.6	41.1	43.2
$\not\!\!E_T$	8.07	9.35	13.4	22.7	23.3	23.6	24.8
Lead Jet E_T	3.76	7.23	14.5	12.0	16.3	17.3	17.9
ΔR(W-Lep, Lead Jet)	19.2	17.4	16.7	13.6	13.8	13.0	12.7
$\Delta\phi$(Leptons,$\not\!\!E_T$)	21.3	20.5	19.1	10.9	10.2	12.4	11.6
m_T(Leptons,$\not\!\!E_T$,Jets)	3.50	1.05	5.96	5.86	4.93	3.93	9.26
$\Delta\phi$(Lep2,$\not\!\!E_T$)	4.42	3.64	4.54	5.31	4.81	4.85	5.60
ΔR b/w Opp. Sign Close Lept.	13.8	13.9	10.7	14.6	11.7	10.9	7.10
Trimass	11.6	9.50	9.14	6.83	6.96	6.96	6.35
Inv. Mass(Lep3,$\not\!\!E_T$,Jets)	7.29	2.78	(0.23)	1.91	1.47	1.94	4.67
H_T(Leptons,$\not\!\!E_T$,Jets)	(0.48)	(0.95)	2.68	6.38	7.14	6.93	5.81
m_T Jets	(1.01)	2.38	(1.01)	(0.98)	(0.18)	2.36	2.49
Dimass(W-Lep,$\not\!\!E_T$)	2.02	(0.07)	2.05	2.80	2.76	2.34	3.09
m_T(W-Lep,$\not\!\!E_T$)	6.55	4.46	(0.72)	1.78	3.44	3.99	3.56
ΔR Opp. Sign Far Lept.	2.82	3.25	2.60	2.40	2.36	2.61	1.83
$\Delta\phi$(Z-Leptons,W-Lepton)	1.55	(1.82)	1.43	(1.19)	2.54	2.64	2.09

Variable(ZH)	160	165	170	175	180	190	200
NJet	45.8	46.6	46.8	47.4	25.8	24.7	22.2
$\not\!\!E_T$	26.7	27.8	27.8	28.4	15.0	13.9	12.7
Lead Jet E_T	19.2	19.0	19.5	20.1	12.2	11.6	10.6
ΔR(W-Lep, Lead Jet)	13.2	12.7	12.1	11.0	7.84	5.53	4.48
$\Delta\phi$(Leptons,$\not\!\!E_T$)	12.0	13.2	12.1	11.0	9.72	7.55	6.82
m_T(Leptons,$\not\!\!E_T$,Jets)	8.62	9.39	9.09	8.52	10.9	9.81	9.26
$\Delta\phi$(Lep2,$\not\!\!E_T$)	8.19	8.11	8.02	6.67	5.48	5.17	4.52
ΔR b/w Opp. Sign Close Lept.	6.54	6.06	5.23	4.95	4.52	3.63	2.81
Trimass	5.84	5.04	4.87	4.87	4.52	3.07	2.66
Inv. Mass(Lep3,$\not\!\!E_T$,Jets)	5.84	6.64	6.60	6.23	6.81	6.93	7.32
H_T(Leptons,$\not\!\!E_T$,Jets)	5.02	5.86	7.97	9.66	51.1	54.4	58.7
m_T Jets	4.28	4.58	4.88	4.79	4.31	3.38	2.53
Dimass(W-Lep,$\not\!\!E_T$)	4.08	4.22	4.68	4.54	3.88	3.98	3.25
m_T(W-Lep,$\not\!\!E_T$)	3.11	2.62	3.28	2.68	3.24	2.93	3.00
ΔR Opp. Sign Far Lept.	2.94	2.61	2.34	2.02	2.45	1.40	1.32
$\Delta\phi$(Z-Leptons,W-Lepton)	2.60	2.59	2.94	1.98	2.07	1.33	1.35

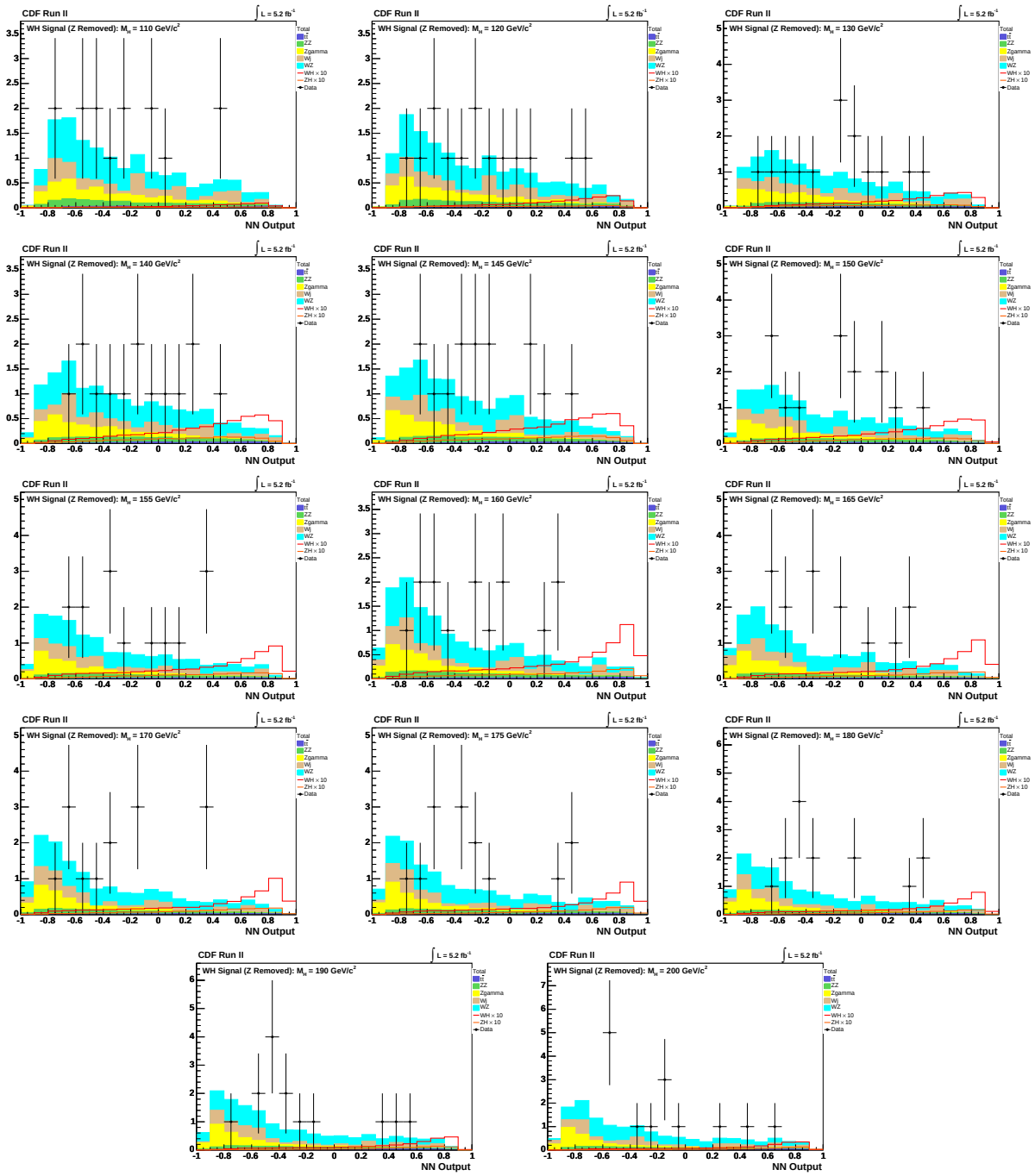

Figure 9.1 Trilepton WH NeuroBayes Neural Network output (linear scale)

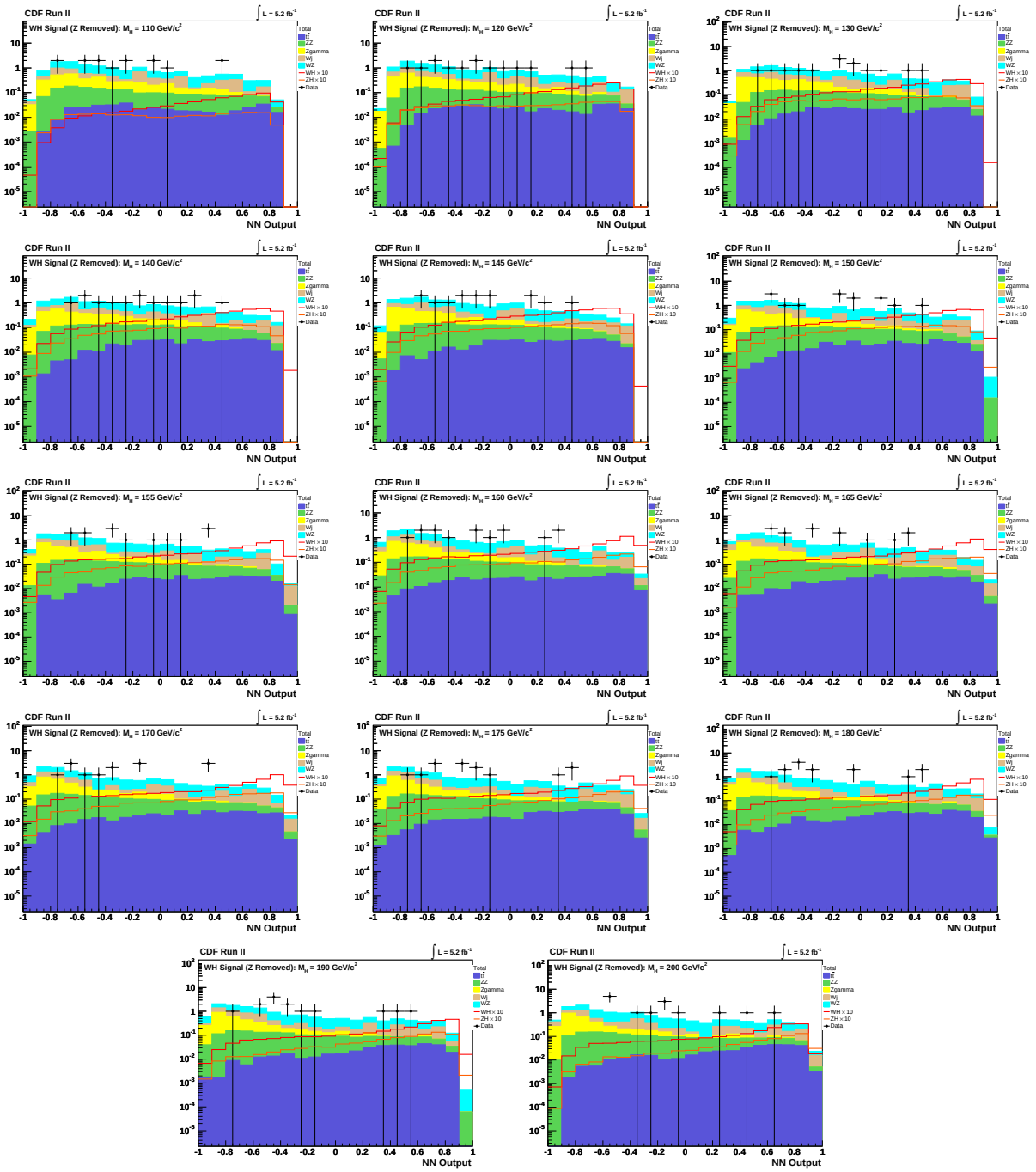

Figure 9.2 Trilepton WH NeuroBayes Neural Network output (logarithmic scale)

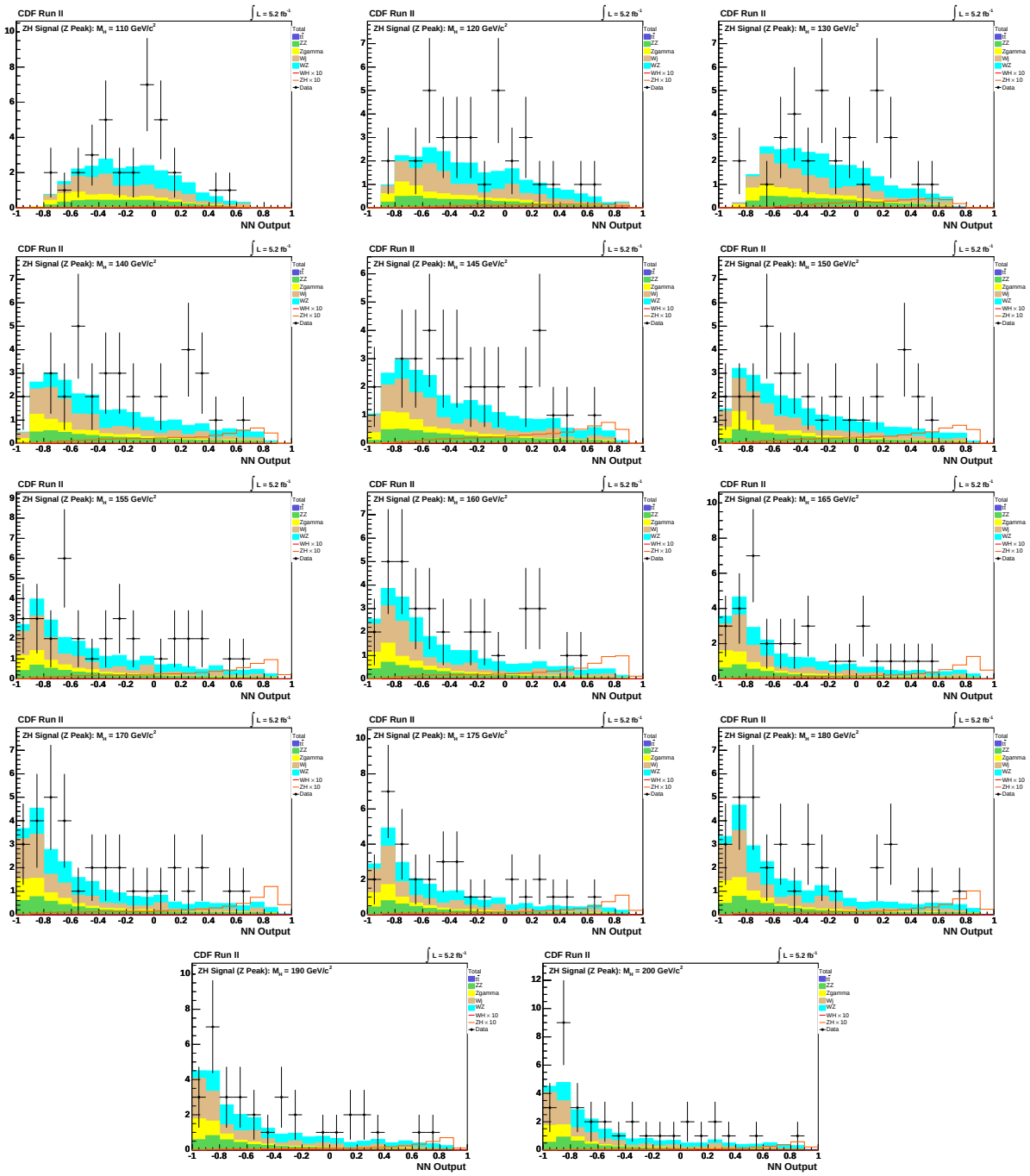

Figure 9.3 Trilepton ZH NeuroBayes Neural Network output (linear scale)

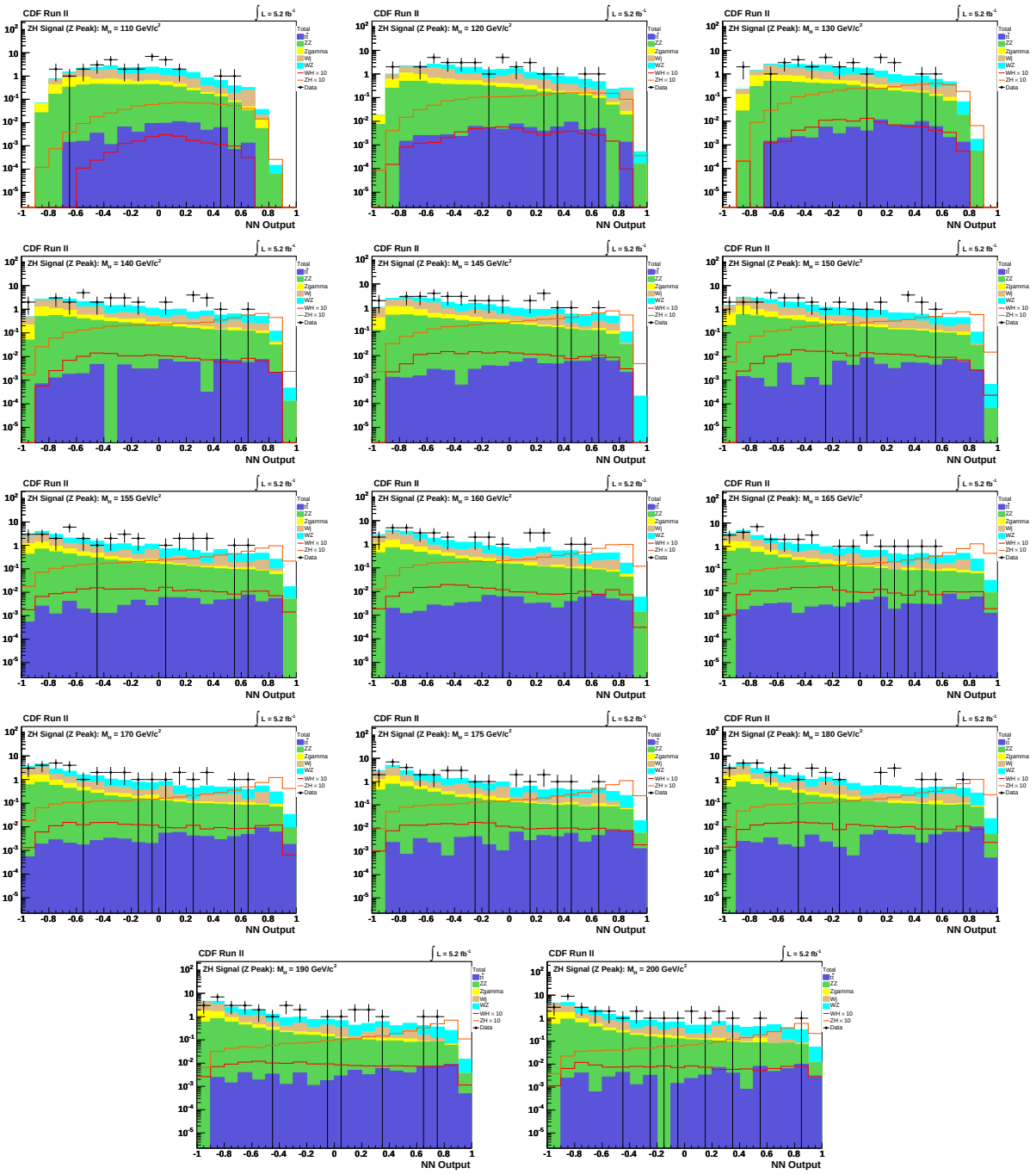

Figure 9.4 Trilepton ZH NeuroBayes Neural Network output (logarithmic scale)

9.4 Control Regions

The modeling of basic kinematic properties and the discriminating variables in the Monte Carlo simulation is tested by comparing the distributions of these variables in the final selected data. Ideally, the modeling of these variables is further tested by creating orthogonal "control regions" which are enhanced in specific major backgrounds and contain minimum possible signal contribution.

The control regions we choose for both the WH and ZH trilepton analyses contain minimal signal (see table 9.4) so cutting them out of the analyses drastically cuts down the background to discriminate against in addition to providing a verification of modelling.

They are:

- WH Analysis Control Region: $10.0 < \not\!\!E_T < 20.0$
- ZH Analysis Control Region: Number of Jets$= 0$

The topology of WH associated production in the trilepton channel also contains at least three neutrinos (more if $W \rightarrow \tau\nu_\tau \rightarrow l_{e,\mu}\nu_{e,\mu}\nu_\tau$ decays are involved), resulting in high missing energy values (see figure A.1). The low $\not\!\!E_T$ region is a natural choice for a control region in the WH analysis since it contains negligible signal contribution and is enriched in $Z\gamma$ and Fakes backgrounds. Also including a $\not\!\!E_T > 20$ cut for the WH signal region substantially enhances the signal to background ratio in the final signal region.

Similarly, the topology of ZH associated production lends to a preference for at least one or two jets (see figures B.5 and A.7) since one of the two Higgs-W-bosons decays hadronically. Only $\sim 10\%$ of the trilepton ZH signal is present in the NJet$= 0$ bin, but much of it's most dominant background, WZ, is. Thus, the NJet$= 0$ bin is a natural choice for the control region of the ZH trilepton analysis. Unfortunately, there are several nefarious difficulties that arise from this choice that must be discussed. First, three of the discriminating variables chosen in the neural network treatment discussed in section 9.6 are undefined when NJet$= 0$ (though can be powerful discriminators among those events that do have at least one jet, serving as yet another argument

for this choice of control region) and NJet must be excluded as a discriminating variable as well since the control region allows it only one possible value by definition (a variable cannot be used to discriminate background from signal when both background and signal must have identical values for that variable). The neural network result for the control region of ZH has the following removed from the list of discriminating variables:

- NJet
- E_T of the leading jet
- ΔR between the W-lepton and the leading jet. Denote the two leptons with dilepton invariant mass $\in [81.0, 101.0]$ GeV (the definition of the *InZPeak* region for the ZH analysis) as the Z-leptons, then the other lepton is denoted the W-lepton.
- Transverse mass of the vector sum of all jets

Further, with the $t\bar{t}$ background being borderline negligible already, our monte carlo sample of $t\bar{t}$ does not contain a single trilepton event in the ZH control region. Summarily, to obtain a neural network result for this *InZPeak* control region we had to retrain a neural network on the signal region (NJet ≥ 1) excluding both the four aforementioned discriminating variables and the $t\bar{t}$ background.

To support the claim that this neural network result for the *InZPeak* control region of the ZH analysis is valid, we first emphasize that the $t\bar{t}$ contribution to the signal region is only 0.02 events expected in 4.8fb^{-1} of data compared to a total background of 20.9 ± 2.64. As such, it's arguable that we could have removed this background from the analysis entirely without any noticeable difference. Second, we chose 16 discriminating variables for the signal region, so losing these four is a serious but not critical loss; the total correlation to target drops from 61.9$\%$ to 52.2$\%$.

While this choice of control region poses challenges, we are rewarded with both a cut that excludes a large portion of the backgrounds with minimal signal loss and with three powerful discriminating variables that would be ill-defined otherwise.

CDF Run II Prebless				$\int \mathcal{L} = 5.3\ \mathrm{fb}^{-1}$		
($m_H = 165\ \mathrm{GeV}/c^2$)	**WH Signal Region**			**ZH Signal Region**		
WZ	0.77	$\pm$	0.11_{syst}	32.0	$\pm$	6.19_{syst}
ZZ	0.72	$\pm$	0.10_{syst}	3.55	$\pm$	0.55_{syst}
$Z\gamma$	19.4	$\pm$	3.31_{syst}	5.56	$\pm$	1.17_{syst}
Fakes (WW,Z+Jets)	7.58	$\pm$	2.27_{syst}	9.43	$\pm$	2.83_{syst}
$t\bar{t}$	0.01	$\pm$	0.002_{syst}	-	$\pm$	-
Total Background	28.4	$\pm$	4.02_{syst}	50.5	$\pm$	7.81_{syst}
WH	0.025	$\pm$	0.003_{syst}	0.06	$\pm$	0.01_{syst}
ZH	0.014	$\pm$	0.002_{syst}	0.06	$\pm$	0.01_{syst}
Total Signal	0.038	$\pm$	0.005_{syst}	0.12	$\pm$	0.02_{syst}
Data	31			49		

High Mass

We provide here the neural net score for the discriminating variables in the WH and ZH trilepton analyses control regions. The MC models the data well.

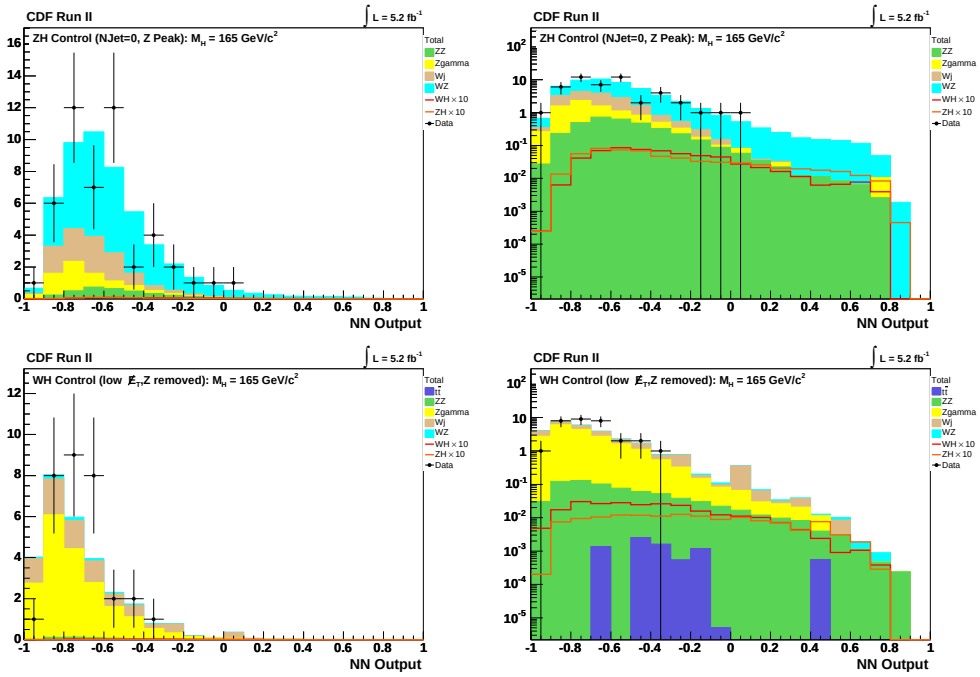

Figure 9.5 WH Control Region (10.0 GeV $< \not\!\!E_T <$ 20.0 GeV) and ZH Control Region (NJet$= 0$) neural net results against samples trained on signal regions.

9.5 Systematic Errors

The systematic uncertainties used are summarized in table 9.7. Most values used are standard to all $H \to WW$ analyses, but since $Z\gamma$ is a new background in this analysis–and a couple other reasons–there are several new systematics particular to this analysis.

- *$Z\gamma$ (and $W\gamma$) Scaling*: Note that the $W\gamma$ background is already scaled down by 17% in other $H \to WW$ analyses due to known mismodelling of photon conversions. We are using the same scale factor for the $Z\gamma$ contribution since the same photon conversion affect is assumed, as such we use the same systematic error associated with this scale factor. Also, we keep this systematic error correlated between the $Z\gamma$ of the trilepton analyses and $W\gamma$ of the dilepton analyses because of the common origin.

- *$Z\gamma$ Higher Order Diagrams*: We have for $W\gamma$ in the dilepton analysis the *$W\gamma$ higher order diagrams* systematic, which accounts for poor MC modeling beyond leading order. Likewise, we assume the same error of 11% for a new *$Z\gamma$ higher order diagrams* systematic since both are modelled by the Bauer MC generator.

- *b-Jet Fake Rate*: Although $t\bar{t}$ is a small contribution to the background for these high m_H standard model Higgs boson in the trilepton case, we do have to account for the peculiar situation that our 3^{rd} lepton is faked from a b-jet and the rate at which a b-jet fakes a lepton–as opposed to a light jet–is not well-known. Further, as a background with two real leptons and one faked, we cannot ignore the possible coverage of $t\bar{t}$ in the data-based Fakes category. We know that the fake rates used in the Fakes category is based on jet samples populated mostly with light jets and presume that b-jets in particular are more likely than light jets to produce a signature that could fake a lepton. Hence, whatever $t\bar{t}$ contribution that exists in the Fakes category is scaled down by the light jet dominated fake rate, meaning it is scaled down too far. To make up for the difference we use an MC $t\bar{t}$ sample that allows reconstructed leptons to match to generator-level leptons, photons, or b-jets (typically, for these reconstructed MC leptons to be considered fully "found" they must pass a matching

criterion to a generator-level lepton or photon only). Now, of course, we have the problem of possible double-counting of $t\bar{t}$ between the MC and what implicit $t\bar{t}$ contribution populates the Fakes category. To account for the double-counting possibility, we assign a systematic error defined to be one half the percentage difference between the MC $t\bar{t}$ sample that allows leptons to match to generator-level leptons, photons, and b-jets; and the MC $t\bar{t}$ sample that allows such matching to generator-level leptons and photons only. The systematic errors adopted are:

  - WH Analysis (*trilep-NoZPeak region*): 0.223
  - ZH Analysis (*trilep-InZPeak region*): 0.231

- *Jet Energy Scaling*: Jet energy scaling is modelled inclusively to all jet bins, so removing the zero-jet bin as a control region for the ZH analysis introduces a slight mismodelling for the signal region. To account for this, we re-run the analysis with different MC samples that have the jet energy scaling increased and decreased by one standard deviation.

  If the jet energy scale is shifted down, then the jets of an event have lower energy, so event count fewer jets on average because fewer jets have enough energy to be considered above the energy threshold to be counted as such. Similarly, if the jet energy scale is shifted up, then the jets of an event have higher energy, so events count more jets on average because more jets have enough energy to be considered above the threshold energy to be counted.

  Singe the ZH analysis signal region only has NJet≥ 1 (the NJet$= 0$ bin is the control region), the events from samples with jet energy scaled down have fewer jets on average so more events are shifted out of the signal region and into the control region. Likewise, events with the jet energy scaled up will count more jets on average and shift events out of the control region and into the signal region. These shifts change the weighted count for the backgrounds for some given integrated luminosity. As such, we must assign a systematic error for each background corresponding to the error of the jet energy scaling.

We then take the average of the percent difference between each and the original samples. Differences necessitating systematic errors arose only for WZ, ZZ, and $Z\gamma$ samples, and only for the ZH analysis.

- WZ (ZH Signal Region): 0.097
- ZZ (ZH Signal Region): 0.052
- $Z\gamma$ (ZH Signal Region): 0.088

We explored the possibility of having a jet energy scaling **shape** systematic as well. That is, even if the total count of a particular process does not change appreciably, we must account for the possibility that the distribution of the process in the neural net output (the templates that serve as the inputs for calculating statistical limits) changes. The subsequent limits could be altered if a process is shifted towards or away from the signal region of the templates. To check, we used the shape systematic error for the limit calculation at the $m_H = 165$ GeV mass point and compared the results to default values. The result is in table 9.8. We see that the shape systematic does not affect the limit results and is therefore not included in the analysis at this time.

- *MC Run Dependence*: The $Z\gamma$ stntuples used cover only periods $0 - 11$, so we assign the customary MC run dependence systematics for such samples. This is determined by comparing a WW sample with partial run dependence (periods $0-7$) with a fully run-dependent WW sample.

- *Lepton, Trigger ID, Luminosity, Parton Distribution Function Model*: Finally, note that we do not use systematic errors for the lepton, trigger ID, luminosity, and PDF model efficiencies because of the scale factor derived from the $W\gamma$ control region in the dilepton analysis. Since we're measuring the $W\gamma$ normalization directly from data, that systematic should cover these effects. However, to be conservative–especially since we measure the scale factor in a control region with selection cuts that differ from our various signal regions–we keep

the systematic uncertainties on the MC that are not related to normalization (higher-order kinematic effects, MC jet modelling).

Systematic Uncertainty	WZ	ZZ	$Z\gamma$	$t\bar{t}$	Fakes	WH	ZH
Diboson Higher Order Diagrams	0.100	0.100					
$t\bar{t}$ Higher Order Diagrams				0.100			
Higgs Higher Order Diagrams						0.100	0.100
PDF Model	0.027	0.027		0.021		0.012	0.009
Lepton ID Efficiencies	0.020	0.020		0.020		0.020	0.020
Trigger Efficiences	0.021	0.021		0.020		0.021	0.021
Light Jet Fake Rates					0.300		
b-Jet Fake Rate*				0.23			
Luminosity	0.059	0.059		0.059		0.059	0.059
MC Run Dependence			0.050*				
Jet Energy Scale	0.098*[a]	0.053*[a]	0.086*[a]			0.084*[a]	0.011*[a]
$Z\gamma$ Higher Order Diagrams*			0.110*				
$W\gamma$ Scaling			0.110*				
σ_{Diboson}	0.060	0.060					
$\sigma_{t\bar{t}}$				0.100			
σ_{VH}						0.050	0.050
$\sigma_{\text{Z}\gamma}$*			0.050*				

Table 9.7 Systematic Uncertainties: Standard values for systematics used in other $H \rightarrow WW$ analyses are used wherever applicable.

[a] Only for the ZH analysis (*trilep-InZPeak* region) because the NJet$= 0$ bin is removed from the signal region and made a control region.

* New to trilepton analysis, not in dilepton analysis.

$m_H = 165$ GeV bin	Exp. Limit-1σ	Median Exp. Limit	Exp. Limit$+1\sigma$
WH Analysis, JES Shape Syst.	6.7	8.9	12.3
WH Analysis, Standard	6.7	8.8	12.4
ZH Analysis, JES Shape Syst.	9.4	12.5	17.7
ZH Analysis, Standard	9.4	12.5	17.2
Trilepton Analyses, JES Shape Syst.	4.7	6.3	8.9
Trilepton Analyses, Standard	4.7	6.3	8.9

Table 9.8 Compare default limit values for the ZH, WH, and combined trilepton analyses. we see that a jet energy scaling shape systematic is not necessary.

9.6 Results

The results of this trilepton analysis present a significant contribution to the $H \rightarrow WW$ combined result. We are poised to solidify and expand the window of standard model Higgs boson exclusion within $163 < m_H < 166$ GeV [18]. In the 165 GeV bin, the WH analysis limits are set at 8.86 times the expected standard model limit; the ZH analysis is set at 12.6 times the expected standard model limit; and the combined trilepton analysis is set at 6.3 times the expected standard model limit. Finally, for the combined $H \rightarrow WW$ analysis result, in the 165 GeV bin the expected limit drops from 1.21[15] to 1.15 while the observed limit drops from 1.23 to 1.08. As such, we are poised to begin excluding the standard model Higgs boson at 95% confidence level with CDF-only analyses in short order.

The limit calculations presented were computed with `HWWLimit` version of `MCLimit`. Expected limits for the ZH, WH, and combined trileptons were calculated in each case with 1,000 iterations of 10,000 pseudoexperiments (1000 iterations of 1000 pseudoexperiments performed 10 times), while 500,000 iterations of 1 pseudoexperiment were performed for the observed results–as is standard. For greater precision, the combined HWW dilepton and trilepton result used 30,000 pseudoexperiments instead of 10,000 for the expected limits, and 5 pseudoexperiment (500,000 iterations each) instead of 1 for the observed limits.

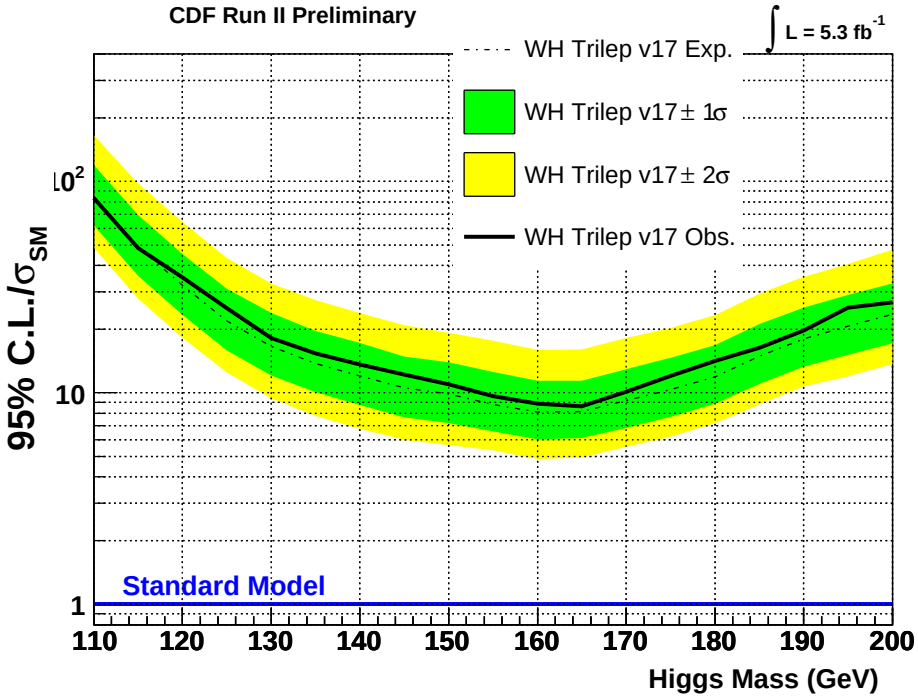

Figure 9.6 Trilepton *NoZPeak* Region Limits

Limits	110	120	130	140	145	150	155
$+2\sigma/\sigma_{\mathrm{SM}}$	180	67.2	35.5	24.4	22.5	20.3	18.4
$+1\sigma/\sigma_{\mathrm{SM}}$	130	48.3	25.3	17.7	16.0	14.5	13.1
Median$/\sigma_{\mathbf{SM}}$	**91.6**	**34.1**	**17.9**	**12.5**	**11.4**	**10.4**	**9.35**
$-1\sigma/\sigma_{\mathrm{SM}}$	67.9	25.1	13.2	9.23	8.40	7.76	7.05
$-2\sigma/\sigma_{\mathrm{SM}}$	54.0	19.9	10.5	7.36	6.67	6.25	5.72
Observed$/\sigma_{\mathbf{SM}}$	**94.4**	**36.9**	**19.9**	**16.5**	**13.9**	**13.8**	**12.2**
Limits	160	165	170	175	180	190	200
$+2\sigma/\sigma_{\mathrm{SM}}$	16.9	17.2	19.8	22.1	25.3	27.1	49.3
$+1\sigma/\sigma_{\mathrm{SM}}$	12.2	12.4	14.0	15.6	18.0	26.8	35.1
Median$/\sigma_{\mathbf{SM}}$	**8.62**	**8.86**	**9.91**	**11.0**	**12.8**	**19.1**	**24.9**
$-1\sigma/\sigma_{\mathrm{SM}}$	6.48	6.71	7.49	8.29	9.62	14.3	18.5
$-2\sigma/\sigma_{\mathrm{SM}}$	5.29	5.60	6.17	6.85	7.90	11.7	15.0
Observed$/\sigma_{\mathbf{SM}}$	**11.1**	**11.0**	**12.6**	**13.6**	**17.3**	**23.9**	**33.3**

Table 9.9 WH trilepton analysis limits for $4.8\mathrm{fb}^{-1}$.

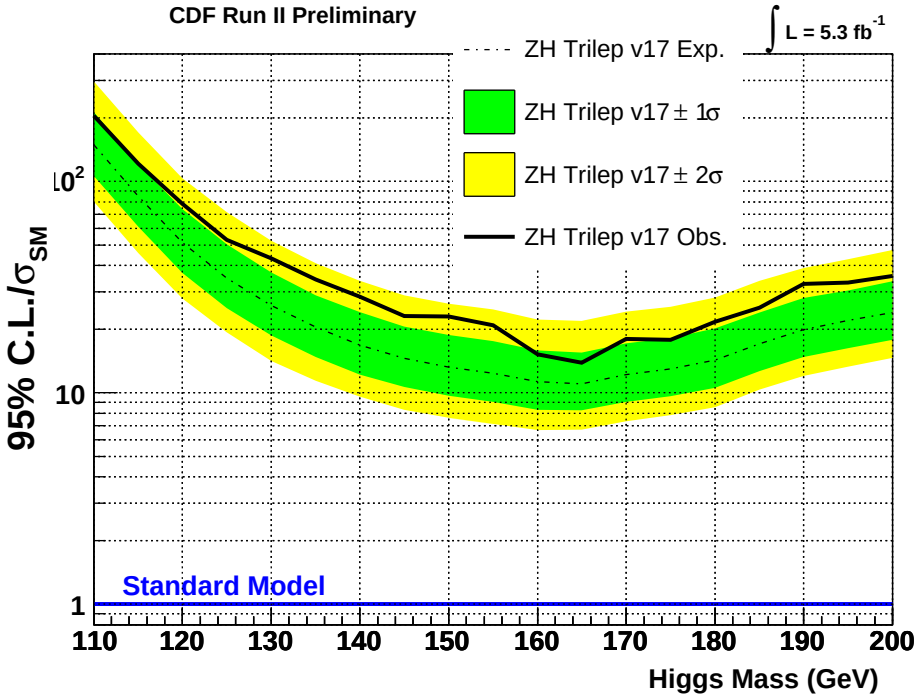

Figure 9.7 Trilepton *InZPeak* Region Limits

Limits	110	120	130	140	145	150	155
$+2\sigma/\sigma_{\mathrm{SM}}$	327	112	57.0	37.3	32.6	29.7	26.7
$+1\sigma/\sigma_{\mathrm{SM}}$	233	80.6	40.6	26.5	23.2	21.1	19.1
Median$/\sigma_{\mathbf{SM}}$	**162**	**56.3**	**28.5**	**18.8**	**16.4**	**14.9**	**13.4**
$-1\sigma/\sigma_{\mathrm{SM}}$	116	40.6	20.5	13.7	11.9	10.8	9.90
$-2\sigma/\sigma_{\mathrm{SM}}$	88.0	31.1	15.7	10.6	9.37	8.54	7.86
Observed$/\sigma_{\mathbf{SM}}$	**192**	**71.9**	**40.8**	**27.0**	**25.2**	**20.3**	**19.1**
Limits	160	165	170	175	180	190	200
$+2\sigma/\sigma_{\mathrm{SM}}$	25.2	24.6	26.8	29.0	31.7	43.3	52.0
$+1\sigma/\sigma_{\mathrm{SM}}$	17.8	17.6	19.1	20.6	22.4	30.8	37.0
Median$/\sigma_{\mathbf{SM}}$	**12.6**	**12.6**	**13.5**	**14.6**	**16.0**	**21.9**	**26.4**
$-1\sigma/\sigma_{\mathrm{SM}}$	9.27	9.44	10.1	10.9	11.9	16.3	19.8
$-2\sigma/\sigma_{\mathrm{SM}}$	7.50	7.65	8.37	8.91	9.68	13.4	16.2
Observed$/\sigma_{\mathbf{SM}}$	**17.0**	**15.8**	**17.8**	**18.7**	**22.1**	**32.8**	**34.5**

Table 9.10 ZH trilepton analysis limits for $4.8\mathrm{fb}^{-1}$.

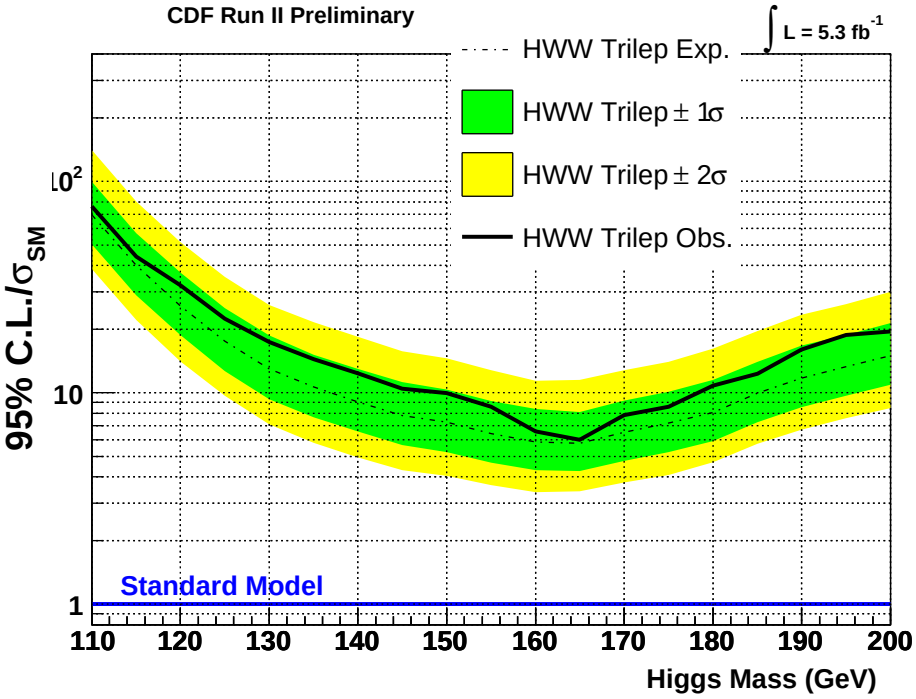

Figure 9.8 Trilepton Combined Limits

Limits	110	120	130	140	145	150	155
$+2\sigma/\sigma_{\mathrm{SM}}$	151	55.0	28.3	19.2	16.9	15.8	13.6
$+1\sigma/\sigma_{\mathrm{SM}}$	108	38.9	20.0	13.7	12.1	11.1	9.74
Median$/\sigma_{\mathbf{SM}}$	**75.8**	**27.4**	**14.0**	**9.63**	**8.55**	**7.79**	**6.84**
$-1\sigma/\sigma_{\mathrm{SM}}$	54.9	20.0	10.2	6.96	6.16	5.69	5.03
$-2\sigma/\sigma_{\mathrm{SM}}$	42.0	15.2	7.81	5.31	4.79	4.45	3.97
Observed$/\sigma_{\mathbf{SM}}$	**77.4**	**30.5**	**17.2**	**13.5**	**12.0**	**10.6**	**9.64**
Limits	160	165	170	175	180	190	200
$+2\sigma/\sigma_{\mathrm{SM}}$	12.5	12.5	13.6	15.3	17.4	24.8	31.5
$+1\sigma/\sigma_{\mathrm{SM}}$	8.93	8.91	9.87	10.9	12.4	17.7	22.4
Median$/\sigma_{\mathbf{SM}}$	**6.33**	**6.31**	**6.95**	**7.72**	**8.73**	**12.6**	**15.8**
$-1\sigma/\sigma_{\mathrm{SM}}$	4.65	4.68	5.16	5.70	6.47	9.27	11.6
$-2\sigma/\sigma_{\mathrm{SM}}$	3.69	3.78	4.17	4.57	5.13	7.36	9.17
Observed$/\sigma_{\mathbf{SM}}$	**8.33**	**7.61**	**8.90**	**9.52**	**12.4**	**18.1**	**22.0**

Table 9.11 Trilepton combined (WH and ZH) analysis limits for $4.8\mathrm{fb}^{-1}$.

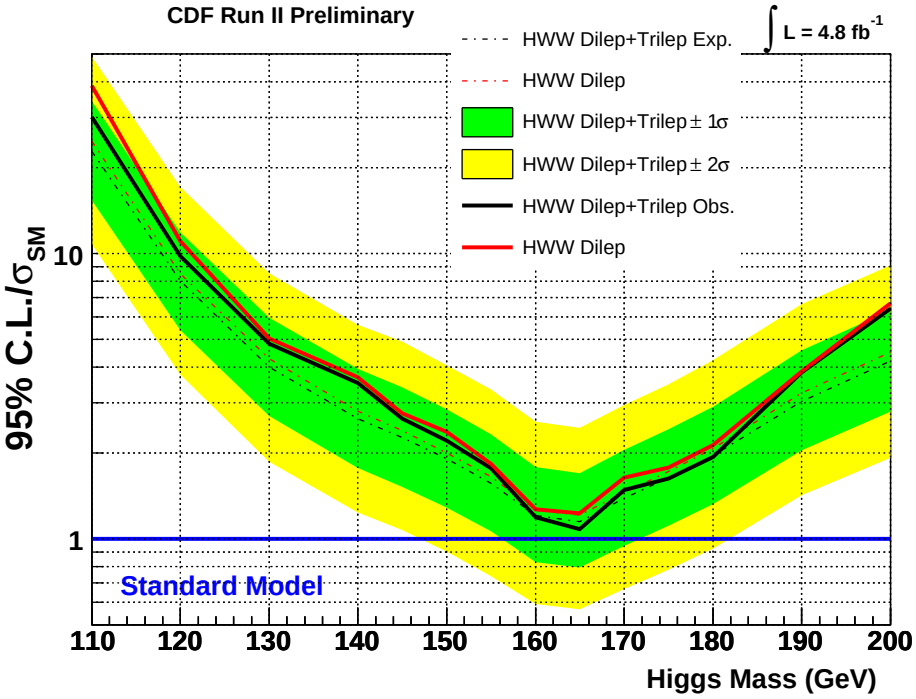

Figure 9.9 HWW+Trilepton Combined Limits

Limits	110	120	130	140	145	150	155
$+2\sigma/\sigma_{\mathrm{SM}}$	49.0	17.1	8.52	5.62	4.91	4.06	3.34
$+1\sigma/\sigma_{\mathrm{SM}}$	34.2	11.9	5.95	3.94	3.39	2.84	2.32
Median/σ_{SM}	**22.8**	**8.02**	**4.01**	**2.64**	**2.27**	**1.91**	**1.57**
$-1\sigma/\sigma_{\mathrm{SM}}$	15.4	5.39	2.70	1.77	1.52	1.29	1.06
$-2\sigma/\sigma_{\mathrm{SM}}$	10.8	3.76	1.86	1.24	1.08	0.90	0.74
Observed/σ_{SM}	**30.1**	**9.79**	**4.83**	**3.52**	**2.64**	**2.21**	**1.77**
Limits	160	165	170	175	180	190	200
$+2\sigma/\sigma_{\mathrm{SM}}$	2.57	2.45	2.95	3.48	4.23	6.65	9.08
$+1\sigma/\sigma_{\mathrm{SM}}$	1.79	1.70	2.05	2.42	2.91	4.57	6.33
Median/σ_{SM}	**1.21**	**1.15**	**1.39**	**1.64**	**1.96**	**3.03**	**4.20**
$-1\sigma/\sigma_{\mathrm{SM}}$	0.83	0.79	0.94	1.11	1.32	2.04	2.80
$-2\sigma/\sigma_{\mathrm{SM}}$	0.59	0.57	0.67	0.78	0.93	1.42	1.93
Observed/σ_{SM}	**1.19**	**1.08**	**1.49**	**1.63**	**1.94**	**3.83**	**6.41**

Table 9.12 HWW w/ Trileptons Combined Expected Sensitivity.

9.7 Conclusions

DISCARD THIS PAGE

Appendix A: Neural Net Input Variables

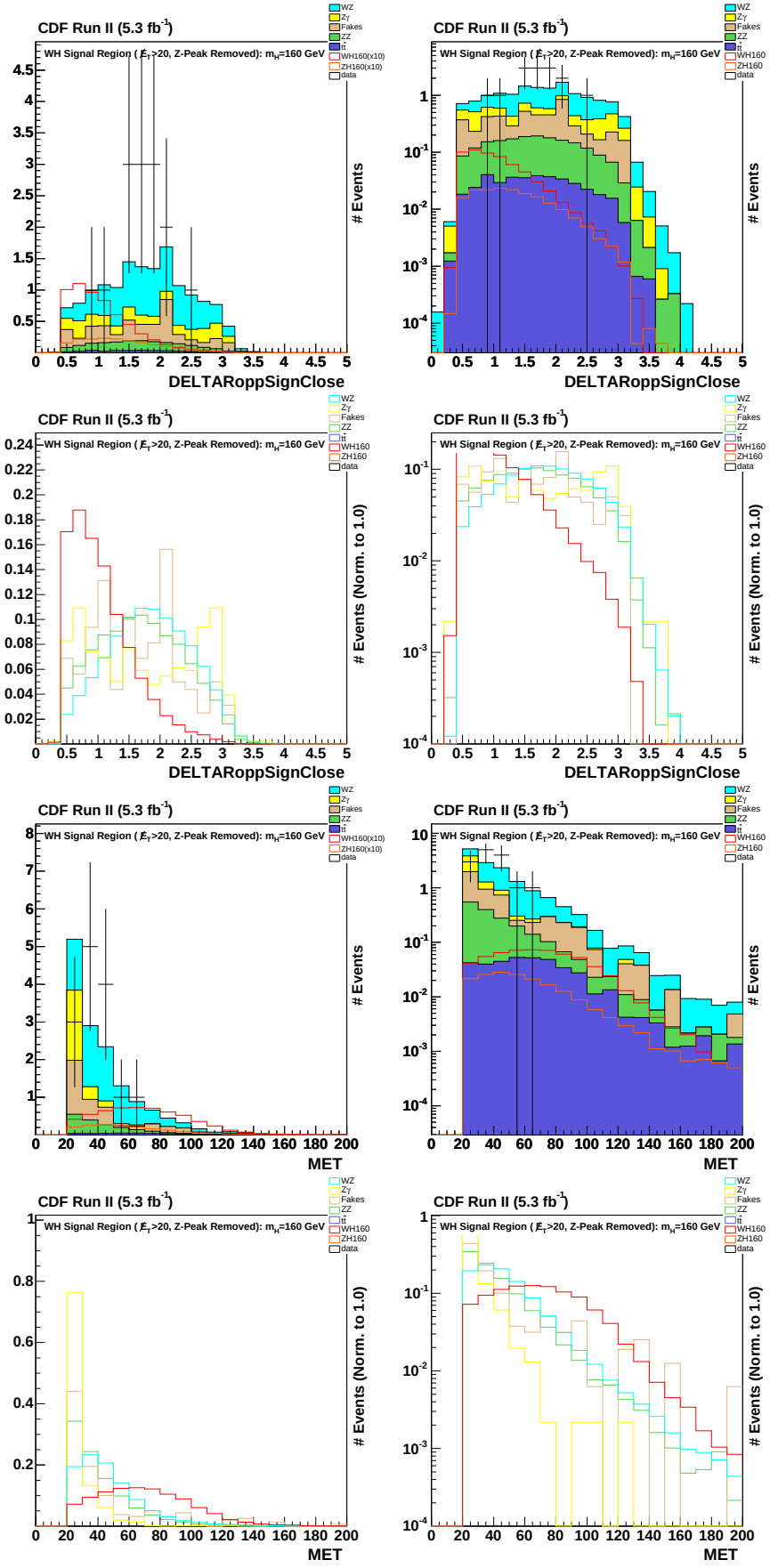

Figure A.1 *NoZPeak* Signal Region (10.0 GeV $< \not\!\!E_T <$ 20.0 GeV): ΔR Opp. Sign Close Leptons, $\not\!\!E_T$.

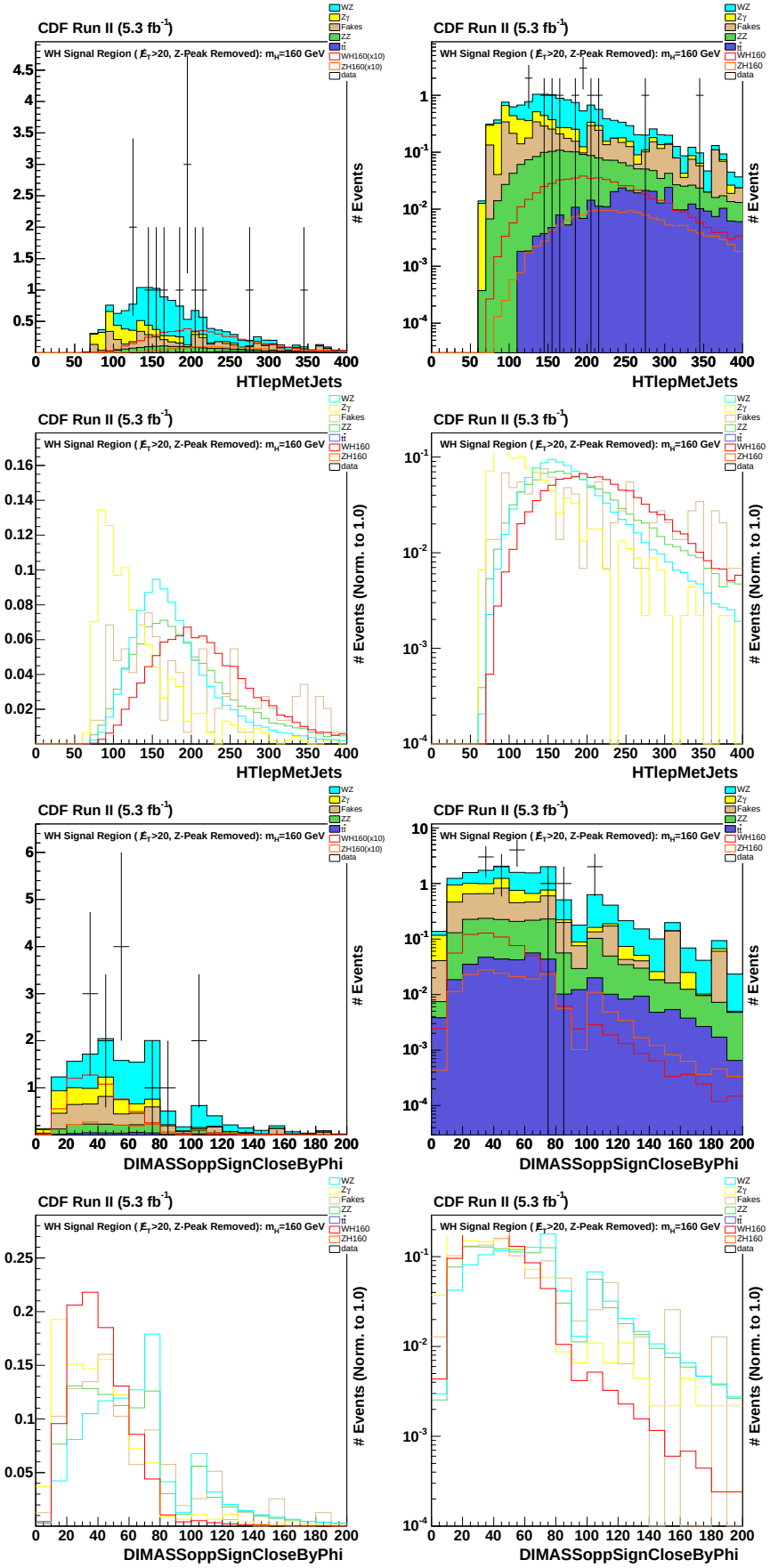

Figure A.2 *NoZPeak* Signal Region (10.0 GeV $< \not\!\!E_T <$ 20.0 GeV): H_T(all leptons, $\not\!\!E_T$, all jets), Dimass Opp. Sign Leptons (closer pair in ϕ).

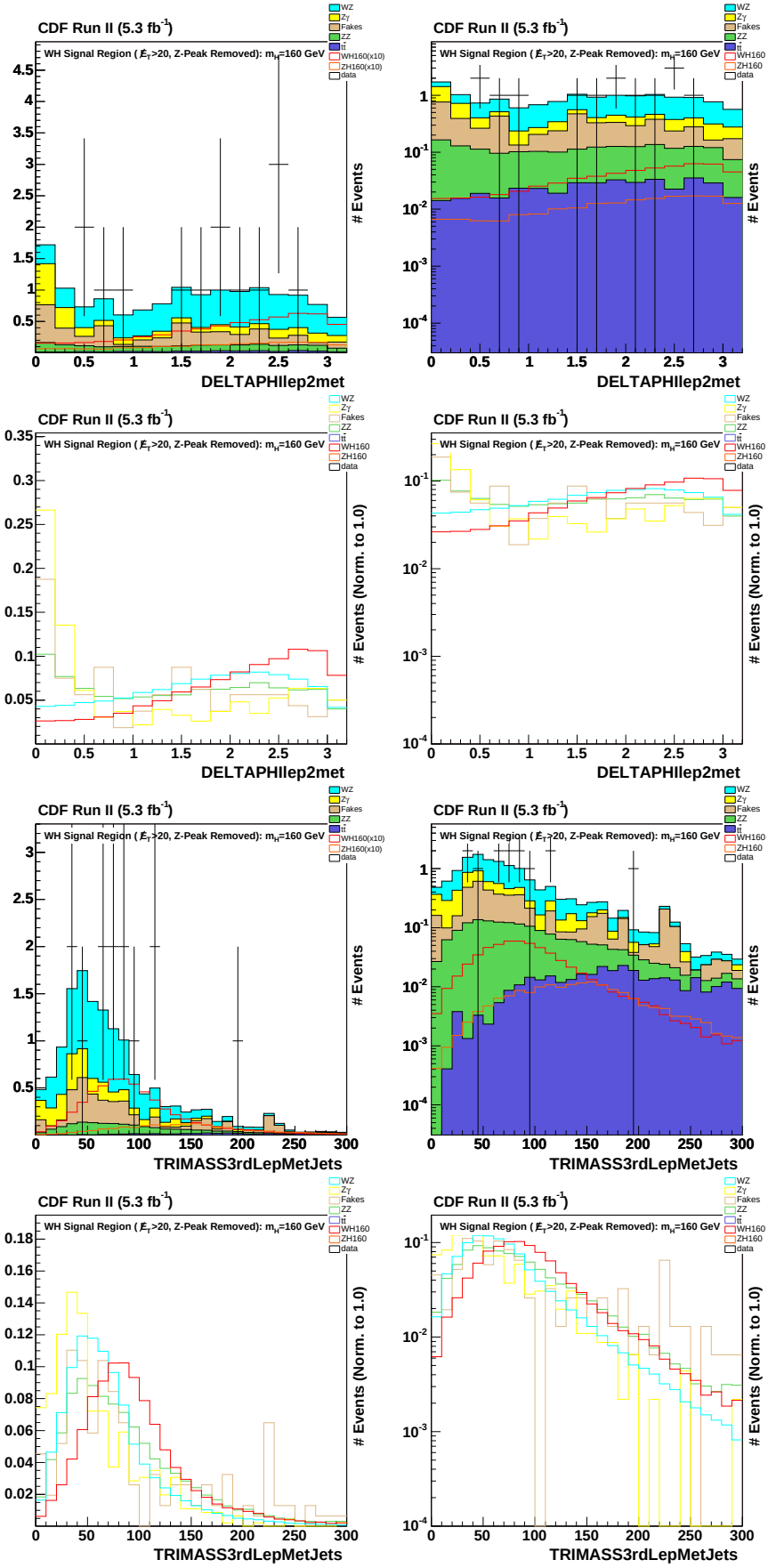

Figure A.3 *NoZPeak* Signal Region (10.0 GeV $< \not\!\!E_T <$ 20.0 GeV): $\Delta\phi$ between the 2nd lepton and $\not\!\!E_T$, Inv. mass of the 3rd lepton+$\not\!\!E_T$+Jets.

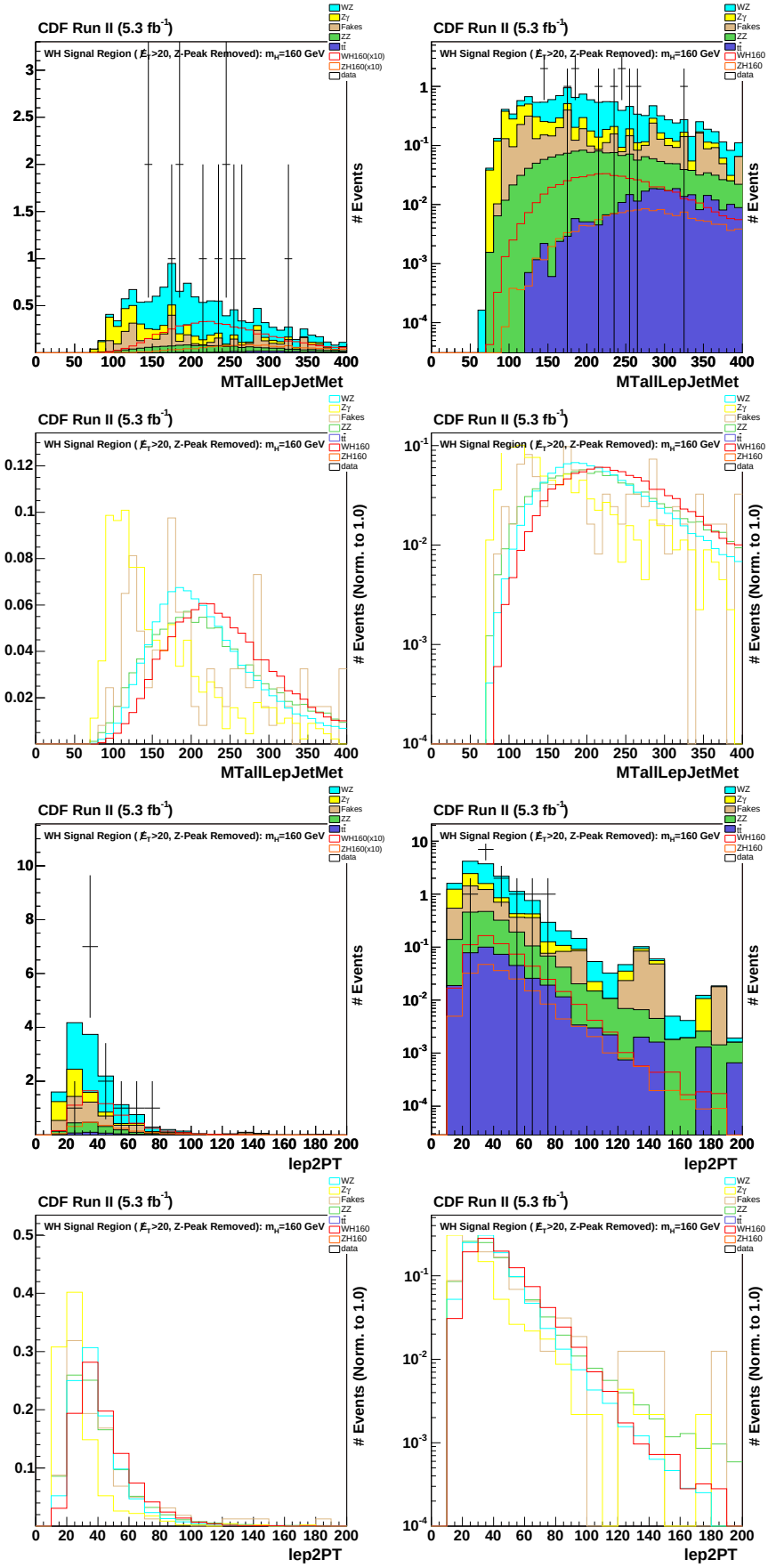

Figure A.4 *NoZPeak* Signal Region (10.0 GeV $< \not\!\!E_T <$ 20.0 GeV): m_T(Leptons,$\not\!\!E_T$,Jets), p_T of 2$^{\text{nd}}$ Lepton

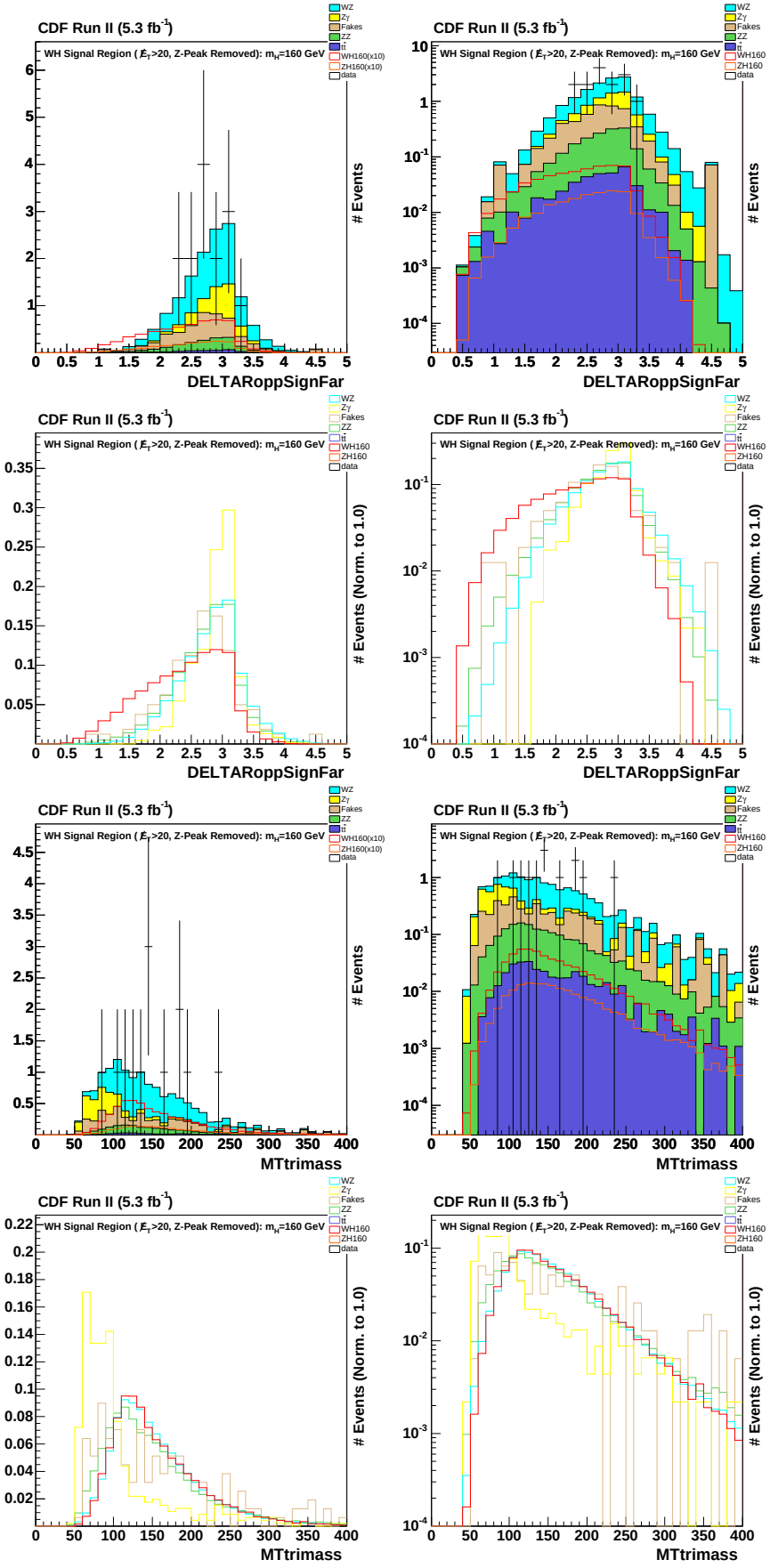

Figure A.5 *NoZPeak* Signal Region (10.0 GeV $< \not\!\!E_T <$ 20.0 GeV): ΔR Opp. Sign Far Leptons, m_T Trilepton Mass.

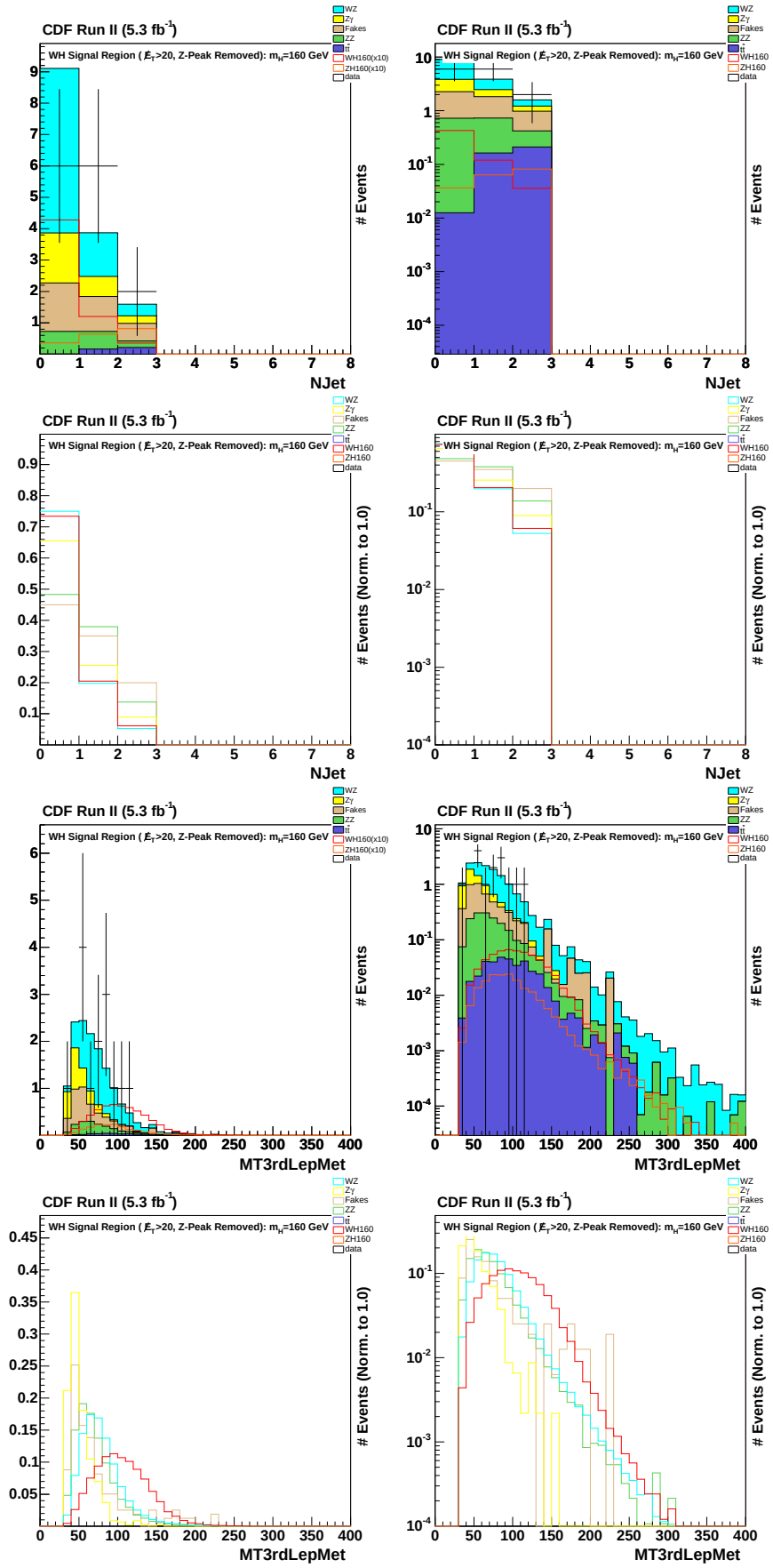

Figure A.6 *NoZPeak* Signal Region (10.0 GeV $< \not\!\!E_T <$ 20.0 GeV): NJet (note that the 0-jet bin is not used in the analysis), m_T (Lep3, $\not\!\!E_T$).

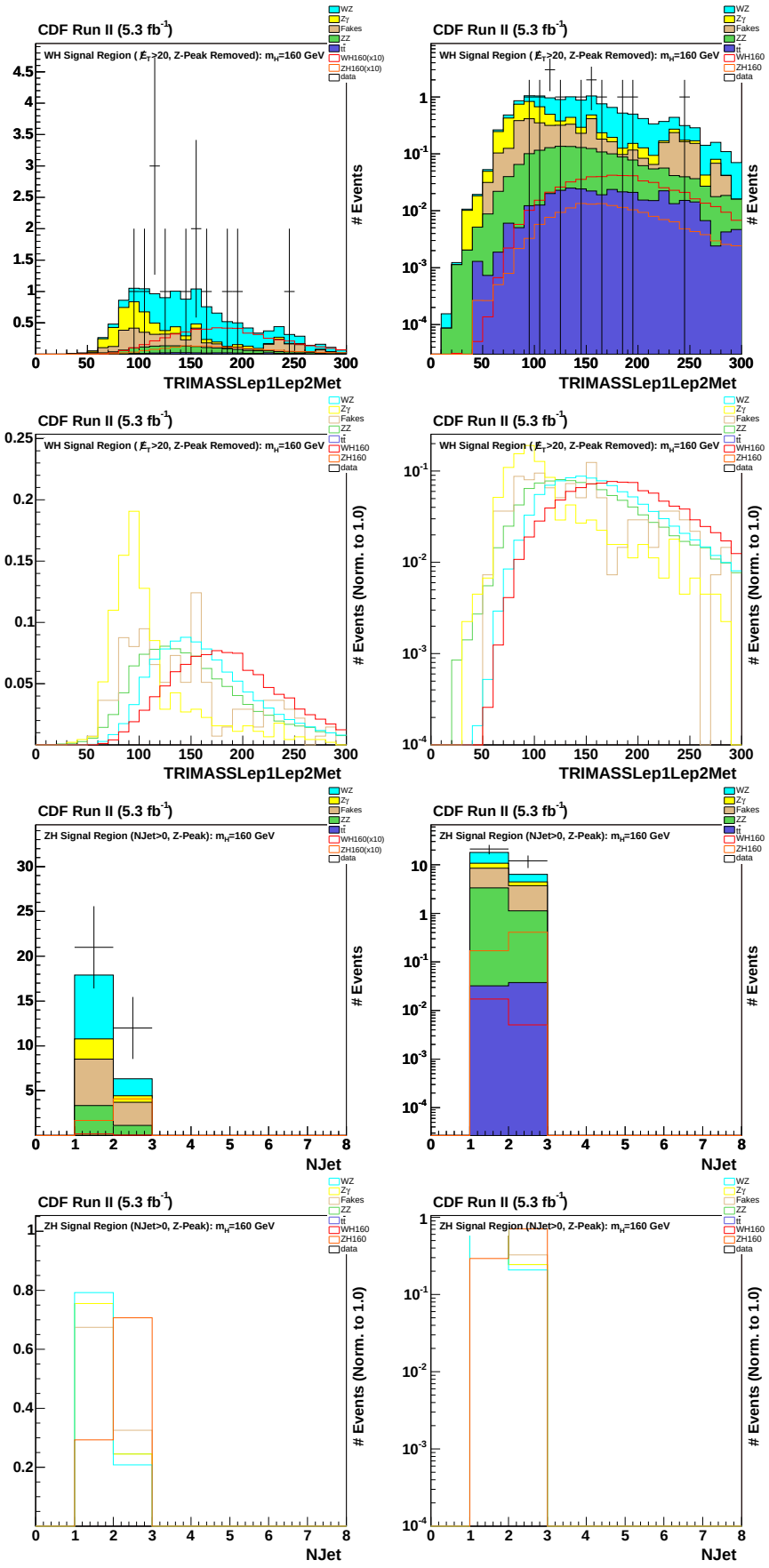

Figure A.7 *NoZPeak* Signal Region (10.0 GeV $< \not\!\!E_T <$ 20.0 GeV): Inv. Mass(Lep1,Lep2,$\not\!\!E_T$). *InZPeak* Signal Region (NJet $\neq$ 0): NJet.

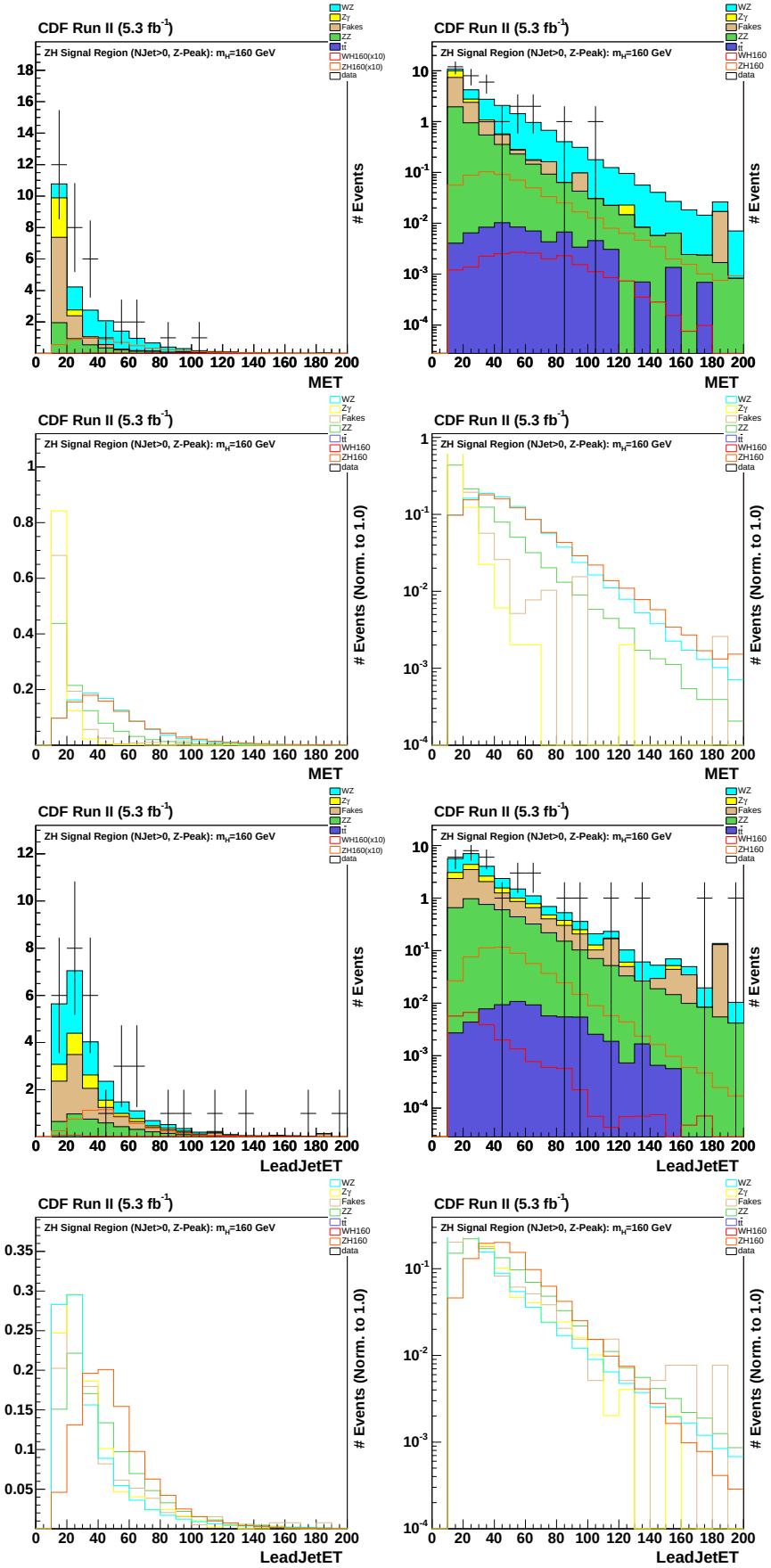

Figure A.8 *InZPeak* Signal Region (NJet $\neq 0$): $\not\!\!E_T$, Lead Jet E_T.

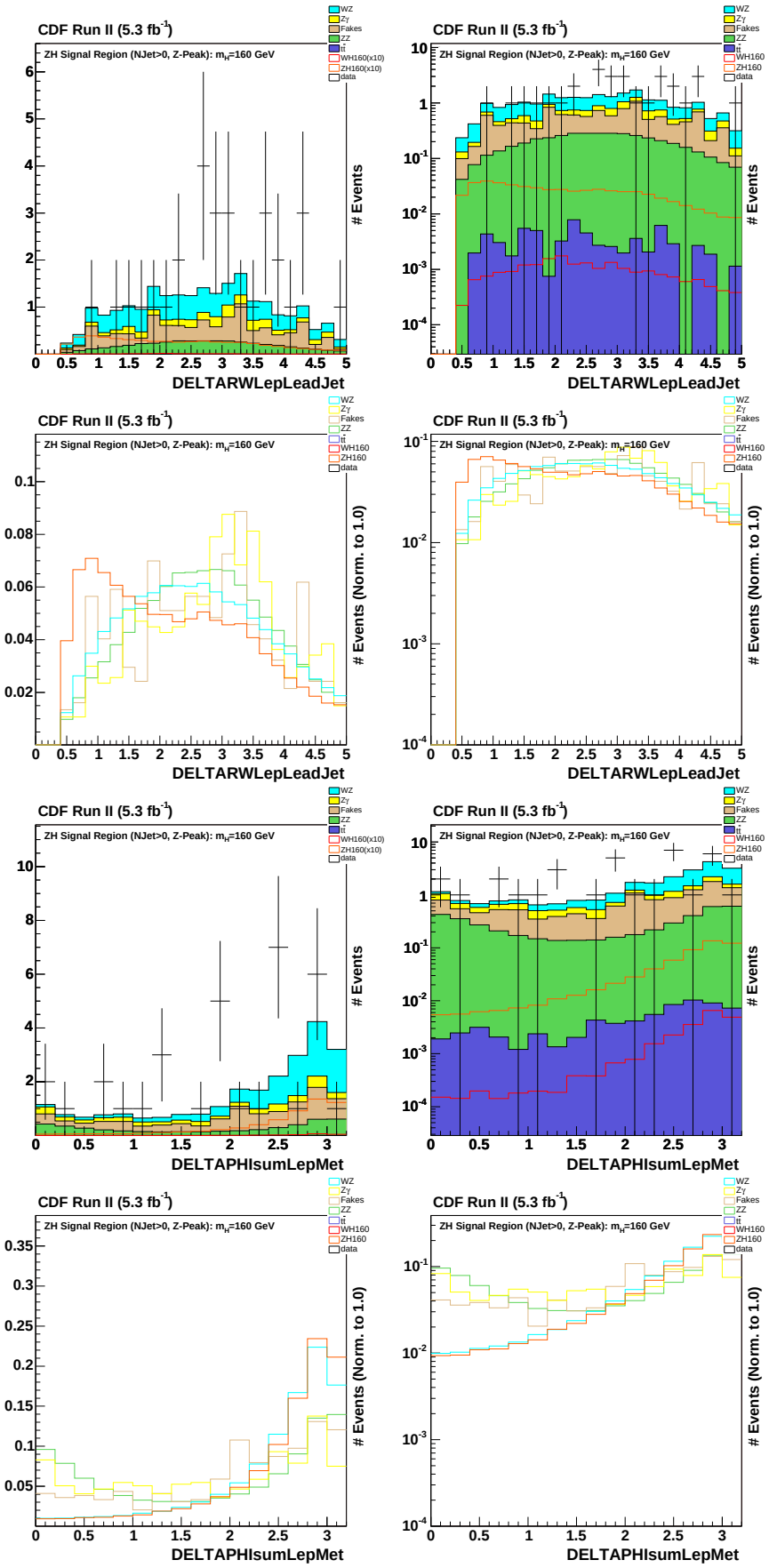

Figure A.9 *InZPeak* Signal Region (NJet $\neq 0$): $\Delta R(W$-Lep, Lead Jet), $\Delta\phi$(Leptons,$\not\!\!E_T$).

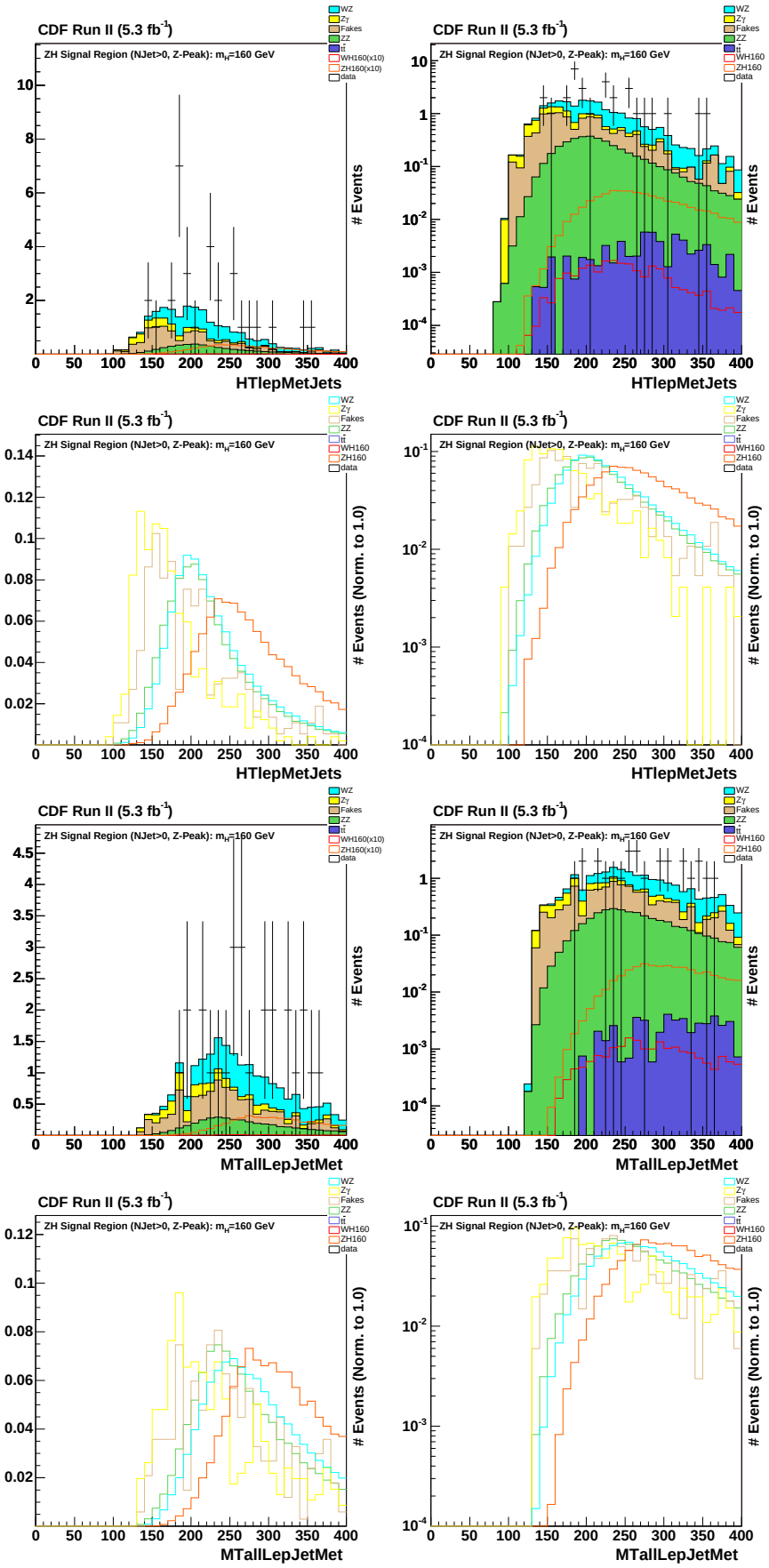

Figure A.10 *InZPeak* Signal Region (NJet $\neq 0$): H_T(Leptons,$\not\!\!E_T$,Jets), m_T(Leptons,$\not\!\!E_T$,Jets).

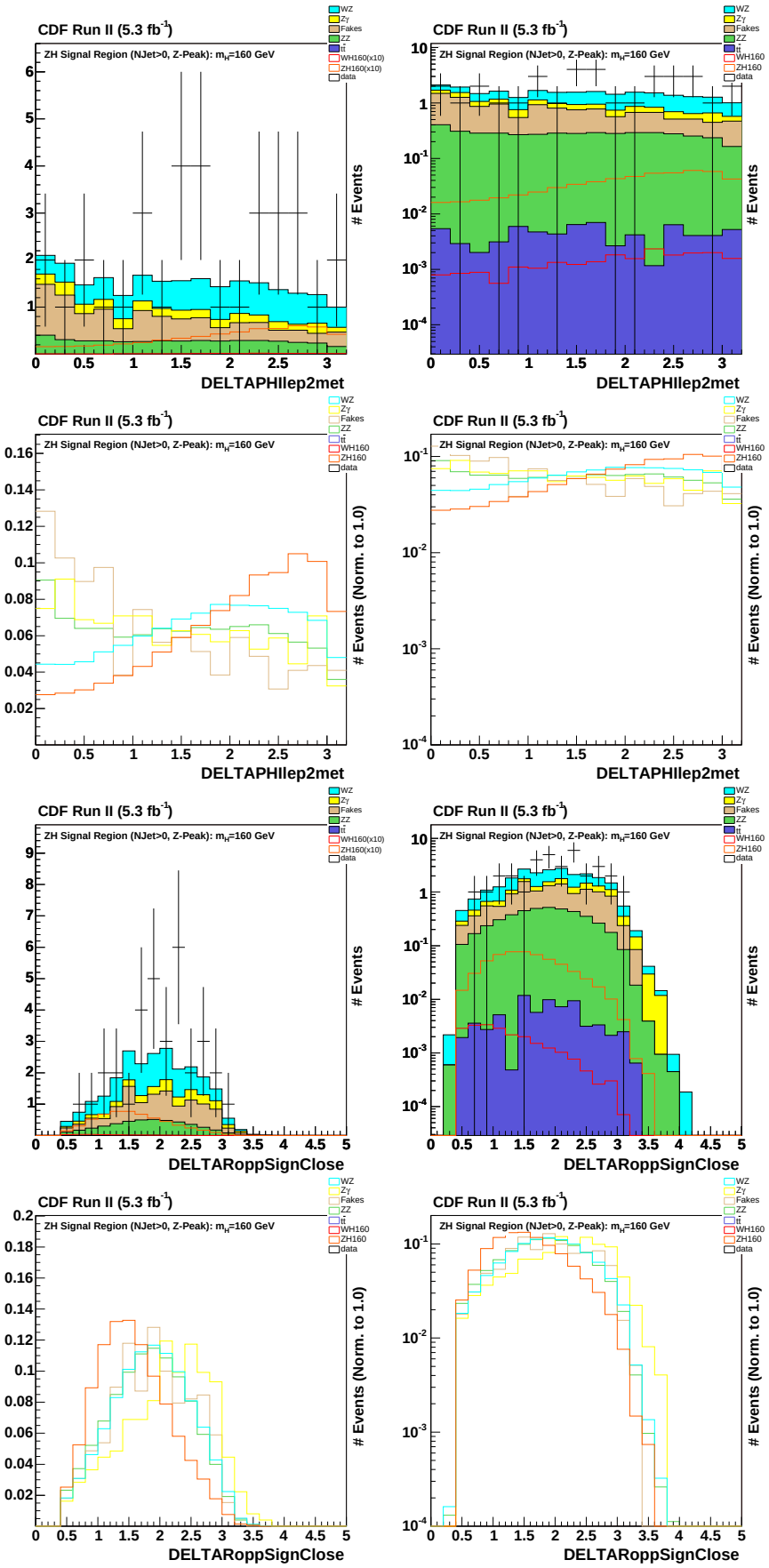

Figure A.11 *InZPeak* Signal Region (NJet $\neq 0$): $\Delta\phi$(Lep2,$\not\!\!E_T$), ΔR b/w Opp. Sign Close Leptons.

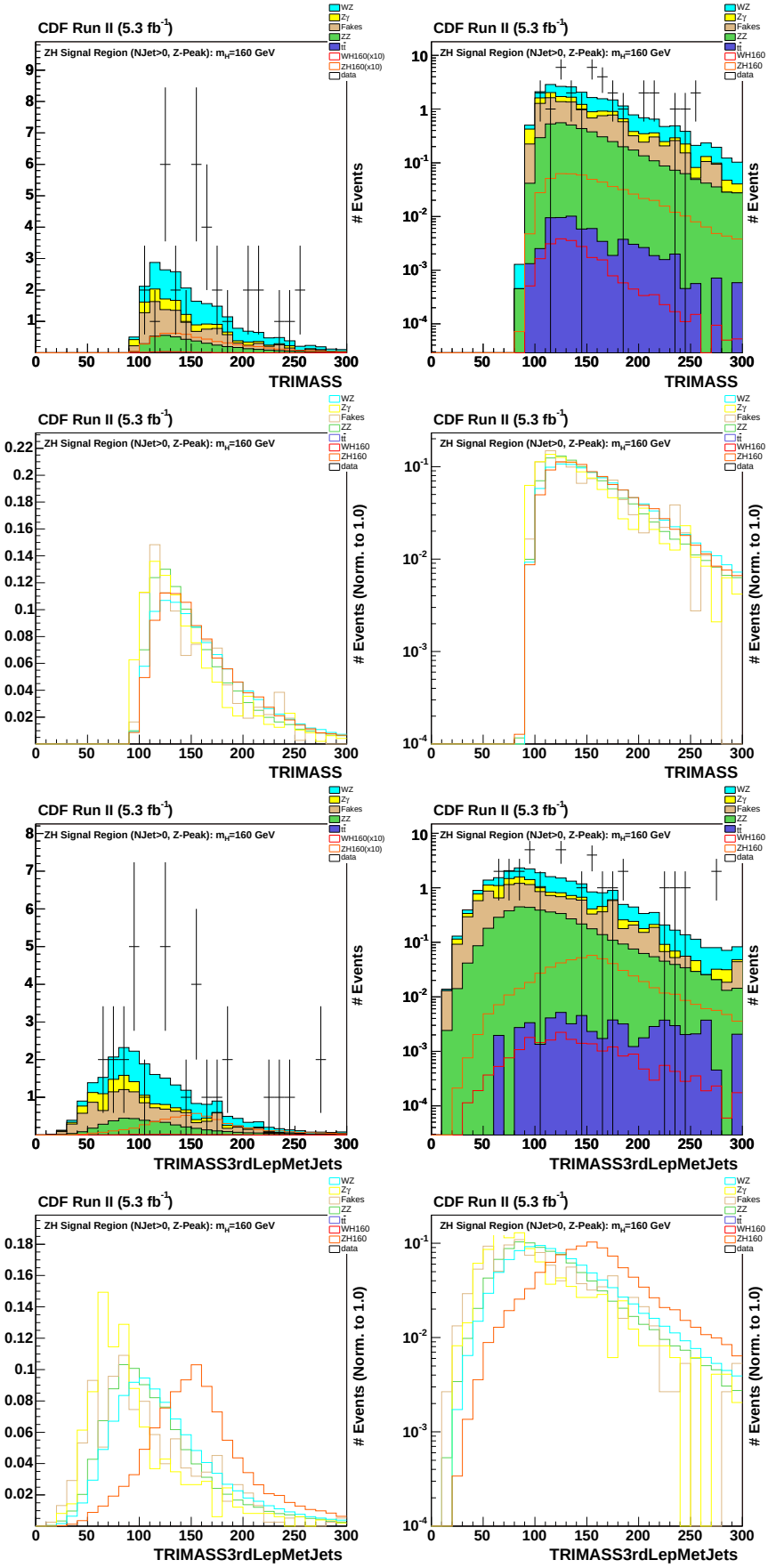

Figure A.12 *InZPeak* Signal Region (NJet $\neq 0$): Trilepton Invariant Mass, Inv. Mass(Lep3,$\not\!\!E_T$,Jets).

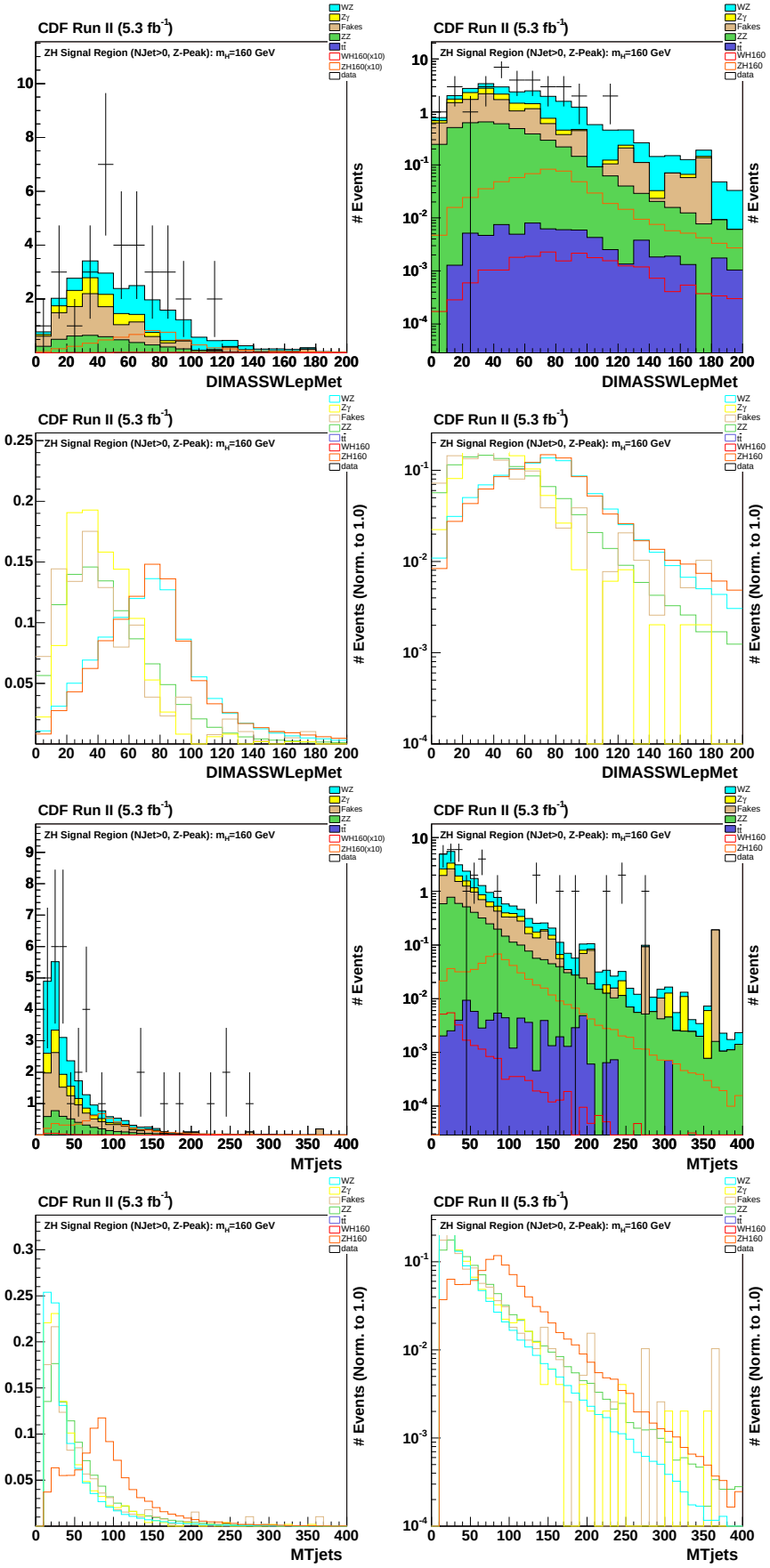

Figure A.13 *InZPeak* Signal Region (NJet $\neq 0$): Dimass(W-Lep,$\not\!\!E_T$), m_T Jets.

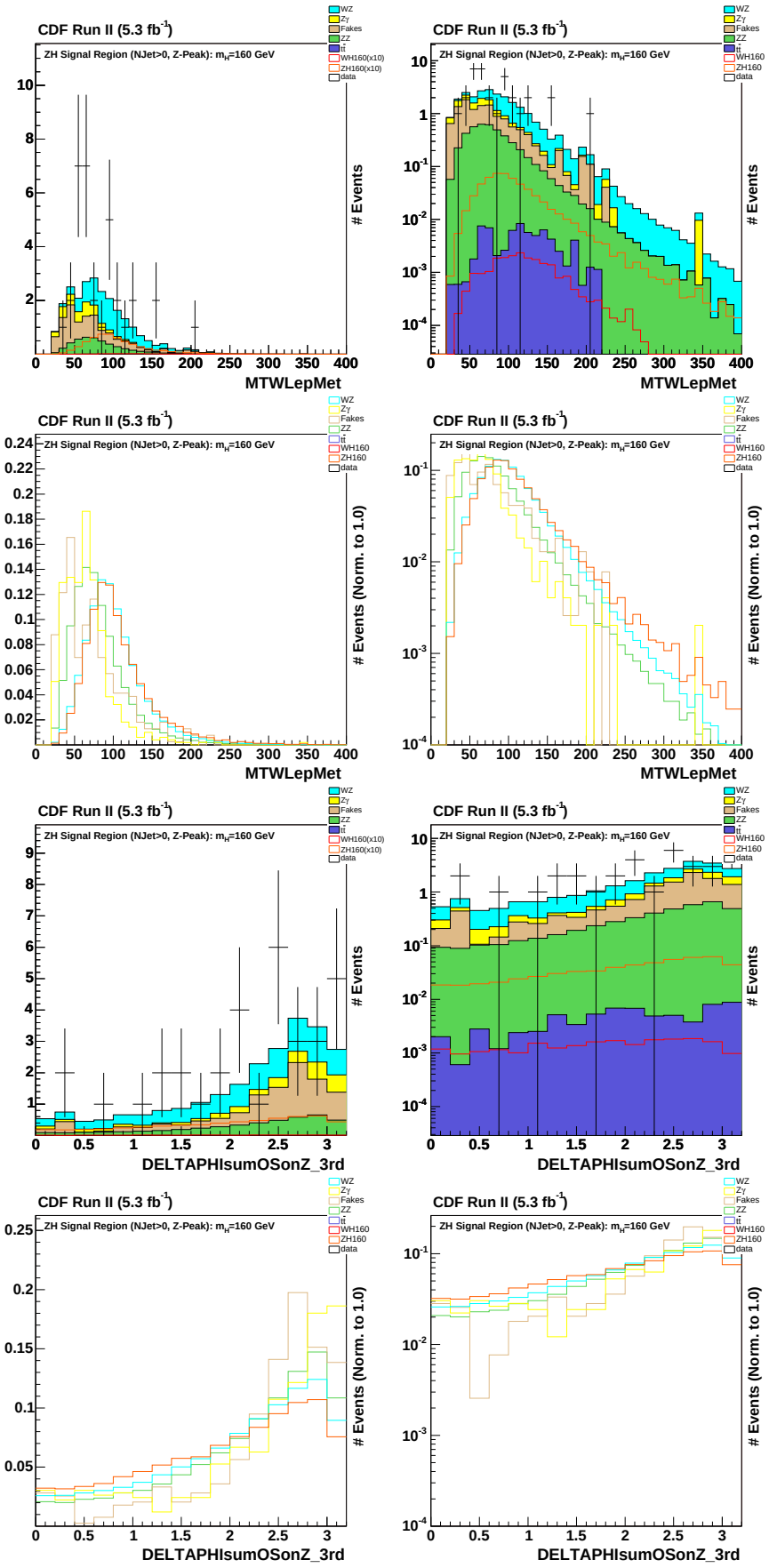

Figure A.14 *InZPeak* Signal Region (NJet $\neq 0$): m_T(W-Lep,$\not\!\!E_T$), $\Delta\phi$(Z-Leptons,W-Lepton).

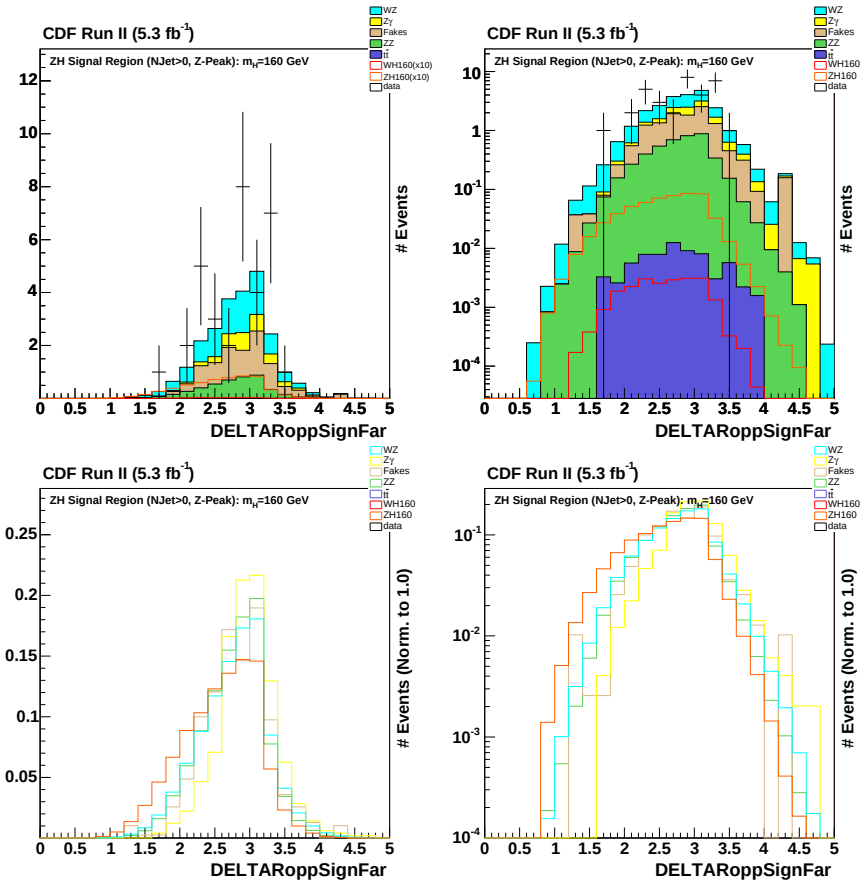

Figure A.15 *InZPeak* Signal Region (NJet $\neq 0$): ΔR Opp. Sign Far Leptons.

Appendix B: Input Variables in Control Regions

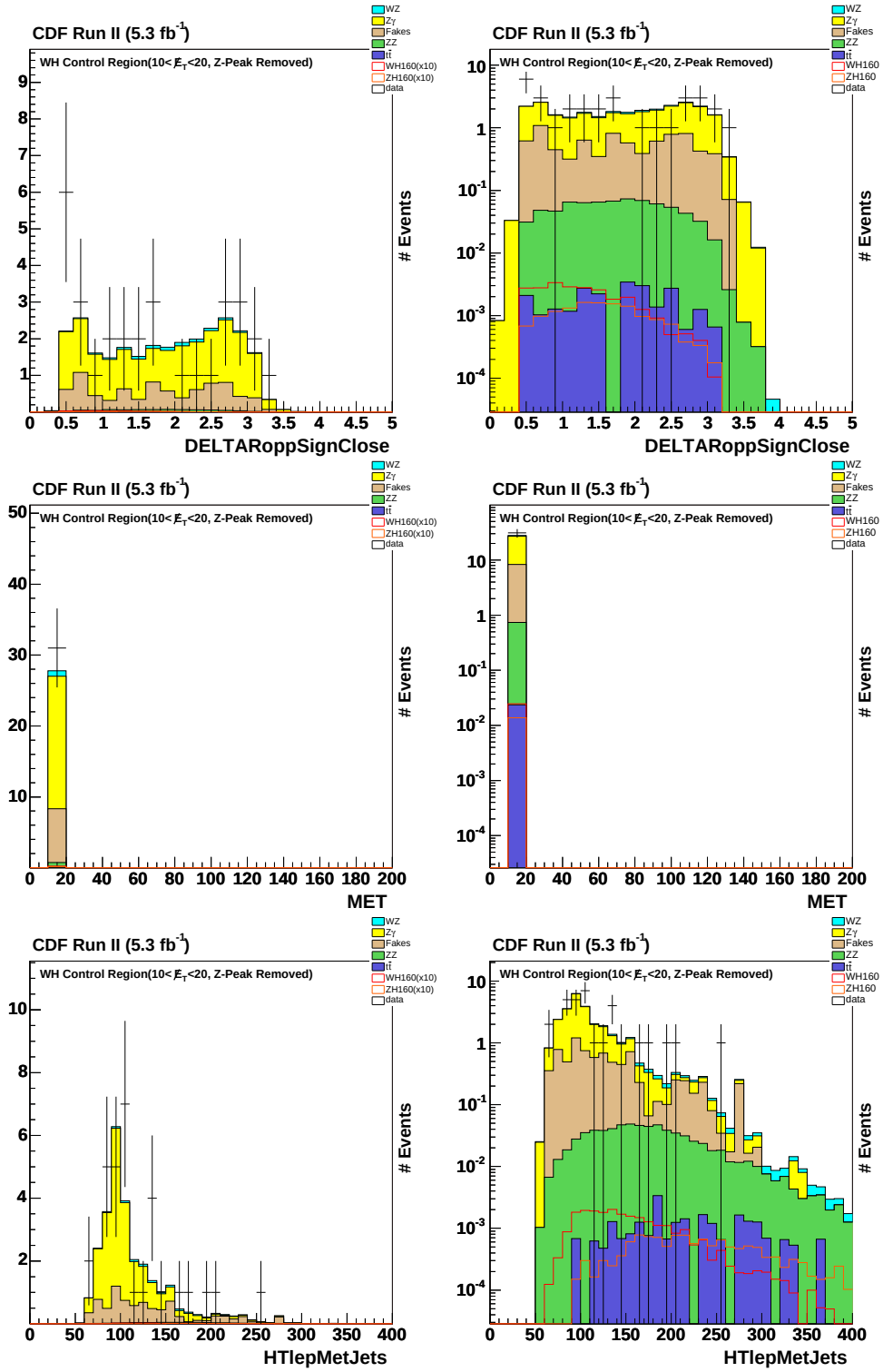

Figure B.1 *NoZPeak* Control Region (10.0 GeV $< \not\!\!E_T <$ 20.0 GeV): ΔR Opp. Sign Close Leptons, $\not\!\!E_T$, H_T(all leptons, $\not\!\!E_T$, all jets).

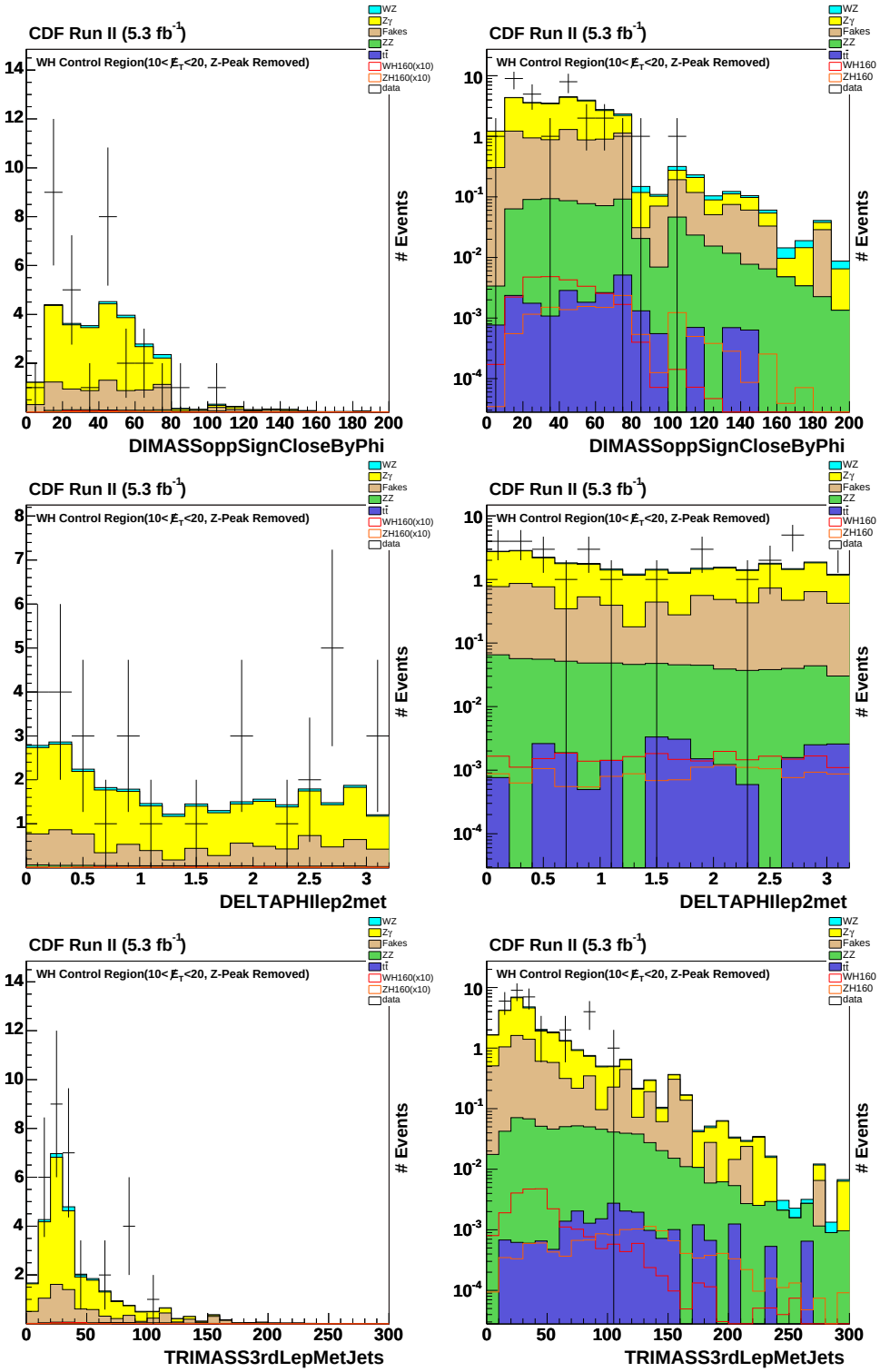

Figure B.2 *NoZPeak* Control Region (10.0 GeV $< \not\!\!E_T <$ 20.0 GeV): Dimass Opp. Sign Leptons (closer pair in ϕ), $\Delta\phi$ between the 2$^{\text{nd}}$ lepton and $\not\!\!E_T$, Inv. mass of the 3$^{\text{rd}}$ lepton+ $\not\!\!E_T$+Jets.

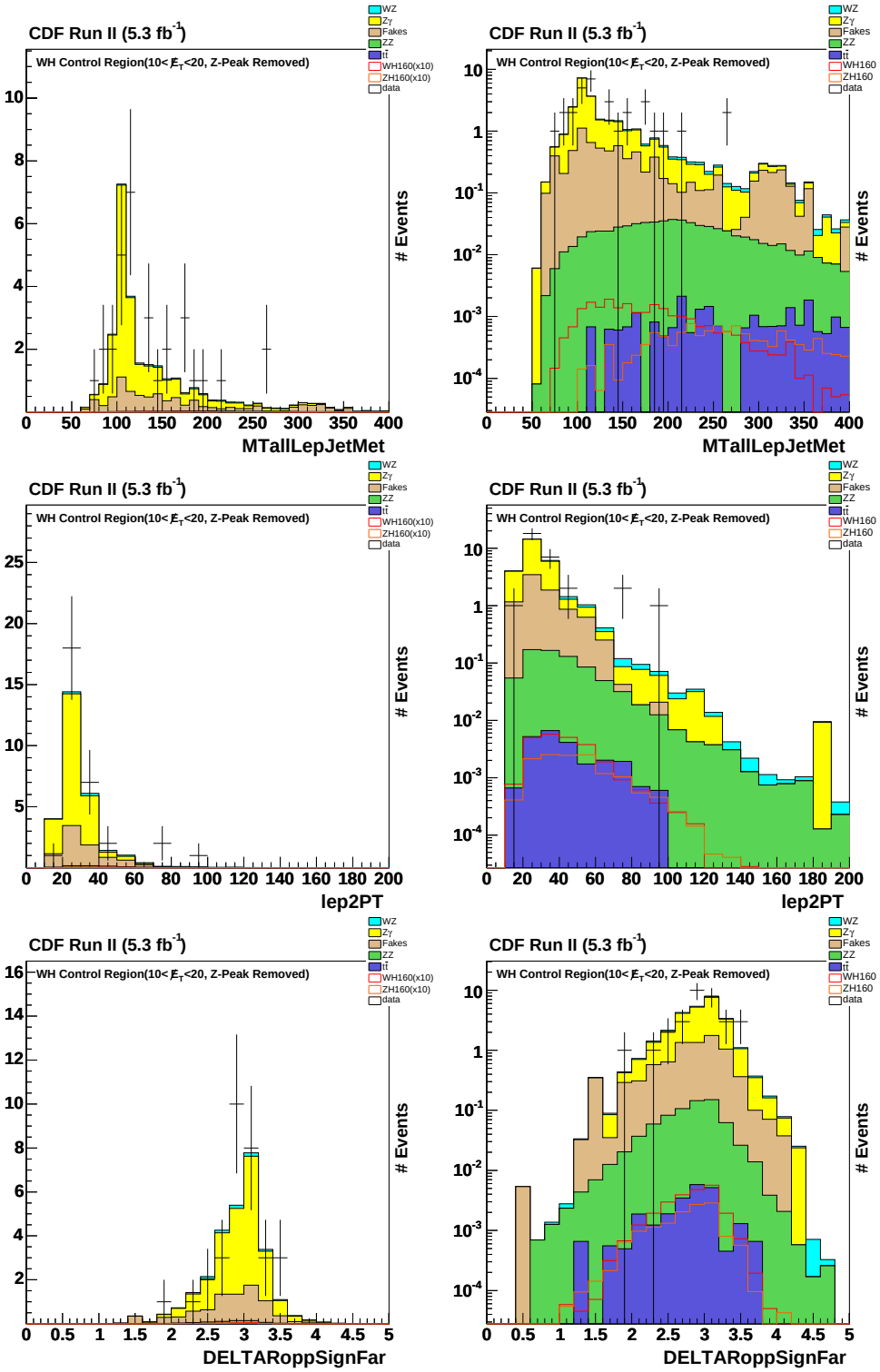

Figure B.3 *NoZPeak* Control Region (10.0 GeV $< \not\!\!E_T <$ 20.0 GeV): m_T(Leptons,$\not\!\!E_T$,Jets), p_T of 2$^{\text{nd}}$ Lepton, ΔR Opp. Sign Far Leptons.

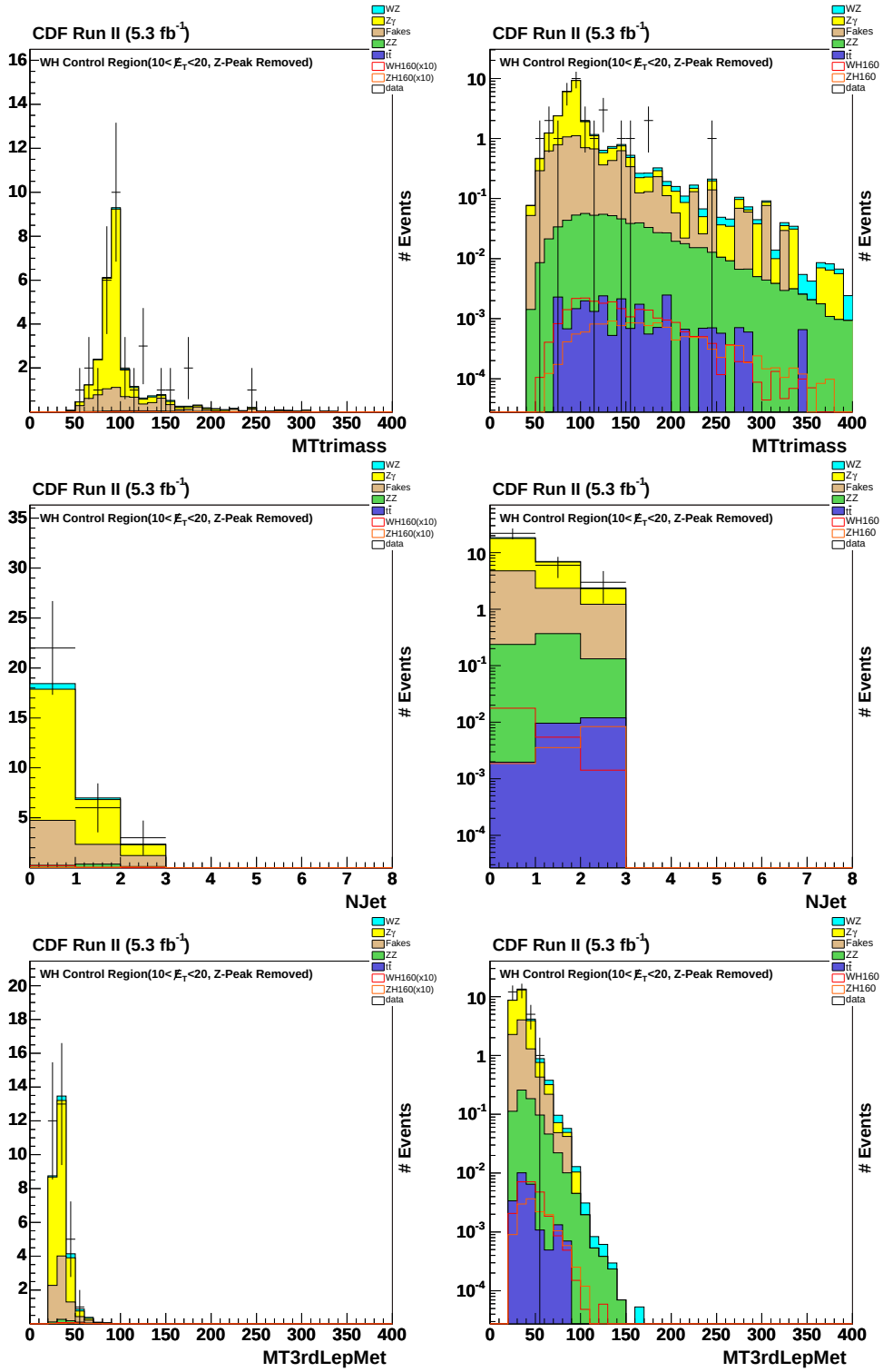

Figure B.4 *NoZPeak* Control Region (10.0 GeV $< \not\!\!E_T <$ 20.0 GeV): m_T Trilepton Mass, NJet, m_T (Lep3, $\not\!\!E_T$).

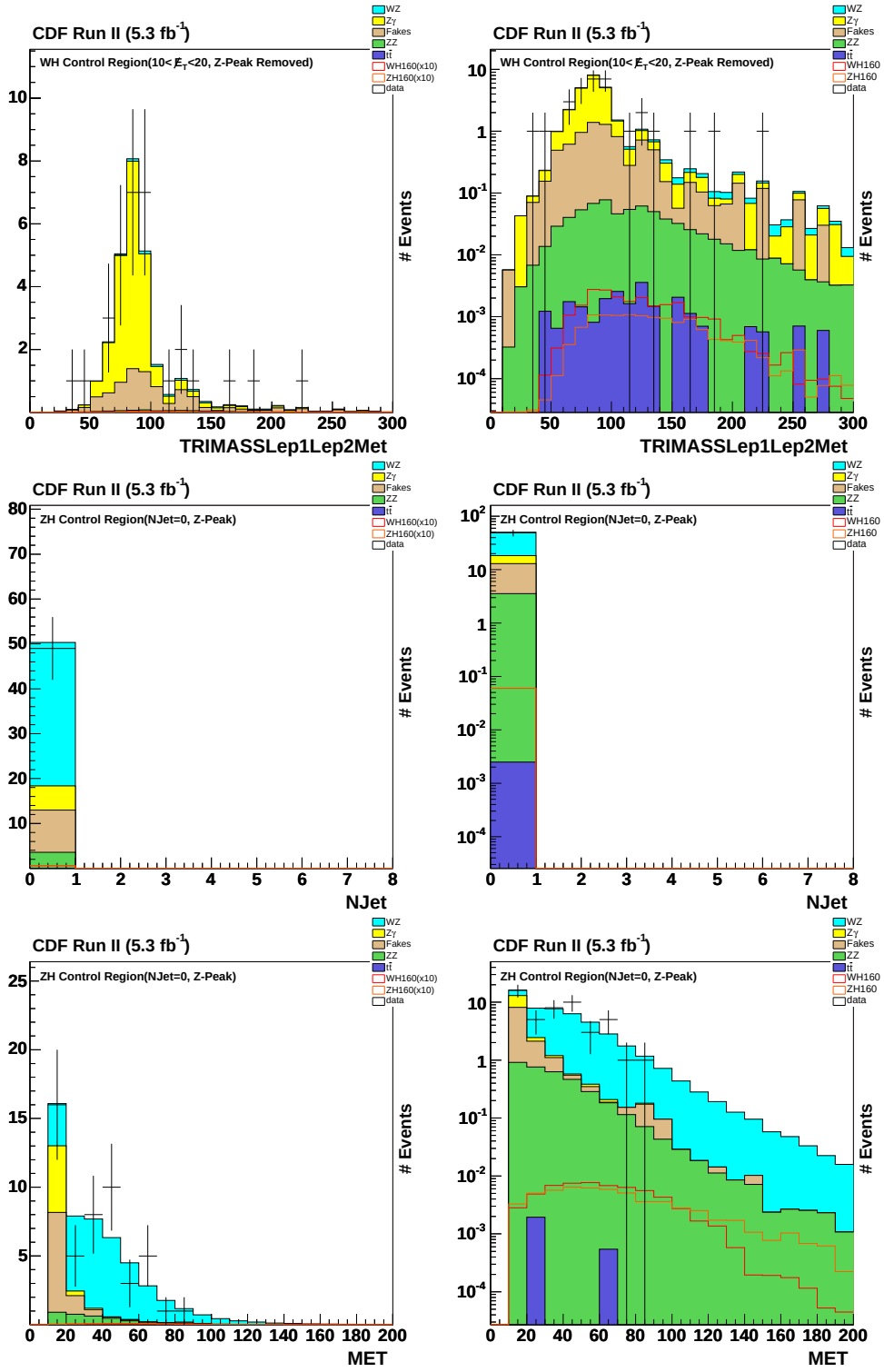

Figure B.5 *NoZPeak* Control Region (10.0 GeV $< \not\!\!E_T <$ 20.0 GeV): Inv. Mass(Lep1,Lep2,$\not\!\!E_T$). *InZPeak* Control Region (NJet=0): NJet, $\not\!\!E_T$.

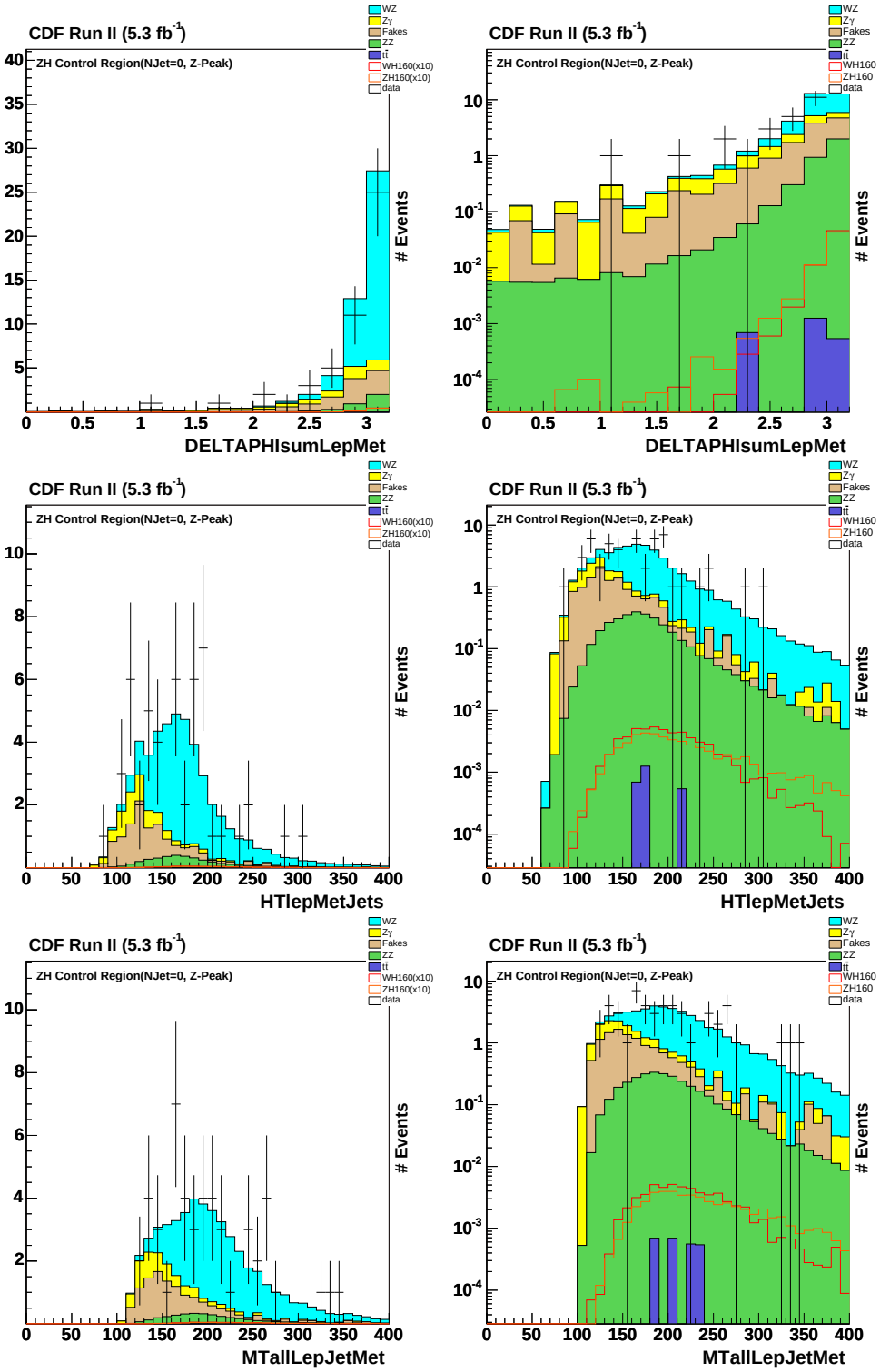

Figure B.6 *InZPeak* Control Region (NJet=0): $\Delta\phi$(Leptons,$\not\!\!E_T$), H_T(Leptons,$\not\!\!E_T$,Jets), m_T(Leptons,$\not\!\!E_T$,Jets)

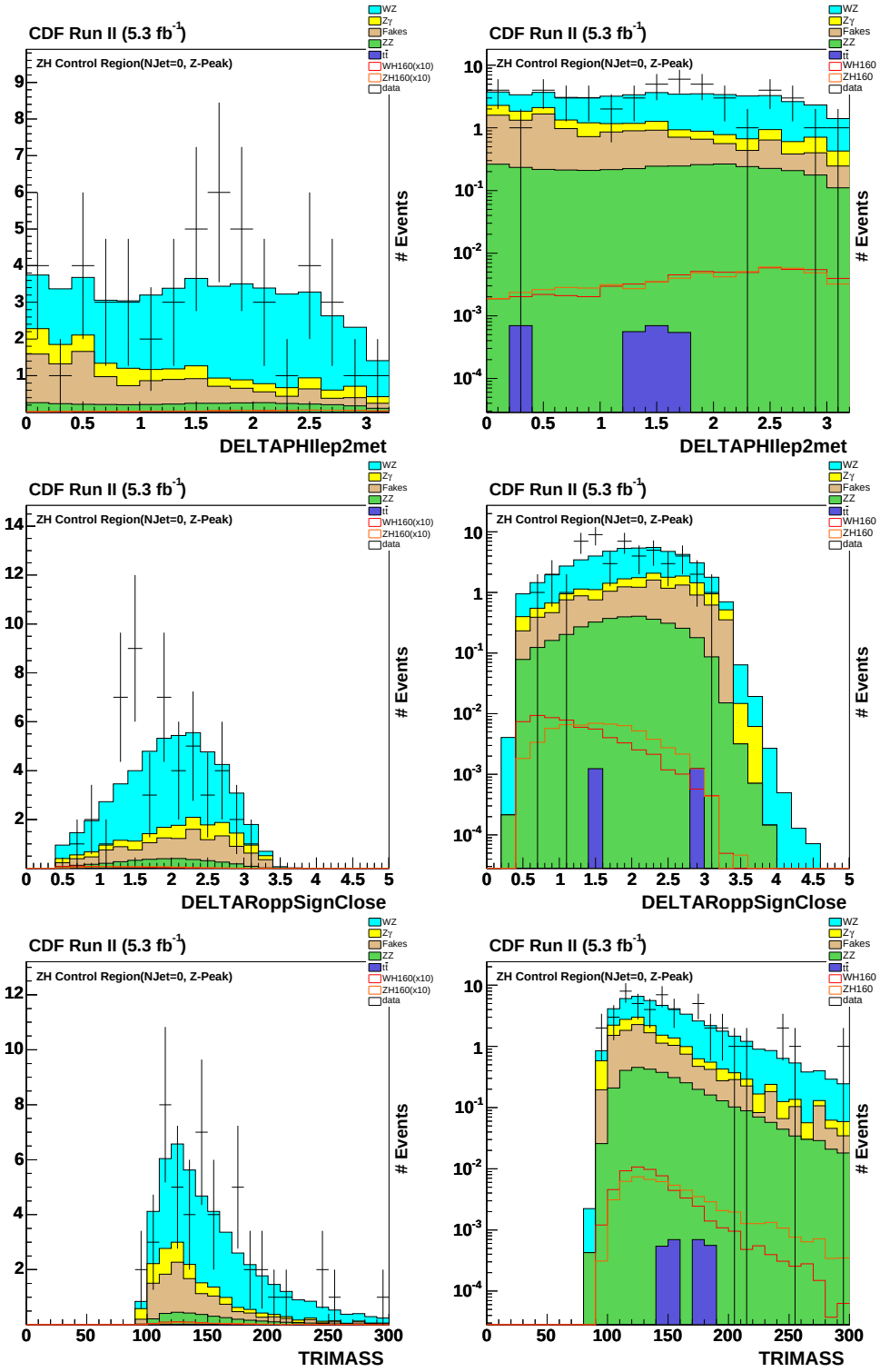

Figure B.7 *InZPeak* Control Region (NJet=0): $\Delta\phi$(Lep2,$\not\!\!E_T$), ΔR b/w Opp. Sign Close Lept, trilepton invariant mass.

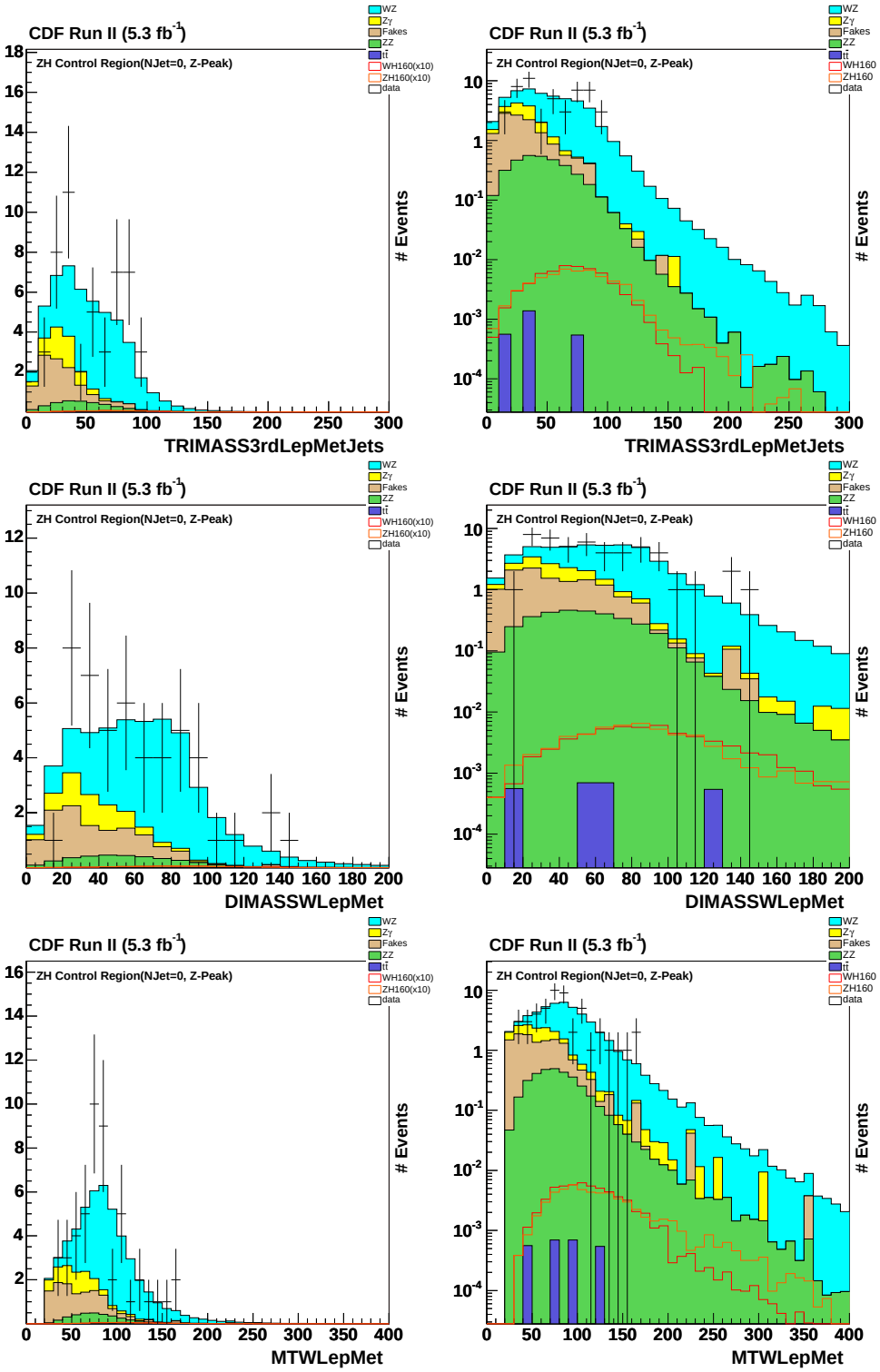

Figure B.8 *InZPeak* Control Region (NJet=0): Inv. Mass(Lep3,$\not\!\!E_T$,Jets), Dimass(W-Lep,$\not\!\!E_T$), m_T(W-Lep,$\not\!\!E_T$).

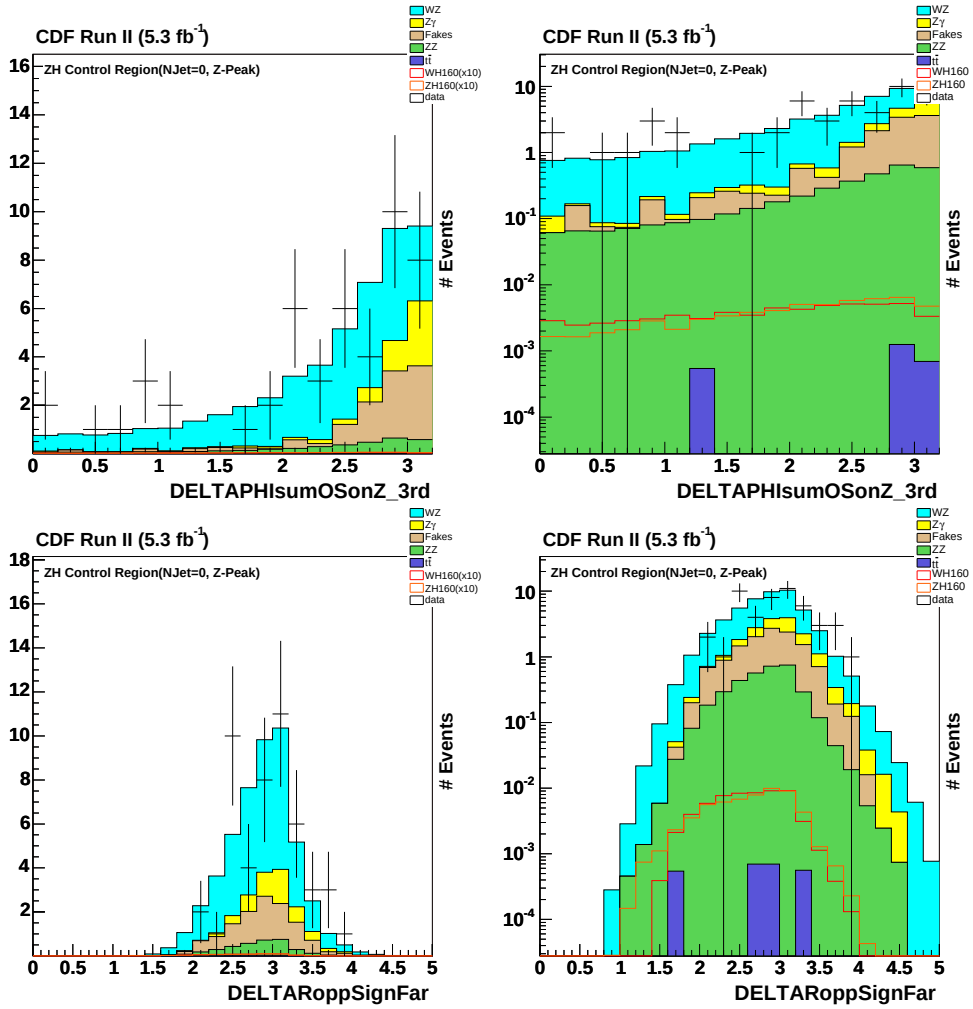

Figure B.9 *InZPeak* Control Region (NJet=0): $\Delta\phi(Z\text{-Leptons}, W\text{-Lepton})$, ΔR Opp. Sign Far Leptons.

Appendix C: $U(1)$ Global Symmetry Breaking

The Standard Model and it's component quantum field theories are based on symmetries of particular groups. Equally important is the concept that symmetries of nature may be spontaneously broken with physical consequences. In this and the subsequent few sections of the appendix, we shall explore the concept of spontaneously broken symmetries because the idea is central to the function of the Higgs boson in the Standard Model.

In this section, we shall explore the concept of spontaneously broken $U(1)$ symmetry for a complex scalar particle. An arbitrary complex field has real and imaginary components, by definition.[12]

$$\phi = \frac{1}{\sqrt{2}}(\phi_1 - i\phi_2) \tag{C.1}$$

It's complex conjugate is then:

$$\phi = \frac{1}{\sqrt{2}}(\phi_1 + i\phi_2) \tag{C.2}$$

We postulate the lagrangian for this particle:

$$\mathcal{L} = (\partial_\mu \phi)^\dagger (\partial^\mu \phi) - m_0^2 \phi^\dagger \phi - \frac{1}{4}\lambda \left(\phi^\dagger \phi\right)^2 \tag{C.3}$$

The first term has the typical form of kinetic energy, the second terms is the potential energy or "rest mass," and the last term governs the possibility of an interaction. If $m_0^2 > 0$, then the lagrangian describes a complex scalar particle with mass m_0.

Denote the last two term as $V(\phi) = m_0^2 \phi^\dagger \phi + \frac{1}{4}\lambda \left(\phi^\dagger \phi\right)^2$, the potential. The task of determining the particle spectrum of the ϕ field reduces to finding the minima of $V(\phi)$ and calculating perturbative oscillations from it.

Recall that the $U(1)$ symmetry group is is the group of angular rotations in the complex plane. We say the lagrangian exhibits a $U(1)$ global symmetry, or is "invariant" under $U(1)$ transformations, because if we rotate the field ϕ in the complex plane by some arbitrary angle α in a manner not dependent on spacetime location

$$\phi \to \phi' = e^{i\alpha}\phi \tag{C.4}$$

then the lagranian does not change

$$\mathcal{L} = (\partial_\mu \phi')^\dagger (\partial^\mu \phi') - m_0^2 \phi'^\dagger \phi' - \frac{1}{4}\lambda \left(\phi'^\dagger \phi'\right)^2 \tag{C.5}$$

$$= \left(\partial_\mu \phi e^{i\alpha}\right)^\dagger \left(\partial^\mu \phi e^{i\alpha}\right) - m_0^2 \phi^\dagger e^{-i\alpha} \phi e^{i\alpha} - \frac{1}{4}\lambda \left(\phi^\dagger e^{-i\alpha} \phi e^{i\alpha}\right)^2 \tag{C.6}$$

$$= (\partial_\mu \phi)^\dagger (\partial^\mu \phi) - m_0^2 \phi^\dagger \phi - \frac{1}{4}\lambda \left(\phi^\dagger \phi\right)^2 \tag{C.7}$$

$$\tag{C.8}$$

Consequently, the physics implied by the lagrangian also does not change. It is important that the rotation is not dependent on spacetime coordinates because if it was, then the partial derivatives would act on the rotation, extra terms would arise, and the lagrangian would therefore not be invariant under the transformation.

Symmetries in physics imply conservation of some property. Invariance to spatial location implies conservation of momentum; Invariance to temporal location implies conservation of energy; etc. In this case, invariance to rotations in the complex plane implies conservation by charge, which can be derived by studying the lagrangian under an infinitesimal $U(1)$ transformation $\phi \to \phi' = (1 + i\alpha)\phi$[25]. However, this is not the task at hand.

If we assume $m_0^2 > 0$, then the potential simply has a unique and stable extremum at the origin. The quantum theoretical prescription for calculating the particle state spectrum is to determine small harmonic oscillations about this minimum. The symmetry about the origin is stable and would remain unbroken.

If, however, $m_0^2 < 0$, then the potential still exhibits the same cylindrical symmetry, but the extremum at the origin is now a maximum and there is a minima ring that assumes the lowest value of the potential. The potential at the origin is unstable, and so it is natural for the symmetry to "break" by having such a state fall to one corresponding to the minima ring.

Determining the particle spectrum now requires choosing some point on the minima circle to perform the perturbative expansion. The minima manifold is found at

$$\frac{dV}{d(\phi^\dagger\phi)} = m_0^2 + \frac{\lambda}{4}2\phi^\dagger\phi = 0 \tag{C.9}$$

$$\phi^\dagger\phi = -\frac{2m_0^2}{\lambda} \tag{C.10}$$

$$v \equiv \sqrt{\phi_1^2 + \phi_2^2} = \sqrt{\frac{-4m_0^2}{\lambda}} \tag{C.11}$$

The new parameter v is then the radius of the circle.

One way to proceed is to expand about the point $\phi_1 = v_1, \phi_2 = 0$. Let

$$\phi(x) = \frac{1}{\sqrt{2}}\left(v + \eta(x) + i\xi(x)\right) \tag{C.12}$$

Then $\eta(x)$ is a field perturbation in the $\Re$ direction and the perturbation $\xi(x)$ in the purely $\Im$ direction. We find the consequent particle spectrum by putting this expression of $\phi(x)$ back into the lagrangian.

$$\mathcal{L} = \left(\partial_\mu\phi\right)^\dagger\left(\partial^\mu\phi\right) - m_0^2\phi^\dagger\phi - \frac{1}{4}\lambda\left(\phi^\dagger\phi\right)^2 \tag{C.13}$$

$$= \frac{1}{2}\left(v + \partial_\mu\eta - i\partial_\mu\xi\right)\left(v + \partial^\mu\eta + i\partial^\mu\xi\right) - \frac{m_0^2}{2}\left(v + \eta - i\xi\right)\left(v + \eta + i\xi\right) \tag{C.14}$$

$$- \frac{1}{16}\lambda\left[\left(v + \eta - i\xi\right)\left(v + \eta + i\xi\right)\right]^2 \tag{C.15}$$

$$= \frac{1}{2}(\partial_\mu\xi)^2 + \frac{1}{2}(\partial_\mu\eta)^2 + m_0^2\eta^2 + (\text{cubic and quartic terms}) \tag{C.16}$$

$$\tag{C.17}$$

From the $m_0^2\eta^2$ term, we see the η-field perturbation is associated with a particle of mass $m_\eta = \sqrt{-2m_0^2}$. There is no mass term for the ξ-field. In attempting to generate a massive gauge boson, spontaneously broken gauge theory has provided its own massless particle.

Pictorially, notice that the η-perturbation (the one that does result in a massive particle) climbs up the potential well while the ξ-perturbation (the massless one) is directed tangent to the circular minima manifold. Perturbing up the potential well implies the existence of an associated massive particle state.

This suggests a possibly more appropriate choice of how to parameterize the field perturbations. Remember that the choice to expand about $\phi_1 = v, \phi_2 = 0$ was arbitrary. Let's parameterize the perturbations in polar, rather than cartesian, coordinates. That way, we need not specify where on the minima manifold we expand around; the argument applies equivalently to all choices. One field perturbation will be in the radial direction, the other in the angular.

$$\phi(x) = \underbrace{\frac{\rho(x)}{\sqrt{2}}}_{\text{Radial Perturbation}} \cdot \underbrace{e^{\frac{i}{v}\theta(x)}}_{\text{Angular Perturbation}} \tag{C.18}$$

Since the minima manifold has a radius v, $\rho(x) = v + h(x)$ (spoiler alert: the letter "h" is chosen for this perturbation off the potential minimum because this is a precursor to the Higgs boson).

Just as before, we put $\phi(x)$ back into the lagrangian and see what the particle spectrum looks like.

$$\mathcal{L} = (\partial_\mu \phi)^\dagger (\partial^\mu \phi) - m_0^2 \phi^\dagger \phi - \frac{1}{4}\lambda \left(\phi^\dagger \phi\right)^2 \tag{C.19}$$

$$= \frac{1}{\sqrt{2}} e^{-\frac{i}{v}\theta(x)} \left[\partial_\mu \rho(x) - \frac{i}{v}\rho(x)\partial_\mu \theta(x)\right] \frac{1}{\sqrt{2}} e^{\frac{i}{v}\theta(x)} \left[\partial^\mu \rho(x) + \frac{i}{v}\rho(x)\partial^\mu \theta(x)\right] \tag{C.20}$$

$$- \frac{1}{2}m_0^2 \rho^2(x) - \frac{1}{16}\lambda \rho^4(x) \tag{C.21}$$

$$= \frac{1}{2}\left[(\partial_\mu \rho)(\partial^\mu \rho) + \frac{1}{v^2}\rho^2 (\partial_\mu \theta)(\partial^\mu \theta)\right] - \frac{1}{2}m_0^2 \rho^2 - \frac{1}{16}\lambda \rho^4 \tag{C.22}$$

$$= \frac{1}{2}(\partial_\mu h + v)(\partial^\mu h + v) + \frac{1}{2v^2}(h+v)^2 (\partial_\mu \theta)^2 - \frac{1}{2}m_0^2 (h^2 + 2vh + v^2) - \frac{1}{16}\lambda (h+v)^4 \tag{C.23}$$

$$= \frac{1}{2}(\partial_\mu h)^2 + v(\partial_\mu h) + \frac{1}{2}v^2 + \left(\frac{1}{2v^2}h^2 + \frac{1}{v^2}hv + \frac{1}{2v^2}v^2\right)(\partial_\mu \theta)^2 \tag{C.24}$$

$$- \frac{1}{2}m_0^2 h^2 - m_0^2 vh - \frac{1}{2}m_0^2 v^2 - \frac{1}{16}\lambda (h+v)^4 \tag{C.25}$$

$$= \frac{1}{2}(\partial_\mu h)^2 + \frac{1}{2}(\partial_\mu \theta)^2 - \frac{1}{2}m_0^2 h^2 + \cdots \tag{C.26}$$

$$\tag{C.27}$$

Hence, choosing any arbitrary location on the minima manifold and calculating the particle spectrum via field perturbations, we have kinetic terms for both $h(x)$ and $\theta(x)$, but a mass term only

for $h(x)$. Also, given this parametrization of $\phi(x)$, the vacuum expectation value is

$$\langle 0 \mid \phi \mid 0 \rangle = \frac{v}{\sqrt{2}} \tag{C.28}$$

This is a situation where a symmetric field potential is spontaneously broken in nature and this breaking manifests in a physics different from the situation of the origin being a stable extremum, in which case the symmetry would not spontaneously break in nature.

Appendix D: $U(1)$ Local Symmetry Breaking

The situation of global $U(1)$ symmetry explored in section C is a special case of the topic of this section, local $U(1)$ symmetry. This scenario is also referred to as the "abelian [commutative] Higgs model."[12] It is not the fully Standard Model version, but still a critical step toward understanding the Higgs sector of the Standard Model. For that reason, the detailed treatment presented in these sections C through F are included in this thesis.

Recall the postulated globally gauge invariant lagrangian from section C.

$$\mathcal{L} = (\partial_\mu \phi)^\dagger (\partial^\mu \phi) - m_0^2 \phi^\dagger \phi - \frac{1}{4}\lambda \left(\phi^\dagger \phi\right)^2 \tag{D.1}$$

To make this lagrangian invariant to local gauge transformations, we must replace the derivatives with "covariant derivatives" to keep the lagrangian invariant under transformation. The covariant derivative is not derived–we postulate the desired covariant derivative and consider its form to be justified by the fact that it works

$$\partial_\mu \rightarrow D_\mu = \partial_\mu + iqA_\mu \tag{D.2}$$

and include a kinetic term for the "gauge field" A_μ that must be included to keep the lagrangian invariant under a local $U(1)$ transformation.

$$\mathcal{L} = [(\partial^\mu + iqA^\mu)\phi]^\dagger [(\partial_\mu + iqA_\mu)\phi] - \frac{1}{4}F_{\mu\nu}F^{\mu\nu} - \frac{1}{4}\lambda(\phi^\dagger\phi)^2 - m_0^2(\phi^\dagger\phi) \tag{D.3}$$

$$\tag{D.4}$$

where $F^{\mu\nu} = \partial^\mu A^\nu - \partial^\nu A^\mu$. Notice this part is the form of the Maxwell lagrangian and A^μ is analogous to the photon. We shall return to this point shortly.

This lagrangian is then invariant to a *local* $U(1)$ field transformation

$$\phi(x) \rightarrow \phi'(x) = e^{-i\alpha(x)}\phi(x) \tag{D.5}$$

or, in infinitesimal form

$$\phi(x) \rightarrow \phi'(x) = (1 - i\alpha(x))\phi(x) \tag{D.6}$$

We still do not know now the gauge field itself transforms. The point of this covariant derivative is to have $D^\mu\phi$ transform the same way ϕ does. So assume

$$D'^\mu\phi' = (1 - i\alpha(x))D^\mu\phi \tag{D.7}$$

to be true and derive the transformation law for A_μ from it.

$$(\partial^\mu + iqA'^\mu)\phi' = (1 - i\alpha(x))(\partial^\mu + iqA^\mu)\phi \tag{D.8}$$

Since this is an infinitesimal transformation, the transformation of A^μ should have a general form $A^\mu \to A'^\mu = A^\mu + \delta A^\mu$. Note that both $\alpha(x)$ and δA^μ are infinitesimals, so any terms infinitesimal to the 2^{nd} order or higher drop.

$$(\partial^\mu + iqA^\mu + iq\delta A^\mu)(1 - i\alpha(x))\phi = (1 - i\alpha(x))(\partial^\mu + iqA^\mu)\phi \tag{D.9}$$

$$(-i\partial^\mu\alpha(x) + iq\delta A^\mu)\phi = (-i\alpha(x)\partial^\mu)\phi \tag{D.10}$$

$$iq\delta A^\mu\phi = (i\partial^\mu\alpha(x) - i\alpha(x)\partial^\mu)\phi \tag{D.11}$$

$$q\delta A^\mu\phi = \partial^\mu(\alpha\phi) - \alpha(\partial^\mu\phi) \tag{D.12}$$

$$q\delta A^\mu\phi = (\partial^\mu\alpha)\phi \tag{D.13}$$

$$\delta A^\mu = \frac{1}{q}\partial^\mu\alpha \tag{D.14}$$

Hence, the gauge field transforms as

$$A^\mu(x) \to A'^\mu(x) = A^\mu(x) + \frac{1}{q}\partial^\mu\alpha(x) \tag{D.15}$$

Now we'll see how the gauge field A^μ absorbs the massless boson θ that was present in the treatment of the global $U(1)$ case in section C.

Recalling the Maxwell term in the lagrangian, let's study the field equation for A^μ

$$\Box A^\nu - \partial^\nu(\partial_\mu A^\mu) = j^\nu_{\text{em}} = iq(\phi^\dagger(\partial^\nu\phi) - (\partial^\nu\phi)^\dagger\phi) - 2q^2A^\nu\phi^\dagger\phi \tag{D.16}$$

Now recall the $U(1)$ field parametrization for spontaneous symmetry breaking

$$\phi(x) = \underbrace{\frac{v + h(x)}{\sqrt{2}}}_{\text{Radial Perturbation}} \cdot \underbrace{e^{-\frac{i}{v}\theta(x)}}_{\text{Angular Perturbation}} \tag{D.17}$$

The current becomes

$$j^\nu_{\text{em}} = iq\Bigg[\frac{1}{\sqrt{2}}(v+h)e^{\frac{i}{v}\theta(x)}\left(\frac{1}{\sqrt{2}}(v+(\partial^\nu h))e^{-\frac{i}{v}\theta(x)}\right)+\frac{1}{\sqrt{2}}(v+h)\left(\frac{-i}{v}(\partial^\nu\theta)\right)e^{-\frac{i}{v}\theta(x)} \tag{D.18}$$

$$-\left(\frac{1}{\sqrt{2}}(v+(\partial^\nu h))e^{\frac{i}{v}\theta(x)}\frac{1}{\sqrt{2}}(v+h)\frac{i}{v}(\partial^\nu\theta)e^{\frac{i}{v}\theta(x)}\right)\frac{1}{\sqrt{2}}(v+h)e^{-\frac{i}{v}\theta(x)}\Bigg] \tag{D.19}$$

$$-2q^2A^\nu\cdot\frac{1}{2}(v+h)^2 \tag{D.20}$$

$$j^\nu_{\text{em}} = -\frac{iq}{2}\Bigg[(v+h)(v+\partial^\nu h)+(v+h)^2\left(\frac{-i}{v}\partial^\nu\theta\right) \tag{D.21}$$

$$-(v+\partial^\nu h)(v+h)-(v+h)^2\left(\frac{i}{v}\partial^\nu\theta\right)\Bigg] \tag{D.22}$$

$$-q^2A^\nu(v+h)^2 \tag{D.23}$$

$$\tag{D.24}$$

$$j^\nu_{\text{em}} = -\frac{iq}{2}\left[\frac{2i}{v}(v+h)^2\partial^\nu\theta\right]-q^2A^\nu(v+h)^2 \tag{D.25}$$

$$j^\nu_{\text{em}} = \frac{q}{v}(v+h)^2\partial^\nu\theta-q^2A^\nu(v+h)^2 \tag{D.26}$$

$$j^\nu_{\text{em}} = -v^2q^2\left(A^\nu-\frac{\partial^\nu\theta}{vq}\right)+\text{higher order terms} \tag{D.27}$$

Using only the linear term for the current, put it back into the field equation for A^ν

$$\Box A^\nu-\partial^\nu(\partial_\mu A^\mu) = j^\nu_{\text{em}} \tag{D.28}$$

$$\Box A^\nu-\partial^\nu(\partial_\mu A^\mu) = -v^2q^2\left(A^\nu-\frac{\partial^\nu\theta}{vq}\right) \tag{D.29}$$

Now recall that a gauge transformation on A^μ has the form $A^\mu(x)\rightarrow A'^\mu(x)+\frac{1}{q}\partial^\mu\alpha(x)$, and notice that the right hand side already has this form. As such, define

$$A'^\nu = A^\nu-\frac{\partial^\nu\theta}{vq} \tag{D.30}$$

Then the field equation becomes

$$\Box A'^\nu-\partial^\nu\partial_\mu A'^\mu = -v^2q^2A'^\nu \tag{D.31}$$

$$\boxed{\left(\Box + v^2 q^2\right) A'^{\nu} - \partial^{\nu}\partial_{\mu} A'^{\mu} = 0} \tag{D.32}$$

Finally, we see that the field equation becomes a free massive vector field for a particle with mass vq. In particular, notice how the appropriate choice of gauge allowed the massless gauge field A^{ν} to absorb the θ ("Goldstone" boson) field term and become massive as a result.

Summarily, generalizing from global to local $U(1)$ symmetry breaking required us to introduce a "gauge field" A^{ν} in order to keep the lagrangian invariant, or symmetric, under $U(1)$ transformations. After deriving the manner in which A^{ν} itself transforms, we were able to choose a particular "gauge," or $U(1)$ transformation, that allows it to absorb the θ field (pertubations along the angular direction of the circular minima manifold of the previous section). In the end, we no longer had a θ field at all, but rather the gauge field A^{ν} that became massive after absorbing the θ field. What has just happened here is important for understanding how the Higgs boson is related to the photon and weak vector boson in the Standard Model theory.

Appendix E: $SU(2)$ Global Symmetry Breaking

The "special unitary group" $SU(2)$ transformations we will be considering in this section are similar to the $U(1)$ case of sections C and D, except that the rotation angle α now becomes rank-2 matrices $\vec{\alpha} \cdot \vec{\tau}$.

To recap, global $U(1)$ symmetry breaking lead to two fields: a massive field $h(x)$ and a massless field $\theta(x)$. Extending to local $U(1)$ symmetry required us to introduce a gauge boson A^ν and we exploited the gauge symmetry to have A^ν absorb the $\theta(x)$ field and become massive. Now, we will see that by generalizing the same arguments to global $SU(2)$ symmetry we will end up with another massive $H(x)$ field and three $\theta(x)$ fields instead of one.

Consider an $SU(2)$ doublet of complex bosons

$$\phi = \begin{bmatrix} \phi^+ \\ \phi^0 \end{bmatrix} = \begin{bmatrix} \frac{1}{\sqrt{2}}(\phi_1 + i\phi_2) \\ \frac{1}{\sqrt{2}}(\phi_3 + i\phi_4) \end{bmatrix} \tag{E.1}$$

where ϕ^+ destroys positively charged particles and creates negatively charged particle, and ϕ^0 destroys neutral particles and creates neutral antiparticles.

Postulate the form of the lagrangian as a direct generalization of the previous two sections

$$\mathcal{L} = (\partial_\mu \phi)^\dagger (\partial^\mu \phi) - m_0^2 \phi^\dagger \phi - \frac{\lambda}{4}(\phi^\dagger \phi)^2 \tag{E.2}$$

where $m_0^2 < 0$. This lagrangian is not only invariant to $SU(2)$ transformations, but also to the global $U(1)$ transformations of section C. We treat the global $SU(2)$ case here, so α is not dependent on spacetime coordinate.

$$\phi \to \phi' = e^{-\frac{i}{2}\vec{\alpha}\cdot\vec{\tau}}\phi \qquad \text{for } SU(2) \tag{E.3}$$

$$\phi \to \phi' = e^{-i\alpha}\phi \qquad \text{for } U(1) \tag{E.4}$$

The minimum occurs at

$$\frac{\partial \mathcal{L}}{\partial(\phi^\dagger \phi)} = -m_0^2 - \frac{\lambda}{2}(\phi^\dagger \phi)_{\text{min}} = 0 \tag{E.5}$$

$$(\phi^\dagger \phi)_{\text{min}} = \frac{-2m_0^2}{\lambda} \equiv \frac{v^2}{2} \tag{E.6}$$

As before, we take the minimum to be the vacuum.

$$\langle 0 \mid \phi^\dagger \phi \mid 0 \rangle = \frac{v^2}{2} = \langle 0 \mid \phi_1^2 + \phi_2^2 + \phi_3^2 + \phi_4^2 \mid 0 \rangle \tag{E.7}$$

To obtain the particle spectrum we expand the fields ϕ about the choice of vacuum. Again, rather than a single point, we have a whole space of minima to choose from. Let,

$$\langle 0 \mid \phi \mid 0 \rangle = \begin{bmatrix} 0 \\ \frac{v}{\sqrt{2}} \end{bmatrix} \tag{E.8}$$

Oscillations about this vacuum choice are parametrized by

$$\phi = e^{-\frac{i}{2}(\vec{\theta}(x)\cdot\vec{\tau})v} \begin{bmatrix} 0 \\ \frac{1}{\sqrt{2}}(v + H(x)) \end{bmatrix} \tag{E.9}$$

We have here three fields $\vec{\theta}$ for possible "angular" oscillations associated with the $SU(2)$ symmetry, and one radial field oscillation $H(x)$. We shall see now that only the $H(x)$ field has nonzero mass, indicating that each $\vec{\theta}$ field oscillates in a direction within the minima manifold, i.e. does not climb the potential just as in the global $U(1)$ case. To do this, put ϕ back into the lagrangian and look for mass terms.

$$\partial^\mu \phi = \begin{bmatrix} 0 \\ -\frac{i}{2v}((\partial^\mu \vec{\theta}) \cdot \vec{\tau}) e^{-\frac{i}{2v}\vec{\theta}\cdot\vec{\tau}} \frac{1}{\sqrt{2}}(v + H) + e^{-\frac{i}{2v}\vec{\theta}\cdot\vec{\tau}} \frac{1}{\sqrt{2}} \partial^\mu H \end{bmatrix} \tag{E.10}$$

$$= e^{-\frac{i}{2v}\vec{\theta}\cdot\vec{\tau}} \begin{bmatrix} 0 \\ \frac{-i}{2\sqrt{2}v}((\partial^\mu \vec{\theta}) \cdot \vec{\tau})(v + H) + \frac{1}{\sqrt{2}} \partial^\mu H \end{bmatrix} \tag{E.11}$$

Similarly,

$$(\partial^\mu \phi)^\dagger = \begin{bmatrix} 0 & \frac{i}{2\sqrt{2}v}((\partial^\mu \vec{\theta}) \cdot \vec{\tau})(v + H) + \frac{1}{\sqrt{2}} \partial^\mu H \end{bmatrix} \tag{E.12}$$

Putting these terms into the lagrangian, we get:

$$\mathcal{L} = \frac{1}{8v^2}(\partial^\mu \vec{\theta} \cdot \vec{\tau})(\partial_\mu \vec{\theta} \cdot \vec{\tau})(v + H)^2 + \frac{1}{2}(\partial^\mu H)(\partial_\mu H) - \frac{m_0^2}{2} v^2 - \frac{m_0^2}{2} vH - \frac{m_0^2}{2} H^2 - \frac{\lambda}{4}(v + H)^4 \tag{E.13}$$

Mass terms with different fields multiplied govern the interaction between the fields. Notice now since $\vec{\theta}(x)$ only appear in an exponent in the field ϕ, it only has derivative terms in the lagrangian. Thus, the particles associated with the $\vec{\theta}$ fields are massless. Only the $H(x)$ has a mass term.

Appendix F: $SU(2)$ Local Symmetry Breaking

Let's now generalize the $SU(2)$ global invariance of the previous section to local invariance in the same manner we did for $U(1)$ transformations in section D.

Local $SU(2)$ gauge transformations have the form

$$\phi(x) \rightarrow \phi'(x) = e^{\frac{ig}{2}\vec{\tau}\cdot\vec{\alpha}(x)}\phi(x) \tag{F.1}$$

where the factor g is inserted to represent the coupling strength.

Just as in the case of electromagnetic interactions, no lagrangian for a free particle can be Lorentz invariant under this local gauge transformation. To make it Lorentz invariant, the derivative must be replaced by a covariant derivative. This way, $D^\mu\phi$ transforms the same way ϕ does, whereas $\partial^\mu\phi$ does not. Just as in the $U(1)$ case, this will necessarily involve the introduction of new gauge fields.

In the $SU(2)$ case,

$$\partial^\mu\phi'(x) = e^{\frac{ig}{2}\vec{\tau}\cdot\vec{\alpha}(x)}(\partial^\mu\phi(x)) + \frac{ig}{2}\vec{\tau}\cdot(\partial^\mu\vec{\alpha}(x))e^{\frac{ig}{2}\vec{\tau}\cdot\vec{\alpha}(x)}\phi(x) \tag{F.2}$$

where it is the second term that breaks the covariance.

The covariant derivative D^μ must act like:

$$D'^\mu\phi'(x) = e^{\frac{ig}{2}\vec{\tau}\cdot\vec{\alpha}(x)}\phi(x)D^\mu\phi(x) \tag{F.3}$$

The form of D^μ is just postulated, then justified by the fact that it works.

$$D^\mu \equiv \partial^\mu + \frac{ig}{2}\vec{\tau}\cdot\vec{W}^\mu \tag{F.4}$$

where $\vec{W}^\mu \equiv (W_1^\mu, W_2^\mu, W_3^\mu)$, a slight precursor to the weak vector bosons.

The $\vec{W}^\mu$ are the $SU(2)$ gauge fields, analogous to the $U(1)$ gauge field A^μ, and the $\vec{\tau}$ are the Pauli spin matrices.

$$\vec{\tau}\cdot\vec{W}^\mu = \begin{bmatrix}0 & 1\\ 1 & 0\end{bmatrix} W_1^\mu + \begin{bmatrix}0 & -i\\ i & 0\end{bmatrix} W_2^\mu + \begin{bmatrix}1 & 0\\ 0 & -1\end{bmatrix} W_3^\mu \tag{F.5}$$

$$= \begin{bmatrix}0 & W_1^\mu\\ W_1^\mu & 0\end{bmatrix} + \begin{bmatrix}0 & -iW_2^\mu\\ iW_2^\mu & 0\end{bmatrix} + \begin{bmatrix}W_3^\mu & 0\\ 0 & -W_3^\mu\end{bmatrix} \tag{F.6}$$

$$= \begin{bmatrix}W_3^\mu & W_1^\mu - iW_2^\mu\\ W_1^\mu + iW_2^\mu & -W_3^\mu\end{bmatrix} \tag{F.7}$$

Remember that the three gauge fields $\vec{W}^\mu$ are spacetime dependent.

Let's examine the $SU(2)$ transformation in infinitesimal form

$$\phi' = \left(1 + \frac{ig}{2}\vec{\tau}\cdot\vec{\epsilon}(x)\right)\phi \tag{F.8}$$

$$\partial\phi' = \left(1 + \frac{ig}{2}\vec{\tau}\cdot\vec{\epsilon}(x)\right)\partial^\mu\phi + \frac{ig}{2}\vec{\tau}\cdot(\partial^\mu\vec{\epsilon})\phi \tag{F.9}$$

We again see the noncovariant term. Let's use the covariant derivative instead.

$$D'^\mu\phi' = \left(1 + \frac{ig}{2}\vec{\tau}\cdot\vec{\epsilon}(x)\right)D^\mu\phi \tag{F.10}$$

$$\left(\partial^\mu + \frac{ig}{2}\vec{\tau}\cdot\vec{W'}^\mu\right)\left[1 + \frac{ig}{2}\vec{\tau}\cdot\vec{\epsilon}(x)\right]\phi = \left[1 + \frac{ig}{2}\vec{\tau}\cdot\vec{\epsilon}(x)\right]\left(\partial^\mu + \frac{ig}{2}\vec{\tau}\cdot\vec{W}^\mu\right)\phi \tag{F.11}$$

So far, we do not know how the gauge fields W^μ transform (notice that both $\vec{W'}^\mu$ and $\vec{W}^\mu$ appear). We proceed by assuming that the previous equality does, in fact, hold; and determine the transformation law for $\vec{W}^\mu$ from it.

The previous equality involves an infinitesimal transformation, so the transformation of $\vec{W}^\mu$ must look something like

$$\vec{W}^\mu \to \vec{W'}^\mu = \vec{W}^\mu + \delta\vec{W}^\mu \tag{F.12}$$

Let's start the algebra.

$$\left[\partial^\mu + \frac{ig}{2}\vec{\tau}\cdot\vec{W'}^\mu\right]\left[1+\frac{ig}{2}\vec{\tau}\cdot\vec{\epsilon}(x)\right]\phi = \left[1+\frac{ig}{2}\vec{\tau}\cdot\vec{\epsilon}(x)\right]\left[\partial^\mu + \frac{ig}{2}\vec{\tau}\cdot\vec{W}^\mu\right]\phi \tag{F.13}$$

$$\left[\partial^\mu + \frac{ig}{2}\vec{\tau}\cdot\vec{W}^\mu + \frac{ig}{2}\vec{\tau}\cdot\delta\vec{W}^\mu\right]\left[1+\frac{ig}{2}\vec{\tau}\cdot\vec{\epsilon}(x)\right]\phi = \left[1+\frac{ig}{2}\vec{\tau}\cdot\vec{\epsilon}(x)\right]\left[\partial^\mu + \frac{ig}{2}\vec{\tau}\cdot\vec{W}^\mu\right]\phi \tag{F.14}$$

$$\left[\frac{ig}{2}\vec{\tau}\cdot\partial^\mu\vec{\epsilon} - \frac{1}{4}g^2(\vec{\tau}\cdot\vec{W}^\mu)(\vec{\tau}\cdot\vec{\epsilon})\frac{ig}{2}\vec{\tau}\cdot\delta\vec{W}^\mu\right]\phi = \left[\frac{ig}{2}(\vec{\tau}\cdot\vec{\epsilon})\partial^\mu - \frac{g^2}{4}(\vec{\tau}\cdot\vec{\epsilon})(\vec{\tau}\cdot\vec{W}^\mu)\right]\phi \tag{F.15}$$

$$\frac{ig}{2}\vec{\tau}\cdot\partial^\mu(\vec{\epsilon}\phi) - \frac{1}{4}g^2(\vec{\tau}\cdot\vec{W}^\mu)(\vec{\tau}\cdot\vec{\epsilon})\phi + \frac{ig}{2}\vec{\tau}\cdot(\delta\vec{W}^\mu)\phi = \frac{ig}{2}\vec{\tau}\cdot(\vec{\epsilon}\partial^\mu\phi) - \frac{g^2}{4}(\vec{\tau}\cdot\vec{\epsilon})(\vec{\tau}\cdot\vec{W}^\mu)\phi \tag{F.16}$$

$$\frac{ig}{2}\vec{\tau}\cdot(\delta\vec{W}^\mu)\phi = \frac{ig}{2}\vec{\tau}\cdot[\vec{\epsilon}(\partial^\mu\phi) - \partial^\mu(\vec{\epsilon}\phi)] + \frac{g^2}{4}\left[(\vec{\tau}\cdot\vec{W}^\mu)(\vec{\tau}\cdot\vec{\epsilon}) - (\vec{\tau}\cdot\vec{\epsilon})(\vec{\tau}\cdot\vec{W}^\mu)\right]\phi \tag{F.17}$$

$$\frac{ig}{2}\vec{\tau}\cdot(\delta\vec{W}^\mu)\phi = \frac{ig}{2}\vec{\tau}\cdot[-(\partial^\mu\vec{\epsilon})\phi] + \frac{g^2}{4}\left[(\vec{\tau}\cdot\vec{W}^\mu)(\vec{\tau}\cdot\vec{\epsilon}) - (\vec{\tau}\cdot\vec{\epsilon})(\vec{\tau}\cdot\vec{W}^\mu)\right]\phi \tag{F.18}$$

$$ig\frac{\vec{\tau}\cdot(\delta\vec{W}^\mu)}{2} = -ig\frac{\vec{\tau}\cdot(\partial^\mu\vec{\epsilon}(x))}{2} + (ig)^2\left[\left(\frac{\vec{\tau}\cdot\vec{\epsilon}}{2}\right)\left(\frac{\vec{\tau}\cdot\vec{W}^\mu}{2}\right) - \left(\frac{\vec{\tau}\cdot\vec{W}^\mu}{2}\right)\left(\frac{\vec{\tau}\cdot\vec{\epsilon}}{2}\right)\right] \tag{F.19}$$

$$\vec{\tau}\cdot(\delta\vec{W}^\mu) = -\vec{\tau}\cdot(\partial^\mu\vec{\epsilon}) - \frac{g}{2}\left[(\vec{\tau}\cdot\vec{\epsilon})\left(\vec{\tau}\cdot\vec{W}^\mu\right) - \left(\vec{\tau}\cdot\vec{W}^\mu\right)(\vec{\tau}\cdot\vec{\epsilon})\right] \tag{F.20}$$

(F.21)

Let's take a closer look at the terms inside the brackets alone.

$$\left[(\vec{\tau}\cdot\vec{\epsilon})\left(\vec{\tau}\cdot\vec{W}^\mu\right) - \left(\vec{\tau}\cdot\vec{W}^\mu\right)(\vec{\tau}\cdot\vec{\epsilon})\right] = \left(\vec{\epsilon}\cdot\vec{W}^\mu + i\vec{\tau}\cdot\vec{\epsilon}\times\vec{W}^\mu\right) - \left(\vec{W}^\mu\cdot\vec{\epsilon} + i\vec{\tau}\cdot\vec{W}^\mu\times\vec{\epsilon}\right) \tag{F.22}$$

$$= i\vec{\tau}\left(\vec{\epsilon}\times\vec{W}^\mu - \vec{W}^\mu\times\vec{\epsilon}\right) \tag{F.23}$$

$$= i\vec{\tau}\left(\vec{\epsilon}\times\vec{W}^\mu - \vec{\epsilon}\times\vec{W}^\mu\right) \tag{F.24}$$

$$= 2i\vec{\tau}\cdot\left(\vec{\epsilon}\times\vec{W}^\mu\right) \tag{F.25}$$

Let's put this back into equation F.20.

$$\vec{\tau} \cdot (\delta \vec{W}^{\mu}) = -\delta^{\mu}\vec{\epsilon}(x) - g\left[\vec{\epsilon}(x) \times \vec{W}^{\mu}\right] \tag{F.26}$$

$$\tag{F.27}$$

This means the infinitesimal piece is

$$\delta \vec{W}^{\mu} = -\partial^{\mu}\vec{\epsilon}(x) - g\left[\vec{\epsilon}(x) \times \vec{W}^{\mu}\right] \tag{F.28}$$

$$\tag{F.29}$$

Generalizing from global to local transformations introduces the extra $\partial^{\mu}\vec{\epsilon}(x)$ term. Hence, the gauge fields for a local $SU(2)$ gauge (phase) transform as

$$\vec{W'}^{\mu} = \vec{W}^{\mu} - \partial^{\mu}\vec{\epsilon}(x) - g\left[\vec{\epsilon}(x) \times \vec{W}^{\mu}\right] \tag{F.30}$$

$$\tag{F.31}$$

Now that we know how the gauge field and the covariant derivative transform with an $SU(2)$ gauge transformation, we can compute the consequences from our basic postulated lagrangian from equation E.2, which can now be repostulated in $SU(2)$ invariant form

$$\mathcal{L} = (D_{\mu}\phi)^{\dagger}(D^{\mu}\phi) - m_0^2\phi^{\dagger}\phi \; - \frac{\lambda}{4}\left(\phi^{\dagger}\phi\right)^2 - \frac{1}{4}\vec{W}_{\mu\nu} \cdot \vec{W}^{\mu\nu} \tag{F.32}$$

where $\vec{W}_{\mu\nu} \equiv \partial_{\mu}\vec{W}_{\nu} - \partial_{\nu}\vec{W}_{\mu} - g\vec{W}_{\mu} \times \vec{W}_{\nu}$, where the last term is necessary because of the non-Abelian nature of the $SU(2)$ group.

Note that if $m_0^2 > 0$, then we just have a system of four scalar particles of mass m_0. However, we are interested in the $m_0^2 < 0$ case. Just as for the $U(1)$ case, we want to find the minima of the potential and find an entire minima manifold.

$$\frac{\partial \mathcal{L}}{\partial(\phi^{\dagger}\phi)} = 0 \tag{F.33}$$

$$(\phi^{\dagger}\phi)_{\text{min}} = -\frac{2m_0^2}{\lambda} = \frac{1}{2}\left(\phi_1^2 + \phi_2^2 + \phi_3^2 + \phi_4^2\right) \tag{F.34}$$

We must choose some particular point on the minima manifold upon which to expand and calculate the particle spectrum, so choose $\phi_1 = \phi_2 = \phi_4 = 0$ and then we are left with

$$\frac{1}{2}\phi_3^2 = \frac{-2m_0^2}{\lambda} \tag{F.35}$$

$$\phi_3 = 2\sqrt{\frac{-m_0^2}{\lambda}} \equiv v \tag{F.36}$$

Then our complex field doublet at this minimum becomes

$$\phi_{\text{min}} = \frac{1}{\sqrt{2}}\begin{bmatrix}\phi_1 + i\phi_2 \\ \phi_3 + i\phi_4\end{bmatrix} = \frac{1}{\sqrt{2}}\begin{bmatrix}0 \\ v\end{bmatrix} \tag{F.37}$$

Again, completely analogous to the $U(1)$ case, we can parametrize perturbations about this minimum as

$$\phi(x) = \frac{\rho(x)}{\sqrt{2}} e^{\frac{i}{v}\vec{\tau}\cdot\vec{\theta(x)}} \quad \text{, where} \tag{F.38}$$

$$\rho(x) = \begin{bmatrix}0 \\ v + h(x)\end{bmatrix} \tag{F.39}$$

This can be see more intuitively when looked at in infinitesimal form.

Nevertheless, we now have an $SU(2)$ gauge invariant lagrangian with covariant derivatives and we know how the introduced gauge fields $\vec{W}^\mu$ change with an $SU(2)$ transformation. As such, the massless $\vec{\theta}(x)$ fields can be gauged away and we are left with massive $\vec{W}^\mu$ and h fields, another example of the Higgs mechanism.

For Standard Model physics, we will be combining this effect for both the $U(1)$ and $SU(2)$ cases to get the massive weak vector bosons and the photon–the higgs will be a necessary consequence. More details will be worked out in sections G, H, and J.

Appendix G: The Higgs Mechanism in the $SU(2) \times U(1)$ Local Spontaneous Symmetry Breaking

Recall that we had a scalar $SU(2)$ doublet

$$\phi = \begin{bmatrix} \phi^+ \\ \phi^0 \end{bmatrix} \tag{G.1}$$

whose lagrangian is

$$\mathcal{L} = (\partial_\mu \phi)^\dagger (\partial^\mu \phi) - m_0^2 \phi^\dagger \phi - \frac{\lambda}{4}(\phi^\dagger \phi)^2 \tag{G.2}$$

This lagrangian is invariant to $U(1)$ global transformations

$$\phi \to \phi' = e^{-i\alpha}\phi \tag{G.3}$$

and global $SU(2)$ transformations

$$\phi \to \phi' = e^{-\frac{i}{2}\vec{\alpha}\cdot\vec{\tau}}\phi \tag{G.4}$$

For a theory that is invariant to local transformations we must introduce three $SU(2)$ gauge fields (see section F) and one $U(1)$ gauge field (see section D). Denote them here as $W_i^\mu(x)$ for $i = 1, 2, 3$ and $B^\mu(x)$, respectively. Also, the derivatives must be replaced with a covariant derivative for both $U(1)$ and $SU(2)$.

$$D^\mu \phi = \left(\partial^\mu + \underbrace{\frac{ig}{2}\vec{\tau}\cdot\vec{W}^\mu}_{SU(2)\text{piece}} + \underbrace{\frac{ig'}{2}B^\mu}_{U(1)\text{piece}} \right) \phi \tag{G.5}$$

Kinetic terms for the new gauge fields must also be included.

$$\vec{F}^{\mu\nu} = \partial^\mu \vec{W}^\nu - \partial^\nu \vec{W}^\mu - g\vec{W}^\mu \times \vec{W}^\nu \tag{G.6}$$

$$G^{\mu\nu} = \partial^\mu B^\nu - \partial^\nu B^\mu \tag{G.7}$$

So the new full lagrangian is

$$\mathcal{L} = (D_\mu \phi)^\dagger (D^\mu \phi) + m_0^2 \phi^\dagger \phi - \frac{\lambda}{4}\left(\phi^\dagger \phi\right)^2 - \frac{1}{4}\vec{F}_{\mu\nu}\cdot\vec{F}^{\mu\nu} - \frac{1}{4}G_{\mu\nu}G^{\mu\nu} \tag{G.8}$$

$$\tag{G.9}$$

We already looked at spontaneous symmetry breaking for the $U(1)$ and $SU(2)$ cases individually, now we want to do so for the product group $SU(2) \times U(1)$ in such a way that we are left with three massive gauge bosons ($W^{\pm}, Z$) and one massless gauge boson (the photon γ). Being massless, the photon corresponds to some symmetry that is left unbroken. Weinberg suggested [12]

$$\langle 0 \mid \phi \mid 0 \rangle = \begin{bmatrix} 0 \\ \frac{\sqrt{2}m_0}{\sqrt{\lambda}} \end{bmatrix} \equiv \begin{bmatrix} 0 \\ \frac{v}{\sqrt{2}} \end{bmatrix} \tag{G.10}$$

This choice leaves the vacuum invariant to a transformation of $U(1)+$ third component of $SU(2)$. That is,

$$(1+\tau_3)\langle 0 \mid \phi \mid 0 \rangle = (1+\tau_3) \begin{bmatrix} 0 \\ \frac{v}{\sqrt{2}} \end{bmatrix} = \begin{bmatrix} 2 & 0 \\ 0 & 0 \end{bmatrix} \begin{bmatrix} 0 \\ \frac{2}{\sqrt{2}} \end{bmatrix} = \begin{bmatrix} 0 \\ 0 \end{bmatrix} \tag{G.11}$$

where the $\vec{\tau}$ are the Pauli matrices. This is also why we eventually find the electric charge to be expressed in terms of weak hypercharge Y and third component of isospin t_3: $Q = \frac{Y}{2} + t_3$ [25]. We are about to see that this interplay between the $U(1)$ symmetry (corresponding to Y) and the third component of $SU(2)$ symmetry (corresponding to t_3) manifests as a mixing of the W_3^{μ} and B^{μ} gauge fields to yield the photon field A^{μ} and the neutral weak vector boson Z.

To consider oscillations about the vacuum, parametrize the degrees of freedom by

$$\phi = e^{-\frac{i}{2v}\vec{\theta}(x)\cdot\vec{\tau}} \begin{bmatrix} 0 \\ \frac{1}{\sqrt{2}}(v + H(x)) \end{bmatrix} \tag{G.12}$$

However, recall that the three $\vec{\theta}$ field perturbations, which would become Goldstone bosons, disappear if we make the appropriate gauge transformation. So we effectively use

$$\phi = \begin{bmatrix} 0 \\ \frac{1}{\sqrt{2}}(v + H(x)) \end{bmatrix} \tag{G.13}$$

The consequences for the lagrangian are (details of how the following form of the lagrangian are calculated are in section J)

$$\mathcal{L} = \frac{1}{2}(\partial_\mu H)(\partial^\mu H) + \frac{m_0^2}{2}(v+H)^2 - \frac{\lambda}{16}(v+H)^4 - \frac{1}{4}\vec{F}_{\mu\nu} \cdot \vec{F}^{\mu\nu} - \frac{1}{4}G_{\mu\nu}G^{\mu\nu} \tag{G.14}$$

$$\mathcal{L} = \frac{1}{2}(\partial_\mu H)(\partial^\mu H) + \frac{m_0^2}{2}(v+H)^2 - \frac{\lambda}{16}(v+H)^4 \tag{G.15}$$

$$- \frac{1}{4}(\partial_\mu W_{1\nu} - \partial_\nu W_{1\mu})(\partial^\mu W_1^\nu - \partial^\nu W_1^\mu) + \frac{1}{8}g^2 v^2 W_{1\nu} W_1^\nu \tag{G.16}$$

$$- \frac{1}{4}(\partial_\mu W_{2\nu} - \partial_\nu W_{2\mu})(\partial^\mu W_2^\nu - \partial^\nu W_2^\mu) + \frac{1}{8}g^2 v^2 W_{2\nu} W_2^\nu \tag{G.17}$$

$$- \frac{1}{4}(\partial_\mu W_{3\nu} - \partial_\nu W_{3\mu})(\partial^\mu W_3^\nu - \partial^\nu W_3^\mu) - \frac{1}{4}G_{\mu\nu}G^{\mu\nu} \tag{G.18}$$

$$+ \frac{1}{8}v^2(gW_{3\mu} - g'B_\mu)(gW_3^\mu - g'B^\mu) + \text{Higgs interactions} \tag{G.19}$$

The second and third lines show that the W_1 and W_2 gauge fields are massive and have the same mass $m_W = \frac{gv}{2}$. These are the W^+, W^- vector gauge bosons in electroweak theory. The Higgs interaction terms are being ignored here because we are focusing on the generation of the Standard Model gauge bosons in this section. In section J, I will go through the details of deriving the full version of this and discuss the interactions between the Higgs and gauge bosons that are produced. The Higgs boson decaying to gauge bosons is precisely the kind of interaction that this dissertation explores experimentally.

The last two lines show that the gauge fields W_3 and B are mixed. The key clue is to notice in the last line it is the combination $(gW_3^\mu - g'B^\mu)$ that has a mass. Introduce the linear combinations

$$Z^\mu \equiv W_3^\mu \cos\theta_W - B^\mu \sin\theta_W \tag{G.20}$$

$$A^\mu \equiv W_3^\mu \sin\theta_W + B^\mu \cos\theta_W \tag{G.21}$$

where

$$\cos\theta_W = \frac{g}{\sqrt{g^2 + g'^2}} \tag{G.22}$$

$$\sin\theta_W = \frac{g'}{\sqrt{g^2 + g'^2}} \tag{G.23}$$

Or, if we invert them

$$B^\mu = A^\mu \cos\theta_W - Z^\mu \sin\theta_W \tag{G.24}$$

$$W_3^\mu = A^\mu \sin\theta_W + Z^\mu \cos\theta_W \tag{G.25}$$

Using this, we can write the last two lines of the lagrangian in terms of A^μ and Z^μ, instead of B^μ and W_3^μ.

$$-\frac{1}{4}(\partial_\mu W_{3\nu}-\partial_\nu W_{3\mu})(\partial^\mu W_3^\nu-\partial^\nu W_3^\mu)-\frac{1}{4}G_{\mu\nu}G^{\mu\nu}+\frac{v^2}{8}(gW_{3\mu}-g'B_\mu)(gW_3^\mu-g'B^\mu) \tag{G.26}$$

$$=-\frac{1}{4}\left(\partial_\mu(Z_\nu\cos\theta_W+A_\nu\sin\theta_W)-\partial_\nu(Z_\mu\cos\theta_W+A_\mu\sin\theta_W)\right) \tag{G.27}$$

$$\cdot\left(\partial^\mu(Z^\nu\cos\theta_W+A^\nu\sin\theta_W)-\partial^\nu(Z^\mu\cos\theta_W+A^\mu\sin\theta_W)\right) \tag{G.28}$$

$$-\frac{1}{4}\left(\partial_\mu(A_\nu\cos\theta_W-Z_\nu\sin\theta_W)-\partial_\nu(A_\mu\cos\theta_W-Z_\mu\sin\theta_W)\right) \tag{G.29}$$

$$\cdot\left(\partial^\mu(A^\nu\cos\theta_W-Z^\nu\sin\theta_W)-\partial^\nu(A^\mu\cos\theta_W-Z^\mu\sin\theta_W)\right) \tag{G.30}$$

$$+\frac{1}{8}v^2\left(g(Z_\mu\cos\theta_W+A_\mu\sin\theta_W)-g'(A_\mu\cos\theta_W-Z_\mu\sin\theta_W)\right) \tag{G.31}$$

$$\cdot\left(g(Z^\mu\cos\theta_W+A^\mu\sin\theta_W)-g'(A^\mu\cos\theta_W-Z^\mu\sin\theta_W)\right) \tag{G.32}$$

$$=-\frac{1}{4}\left((\partial_\mu Z_\nu-\partial_\nu Z_\mu)\cos\theta_W+(\partial_\mu A_\nu-\partial_\nu A_\mu)\sin\theta_W\right) \tag{G.33}$$

$$\cdot\left((\partial^\mu Z^\nu-\partial^\nu Z^\mu)\cos\theta_W+(\partial^\mu A^\nu-\partial^\nu A^\mu)\sin\theta_W\right) \tag{G.34}$$

$$-\frac{1}{4}\left((\partial_\mu A_\nu-\partial_\nu A_\mu)\cos\theta_W-(\partial_\mu Z_\nu-\partial_\nu Z_\mu)\sin\theta_W\right) \tag{G.35}$$

$$\cdot\left((\partial^\mu A^\nu-\partial^\nu A^\mu)\cos\theta_W-(\partial^\mu Z^\nu-\partial^\nu Z^\mu)\sin\theta_W\right) \tag{G.36}$$

$$+\frac{1}{8}v^2\left(Z_\mu(g\cos\theta_W+g'\sin\theta_W)+A_\mu(g\sin\theta_W-g'\cos\theta_W)\right) \tag{G.37}$$

$$\cdot\left(Z^\mu(g\cos\theta_W+g'\sin\theta_W)+A^\mu(g\sin\theta_W-g'\cos\theta_W)\right) \tag{G.38}$$

Define $\mathcal{F}_{\mu\nu}\equiv\partial_\mu A_\nu-\partial_\nu A_\mu$ and $Z_{\mu\nu}\equiv\partial_\mu Z_\nu-\partial_\nu Z_\mu$.

$$=-\frac{1}{4}(Z_{\mu\nu}\cos\theta_W+\mathcal{F}_{\mu\nu}\sin\theta_W)(Z^{\mu\nu}\cos\theta_W+\mathcal{F}^{\mu\nu}\sin\theta_W) \tag{G.39}$$

$$-\frac{1}{4}(\mathcal{F}_{\mu\nu}\cos\theta_W-Z_{\mu\nu}\sin\theta_W)(\mathcal{F}^{\mu\nu}\cos\theta_W-Z^{\mu\nu}\sin\theta_W) \tag{G.40}$$

$$\frac{1}{8}v^2\left(Z_\mu\frac{g^2+g'^2}{\sqrt{g^2+g'^2}}+A_\mu\frac{gg'-g'g}{\sqrt{g^2+g'^2}}\right)\cdot\left(Z^\mu\frac{g^2+g'^2}{\sqrt{g^2+g'^2}}+A^\mu\frac{gg'-g'g}{\sqrt{g^2+g'^2}}\right) \tag{G.41}$$

$$=-\frac{1}{4}\left(Z_{\mu\nu}Z^{\mu\nu}+\mathcal{F}_{\mu\nu}\mathcal{F}^{\mu\nu}\right)+\frac{1}{8}v^2Z_\mu Z^\mu(g^2+g'^2) \tag{G.42}$$

Hence, we have unmixed the two fields. They become the Z boson and the photon.

$$m_Z = \frac{1}{2}v^2\sqrt{g^2 + g'^2} = \frac{m_W}{\cos\theta_W} \tag{G.43}$$

$$m_A = 0 \tag{G.44}$$

Now that we have our lagrangian in a usable form, we can finally starting calculating the characteristics of Standard Model particles.

Appendix H: The $SU(2)_L \times U(1)_Y$ Local Gauge Invariant Lagrangian and the [massless] Fermions

We know now from section G what our postulated lagrangian should look like in order to be both $U(1)$ and $SU(2)$ invariant, which necessarily involved the weak vector bosons and the photon. Let's look at $SU(2) \times U(1)$ gauge invariance for the first generation of quarks; the calcuation is identical for the higher generations. The calculation for the lepton generations is also very similar and so not repeated in this dissertation.

The Higgs mechanism is *not* included here so the quarks will still be massless; that will be dealt with in section I. Instead, we will deal with fermions that appear as a left-handed doublet and right-handed singlets for both particles. In the end, we will have computed the lagrangian that tells us how these fermions interact with each other, the weak vector gauge bosons, and the photon. The mass terms will, in the absence of the Higgs mechanism, be also absent for this section.

Suppose we have the (fermion) quark doublet

$$q = \begin{bmatrix} u \\ d \end{bmatrix} \tag{H.1}$$

and recall that

$$\psi_L = \left(\frac{1 - \gamma_5}{2} \right) \psi \tag{H.2}$$

$$\psi_R = \left(\frac{1 + \gamma_5}{2} \right) \psi \tag{H.3}$$

are relations distinguishing the left and right handed components.

As always, we must postulate a lagrangian. In the sections exploring $U(1)$ and $SU(2)$ symmetries, we used generalizations of the Klein-Gordon equation's lagrangian for scalar particles. Now we want to look at spin-$1/2$ fermions, so we must use the Dirac lagrangian in our gauge invariant form. This is why I want to explore the case of massless fermions before adding in mass generation from the Higgs mechanism.[25]

Recall the Dirac lagrangian

$$\mathcal{L} = i\bar{\psi}\gamma_\mu \partial^\mu \psi - m\bar{\psi}\psi \tag{H.4}$$

Now we want a massless version for a fermion doublet:

$$\mathcal{L} = \bar{q} i \not{D} q \tag{H.5}$$

$$\mathcal{L} = \bar{q}_L i \not{D}_L q_L + \bar{u}_R i \not{D}_R u_R + \bar{d}_R i \not{D}_R d_R \tag{H.6}$$

where the covariant derivative for the doublet $\not{D}_L$ is $SU(2) \times U(1)$ invariant, and $\not{D}_R$ is only $U(1)$ invariant for the singlet:

$$D_L^\rho = \partial^\rho + \frac{ig}{2}\vec{\tau} \cdot \vec{W}^\rho + \frac{ig'Y}{2} B^\rho \tag{H.7}$$

$$D_R^\rho = \partial^\rho + \frac{ig'Y}{2} B^\rho \tag{H.8}$$

H.1 The $\mathcal{L}_R$ terms

$$\mathcal{L}_R = \bar{u}_R i \not{D} u_R + \bar{d}_R i \not{D} d_R \tag{H.9}$$

$$= \bar{u}_R i \gamma_\rho \left(\partial^\rho \ - \frac{ig'Y}{2} B^\rho \right) u_R + \bar{d}_R i \gamma_\rho \left(\partial^\rho \ - \frac{ig'Y}{2} B^\rho \right) d_R \tag{H.10}$$

$$= i \bar{u}_R \gamma_\rho (\partial^\rho u_R) - \frac{g'Y}{2} \bar{u}_R \gamma_\rho B^\rho u_R + i \bar{d}_R \gamma_\rho (\partial^\rho d_R) - \frac{g'Y}{2} \bar{d}_R \gamma_\rho B^\rho d_R \tag{H.11}$$

$$= i u_R^\dagger \gamma_0 \gamma_\rho (\partial^\rho u_R) - \frac{g'Y}{2} u_R^\dagger \gamma_0 \gamma_\rho B^\rho u_R + i d_R^\dagger \gamma_0 \gamma_\rho (\partial^\rho d_R) - \frac{g'Y}{2} d_R^\dagger \gamma_0 \gamma_\rho B^\rho d_R \tag{H.12}$$

$$= i u^\dagger \left(\frac{1+\gamma_5}{2} \right) \gamma_0 \gamma_\rho \left(\frac{1+\gamma_5}{2} \right) (\partial^\rho u) - \frac{g'Y}{2} u^\dagger \left(\frac{1+\gamma_5}{2} \right) \gamma_0 \gamma_\rho B^\rho \left(\frac{1+\gamma_5}{2} \right) u \tag{H.13}$$

$$+ i d^\dagger \left(\frac{1+\gamma_5}{2} \right) \gamma_0 \gamma_\rho \left(\frac{1+\gamma_5}{2} \right) (\partial^\rho d) - \frac{g'Y}{2} d^\dagger \left(\frac{1+\gamma_5}{2} \right) \gamma_0 \gamma_\rho B^\rho \left(\frac{1+\gamma_5}{2} \right) d \tag{H.14}$$

$$\tag{H.15}$$

Use the fact that γ_5 anticommutes with the other γ_μ's, so $\{\gamma_5, \gamma_\mu\} = 0 \Rightarrow \left(\frac{1+\gamma_5}{2}\right)\gamma_\mu = \left(\frac{\gamma_\mu + \gamma_5\gamma_\mu}{2}\right) = \left(\frac{\gamma_\mu + (-\gamma_\mu\gamma_5)}{2}\right) = \gamma_\mu\left(\frac{1-\gamma_5}{2}\right)$. Also, note that after $\left(\frac{1+\gamma_5}{2}\right)$ commutes past $\gamma_0\gamma_\rho$, $\left(\frac{1+\gamma_5}{2}\right)\left(\frac{1+\gamma_5}{2}\right) =$

$\left(\frac{1+\gamma_5}{2}\right)$.

$$\Rightarrow \mathcal{L}_R = i\bar{u}\gamma_\rho \left(\frac{1+\gamma_5}{2}\right)(\partial^\rho u) - \frac{g'Y}{2}\bar{u}\gamma_\rho B^\rho \left(\frac{1+\gamma_5}{2}\right) u \tag{H.16}$$

$$+ i\bar{d}\gamma_\rho \left(\frac{1+\gamma_5}{2}\right)(\partial^\rho d) - \frac{g'Y}{2}\bar{d}\gamma_\rho B^\rho \left(\frac{1+\gamma_5}{2}\right) d \tag{H.17}$$

We will return to these terms later.

H.2 The $\mathcal{L}_L$ terms

$$\mathcal{L}_L = \bar{q}_L i \not{D} q_L \tag{H.18}$$

As before, note that $\bar{u}_L = u^\dagger \left(\frac{1-\gamma_5}{2}\right)\gamma_0$ and also that

$$\bar{q}_L = \overline{\begin{bmatrix} u_L \\ d_L \end{bmatrix}} = \begin{bmatrix} \bar{u}_L & \bar{d}_L \end{bmatrix} \tag{H.19}$$

$$\mathcal{L}_L = \begin{bmatrix} \bar{u}_L & \bar{d}_L \end{bmatrix} i\gamma_\rho D^\rho \begin{bmatrix} u_L \\ d_L \end{bmatrix} \tag{H.20}$$

$$= \begin{bmatrix} \bar{u}_L & \bar{d}_L \end{bmatrix} i\gamma_\rho \left(\partial^\rho + \frac{ig}{2}\vec{\tau}\cdot\vec{W}^\rho + \frac{ig'Y}{2}B^\rho\right) \begin{bmatrix} u_L \\ d_L \end{bmatrix} \tag{H.21}$$

$$= \underbrace{i \begin{bmatrix} \bar{u}_L & \bar{d}_L \end{bmatrix} \gamma_\rho \partial^\rho \begin{bmatrix} u_L \\ d_L \end{bmatrix}}_{\text{II.A}} \underbrace{- \frac{g}{2} \begin{bmatrix} \bar{u}_L & \bar{d}_L \end{bmatrix} \gamma_\rho \vec{\tau}\cdot\vec{W}^\rho \begin{bmatrix} u_L \\ d_L \end{bmatrix}}_{\text{II.B}} \underbrace{- \begin{bmatrix} \bar{u}_L & \bar{d}_L \end{bmatrix} \frac{g'Y}{2}\gamma_\rho B^\rho \begin{bmatrix} u_L \\ d_L \end{bmatrix}}_{\text{II.C}} \tag{H.22}$$

II.A The Derivative Terms

$$i\begin{bmatrix}\bar{u}_L & \bar{d}_L\end{bmatrix}\gamma_\rho\partial^\rho\begin{bmatrix}u_L\\ d_L\end{bmatrix} = i\begin{bmatrix}\bar{u}_L & \bar{d}_L\end{bmatrix}\begin{bmatrix}\partial\!\!\!/ u_L\\ \partial\!\!\!/ d_L\end{bmatrix} \tag{H.23}$$

$$= i\bar{u}_L\partial\!\!\!/ u_L + i\bar{d}_L\partial\!\!\!/ d_L \tag{H.24}$$

$$= iu^\dagger\left(\frac{1-\gamma_5}{2}\right)\gamma_0\gamma_\rho\left(\frac{1-\gamma_5}{2}\right)(\partial^\rho u) + id^\dagger\left(\frac{1-\gamma_5}{2}\right)\gamma_0\gamma_\rho\left(\frac{1-\gamma_5}{2}\right)(\partial^\rho d) \tag{H.25}$$

$$= iu^\dagger\gamma_0\left(\frac{1+\gamma_5}{2}\right)\gamma_\rho\left(\frac{1-\gamma_5}{2}\right)(\partial^\rho u) + id^\dagger\gamma_0\left(\frac{1+\gamma_5}{2}\right)\gamma_\rho\left(\frac{1-\gamma_5}{2}\right)(\partial^\rho d) \tag{H.26}$$

$$= iu^\dagger\gamma_0\gamma_\rho\left(\frac{1-\gamma_5}{2}\right)^2(\partial^\rho u) + id^\dagger\gamma_0\gamma_\rho\left(\frac{1-\gamma_5}{2}\right)^2(\partial^\rho d) \tag{H.27}$$

$$= iu^\dagger\gamma_0\gamma_\rho\left(\frac{1-\gamma_5}{2}\right)(\partial^\rho u) + id^\dagger\gamma_0\gamma_\rho\left(\frac{1-\gamma_5}{2}\right)(\partial^\rho d) \tag{H.28}$$

$$= i\bar{u}\gamma_\rho\left(\frac{1-\gamma_5}{2}\right)(\partial^\rho u) + i\bar{d}\gamma_\rho\left(\frac{1-\gamma_5}{2}\right)(\partial^\rho d) \tag{H.29}$$

II.B The $W, W^\dagger, W_3$ Terms The key here is to express

$$\frac{1}{2}\vec{\tau}\cdot\vec{W}^\mu = \frac{1}{2}\left[\tau_1 W_1^\mu + \tau_2 W_2^\mu + \tau_3 W_3^\mu\right] \tag{H.30}$$

$$= \frac{1}{\sqrt{2}}\left[\tau_+\left(\frac{W_1^\mu - iW_2^\mu}{\sqrt{2}}\right)\tau_-\left(\frac{W_1^\mu + iW_2^\mu}{\sqrt{2}}\right)\right] + \frac{1}{2}\tau_3 W_3^\mu \tag{H.31}$$

$$= \frac{1}{\sqrt{2}}\left[\tau_+ W^\mu + \tau_- W_\mu^\dagger\right] + \frac{1}{2}\tau_3 W_3^\mu \tag{H.32}$$

Where we denote

$$\tau_+ \equiv \frac{1}{2}(\tau_1 + i\tau_2) = \frac{1}{2}\left[\begin{bmatrix}0 & 1\\ 1 & 0\end{bmatrix} + i\begin{bmatrix}0 & -i\\ i & 0\end{bmatrix}\right] = \frac{1}{2}\begin{bmatrix}0 & 2\\ 0 & 0\end{bmatrix} = \begin{bmatrix}0 & 1\\ 0 & 0\end{bmatrix} \tag{H.33}$$

$$\tau_- \equiv \frac{1}{2}(\tau_1 - i\tau_2) = \frac{1}{2}\left[\begin{bmatrix}0 & 1\\ 1 & 0\end{bmatrix} - i\begin{bmatrix}0 & -i\\ i & 0\end{bmatrix}\right] = \frac{1}{2}\begin{bmatrix}0 & 0\\ 2 & 0\end{bmatrix} = \begin{bmatrix}0 & 0\\ 1 & 0\end{bmatrix} \tag{H.34}$$

$$W^\mu \equiv \frac{W_1^\mu - iW_2^\mu}{\sqrt{2}} \tag{H.35}$$

$$W^{\mu\dagger} \equiv \frac{W_1^\mu + iW_2^\mu}{\sqrt{2}} \tag{H.36}$$

The reason we want to do this is for the following:

$$\frac{1}{\sqrt{2}}\tau_+ W^\mu \begin{bmatrix} u_L \\ d_L \end{bmatrix} = \frac{1}{\sqrt{2}} \begin{bmatrix} 0 & W^\mu \\ 0 & 0 \end{bmatrix} \begin{bmatrix} u_L \\ d_L \end{bmatrix} = \frac{1}{\sqrt{2}} \begin{bmatrix} W^\mu d_L \\ 0 \end{bmatrix} = \frac{W^\mu}{\sqrt{2}} \begin{bmatrix} d_L \\ 0 \end{bmatrix} \tag{H.37}$$

$$\frac{1}{\sqrt{2}}\tau_+ W^{\mu\dagger} \begin{bmatrix} u_L \\ d_L \end{bmatrix} = \frac{1}{\sqrt{2}} \begin{bmatrix} 0 & 0 \\ W^{\mu\dagger} & 0 \end{bmatrix} \begin{bmatrix} u_L \\ d_L \end{bmatrix} = \frac{1}{\sqrt{2}} \begin{bmatrix} 0 \\ W^{\mu\dagger} u_L \end{bmatrix} = \frac{W^\mu}{\sqrt{2}} \begin{bmatrix} 0 \\ u_L \end{bmatrix} \tag{H.38}$$

Notice how the u_L and d_L fields switch positions in the vector. This is what will subsequently allow interactions between these fields via the gauge bosons W^μ.

Lastly,

$$\frac{1}{2}\tau_3 W_3^\mu \begin{bmatrix} u_L \\ d_L \end{bmatrix} = \frac{1}{2} \begin{bmatrix} 1 & 0 \\ 0 & -1 \end{bmatrix} \begin{bmatrix} W_3^\mu u_L \\ W_3^\mu d_L \end{bmatrix} = \frac{1}{2} \begin{bmatrix} W_3^\mu u_L \\ -W_3^\mu d_L \end{bmatrix} = \frac{W_3^\mu}{2} \begin{bmatrix} u_L \\ -d_L \end{bmatrix} \tag{H.39}$$

Now we are ready to return to the term II.B from the lagrangian.

$$\frac{g}{2} \begin{bmatrix} \bar{u}_L & \bar{d}_L \end{bmatrix} \gamma_\rho \vec{\tau} \cdot \vec{W^\rho} \begin{bmatrix} u_L \\ d_L \end{bmatrix} \tag{H.40}$$

$$= g \begin{bmatrix} \bar{u}_L & \bar{d}_L \end{bmatrix} \gamma_\rho \left(\frac{1}{2}\tau_+ (W_1^\rho - iW_2^\rho) + \frac{1}{2}\tau_- (W_1^\rho + iW_2^\rho) + \frac{1}{2}\tau_3 W_3^\rho \right) \begin{bmatrix} u_L \\ d_L \end{bmatrix} \tag{H.41}$$

$$= g \begin{bmatrix} \bar{u}_L & \bar{d}_L \end{bmatrix} \gamma_\rho \left(\frac{1}{\sqrt{2}}\tau_+ W^\rho + \frac{1}{\sqrt{2}}\tau_- W^{\rho\dagger} + \frac{1}{2}\tau_3 W_3^\rho \right) \begin{bmatrix} u_L \\ d_L \end{bmatrix} \tag{H.42}$$

$$= g \begin{bmatrix} \bar{u}_L & \bar{d}_L \end{bmatrix} \gamma_\rho \left(\frac{1}{\sqrt{2}} W^\rho \begin{bmatrix} d_L \\ 0 \end{bmatrix} + \frac{1}{\sqrt{2}} W^{\rho\dagger} \begin{bmatrix} 0 \\ u_L \end{bmatrix} + \frac{1}{2} W_3^\rho \begin{bmatrix} u_L \\ -d_L \end{bmatrix} \right) \tag{H.43}$$

$$= \frac{1}{\sqrt{2}} g \begin{bmatrix} \bar{u}_L & \bar{d}_L \end{bmatrix} \begin{bmatrix} \not{W}^\rho d_L \\ 0 \end{bmatrix} \frac{1}{\sqrt{2}} g \begin{bmatrix} \bar{u}_L & \bar{d}_L \end{bmatrix} \begin{bmatrix} 0 \\ \not{W}^{\dagger\rho} u_L \end{bmatrix} \frac{1}{2} g \begin{bmatrix} \bar{u}_L & \bar{d}_L \end{bmatrix} \begin{bmatrix} \not{W}_3^\rho u_L \\ -\not{W}_3^\rho d_L \end{bmatrix} \tag{H.44}$$

$$= \frac{1}{\sqrt{2}} g \bar{u}_L \not{W}^\rho d_L + \frac{1}{\sqrt{2}} g \bar{d}_L \not{W}^{\dagger\rho} u_L + \frac{1}{2} g \bar{u}_L \not{W}_3^\rho u_L + \frac{1}{2} g \bar{d}_L \left(-\not{W}_3^\rho d_L \right) \tag{H.45}$$

$$\tag{H.46}$$

$$\frac{g}{2}\begin{bmatrix}\bar{u}_L & \bar{d}_L\end{bmatrix}\gamma_\rho\vec{\tau}\cdot\vec{W^\rho}\begin{bmatrix}u_L\\ d_L\end{bmatrix} \tag{H.47}$$

$$= \frac{1}{\sqrt{2}}gu_L^\dagger\gamma_0\gamma_\rho W^\rho d_L + \frac{1}{\sqrt{2}}gd_L^\dagger\gamma_0\gamma_\rho W^{\rho\dagger}u_L + \frac{1}{2}gu_L^\dagger\gamma_0\gamma_\rho W_3^\rho u_L - \frac{1}{2}gd_L^\dagger\gamma_0\gamma_\rho W_3^\rho d_L \tag{H.48}$$

$$= \frac{1}{\sqrt{2}}gu^\dagger\left(\frac{1-\gamma_5}{2}\right)\gamma_0\gamma_\rho W^\rho\left(\frac{1-\gamma_5}{2}\right)d + \frac{1}{\sqrt{2}}gd^\dagger\left(\frac{1-\gamma_5}{2}\right)\gamma_0\gamma_\rho W^{\rho\dagger}\left(\frac{1-\gamma_5}{2}\right)u \tag{H.49}$$

$$+ \frac{1}{2}gu^\dagger\left(\frac{1-\gamma_5}{2}\right)\gamma_0\gamma_\rho W_3^\rho\left(\frac{1-\gamma_5}{2}\right)u - \frac{1}{2}gd^\dagger\left(\frac{1-\gamma_5}{2}\right)\gamma_0\gamma_\rho W_3^\rho\left(\frac{1-\gamma_5}{2}\right)d \tag{H.50}$$

$$= \frac{1}{\sqrt{2}}g\bar{u}\gamma_\rho W^\rho\left(\frac{1-\gamma_5}{2}\right)d + \frac{1}{\sqrt{2}}g\bar{d}\gamma_\rho W^{\rho\dagger}\left(\frac{1-\gamma_5}{2}\right)u \tag{H.51}$$

$$+ \frac{1}{2}g\bar{u}\gamma_\rho W_3^\rho\left(\frac{1-\gamma_5}{2}\right)u - \frac{1}{2}g\bar{d}\gamma_\rho W_3^\rho\left(\frac{1-\gamma_5}{2}\right)d \tag{H.52}$$

It is important to note that while these terms do describe quark interactions, the vertex factors here are not in their final Standard Model form. There are still the CKM matrix elements that govern the strength of the interactions to deal with. The proper form with the CKM matrix elements follows directly from the presence of the Higgs field and is therefore excluded from this section. That problem requires separate treatment.

II.C The B^ρ Field Terms

$$\begin{bmatrix}\bar{u}_L & \bar{d}_L\end{bmatrix}\frac{g'Y}{2}\gamma_\rho B^\rho\begin{bmatrix}u_L\\ d_L\end{bmatrix} \tag{H.53}$$

$$=\frac{g'Y}{2}\begin{bmatrix}\bar{u}_L & \bar{d}_L\end{bmatrix}\begin{bmatrix}\not{B}u_L\\ \not{B}d_L\end{bmatrix} \tag{H.54}$$

$$=\frac{g'Y}{2}\left[\bar{u}_L\not{B}u_L+\bar{d}_L\not{B}d_L\right] \tag{H.55}$$

$$=\frac{g'Y}{2}\left[u_L^\dagger\gamma_0\gamma_\rho B^\rho u_L+d_L^\dagger\gamma_0\gamma_\rho B^\rho d_L\right] \tag{H.56}$$

$$=\frac{g'Y}{2}\left[u^\dagger\left(\frac{1-\gamma_5}{2}\right)\gamma_0\gamma_\rho B^\rho\left(\frac{1-\gamma_5}{2}\right)u+d^\dagger\left(\frac{1-\gamma_5}{2}\right)\gamma_0\gamma_\rho B^\rho\left(\frac{1-\gamma_5}{2}\right)d\right] \tag{H.57}$$

$$=\frac{g'Y}{2}\left[\bar{u}\gamma_\rho\left(\frac{1-\gamma_5}{2}\right)B^\rho u+\bar{d}\gamma_\rho\left(\frac{1-\gamma_5}{2}\right)B^\rho d\right] \tag{H.58}$$

H.3 Find the Z-boson and Photon Interactions

The next task is to mix these terms with the W_3^μ terms from before to yield the photon and Z-boson interactions with the quarks. Note that the work of mixing these fields into A^μ and Z^μ was done in G. So we are going to collect the B^ρ and W_3^ρ terms from II.A, II.B, and II.C, then switch to expressing those terms with A^μ and Z^μ instead. This will yield quark interactions with the photon and Z-boson. Afterward, we will collect all the terms of the lagrangian and express it in a manner that elucidates the electroweak physics of quarks.

$$-\frac{g'Y}{2}\bar{u}\gamma_\rho B^\rho\left(\frac{1+\gamma_5}{2}\right)u-\frac{g'Y}{2}\bar{d}\gamma_\rho B^\rho\left(\frac{1+\gamma_5}{2}\right)d \tag{H.59}$$

$$-\frac{1}{2}g\bar{u}\gamma_\rho W_3^\rho\left(\frac{1-\gamma_5}{2}\right)u+\frac{1}{2}g\bar{d}\gamma_\rho W_3^\rho\left(\frac{1-\gamma_5}{2}\right)d \tag{H.60}$$

$$-\frac{g'Y}{2}\bar{u}\gamma_\rho\left(\frac{1-\gamma_5}{2}\right)B^\rho u-\frac{g'Y}{2}\bar{d}\gamma_\rho\left(\frac{1-\gamma_5}{2}\right)B^\rho d \tag{H.61}$$

$$=-\frac{g'Y}{2}\bar{u}\gamma_\rho\left(\frac{1+\gamma_5}{2}\right)u(-Z^\rho\sin\theta_W+A^\rho\cos\theta_W) \tag{H.62}$$

$$-\frac{g'Y}{2}\bar{d}\gamma_\rho\left(\frac{1+\gamma_5}{2}\right)d(-Z^\rho\sin\theta_W+A^\rho\cos\theta_W) \tag{H.63}$$

$$-\frac{g}{2}\bar{u}\gamma_\rho\left(\frac{1-\gamma_5}{2}\right)u(Z^\rho\cos\theta_W+A^\rho\sin\theta_W) \tag{H.64}$$

$$+\frac{g}{2}\bar{d}\gamma_\rho\left(\frac{1-\gamma_5}{2}\right)d(Z^\rho\cos\theta_W+A^\rho\sin\theta_W) \tag{H.65}$$

$$-\frac{g'Y}{2}\bar{u}\gamma_\rho\left(\frac{1-\gamma_5}{2}\right)u(-Z^\rho\sin\theta_W+A^\rho\cos\theta_W) \tag{H.66}$$

$$-\frac{g'Y}{2}\bar{d}\gamma_\rho\left(\frac{1-\gamma_5}{2}\right)d(-Z^\rho\sin\theta_W+A^\rho\cos\theta_W) \tag{H.67}$$

Use $Y = 1/3$ for u_L; $Y = 4/3$ for u_R; $Y = 1/3$ for d_L; and $Y = -2/3$ for d_R [12].

$$= -\frac{2g'}{3}\bar{u}\gamma_\rho\left(\frac{1+\gamma_5}{2}\right)u(-Z^\rho\sin\theta_W + A^\rho\cos\theta_W) \tag{H.68}$$

$$+ \frac{g'}{3}\bar{d}\gamma_\rho\left(\frac{1+\gamma_5}{2}\right)d(-Z^\rho\sin\theta_W + A^\rho\cos\theta_W) \tag{H.69}$$

$$- \frac{g}{2}\bar{u}\gamma_\rho\left(\frac{1-\gamma_5}{2}\right)u(Z^\rho\cos\theta_W + A^\rho\sin\theta_W) \tag{H.70}$$

$$+ \frac{g}{2}\bar{d}\gamma_\rho\left(\frac{1-\gamma_5}{2}\right)d(Z^\rho\cos\theta_W + A^\rho\sin\theta_W) \tag{H.71}$$

$$- \frac{g'}{6}\bar{u}\gamma_\rho\left(\frac{1-\gamma_5}{2}\right)u(-Z^\rho\sin\theta_W + A^\rho\cos\theta_W) \tag{H.72}$$

$$- \frac{g'}{6}\bar{d}\gamma_\rho\left(\frac{1-\gamma_5}{2}\right)d(-Z^\rho\sin\theta_W + A^\rho\cos\theta_W) \tag{H.73}$$

$$= \frac{2g'}{3}\bar{u}\gamma_\rho\left(\frac{1+\gamma_5}{2}\right)u(Z^\rho\sin\theta_W) - \frac{2g'}{3}\bar{u}\gamma_\rho\left(\frac{1+\gamma_5}{2}\right)u(A^\rho\cos\theta_W) \tag{H.74}$$

$$- \frac{g'}{3}\bar{d}\gamma_\rho\left(\frac{1+\gamma_5}{2}\right)d(Z^\rho\sin\theta_W) + \frac{g'}{3}\bar{d}\gamma_\rho\left(\frac{1+\gamma_5}{2}\right)d(A^\rho\cos\theta_W) \tag{H.75}$$

$$+ \bar{u}\gamma_\rho\left(\frac{1-\gamma_5}{2}\right)uZ^\rho\left(-\frac{1}{2}g\cos\theta_W + \frac{1}{6}g'\sin\theta_W\right) \tag{H.76}$$

$$+ \bar{u}\gamma_\rho\left(\frac{1-\gamma_5}{2}\right)uA^\rho\left(-\frac{1}{2}g\sin\theta_W - \frac{1}{6}g'\cos\theta_W\right) \tag{H.77}$$

$$+ \bar{d}\gamma_\rho\left(\frac{1-\gamma_5}{2}\right)dZ^\rho\left(\frac{1}{2}g\cos\theta_W + \frac{1}{6}g'\sin\theta_W\right) \tag{H.78}$$

$$+ \bar{d}\gamma_\rho\left(\frac{1-\gamma_5}{2}\right)dA^\rho\left(\frac{1}{2}g\sin\theta_W - \frac{1}{6}g'\cos\theta_W\right) \tag{H.79}$$

$$\tag{H.80}$$

Now use $g' = g\frac{\sin\theta_W}{\cos\theta_W}$ in all terms.

$$= \frac{2}{3}\bar{u}\gamma_\rho\left(\frac{1+\gamma_5}{2}\right)uZ^\rho\left(g\frac{\sin\theta_W}{\cos\theta_W}\sin\theta_W\right) \tag{H.81}$$

$$-\frac{2}{3}\bar{u}\gamma_\rho\left(\frac{1+\gamma_5}{2}\right)uA^\rho\left(g\sin\theta_W\right) \tag{H.82}$$

$$-\frac{1}{3}\bar{d}\gamma_\rho\left(\frac{1+\gamma_5}{2}\right)d\ Z^\rho\left(g\frac{\sin\theta_W}{\cos\theta_W}\sin\theta_W\right) \tag{H.83}$$

$$+\frac{1}{3}\bar{d}\gamma_\rho\left(\frac{1+\gamma_5}{2}\right)d\ A^\rho g\sin\theta_W \tag{H.84}$$

$$\bar{u}\gamma_\rho\left(\frac{1-\gamma_5}{2}\right)uZ^\rho\left(-\frac{1}{2}g\cos\theta_W+\frac{1}{6}g\frac{\sin\theta_W}{\cos\theta_W}\sin\theta_W\right) \tag{H.85}$$

$$\bar{u}\gamma_\rho\left(\frac{1-\gamma_5}{2}\right)uA^\rho\left(-\frac{1}{2}g\sin\theta_W-\frac{1}{6}g\sin\theta_W\right) \tag{H.86}$$

$$\bar{d}\gamma_\rho\left(\frac{1-\gamma_5}{2}\right)uZ^\rho\left(\frac{1}{2}g\cos\theta_W+\frac{1}{6}g\frac{\sin\theta_W}{\cos\theta_W}\sin\theta_W\right) \tag{H.87}$$

$$\bar{d}\gamma_\rho\left(\frac{1-\gamma_5}{2}\right)dA^\rho\left(\frac{1}{2}g\sin\theta_W-\frac{1}{6}g\sin\theta_W\right) \tag{H.88}$$

$$\tag{H.89}$$

$$= \frac{2g}{3}\bar{u}\gamma_\rho\left(\frac{1+\gamma_5}{2}\right)uZ^\rho\left(\frac{\sin^2\theta_W}{\cos\theta_W}\right)-\frac{2g}{3}\bar{u}\gamma_\rho\left(\frac{1+\gamma_5}{2}\right)uA^\rho\sin\theta_W \tag{H.90}$$

$$-\frac{g}{3}\bar{d}\gamma_\rho\left(\frac{1+\gamma_5}{2}\right)d\ Z^\rho\left(\frac{\sin^2\theta_W}{\cos\theta_W}\right)+\frac{g}{3}\bar{d}\gamma_\rho\left(\frac{1+\gamma_5}{2}\right)d\ A^\rho\sin\theta_W \tag{H.91}$$

$$+\frac{g}{2\cos\theta_W}\bar{u}\gamma_\rho\left(\frac{1-\gamma_5}{2}\right)uZ^\rho\left(-\cos^2\theta_W+\frac{1}{3}\sin^2\theta_W\right) \tag{H.92}$$

$$-\frac{2g}{3}\bar{u}\gamma_\rho\left(\frac{1-\gamma_5}{2}\right)uA^\rho\sin\theta_W \tag{H.93}$$

$$+\frac{g}{2\cos\theta_W}\bar{d}\gamma_\rho\left(\frac{1-\gamma_5}{2}\right)d\ Z^\rho\left(\cos^2\theta_W+\frac{1}{3}\sin^2\theta_W\right) \tag{H.94}$$

$$+\frac{g}{3}\bar{d}\gamma_\rho\left(\frac{1-\gamma_5}{2}\right)d\ A^\rho\sin\theta_W \tag{H.95}$$

Use these trigonometric relations,

$$-\cos^2\theta_W + \frac{1}{3}\sin^2\theta_W = -1 + \frac{4}{3}\sin^2\theta_W \tag{H.96}$$

$$\cos^2\theta_W + \frac{1}{3}\sin^2\theta_W = 1 - \frac{2}{3}\sin^2\theta_W \tag{H.97}$$

$$\left(\frac{1-\gamma_5}{2}\right) + \left(\frac{1+\gamma_5}{2}\right) = 1 \tag{H.98}$$

and the electric charge defined as $e_0 = g\sin\theta_W$ in recollecting all the terms of the lagrangian, which now has the form:

$$\mathcal{L} = i\bar{u}\gamma_\rho\left(\frac{1+\gamma_5}{2}\right)(\partial^\rho u) + i\bar{d}\gamma_\rho\left(\frac{1+\gamma_5}{2}\right)(\partial^\rho d) + i\bar{u}\gamma_\rho\left(\frac{1-\gamma_5}{2}\right)(\partial^\rho u) + i\bar{d}\gamma_\rho\left(\frac{1-\gamma_5}{2}\right)(\partial^\rho d) \tag{H.99}$$

$$+ \frac{1}{\sqrt{2}}g\bar{u}\gamma_\rho W^\rho\left(\frac{1-\gamma_5}{2}\right)d + \frac{1}{\sqrt{2}}g\bar{d}\gamma_\rho W^{\rho\dagger}\left(\frac{1-\gamma_5}{2}\right)u \tag{H.100}$$

$$+ \frac{g}{2\cos\theta_W}Z^\rho\left[\bar{u}\gamma_\rho\left(\frac{1+\gamma_5}{2}\right)u\left(\frac{4}{3}\sin^2\theta_W\right) - \bar{d}\gamma_\rho\left(\frac{1+\gamma_5}{2}\right)d\left(\frac{2}{3}\sin^2\theta_W\right)\right. \tag{H.101}$$

$$\left. + \bar{u}\gamma_\rho\left(\frac{1-\gamma_5}{2}\right)u\left(-1+\frac{4}{3}\sin^2\theta_W\right) - \bar{d}\gamma_\rho\left(\frac{1-\gamma_5}{2}\right)d\left(-1+\frac{2}{3}\sin^2\theta_W\right)\right] \tag{H.102}$$

$$- \frac{2e_0}{3}\bar{u}\gamma_\rho u A^\rho + \frac{e_0}{3}\bar{d}\gamma_\rho d A^\rho \tag{H.103}$$

$$\tag{H.104}$$

Appendix I: The Higgs Mechanism and Fermion Mass Generation

Recall from section H that the kinetic part of a free Dirac fermion does not mix the left and right components of the field:

$$\bar{\psi}\gamma_\mu\partial^\mu\psi = \bar{\psi}_R\gamma_\mu\partial^\mu\psi_R + \bar{\psi}_L\gamma_\mu\partial^\mu\psi_L \tag{I.1}$$

Because of this, we can gauge the left and right handed components differently. Weak interactions are parity violating in the Standard Model and the $SU(2)_L$ covariant derivative acts only on the left-handed term. However, a Dirac mass term has the form

$$-m\left(\bar{\psi}_L\psi_R + \bar{\psi}_R\psi_L\right) \tag{I.2}$$

when we write the left and right handed components separately. So the components are coupled, meaning any such mass term breaks $SU(2)_L$ gauge invariance.

In a theory with spontaneous symmetry breaking, there is a way of giving mass to fermions without explicitly introducing gauge invariance breaking mass terms in the lagrangian. Consider the electron $SU(2)_L$ doublet

$$l = \begin{bmatrix} \nu \\ e \end{bmatrix}_L \tag{I.3}$$

the Higgs doublet

$$\phi = \begin{bmatrix} \phi^+ \\ \phi^0 \end{bmatrix} \tag{I.4}$$

$$\phi^+ = \frac{1}{\sqrt{2}}(\phi_1 - i\phi_2) \tag{I.5}$$

$$\phi^0 = \frac{1}{\sqrt{2}}(\phi_3 - i\phi_4) \tag{I.6}$$

and the right handed electron singlet in a Yukawa model.

$$\mathcal{L}_e = -g_e\bar{l}_L\phi e_R - g_e\bar{e}_R\phi^\dagger l_L \tag{I.7}$$

It is important to notice that the structure of these terms has two $SU(2)_L$ doublets multiplied to form an $SU(2)_L$ scalar $(\bar{l}_L\phi, \phi^\dagger l)$, and that scalar multiplies the $SU(2)_L$ scalar R-component. So this lagrangian is $SU(2)_L$ invariant and the symmetry is preserved.[12]

Recall from section G that the vacuum expectation value of the Higgs doublet assumes the value

$$\langle 0 \mid \phi \mid 0 \rangle = \begin{bmatrix} 0 \\ \frac{v}{\sqrt{2}} \end{bmatrix} \tag{I.8}$$

but that section dealt with a scalar Klein-Gordon particle. The consequence for a fermion doublet in this lagrangian is

$$\mathcal{L}_e = -g_e \bar{l}_L \phi e_R - g_e \bar{e}_R \phi^\dagger l_L \tag{I.9}$$

$$= -g_e \overline{\begin{bmatrix} \nu_L \\ e_L \end{bmatrix}} \phi e_R - g_e \bar{e}_R \phi^\dagger \begin{bmatrix} \nu_L \\ e_L \end{bmatrix} \tag{I.10}$$

$$= -g_e \begin{bmatrix} \bar{\nu}_L & \bar{e}_L \end{bmatrix} \begin{bmatrix} \phi^+ \\ \phi^0 \end{bmatrix} e_R - g_e \bar{e}_R \begin{bmatrix} \phi^+ & \phi^0 \end{bmatrix} \begin{bmatrix} \nu_L \\ e_L \end{bmatrix} \tag{I.11}$$

$$= -g_e(\bar{\nu}_L \phi^+ + \bar{e}_L \phi^0) e_R - g_e \bar{e}_R (\phi^+ \nu_L + \phi^0 e_L) \tag{I.12}$$

$$= -g_e \left[\bar{\nu}_L \phi^+ e_R + \bar{e}_L \phi^0 e_R + \bar{e}_R \phi^+ \nu_L + \bar{e}_R \phi^0 e_L \right] \tag{I.13}$$

Take on the vacuum expectation values.

$$\langle 0 \mid \mathcal{L}_e \mid 0 \rangle = -g_e \left[\bar{\nu}_L \underbrace{\langle 0 \mid \phi^+ \mid 0 \rangle}_{=0} e_R + \bar{e}_L \underbrace{\langle 0 \mid \phi^0 \mid 0 \rangle}_{\frac{v}{\sqrt{2}}} e_R + \bar{e}_R \underbrace{\langle 0 \mid \phi^+ \mid 0 \rangle}_{=0} \nu_L + \bar{e}_R \underbrace{\langle 0 \mid \phi^0 \mid 0 \rangle}_{\frac{v}{\sqrt{2}}} e_L \right] \tag{I.14}$$

$$= -\frac{g_e v}{\sqrt{2}} \left[\bar{e}_L e_R + \bar{e}_R e_L \right] \tag{I.15}$$

This is exactly a Dirac mass with $m_e = \frac{g_e v}{\sqrt{2}}$. That was precisely the vacuum. Now let's see that if we consider also oscillations about the vacuum we generate a coupling between the electron and the Higgs field. In the last line, use $v + H$ instead of just v.

$$\langle 0 \mid \mathcal{L}_e \mid 0 \rangle = -\frac{g_e v}{\sqrt{2}} \left[\bar{e}_L (v + H) e_R + \bar{e}_R (v + H) e_L \right] \tag{I.16}$$

$$= -\frac{g_e v}{\sqrt{2}} \left[v \bar{e}_L e_R + \bar{e}_L H e_R + v \bar{e}_R e_L + \bar{e}_R H e_L \right] \tag{I.17}$$

$$= -\frac{g_e v}{\sqrt{2}} \left[v e^\dagger \left(\frac{1 - \gamma_5}{2} \right) \gamma_0 \left(\frac{1 + \gamma_5}{2} \right) e + e^\dagger \left(\frac{1 - \gamma_5}{2} \right) \gamma_0 H \left(\frac{1 + \gamma_5}{2} \right) e \right. \tag{I.18}$$

$$\left. + v e^\dagger \left(\frac{1 + \gamma_5}{2} \right) \gamma_0 \left(\frac{1 - \gamma_5}{2} \right) e + e^\dagger \left(\frac{1 + \gamma_5}{2} \right) \gamma_0 H \left(\frac{1 - \gamma_5}{2} \right) e \right] \tag{I.19}$$

$$= -\frac{g_e v}{\sqrt{2}} \left[v \bar{e} \left(\frac{1 + \gamma_5}{2} \right) e + \bar{e} H e \left(\frac{1 + \gamma_5}{2} \right) + v \bar{e} \left(\frac{1 - \gamma_5}{2} \right) e + \bar{e} H e \left(\frac{1 - \gamma_5}{2} \right) \right] \tag{I.20}$$

$$= -\frac{g_e v}{\sqrt{2}} \left[\underbrace{v \bar{e} e}_{\text{Dirac electron mass}} + \underbrace{\bar{e} H e}_{\text{electron-Higgs coupling}} \right] \tag{I.21}$$

Notice for the coupling term

$$\left(\frac{-g_e}{\sqrt{2}} \right) \bar{e} H e = \left(-\frac{m_e}{v} \right) \bar{e} H e = \left(-\frac{g m_e}{2 m_W} \right) \bar{e} H e \tag{I.22}$$

So in addition to interations of the form $f \bar{f} \to (\gamma \text{ or } Z^0) \to W^+ W^-$ we also have the possibility $f \bar{f} \to H \to W^+ W^-$. The presence of the fermion mass in the coupling to the Higgs is significant.

We must now recall that if an $SU(2)$ doublet transforms as

$$l' = e^{\frac{i}{2} \vec{\alpha} \cdot \vec{\tau}} l \tag{I.23}$$

then the charge conjugate states

$$i \tau_2 \begin{bmatrix} u^* \\ d^* \end{bmatrix} \tag{I.24}$$

transform the same way. So then the charge conjugate of the Higgs field is

$$\phi_c = i\tau_2\phi^* \tag{I.25}$$

$$= i\begin{bmatrix} 0 & -i \\ i & 0 \end{bmatrix}\begin{bmatrix} \phi^+ \\ \phi^0 \end{bmatrix}^* \tag{I.26}$$

$$= \begin{bmatrix} 0 & 1 \\ -1 & 0 \end{bmatrix}\begin{bmatrix} \frac{1}{\sqrt{2}}(\phi_1 - i\phi_2)^* \\ \frac{1}{\sqrt{2}}(\phi_3 - i\phi_4)^* \end{bmatrix} \tag{I.27}$$

$$= \begin{bmatrix} 0 & 1 \\ -1 & 0 \end{bmatrix}\begin{bmatrix} \frac{1}{\sqrt{2}}(\phi_1 + i\phi_2) \\ \frac{1}{\sqrt{2}}(\phi_3 + i\phi_4) \end{bmatrix} \tag{I.28}$$

$$= \begin{bmatrix} \frac{1}{\sqrt{2}}(\phi_3 + i\phi_4) \\ -\frac{1}{\sqrt{2}}(\phi_1 + i\phi_2) \end{bmatrix} \tag{I.29}$$

$$\equiv \begin{bmatrix} \phi^{0\dagger} \\ -\phi^- \end{bmatrix} \tag{I.30}$$

ϕ_c is also an $SU(2)$ doublet which transforms the same way ϕ does.

Note that in the use of the ϕ Higgs doublet we could not use the terms $\bar{l}_L\phi\nu_R$ or $\bar{\nu}_R\phi^\dagger l_L$ in the lagrangian (ν_R has replaced e_R) because it leads to unphysical terms $\bar{e}_L\nu_R$ and $\bar{\nu}_R e_L$. With the Higgs conjugate field doublet ϕ_c we may include $\bar{l}_L\phi_c\nu_R$ and $\bar{\nu}_R\phi_c^\dagger l_L$ terms (but not $\bar{l}_L\phi_c e_R$ and $\bar{e}_R\phi_c^\dagger l_L$ terms for the same reasons just discussed) which yield Dirac masses for the neutrinos as well as Higgs interactions. Observe,

$$\mathcal{L}_\nu = -g_\nu\left[\bar{l}_L\phi\nu_R + \bar{\nu}_R\phi^\dagger l_L\right] \tag{I.31}$$

$$= -g_\nu\left[\begin{bmatrix}\bar{\nu}_L & \bar{e}_L\end{bmatrix}\begin{bmatrix}\phi^{0\dagger} \\ -\phi^-\end{bmatrix}\nu_R + \begin{bmatrix}\phi^0 & -\phi^{-\dagger}\end{bmatrix}\begin{bmatrix}\nu_L \\ e_L\end{bmatrix}\right] \tag{I.32}$$

$$= -g_\nu\left[\left(\bar{\nu}_L\phi^{0\dagger} - \bar{e}_L\phi^-\right)\nu_R + \bar{\nu}_R\left(\phi^0\nu_L - \phi^{-\dagger}e_L\right)\right] \tag{I.33}$$

$$= -g_\nu\left[\bar{\nu}_L\phi^{0\dagger}\nu_R - \bar{e}_L\phi^-\nu_R + \bar{\nu}_R\phi^0\nu_L - \bar{\nu}_R\phi^{-\dagger}e_L\right] \tag{I.34}$$

Take the vacuum expectation value and all ϕ^- terms vanish. The ϕ^0 factors become $\frac{1}{\sqrt{2}}(v+H)$ again.

$$\langle 0 \mid \mathcal{L}_\nu \mid 0 \rangle = -\frac{g_\nu}{\sqrt{2}}\left[\bar{\nu}_L(v+H)\nu_R + \bar{\nu}_R(v+H)\nu_L\right] \tag{I.35}$$

$$= -\frac{g_\nu}{\sqrt{2}}\left[\underbrace{v\bar{\nu}_L\nu_R + v\bar{\nu}_R\nu_L}_{\text{Dirac Mass}} + \underbrace{\bar{\nu}_L H\nu_R + \bar{\nu}_R H\nu_L}_{\nu\text{-Higgs Interaction}}\right] \tag{I.36}$$

$$= -\frac{g_\nu}{\sqrt{2}}\left[v\bar{\nu}\nu + \bar{\nu}H\nu\right] \tag{I.37}$$

Summarily, to give the electron-neutrino $SU(2)$ doublet mass (as well as the other lepton and quark doublets), we are adding more terms to the lagrangian derived at the end of section H of the form:

$$\mathcal{L}_{f,\text{Higgs}} = \sum_{l=e,\mu,\tau}\left[-\frac{g_l}{\sqrt{2}}\left[v\bar{l}l + \bar{l}Hl\right] - \frac{g_{\nu_l}}{\sqrt{2}}\left[v\bar{\nu}_l\nu_l + \bar{\nu}_l H\nu_l\right]\right] \tag{I.38}$$

for the three lepton generations and similar terms for the three quark doublets. Because of the Higgs mechanism, we now have sensible masses for Standard Model particles.

Appendix J: The Higgs Sector in Standard Model Electroweak Physics

Let's refer back to section G, line G.15. We shall now see the details of how we go from the postulated $SU(2) \times U(1)$ invariant lagrangian for a scalar particle to a form that determines the physics it implies.

Recall the lagrangian for the (scalar) Higgs sector is

$$\mathcal{L} = (D_\mu \phi)^\dagger (D^\mu \phi) + m_0^2 \phi^\dagger \phi - \frac{\lambda}{4} \left(\phi^\dagger \phi\right)^2 - \frac{1}{4} \vec{F}_{\mu\nu} \cdot \vec{F}^{\mu\nu} - \frac{1}{4} G_{\mu\nu} G^{\mu\nu} \tag{J.1}$$

$$\tag{J.2}$$

for

$$\vec{F}^{\mu\nu} = \partial^\mu \vec{W}^\nu - \partial^\nu \vec{W}^\mu - g \vec{W}^\mu \times \vec{W}^\nu \tag{J.3}$$

$$G^{\mu\nu} = \partial^\mu B^\nu - \partial^\nu B^\mu \tag{J.4}$$

$$D^\mu \phi = \left(\partial^\mu + \underbrace{\frac{ig}{2} \vec{\tau} \cdot \vec{W}^\mu}_{SU(2)\text{piece}} + \underbrace{\frac{ig'}{2} B^\mu}_{U(1)\text{piece}} \right) \phi \tag{J.5}$$

Consider only the first term for now.

$$(D^\mu \phi)^\dagger (D^\mu \phi) = \left(\partial_\mu \phi + \frac{ig}{2} \vec{\tau} \cdot \vec{W}_\mu \phi + \frac{ig' Y}{2} B_\mu \phi \right)^\dagger \left(\partial^\mu \phi + \frac{ig}{2} \vec{\tau} \cdot \vec{W}^\mu \phi + \frac{ig' Y}{2} B^\mu \phi \right) \tag{J.6}$$

$$= (\partial_\mu \phi)^\dagger (\partial^\mu \phi) \tag{J.7}$$

$$+ (\partial_\mu \phi)^\dagger \left(\frac{ig}{2} \vec{\tau} \cdot \vec{W}^\mu \phi + \frac{ig' Y}{2} B^\mu \phi \right) + \left(\frac{ig}{2} \vec{\tau} \cdot \vec{W}_\mu \phi + \frac{ig' Y}{2} B_\mu \phi \right)^\dagger (\partial^\mu \phi) \tag{J.8}$$

$$+ \left[\frac{ig}{2} \vec{\tau} \cdot \vec{W}_\mu \phi + \frac{ig' Y}{2} B_\mu \phi \right]^\dagger \left[\frac{ig}{2} \vec{\tau} \cdot \vec{W}^\mu \phi + \frac{ig' Y}{2} B^\mu \phi \right] \tag{J.9}$$

Now let's work on the last line of this. Note that in my expression of the Higgs doublet I'll be skipping straight to vacuum expectation values.

$$\frac{ig}{2}\vec{\tau}\cdot\vec{W}_\mu\phi+\frac{ig'Y}{2}B_\mu\phi=\frac{ig}{2}\left[\begin{bmatrix}0&1\\1&0\end{bmatrix}W_{1\mu}+\begin{bmatrix}0&-i\\i&0\end{bmatrix}W_{2\mu}+\begin{bmatrix}1&0\\0&-1\end{bmatrix}W_{3\mu}\right]\begin{bmatrix}0\\\frac{1}{\sqrt{2}}(v+H)\end{bmatrix} \tag{J.10}$$

$$+\frac{ig'Y}{2}B_\mu\begin{bmatrix}0\\\frac{1}{\sqrt{2}}(v+H)\end{bmatrix} \tag{J.11}$$

$$=\frac{ig}{2}\left[\begin{bmatrix}\frac{1}{\sqrt{2}}W_{1\mu}(v+H)\\0\end{bmatrix}+\begin{bmatrix}\frac{-i}{\sqrt{2}}W_{2\mu}(v+H)\\0\end{bmatrix}+\begin{bmatrix}0\\\frac{-1}{\sqrt{2}}W_{3\mu}(v+H)\end{bmatrix}\right] \tag{J.12}$$

$$+\begin{bmatrix}0\\\frac{ig'Y}{2\sqrt{2}}B_\mu(v+H)\end{bmatrix} \tag{J.13}$$

$$=\begin{bmatrix}\frac{ig}{2\sqrt{2}}W_{1\mu}(v+H)+\frac{g}{2\sqrt{2}}W_{2\mu}(v+H)\\\frac{-ig}{2\sqrt{2}}W_{3\mu}(v+H)+\frac{ig'Y}{2\sqrt{2}}B_\mu(v+H)\end{bmatrix} \tag{J.14}$$

$$=\begin{bmatrix}\frac{ig}{2}(W_{1\mu}-iW_{2\mu})\frac{1}{\sqrt{2}}(v+H)\\-\frac{ig}{2}W_{3\mu}\frac{1}{\sqrt{2}}(v+H)+\frac{ig'Y}{2}B_\mu\frac{1}{\sqrt{2}}(v+H)\end{bmatrix} \tag{J.15}$$

Next, multiply this by it's Hermitian conjugate from the left:

$$\left[-\tfrac{ig}{2}(W_{1\mu}+iW_{2\mu})\tfrac{1}{\sqrt{2}}(v+H) \quad \tfrac{ig}{2}W_{3\mu}\tfrac{1}{\sqrt{2}}(v+H)-\tfrac{ig'Y}{2}B_\mu\tfrac{1}{\sqrt{2}}(v+H)\right] \tag{J.16}$$

$$\begin{bmatrix} \tfrac{ig}{2}(W_1^\mu - iW_2^\mu)\tfrac{1}{\sqrt{2}}(v+H) \\ -\tfrac{ig}{2}W_3^\mu\tfrac{1}{\sqrt{2}}(v+H)+\tfrac{ig'Y}{2}B^\mu\tfrac{1}{\sqrt{2}}(v+H)\end{bmatrix} \tag{J.17}$$

$$= \frac{g^2}{4}\left|W_1-iW_2\right|^2\frac{1}{2}(v+H)^2+\frac{g^2}{4}|W_3|^2\frac{1}{2}(v+H)^2-\frac{gg'Y}{4}W_{3\mu}B^\mu\frac{1}{2}(v+H)^2 \tag{J.18}$$

$$-\frac{gg'Y}{4}W_3^\mu B_\mu\frac{1}{2}(v+H)^2+\frac{g'^2Y^2}{4}|B|^2\frac{1}{2}(v+H)^2 \tag{J.19}$$

$$= \frac{g^2}{4}W_\mu^\dagger W^\mu v^2+\frac{g^2}{2}W_\mu^\dagger W_\mu vH+\frac{g^2}{4}W_\mu^\dagger W^\mu H+\frac{g^2}{8}|W_3|^2v^2+\frac{g^2}{4}|W_3|^2vH+\frac{g^2}{8}|W_3|^2H^2 \tag{J.20}$$

$$-\frac{gg'Y}{4}W_{3\mu}B^\mu v^2-\frac{gg'Y}{2}W_{3\mu}B^\mu vH-\frac{gg'Y}{2}W_{3\mu}B^\mu H^2 \tag{J.21}$$

$$+\frac{g'^2Y^2}{8}|B|^2v^2+\frac{g'^2Y^2}{4}|B|^2vH+\frac{g'^2Y^2}{8}|B|^2H^2 \tag{J.22}$$

Now we have mass terms for the gauge boson fields and interaction terms among the gauge and Higgs bosons. With that done, let's go back and deal with the terms from lines J.7 and J.8.

$$(\partial_\mu\phi)^\dagger(\partial^\mu\phi)=\left[0 \quad \tfrac{1}{\sqrt{2}}(\partial_\mu v+\partial_\mu H)\right]\begin{bmatrix}0\\ \tfrac{1}{\sqrt{2}}(\partial_\mu v+\partial_\mu H)\end{bmatrix}=\frac{1}{2}(\partial_\mu H)(\partial^\mu H) \tag{J.23}$$

$$(\partial_\mu\phi)^\dagger\left(\frac{ig}{2}\vec{\tau}\cdot\vec{W}^\mu\phi+\frac{ig'Y}{2}B^\mu\phi\right)=-\frac{ig}{4}(\partial_\mu H)W_3^\mu(v+H)+\frac{ig'Y}{2}(\partial_\mu H)B^\mu(v+H) \tag{J.24}$$

$$\left(\frac{ig}{2}\vec{\tau}\cdot\vec{W}^\mu\phi+\frac{ig'Y}{2}B^\mu\phi\right)^\dagger(\partial^\mu\phi)=\frac{ig}{4}W_{3\mu}(v+H)(\partial^\mu H)-\frac{ig'Y}{4}B_\mu(v+H)(\partial^\mu H) \tag{J.25}$$

We are now ready to put the first term of the lagrangian back together.

$$(D_\mu\phi)^\dagger (D^\mu\phi) = \frac{1}{2}(\partial_\mu H)(\partial^\mu H) - \frac{ig}{4}(\partial_\mu H)W_3^\mu(v+H) + \frac{ig'Y}{4}(\partial_\mu H)B^\mu(v+H) \quad \text{(J.26)}$$

$$+ \frac{ig}{4}W_{3\mu}(v+H)(\partial^\mu H) - \frac{ig'Y}{4}B_\mu(v+H)(\partial^\mu H) \quad \text{(J.27)}$$

$$+ \frac{g^2}{4}W_\mu^\dagger W^\mu v^2 + \frac{g^2}{2}W_\mu^\dagger W^\mu vH + \frac{g^2}{4}W_\mu^\dagger W^\mu H^2 \quad \text{(J.28)}$$

$$+ \frac{g^2}{8}|W_3|^2v^2 + \frac{g^2}{4}|W_3|^2vH + \frac{g^2}{8}|W_3|^2H^2 \quad \text{(J.29)}$$

$$- \frac{gg'Y}{4}W_{3\mu}B^\mu v^2 - \frac{gg'Y}{4}W_{3\mu}B^\mu vH - \frac{gg'Y}{4}W_{3\mu}B^\mu H^2 \quad \text{(J.30)}$$

$$+ \frac{g'^2Y}{8}|B|^2v^2 + \frac{g'^2Y}{4}|B|^2vH + \frac{g'^2Y}{8}|B|^2H^2 \quad \text{(J.31)}$$

And the $SU(2)$ gauge fields kinetic terms:

$$\vec{F}_{\mu\nu}\cdot\vec{F}^{\mu\nu} = (\partial_\mu\vec{W}_\nu - \partial_\nu\vec{W}_\mu - g\vec{W}_\mu\times\vec{W}_\nu)\cdot(\partial^\mu\vec{W}^\nu - \partial^\nu\vec{W}^\mu - g\vec{W}^\mu\times\vec{W}^\nu) \quad \text{(J.32)}$$

$$= (\partial_\mu\vec{W}_\nu - \partial_\nu\vec{W}_\mu)\cdot(\partial^\mu\vec{W}^\nu - \partial^\nu\vec{W}^\mu) - g(\partial_\mu\vec{W}_\nu - \partial_\nu\vec{W}_\mu)\cdot(\vec{W}^\mu\times\vec{W}^\nu) \quad \text{(J.33)}$$

$$- g(\vec{W}_\mu\times\vec{W}_\nu)\cdot(\partial^\mu\vec{W}^\nu - \partial^\nu\vec{W}^\mu) + g^2(\vec{W}_\mu\times\vec{W}_\nu)\cdot(\vec{W}^\mu\times\vec{W}^\nu) \quad \text{(J.34)}$$

$$= (\partial_\mu\vec{W}_\nu - \partial_\nu\vec{W}_\mu)\cdot(\partial^\mu\vec{W}^\nu - \partial^\nu\vec{W}^\mu) - 2g(\vec{W}_\mu\times\vec{W}_\nu)\cdot(\partial^\mu\vec{W}^\nu - \partial^\nu\vec{W}^\mu) \quad \text{(J.35)}$$

$$+ g^2\left[|W_\mu|^2|W_\nu|^2 - |\vec{W}_\mu\cdot\vec{W}_\nu|^2\right] \quad \text{(J.36)}$$

$$\quad \text{(J.37)}$$

Now we're ready to put the lagrangian back together. After a little algebra:

$$\mathcal{L} = \underbrace{\frac{1}{2}(\partial_\mu H)(\partial^\mu H) + \frac{1}{2}m_0^2(v+H)^2 - \frac{\lambda}{16}(v+H)^4}_{\text{Higgs kinetic, mass, and self-interaction terms}} \tag{J.38}$$

$$\underbrace{- \frac{1}{4}(\partial_\mu W_{1\nu} - \partial_\nu W_{1\mu})(\partial^\mu W_1^\nu - \partial^\nu W_1^\mu) - \frac{1}{4}(\partial_\mu W_{2\nu} - \partial_\nu W_{2\mu})(\partial^\mu W_2^\nu - \partial^\nu W_2^\mu)}_{W^\pm \text{ kinetic terms}}$$

(J.39)

$$- \frac{1}{4}(\partial_\mu W_{3\nu} - \partial_\nu W_{3\mu})(\partial^\mu W_3^\nu - \partial^\nu W_3^\mu) - \frac{1}{4}G_{\mu\nu}G^{\mu\nu} \tag{J.40}$$

$$\underbrace{+ \frac{1}{8}v^2(gW_{3\mu} - g'YB_\mu)(gW_3^\mu - g'YB^\mu)}_{\text{Terms that become the } Z\text{-boson and photon}} \tag{J.41}$$

$$+ \frac{g^2v^2}{4}W_\mu^\dagger W^\mu + \frac{g^2v}{2}W_\mu^\dagger W^\mu H + \frac{g^2}{4}W_\mu^\dagger W^\mu H^2 + \frac{g^2v}{4}|W_3|^2 H + \frac{g^2}{8}|W_3|^2 H^2 \tag{J.42}$$

$$\underbrace{- \frac{gg'Yv}{2}W_{3\mu}B^\mu H - \frac{gg'Y}{2}W_{3\mu}B^\mu H^2 + \frac{g'^2Y^2v}{4}|B|^2 H + \frac{g'^2Y^2}{8}|B|^2 H^2}_{W^\pm \text{ mass,trilinear, quadrilinear couplings with the Higgs}} \tag{J.43}$$

$$\underbrace{\frac{1}{2}g(\vec{W}_\mu \times \vec{W}_\nu)\cdot(\partial^\mu \vec{W}^\mu - \partial^\nu \vec{W}^\mu) - \frac{1}{4}g^2\left[|W_\mu|^2|W_\nu|^2 - |\vec{W}_\mu \cdot \vec{W}_\nu|^2\right]}_{\text{Quadrilinear couplings among the gauge bosons}} \tag{J.44}$$

Appendix K: WH Production Amplitude

The Tevatron consists of a proton beam colliding with an antiproton beam. So let's consider this interaction when an up quark interacts with an anti-down quark; the interaction of an anti-up quark with a down quark follows analogously. The full Lagrangian for the interaction is the sum of the Higgs Sector of the Standard Model Lagrangian with the Lagrangian for a quark doublet.

$$\mathcal{L} = \underbrace{\frac{1}{2}\left(\partial_\mu H\right)\left(\partial^\mu H\right) + \frac{1}{2}\mu^2 H^2 + \frac{g^2 v^2}{4} W_\mu^\dagger W^\mu + \frac{g^2 v}{2} W_\mu^\dagger W^\mu H}_{\text{Higgs Sector}} \tag{K.1}$$

$$\underbrace{-\frac{1}{4}\sum_{i=1,2}\left(\partial_\mu W_{i\nu} - \partial_\nu W_{i\mu}\right)\left(\partial^\mu W_i^\nu - \partial^\nu W_i^\mu\right)}_{\text{W boson kinetic terms}} \tag{K.2}$$

$$\underbrace{+i\overline{u}\gamma_\rho\left(\frac{1-\gamma_5}{2}\right)\partial^\rho u + i\overline{d}\gamma_\rho\left(\frac{1-\gamma_5}{2}\right)\partial^\rho d + \frac{gV_{ud}}{\sqrt{2}}\overline{d}\gamma_\rho W^{\dagger\rho}\left(\frac{1-\gamma_5}{2}\right)u}_{\text{Quark Doublet}} \tag{K.3}$$

To calculate the cross section for this interaction, I want the interaction Lagrangian, which is found by just collecting the interaction terms in the above Lagrangian.

$$\mathcal{L}_I = \frac{g^2 v}{2} W_\mu^\dagger W^\mu H + \frac{gV_{ud}}{\sqrt{2}}\overline{d}\gamma_\rho W^{\rho\dagger}\left(\frac{1-\gamma_5}{2}\right)u \tag{K.4}$$

I would like to change the form of the coefficients to be expressed in terms of the W mass and electric charge. Using $m_W = \frac{gv}{2}$ and $e_0 = g\sin\theta_W$,

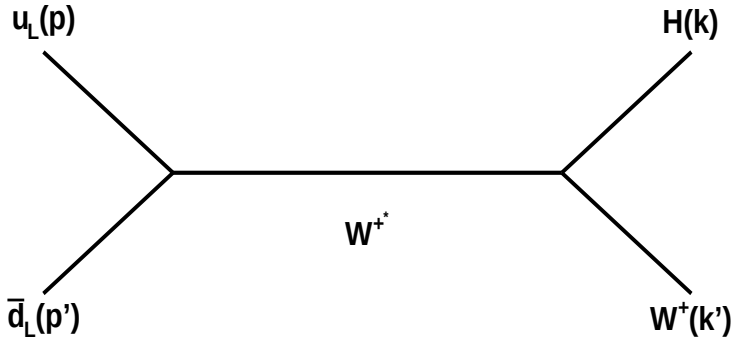

Figure K.1 Associated Production with a W boson

$$\mathcal{L}_I = \frac{2m_W^2}{v} W_\mu^\dagger W^\mu H + \frac{e_0 V_{ud}}{\sqrt{2}\sin\theta_W} \bar{d}\gamma_\rho W^{\rho\dagger} \left(\frac{1-\gamma_5}{2}\right) u \tag{K.5}$$

Later, I'll re-express the leftover v in terms of the Fermi Coupling Constant $G_F = \sqrt{2}/2v^2$. This way, I'll be able to express the cross section in terms of measured quantities.

From the interaction Lagrangian density I need the interaction Hamiltonian density.

$$\mathcal{H}_I(x) = \pi(x)\dot{\Phi}(x) - \mathcal{L}_I(x) \tag{K.6}$$

where $\Phi(x)$ is a position-space field and $\pi(x)$ is its conjugate momentum field. However, in this case there are no time-derivatives of fields in the interaction Lagrangian density. So it is simply

$$\mathcal{H}_I(x) = -\mathcal{L}(x) \tag{K.7}$$

$$= -\underbrace{\frac{2m_W^2}{v} W_\mu^\dagger W^\mu H}_{\mathcal{H}_{IH}(x)} - \underbrace{\frac{e_0 V_{ud}}{\sqrt{2}\sin\theta_W} \bar{d}\gamma_\rho W^{\rho\dagger} \left(\frac{1-\gamma_5}{2}\right) u}_{\mathcal{H}_{Iq}(x)} \tag{K.8}$$

$$\Rightarrow \mathcal{H}_I(x) = \mathcal{H}_{IH}(x) + \mathcal{H}_{Iq}(x) \tag{K.9}$$

The scattering matrix for this interaction is[33]

$$\langle k'; k \mid S \mid p'; p\rangle = \langle k'; k \mid 1 \mid p'; p\rangle + i\langle k'; k \mid T \mid p'; p\rangle \tag{K.10}$$

where we recall that the scattering matrix is defined as the time-evolution operator as $t \to \infty$.

$$\langle k'; k \mid S \mid p'; p\rangle = \lim_{t\to\infty} \langle k'; k \mid e^{iH(2t)} \mid p'; p\rangle \tag{K.11}$$

The interaction component here is what I want to calculate. From (4.90) Peskin and Schroeder[33]

$$i\langle k'; k \mid T \mid p'; p\rangle = \lim_{t\to\infty(1-i\varepsilon)} \langle k'; k \mid T \exp\left[-i\int_{-t}^{t} dt' H_I(t')\right] \mid p'; p\rangle \tag{K.12}$$

That exponential expands as (from (4.22) Peskin and Schroeder[33]):

$$T\exp\left[-i\int_{-t}^{t} dt' H_I(t')\right] = 1 + (-i)\int_{-t}^{t} dt_1 H_I(t_1) + \frac{(-i)^2}{2!}\iint_{-t}^{t} dt_1 dt_2 T\left[H_I(t_1)H_I(t_2)\right] + \cdots \tag{K.13}$$

As we are beginning and ending with two particle states, the second order term is the first that can contribute to this interaction, and any higher-order terms contain loops that we do not address here. The interaction part of the scattering matrix element becomes

$$i\langle k';k \mid T \mid p';p\rangle \cong \langle k';k \mid \frac{(-i)^2}{2!}\iint_{-t}^{t} dt_1 dt_2 T\left[H_I(x_1)H_I(x_2)\right] \mid p';p\rangle \tag{K.14}$$

where $H_I(x) = \int d^3\vec{x}\mathcal{H}_I(x) = \int d^3\vec{x}\left[\mathcal{H}_{IH}(x) + \mathcal{H}_{Iq}(x)\right]$, and in the Hamiltonian I replaced the variable t with full spacetime variable $x = (t, x_1, x_2, x_3)$ because all components now come into play.

$$= \langle k';k \mid \frac{(-i)^2}{2}\iint dt_1 dt_2 T\left[\int d^3\vec{x}_1\mathcal{H}_I(x_1)\int d^3\vec{x}_2\mathcal{H}_I(x_2)\right] \mid p';p\rangle \tag{K.15}$$

$$= \langle k';k \mid \frac{(-i)^2}{2} T\left[\int d^4x_1\mathcal{H}_I(x_1)\int d^4x_2\mathcal{H}_I(x_2)\right] \tag{K.16}$$

$$= \frac{(-i)^2}{2}\iint d^4x_1 d^4x_2\langle k';k \mid T\left[\mathcal{H}_I(x_1)\mathcal{H}_I(x_2)\right] \mid p';p\rangle \tag{K.17}$$

$$= \frac{(-i)^2}{2}\iint d^4x_1 d^4x_2\langle k';k \mid T[\mathcal{H}_{IH}(x_1)\mathcal{H}_{IH}(x_2) + \mathcal{H}_{IH}(x_1)\mathcal{H}_{Iq}(x_2) + \tag{K.18}$$

$$\mathcal{H}_{Iq}(x_1)\mathcal{H}_{IH}(x_2) + \mathcal{H}_{Iq}(x_1)\mathcal{H}_{Iq}(x_2)] \mid p';p\rangle \tag{K.19}$$

Since I have an interaction that involves both the quark doublet and the Higgs, the $\mathcal{H}_{IH}(x_1)\mathcal{H}_{IH}(x_2)$ and $\mathcal{H}_{Iq}(x_1)\mathcal{H}_{Iq}(x_2)$ terms do not contribute.

$$= \frac{(-i)^2}{2}\iint d^4x_1 d^4x_2\langle k';k \mid T\left[\mathcal{H}_{IH}(x_1)\mathcal{H}_{Iq}(x_2) + \mathcal{H}_{Iq}(x_1)\mathcal{H}_{IH}(x_2) + \right] \mid p';p\rangle \tag{K.20}$$

Next, I have to calculate these two time-ordered products inside the brackets. Using terms from expression K.9 above,

$$T\left[\mathcal{H}_{Iq}(x_1)\mathcal{H}_{IH}(x_2)\right] = \frac{2e_0 m_W^2 V_{ud}}{v\sqrt{2}\sin\theta_W} T\left[W_\mu^\dagger(x_1)W^\mu(x_1)H(x_1)\bar{d}(x_2)\not{W}^\dagger(x_2)\left(\frac{1-\gamma_5}{2}\right)u(x_2)\right] \tag{K.21}$$

$$= \frac{2e_0 m_W^2 V_{ud}}{v\sqrt{2}\sin\theta_W} N[W_\mu^\dagger(x_1)W^\mu(x_1)H(x_1)\bar{d}(x_2)\not{W}^\dagger(x_2)\left(\frac{1-\gamma_5}{2}\right)u(x_2) \tag{K.22}$$

$$+ \text{ all contractions}] \tag{K.23}$$

The N operator indicates we explore all possible combination of field contractions, most of which vanish as irrelevant. Field contractions will be expressed notationally as $\overline{A(x)B(x)C(x)}$ to contract

field A with field C.

$$= \frac{2e_0 m_W^2 V_{ud}}{v\sqrt{2}\sin\theta_W} N[W_\mu^\dagger(x_1)W^\mu(x_1)H(x_1)\bar{d}(x_2)W^\dagger(x_2)\left(\frac{1-\gamma_5}{2}\right)u(x_2) \tag{K.24}$$

$$+\overbrace{W_\mu^\dagger(x_1)W^\mu(x_1)}H(x_1)\bar{d}(x_2)W^\dagger(x_2)\left(\frac{1-\gamma_5}{2}\right)u(x_2) \tag{K.25}$$

$$+\overbrace{W_\mu^\dagger(x_1)W^\mu(x_1)H(x_1)}\bar{d}(x_2)W^\dagger(x_2)\left(\frac{1-\gamma_5}{2}\right)u(x_2) \tag{K.26}$$

$$+\overbrace{W_\mu^\dagger(x_1)W^\mu(x_1)H(x_1)\bar{d}(x_2)}W^\dagger(x_2)\left(\frac{1-\gamma_5}{2}\right)u(x_2) \tag{K.27}$$

$$+\overbrace{W_\mu^\dagger(x_1)W^\mu(x_1)H(x_1)\bar{d}(x_2)W^\dagger(x_2)}\left(\frac{1-\gamma_5}{2}\right)u(x_2) \tag{K.28}$$

$$+\overbrace{W_\mu^\dagger(x_1)W^\mu(x_1)H(x_1)\bar{d}(x_2)W^\dagger(x_2)\left(\frac{1-\gamma_5}{2}\right)u(x_2)} \tag{K.29}$$

$$+W_\mu^\dagger(x_1)\overbrace{W^\mu(x_1)H(x_1)}\bar{d}(x_2)W^\dagger(x_2)\left(\frac{1-\gamma_5}{2}\right)u(x_2) \tag{K.30}$$

$$+W_\mu^\dagger(x_1)\overbrace{W^\mu(x_1)H(x_1)\bar{d}(x_2)}W^\dagger(x_2)\left(\frac{1-\gamma_5}{2}\right)u(x_2) \tag{K.31}$$

$$+W_\mu^\dagger(x_1)\overbrace{W^\mu(x_1)H(x_1)\bar{d}(x_2)W^\dagger(x_2)}\left(\frac{1-\gamma_5}{2}\right)u(x_2) \tag{K.32}$$

$$+W_\mu^\dagger(x_1)\overbrace{W^\mu(x_1)H(x_1)\bar{d}(x_2)W^\dagger(x_2)\left(\frac{1-\gamma_5}{2}\right)u(x_2)} \tag{K.33}$$

$$+W_\mu^\dagger(x_1)W^\mu(x_1)\overbrace{H(x_1)\bar{d}(x_2)}W^\dagger(x_2)\left(\frac{1-\gamma_5}{2}\right)u(x_2) \tag{K.34}$$

$$+W_\mu^\dagger(x_1)W^\mu(x_1)\overbrace{H(x_1)\bar{d}(x_2)W^\dagger(x_2)}\left(\frac{1-\gamma_5}{2}\right)u(x_2) \tag{K.35}$$

$$+W_\mu^\dagger(x_1)W^\mu(x_1)\overbrace{H(x_1)\bar{d}(x_2)W^\dagger(x_2)\left(\frac{1-\gamma_5}{2}\right)u(x_2)} \tag{K.36}$$

$$+W_\mu^\dagger(x_1)W^\mu(x_1)H(x_1)\overbrace{\bar{d}(x_2)W^\dagger(x_2)}\left(\frac{1-\gamma_5}{2}\right)u(x_2) \tag{K.37}$$

$$+W_\mu^\dagger(x_1)W^\mu(x_1)H(x_1)\overbrace{\bar{d}(x_2)W^\dagger(x_2)\left(\frac{1-\gamma_5}{2}\right)u(x_2)} \tag{K.38}$$

$$+W_\mu^\dagger(x_1)W^\mu(x_1)H(x_1)\bar{d}(x_2)\overbrace{W^\dagger(x_2)\left(\frac{1-\gamma_5}{2}\right)u(x_2)} \tag{K.39}$$

$$+\text{terms with more than one contraction}] \tag{K.40}$$

There some important characteristics to note which will greatly simplify this mess:

- Since we are dealing only with the tree-level production process, terms with more than one contraction are automatically irrelevant.
- Contracted fields at the same spacetime coordinate constitute loops so they are not involved in tree-level interactions.
- Contractions between fields of different types vanish. Physically, the contracted fields are the propagator in the feynman diagram.
- If there are no contractions of a particular field at x_1 with a field at x_2, then there is no interaction between the initial and final states.
- The initial and final particle fields must be uncontracted. They contract with the initial and final state vectors later.

Hence, the only term left is the one that contracts $W^{\mu}(x_1)$ to $W^{\nu\dagger}(x_2)$ in expression K.28– this establishes the physical propagation of a W-boson field from spacetime coordinate x_1 to x_2. Notice that this is the only transition from initial to final states possible at tree-level.

Taking a step back to expression K.20, here's where we are:

$$i\langle k';k \mid T \mid p';p\rangle = \frac{(-i)^2 e_0 m_W^2 V_{ud}}{v\sqrt{2}\sin\theta_W}\times \tag{K.41}$$

$$\iint d^4x_1 d^4x_2 \langle k';k \mid [W_\mu^\dagger(x_1)\,\overline{W^\mu(x_1)H(x_1)\bar{d}(x_2)\gamma_\rho W^{\rho\dagger}(x_2)}\left(\frac{1-\gamma_5}{2}\right)u(x_2) \tag{K.42}$$

$$+\,\bar{d}(x_1)\gamma_\rho\,\overline{W^{\rho\dagger}(x_1)\left(\frac{1-\gamma_5}{2}\right)u(x_1)W_\mu^\dagger(x_2)W^\mu(x_2)}\,H(x_2)] \mid p';p\rangle \tag{K.43}$$

$$i\langle k';k \mid T \mid p';p\rangle = \frac{(-i)^2 e_0 m_W^2 V_{ud}}{v\sqrt{2}\sin\theta_W}\times \tag{K.44}$$

$$\iint d^4x_1 d^4x_2 \langle k';k \mid W_\mu^\dagger(x_1)\,\overline{W^\mu(x_1)H(x_1)\bar{d}(x_2)\gamma_\rho W^{\rho\dagger}(x_2)}\left(\frac{1-\gamma_5}{2}\right)u(x_2) \mid p';p\rangle \tag{K.45}$$

$$+\,\frac{(-i)^2 e_0 m_W^2 V_{ud}}{v\sqrt{2}\sin\theta_W}\times \tag{K.46}$$

$$\iint d^4x_1 d^4x_2 \langle k';k \mid \bar{d}(x_1)\gamma_\rho\,\overline{W^{\rho\dagger}(x_1)\left(\frac{1-\gamma_5}{2}\right)u(x_1)W_\mu^\dagger(x_2)W^\mu(x_2)}\,H(x_2)] \mid p';p \tag{K.47}$$

The two terms cover two Feynman diagrams:

- u and $\bar{d}$ quarks interact at spacetime coordinate x_1 to become a virtual W^+, which then radiates a Higgs boson at spacetime coordinate x_2.
- The same situation with spacetime coordinates x_1 and x_2 reversed.

The uncontracted terms now contract with the initial and final state vectors, corresponding physically to the incoming and outgoing particles of the Feynman diagram. They contract as

follows:

$$\overline{\langle k' \mid W_\mu^\dagger(x)} = \langle 0 \mid \epsilon_\mu^{s\,*}(k') e^{ik'\cdot x} \tag{K.48}$$

$$\overline{\langle k \mid H(x)} = \langle 0 \mid e^{ik\cdot x} \tag{K.49}$$

$$\overline{\bar{d}(x) \mid p'\rangle} = e^{-ip'\cdot x} \bar{d}^{r_1}(p') \mid 0\rangle \tag{K.50}$$

$$\overline{u(x) \mid p\rangle} = e^{-ip\cdot x} u^{r_2}(p) \mid 0\rangle \tag{K.51}$$

where r_1, r_2 are the fermion spins.

In position-space, the W propagator includes an integral over the momentum q:

$$\overline{W^{\rho\dagger}(x_1) W^{\mu}(x_2)} = \int \frac{d^4q}{(2\pi)^4} i \left[\frac{-g^{\mu\rho} + \frac{q^\mu q^\rho}{m_W^2}}{q^2 - m_W^2 + i\varepsilon} \right] e^{-iq\cdot(x_1 - x_2)} \tag{K.52}$$

$$\tag{K.53}$$

Let's make the replacements in the scattering matrix.

$$i\langle k'; k \mid T \mid p'; p\rangle = \frac{(-i)^2 e_0 m_W^2 V_{ud}}{v\sqrt{2}\sin\theta_W} \times \tag{K.54}$$

$$\iint d^4x_1 d^4x_2 [\underbrace{\langle 0 \mid \epsilon_\mu^{s\,*}(k') e^{ik'\cdot x_1}}_{W^\dagger} \underbrace{\langle 0 \mid e^{ik\cdot x_1}}_{H} \underbrace{\int \frac{d^4q}{(2\pi)^4} i \left[\frac{-g^{\mu\rho} + \frac{q^\mu q^\rho}{m_W^2}}{q^2 - m_W^2 + i\varepsilon} \right] e^{-iq\cdot(x_2 - x_1)}}_{W-\text{propagator}} \tag{K.55}$$

$$\underbrace{e^{-ip'\cdot x_2} \bar{d}^{r_1}(p') \mid 0\rangle}_{\bar{d}} \gamma_\rho \left(\frac{1 - \gamma_5}{2} \right) \underbrace{e^{-ip\cdot x_2} u^{r_2}(p) \mid 0\rangle}_{u}] \tag{K.56}$$

$$+ \frac{(-i)^2 e_0 m_W^2 V_{ud}}{v\sqrt{2}\sin\theta_W} \times \tag{K.57}$$

$$\iint d^4x_1 d^4x_2 [\underbrace{e^{-ip'\cdot x_1} \bar{d}^{r_1}(p') \mid 0\rangle}_{\bar{d}} \gamma_\rho \underbrace{\int \frac{d^4q}{(2\pi)^4} i \left[\frac{-g^{\mu\rho} + \frac{q^\mu q^\rho}{m_W^2}}{q^2 - m_W^2 + i\varepsilon} \right] e^{-iq\cdot(x_1 - x_2)}}_{W-\text{propagator}} \left(\frac{1 - \gamma_5}{2} \right) \tag{K.58}$$

$$\underbrace{e^{-ip\cdot x_1} u^{r_2}(p) \mid 0\rangle}_{u} \underbrace{\langle 0 \mid \epsilon_\mu^{s\,*}(k') e^{ik'\cdot x_2}}_{W^\dagger} \underbrace{\langle 0 \mid e^{ik\cdot x_2}}_{H}] \tag{K.59}$$

Integrating x_1 and x_2 over the exponentials is the very definition–or one of many–of a 4-dim Dirac delta function.

$$i\langle k';k \mid T \mid p';p\rangle = \left[\frac{i(-i)^2 e_0 m_W^2 V_{ud}}{v\sqrt{2}\sin\theta_W}\right]\int d^4q \epsilon_\mu^{s\,*}(k')\left[\frac{-g^{\mu\rho}+\frac{q^\mu q^\rho}{m_W^2}}{q^2-m_W^2+i\varepsilon}\right]\bar{d}^{r_1}(p') \tag{K.60}$$

$$\gamma_\rho\left(\frac{1-\gamma_5}{2}\right)u^{r_2}(p)(2\pi)^4\delta^4(-k'-k-q)\delta^4(p'+p+q) \tag{K.61}$$

$$+\left[\frac{i(-i)^2 e_0 m_W^2 V_{ud}}{v\sqrt{2}\sin\theta_W}\right]\int d^4q \bar{d}^{r_1}(p')\gamma_\rho\left(\frac{1-\gamma_5}{2}\right)u^{r_2}(p) \tag{K.62}$$

$$\left[\frac{-g^{\mu\rho}+\frac{q^\mu q^\rho}{m_W^2}}{q^2-m_W^2+i\varepsilon}\right]\epsilon_\mu^{s\,*}(k')(2\pi)^4\delta^4(-k'-k-q)\delta^4(p'+p+q) \tag{K.63}$$

$$i\langle k';k \mid T \mid p';p\rangle = \left[\frac{i(-i)^2 e_0 m_W^2 V_{ud}}{v\sqrt{2}\sin\theta_W}\right](2\pi)^4\epsilon_\mu^{s\,*}(k')\left[\frac{-g^{\mu\rho}+\frac{q^\mu q^\rho}{m_W^2}}{q^2-m_W^2+i\varepsilon}\right]\bar{d}^{r_1}(p')\gamma_\rho \tag{K.64}$$

$$\left(\frac{1-\gamma_5}{2}\right)u^{r_2}(p)\delta^4(p'+p-k'-k) \tag{K.65}$$

$$+\left[\frac{i(-i)^2 e_0 m_W^2 V_{ud}}{v\sqrt{2}\sin\theta_W}\right](2\pi)^4\bar{d}^{r_1}(p')\gamma_\rho\left(\frac{1-\gamma_5}{2}\right)u^{r_2}(p) \tag{K.66}$$

$$\left[\frac{-g^{\mu\rho}+\frac{q^\mu q^\rho}{m_W^2}}{q^2-m_W^2+i\varepsilon}\right]\epsilon_\mu^{s\,*}(k')\delta^4(p'+p-k'-k) \tag{K.67}$$

Now that the integral over q has been carried out over the δ-functions, it is understood that $q = k'+k = p'+p$ explicitly now.

$$i\langle k';k \mid T \mid p';p\rangle = \left[\frac{-2ie_0 m_W^2 V_{ud}}{v\sqrt{2}\sin\theta_W}\right](2\pi)^4\epsilon_\mu^{s\,*}(k')\left[\frac{-g^{\mu\rho}+\frac{q^\mu q^\rho}{m_W^2}}{q^2-m_W^2+i\varepsilon}\right] \tag{K.68}$$

$$\bar{d}^{r_1}(p')\gamma_\rho\left(\frac{1-\gamma_5}{2}\right)u^{r_2}(p)\delta^4(p'+p-k'-k) \tag{K.69}$$

Recall from Peskin and Schroeder (4.73)[33]

$$i\langle k';k \mid T \mid p';p\rangle = (2\pi)^4\delta^4(p'+p-k'-k)\cdot i\mathcal{M}(p',p\to k',k) \tag{K.70}$$

Finally, the invariant amplitude for Higgs associated production with a W^+-boson is

$$\boxed{i\mathcal{M} = \left[\frac{-2ie_0 m_W^2 V_{ud}}{v\sqrt{2}\sin\theta_W}\right]\epsilon_\mu^{s\,*}(k')\left[\frac{-g^{\mu\rho}+\frac{q^\mu q^\rho}{m_W^2}}{q^2-m_W^2+i\varepsilon}\right]\bar{d}^{r_1}(p')\gamma_\rho\left(\frac{1-\gamma_5}{2}\right)u^{r_2}(p)} \tag{K.71}$$

Appendix L: $H \to WW$ Lagrangian Density To Invariant Amplitude

For a Higgs boson decay to two W bosons, the Lagrangian density comes from the Higgs sector of the standard model Lagrangian. The Z boson and photon terms can be excluded.

$$\mathcal{L} = \underbrace{\frac{1}{2}\left(\partial_\mu H\right)\left(\partial^\mu H\right) + \frac{1}{2}\mu^2 H^2 + \frac{g^2 v^2}{4} W_\mu^\dagger W^\mu + \frac{g^2 v}{2} W_\mu^\dagger W^\mu H}_{\text{Higgs Sector}}$$
$$\underbrace{-\frac{1}{4}\sum_{i=1,2}\left(\partial_\mu W_{i\nu} - \partial_\nu W_{i\mu}\right)\left(\partial^\mu W_i^\mu - \partial^\nu W_i^\mu\right)}_{\text{W boson kinetic terms}}$$

To calculate the invariant amplitude for the decay, I want the interaction Lagrangian.

$$\mathcal{L} = \frac{g^2 v}{2} W_\mu^\dagger W^\mu H$$

From this I need the interaction Hamiltonian density.

$$\mathcal{H}_I = \sum_{\text{fields}} \pi(x)\dot{\Phi}(x) - \mathcal{L}_I(x)$$

where $\Phi(x)$ is a position-space field and $\pi(x)$ is its conjugate momentum field. However, in this case there are no time-derivatives of fields in the interaction Lagrangian density. So it is simply

$$\begin{aligned}\mathcal{H}_I(x) &= -\mathcal{L} \\ &= -\frac{g^2 v}{2} W_\mu^\dagger W^\mu H\end{aligned}$$

The scattering matrix for this interaction is

$$\langle k_1, k_2|S|p\rangle = \langle k_1, k_2|1|p\rangle + i\langle k_1, k_2|T|p\rangle$$

where we recall that the scattering matrix is defined as the time-evolution operator as $t \to \infty$.

$$\langle k_1, k_2|S|p\rangle = \lim_{t\to\infty}\langle k_1, k_2|e^{iH(2t)}|p\rangle$$

The interaction component here is what I want to calculate. From (4.90) Peskin,

$$i\langle k_1, k_2|T|p\rangle = \lim_{t\to\infty(1-i\varepsilon)} \langle k_1, k_2|T\exp\left[-i\int_{-t}^{t} dt' H_I(t')\right]|p\rangle$$

That exponential expands as (from (4.22) Peskin)

$$T\exp\left[-i\int_{-t}^{t} dt' H_I(t')\right] = 1 + (-i)\int_{-t}^{t} dt_1 H_I(t_1) + \frac{(-i)^2}{2!}\iint_{-t}^{t} dt_1 dt_2 T\left[H_I(t_1)H_I(t_2)\right] + \cdots$$

This scenario is just a tree-level decay–there are no loops to consider or propagators between two spacetime coordinates x_1 and x_2. Hence, let's consider only the contribution from the 1st order term. The interaction part of the scattering matrix becomes

$$i\langle k_1, k_2|T|p\rangle \cong \langle k_1, k_2|(-i)\int_{-t}^{t} dt_1 H_I(x_1)|p\rangle$$

where $H_I(x) = \int d^3x \mathcal{H}_I(x)$, and in the Hamiltonian I replaced the variable t with the full space-time variable x because all components now come into play.

$$\begin{aligned}
i\langle k_1, k_2|T|p\rangle &= (-i)\langle k_1, k_2|\int_{-t}^{t} dt_1 \int d^3x \mathcal{H}_I(x)|p\rangle \\
&= -i\langle k_1, k_2|\int d^4x \mathcal{H}_I(x)|p\rangle \\
&= -i\int d^4x \langle k_1, k_2|\mathcal{H}_I(x)|p\rangle \\
&= -i\int d^4x \langle k_1, k_2|\frac{-g^2 v}{2} W_\mu^\dagger W^\mu H|p\rangle \\
&= \frac{-ig^2 v}{2}\int d^4x \langle k_1, k_2|W_\mu^\dagger W^\mu H|p\rangle
\end{aligned}$$

Assume the fields are now contracted with their state vectors.

If we go to my contractions section:

$$\langle k|W_\mu(x) = \langle 0|\varepsilon^*_\mu(k,\lambda)e^{ik\cdot x}$$
$$H|p\rangle = e^{-ip\cdot x}|0\rangle$$

Using these

$$\begin{aligned} i\langle k_1,k_2|T|p\rangle &= \frac{ig^2v}{2}\int d^4x\epsilon^*_\mu(k_1,\lambda_1)e^{ik_1\cdot x}\epsilon^{*^\mu}(k_2,\lambda_2)e^{ik_2\cdot x}e^{-ip\cdot x} \\ &= \frac{ig^2v}{2}\int d^4x\epsilon^*_\mu(k_1,\lambda_1)\epsilon^{*^\mu}(k_2,\lambda_2)e^{i(k_1+k_2-p)\cdot x} \\ &= \frac{ig^2v}{2}\epsilon^*_\mu(k_1,\lambda_1)\epsilon^{*^\mu}(k_2,\lambda_2)\delta^4(k_1+k_2-p)(2\pi)^4 \end{aligned}$$

Recall from (4.73) Peskin

$$\begin{aligned} i\langle k_1,k_2|T|p\rangle &= (2\pi)^4\delta^4(k_1+k_2-p)\cdot i\mathcal{M}(p\to k_1,k_2) \\ \Rightarrow i\mathcal{M} &= \frac{ig^2v}{2}\epsilon^*_\mu(k_1,\lambda_1)\epsilon^{*^\mu}(k_2,\lambda_2) \end{aligned}$$

Appendix M: $H \to WW$ Invariant Amplitude to Decay Rate (Γ)

The decay rate from (4.83) Peskin is

$$\Gamma = \frac{1}{2m_H}\left[\frac{d^3k_1}{2E_1(2\pi)^3}\frac{d^3k_2}{2E_2(2\pi)^3}\right]\sum_{\lambda_1,\lambda_2}|\mathcal{M}|^2(2\pi)^4\delta^4(k_1+k_2-p)$$

So let's square the amplitude

$$\begin{aligned} i\mathcal{M} &= igm_W\epsilon^*_\mu(k_1,\lambda_1)\epsilon^{*^\mu}(k_2,\lambda_2) \\ |\mathcal{M}|^2 &= g^2m_W^2\left(\epsilon^*_\mu(k_1,\lambda_1)\epsilon_\nu(k_1,\lambda_1)\right)\left(\epsilon^{*^\mu}(k_2,\lambda_2)\epsilon^\nu(k_2,\lambda_2)\right) \end{aligned}$$

Now deal with the spin sum

$$\begin{aligned} \sum_{\lambda_1,\lambda_2}|\mathcal{M}|^2 &= g^2m_W^2\sum_{\lambda_1,\lambda_2}\left(\epsilon^*_\mu(k_1,\lambda_1)\epsilon_\nu(k_1,\lambda_1)\right)\left(\epsilon^{*^\mu}(k_2,\lambda_2)\epsilon^\nu(k_2,\lambda_2)\right) \\ &= g^2m_W^2\left(-g_{\mu\nu}+\frac{k_{1\mu}k_{1\nu}}{m_W^2}\right)\left(-g^{\mu\nu}+\frac{k_2^\mu k_2^\nu}{m_W^2}\right) \\ &= g^2m_W^2\left(g_{\mu\nu}g^{\mu\nu}-g_{\mu\nu}\frac{k_2^\mu k_2^\nu}{m_W^2}-g^{\mu\nu}\frac{k_{1\mu}k_{1\nu}}{m_W^2}+\frac{k_{1\mu}k_{1\nu}k_2^\mu k_2^\nu}{m_W^2}\right) \\ &= g^2m_W^2\left(4-\frac{k_2^2}{m_W^2}-\frac{k_1^2}{m_W^2}+\frac{(k_1\cdot k_2)^2}{m_W^4}\right) \end{aligned}$$

Recall that in a reaction the 4-momentum squared is a relativistic invariant. Using this invariant, we may alternate among before and after the decay, and viewing from the lab frame or CM frame (or any other frame). In this case, let's try before and after decay entirely in the CM frame. This means $\vec{p}=0$, and for the W boson energy and momenta $E_1=E_2=E$, $\vec{k}_1=-\vec{k}_2\equiv\vec{k}$.

$$\Rightarrow \frac{k^2}{m_W^2}=\frac{E^2-|\vec{k}|^2}{m_W^2}=\frac{(m_W^2+|\vec{k}|^2)-|\vec{k}|^2}{m_W^2}=1$$

Also,

$$\begin{aligned}(m_H, 0)^2 &= (E_1 + E_2, \vec{k}_1 + \vec{k}_2 = 0)^2 \\ m_H^2 &= 4E_2^2 = 4(m_W^2 + |\vec{k}|^2) \\ m_H^2 &= 4m_W^2 + 4|\vec{k}|^2 \\ m_H^2 - 2m_W^2 &= 2(m_W^2 + 2|\vec{k}|^2) \\ \frac{m_H^2 - 2m_W^2}{2} &= k_1 \cdot k_2\end{aligned}$$

where in the last line I used

$$\begin{aligned}k_1 \cdot k_2 &= (E_1, \vec{k}_1) \cdot (E_2, \vec{k}_2) \\ &= (E, \vec{k}) \cdot (E_2, -\vec{k}) \\ &= E^2 + |\vec{k}|^2 \\ &= (m_W^2 + |\vec{k}|^2) + |\vec{k}|^2 \\ &= m_W^2 + 2|\vec{k}|^2\end{aligned}$$

Now we may put these results back into the spin-summed invariant amplitude.

$$\begin{aligned}\sum_{\lambda_1,\lambda_2} |\mathcal{M}|^2 &= g^2 m_W^2 \left(4 - 1 - 1 + \frac{(m_H^2 - 2m_W^2)^2}{4m_W^4}\right) \\ &= g^2 m_W^2 \left(2 + \frac{m_H^2 - 4m_W^2 m_H^2 + 4m_W^4}{4m_W^4}\right) \\ &= g^2 m_W^2 \left(2 + \frac{m_H^4}{4m_W^4} - \frac{m_H^2}{m_W^2} + 1\right) \\ &= g^2 m_W^2 \left(\frac{3m_H^4}{4m_W^4} \cdot \frac{4m_W^4}{m_H^4} + \frac{m_H^4}{4m_W^4} - \frac{m_H^4}{4m_W^4} \cdot \frac{4m_W^4}{m_H^4} \cdot \frac{m_H^2}{m_W^2}\right) \\ &= g^2 m_W^2 \frac{m_H^4}{4m_W^4} \left(1 + \frac{12m_W^4}{m_H^4} - \frac{4m_W^2}{m_H^2}\right) \\ &= \frac{g^2 m_H^4}{4m_W^4} \left(1 - \frac{4m_W^2}{m_H^2} + \frac{12m_W^4}{m_H^4}\right)\end{aligned}$$

Put this into the decay rate.

$$d\Gamma = \frac{1}{2m_H}\left[\frac{d^3k_1}{2E_1(2\pi)^3}\frac{d^3k_2}{2E_2(2\pi)^3}\right]\frac{g^2m_H^4}{4m_W^4}\left(1-\frac{4m_W^2}{m_H^2}+\frac{12m_W^4}{m_H^4}\right)(2\pi)^4\delta^4(k_1+k_2-p)$$

$$\Gamma = \frac{g^2m_H^3}{32(2\pi)^2m_W^2}\left(1-\frac{4m_W^2}{m_H^2}+\frac{12m_W^4}{m_H^4}\right)\int\frac{d^3\vec{k}_1}{E_1}\frac{d^3\vec{k}_2}{E_2}\delta(E_1+E_2-E_p)\delta^3(\vec{k}_1+\vec{k}_2-\vec{p})$$

In the CM frame, $E_p = m_H$ and $\vec{p} = 0$.

$$\Gamma = \frac{g^2m_H^3}{32(2\pi)^2m_W^2}\left(1-\frac{4m_W^2}{m_H^2}+\frac{12m_W^4}{m_H^4}\right)\int\frac{d^3\vec{k}_1}{E_1}\frac{d^3\vec{k}_2}{E_2}\delta(E_1+E_2-m_H)\delta^3(\vec{k}_1+\vec{k}_2)$$

$$\Gamma = \frac{g^2m_H^3}{32(2\pi)^2m_W^2}\left(1-\frac{4m_W^2}{m_H^2}+\frac{12m_W^4}{m_H^4}\right)\int\frac{d^3\vec{k}}{\sqrt{m_W^2+|\vec{k}_1|^2}}\frac{d^3\vec{k}}{\sqrt{m_W^2+|\vec{k}_2|^2}}\delta(E_1+E_2-m_H)\delta^3(\vec{k}_1+\vec{k}$$

Perform the k_2 integration. Because of $\delta^3(\vec{k}_1+\vec{k}_2)$, this will just enforce $\vec{k}_1 = -\vec{k}_2 \Rightarrow |\vec{k}_1|^2 = |\vec{k}_2|^2$. Since we are dealing only with these momenta squared now, let's drop the index and just use $|\vec{k}|$.

$$\Gamma = \frac{g^2m_H^3}{32(2\pi)^2m_W^2}\left(1-\frac{4m_W^2}{m_H^2}+\frac{12m_W^4}{m_H^4}\right)\int\frac{d^3\vec{k}}{m_W^2+|\vec{k}|^2}\delta(E_1+E_2-m_H)$$

Express the remaining differential in spherical coordinates $d^3\vec{k} = |\vec{k}|^2d|\vec{k}|\sin\theta d\theta d\phi$, where $\int\sin\theta d\theta d\phi = 4\pi$.

$$\Gamma = \frac{g^2m_H^3}{32(2\pi)^2m_W^2}\left(1-\frac{4m_W^2}{m_H^2}+\frac{12m_W^4}{m_H^4}\right)\int\frac{|\vec{k}|^2d|\vec{k}|\sin\theta d\theta d\phi}{m_W^2+|\vec{k}|^2}\delta(E_1+E_2-m_H)$$

In the CM frame, $E_1 = E_2 = \sqrt{m_W^2+|\vec{k}|^2}$.

$$\Gamma = \frac{g^2m_H^3}{8(4\pi)m_W^2}\left(1-\frac{4m_W^2}{m_H^2}+\frac{12m_W^4}{m_H^4}\right)\int d|\vec{k}|\frac{|\vec{k}|^2}{m_W^2+|\vec{k}|^2}\delta\left(2\sqrt{m_W^2+|\vec{k}|^2}-m_H\right)$$

We must take care here. The integral is over $|\vec{k}|$ but the argument of the δ-function has more than one zero, so there is an ambiguity of which value $|\vec{k}|$ should take from the integration. Fortunately, it is possible to expand the δ-function as follows:

$$\delta(f(x)) = \sum_j \frac{1}{f'\left(x_0^j\right)} \delta\left(x - x_0^j\right)$$

where j counts over the zeros of $f(x)$ and $f' = \frac{df}{dx}$. Let $f(k) = 2\sqrt{m_W^2 + |\vec{k}|^2} - m_H$ and find the zeros:

$$\begin{aligned} m_H &= 2\sqrt{m_W^2 + |\vec{k}|^2} \\ \frac{m_H^2}{4} &= m_W^2 + |\vec{k}|^2 \\ \frac{1}{4}\left(m_H^2 - 2m_W^2\right) &= k^2 \\ \pm\frac{1}{2}\sqrt{m_H^2 - 2m_W^2} &= k \end{aligned}$$

However, a negative momentum magnitude doesn't make sense so we only use the positive one.

$$\begin{aligned} f'(k) &= \frac{2k}{\sqrt{m_W^2 + k^2}} \\ f'(k_0) &= \frac{\sqrt{m_H^2 - 4m_W^2}}{\sqrt{m_W^2 + \frac{1}{4}m_H^2 - m_W^2}} \\ f'(k_0) &= \frac{\sqrt{m_H^2 - 4m_W^2}}{\frac{1}{2}m_H^2} \\ f'(k_0) &= \frac{2}{m_H}\sqrt{m_H^2 - 4m_W^2} \\ \Rightarrow \delta(f(k)) &= -\frac{m_H}{2\sqrt{m_H^2 - 4m_W^2}} \delta\left(|\vec{k}| - \frac{1}{2}\sqrt{m_H^2 - 4m_W^2}\right) \end{aligned}$$

Put this into the decay rate.

$$\begin{aligned}
\Gamma &= \frac{g^2 m_H^3}{32\pi m_W^2}\left(1-\frac{4m_W^2}{m_H^2}+\frac{12m_W^4}{m_H^4}\right)\int d|\vec{k}|\frac{|\vec{k}|^2}{m_W^2+|\vec{k}|^2}\frac{m_H}{2\sqrt{m_H^2-4m_W^2}}\delta\left(|\vec{k}|-\frac{1}{2}\sqrt{m_H^2-4m_W^2}\right)\\
&= \frac{g^2 m_H^3}{32\pi m_W^2}\left(1-\frac{4m_W^2}{m_H^2}+\frac{12m_W^4}{m_H^4}\right)\frac{\frac{1}{4}(m_H^2-4m_W^2)}{m_W^2+\frac{1}{4}(m_H^2-4m_W^2)}\frac{m_H}{2\sqrt{m_H^2-4m_W^2}}\\
&= \frac{g^2 m_H^3}{32\pi m_W^2}\left(1-\frac{4m_W^2}{m_H^2}+\frac{12m_W^4}{m_H^4}\right)\frac{\frac{1}{4}(m_H^2-4m_W^2)}{\frac{1}{4}m_H^2}\frac{m_H}{2\sqrt{m_H^2-4m_W^2}}\\
&= \frac{g^2 m_H^3}{32\pi m_W^2}\left(1-\frac{4m_W^2}{m_H^2}+\frac{12m_W^4}{m_H^4}\right)\frac{\sqrt{m_H^2-4m_W^2}}{2m_H}\\
&= \frac{g^2 m_H^3}{64\pi m_W^2}\left(1-\frac{4m_W^2}{m_H^2}+\frac{12m_W^4}{m_H^4}\right)\sqrt{1-\frac{4m_W^2}{m_H^2}}\\
&= \boxed{\frac{G_F m_H^3}{8\sqrt{2}\pi}\left(1-\frac{4m_W^2}{m_H^2}+\frac{12m_W^4}{m_H^4}\right)\sqrt{1-\frac{4m_W^2}{m_H^2}}}
\end{aligned}$$

where $G_F = \frac{\sqrt{2}g^2}{8m_W^2} \Rightarrow \frac{G_F}{\sqrt{2}} = \frac{g^2}{8m_W^2}$.

Appendix N: WZ Cross Section Measurement in 5.9fb^{-1}

LIST OF REFERENCES

[1] Fermilab's chain of accelerators, accelerator details: the antiproton source. Website, August 2000. http://www-bd.fnal.gov/public/antiproton.html.

[2] Fermilab's chain of accelerators, accelerator details: the main injector. Website, August 2000. http://www-bd.fnal.gov/public/maininj.html.

[3] Fermilab's chain of accelerators, accelerator details: the proton source. Website, August 2000. http://www-bd.fnal.gov/public/tevatron.html.

[4] Layer 00. Website, November 2000. http://www-cdf.fnal.gov/internal/upgrades/layer00/layer00.html.

[5] Svx ii homepage. Website, September 2000. http://www-cdf.fnal.gov/internal/upgrades/svxii/svxii_home.html.

[6] Intermediate silicon layers. Website, February 2001. http://www-cdf.fnal.gov/internal/upgrades/isl/isl.html.

[7] Fermilab: Tevatron luminosity. Website, March 2002. http://www.fnal.gov/pub/now/tevlum.html.

[8] Cdf central outer tracker. Website, November 2004. http://www-cdf.fnal.gov/internal/upgrades/cot/.

[9] Run ii luminosity. Website, August 2006. http://www-d0.fnal.gov/runcoor/RUN/run2_lumi.html.

[10] Fermilab today. Website, June 2008. http://www.fnal.gov/pub/today/archive_2008/today08-06-18.html.

[11] Cdf run2 triggers and filters report group triggers and bits on cdf online production report – physics table physics_5_04_v-3. Website, March 2010. http://cdfdbb.fnal.gov:8520/cdfr2/databases?tdt=phy&tdv=PHYSICS_5_04_v-3.

[12] I. J. R. Aitchison and A. J. G. Hey. *Gauge Theories in Particle Physics. Vol. 2: QCD and the Electroweak Theory*. Institute of Physics Publishing, Philadelphia, 2004.

[13] A B Balantekin, editor. *Journal of Physics G Nuclear and Particle Physics*, volume 33. Institute of Physics, 2006.

[14] D. Benjamin, , M. Kruse, Seig Oh, Geumbong Yu, P. Bussey, E. James, D. Hidas, S. Jindariani, B. Rutherford, R. Lysak, M. Herndon, J. Nett, J. Pursley, M. d'Errico, S.P. Griso, D. Lucchesi, A. Robson, R. St.Denis, Maria d'Errico, Donatella Lucchesi, and Anadi Canepa. Search for $h \to ww$ production using 5.3 fb^{-1}. CDF/PHYS/EXOTIC/CDFR/10086, 2010.

[15] D. Benjamin, M. Kruse, P. Bussey, E. James, D. Hidas, S. Jindariani, B. Rutherford, R. Lysak, M. Herndon, J. Nett, J. Pursley, M. d'Errico, S.P. Griso, D. Lucchesi, A. Robson, and R. St.Denis. Search for $h \to ww$ production in the low m_{ll} region using 4.8 fb^{-1}. CDF/PHYS/EXOTIC/CDFR/9864, 2009.

[16] D. Benjamin, M. Kruse, P. Bussey, E. James, D. Hidas, S. Jindariani, B. Rutherford, R. Lysak, M. Herndon, J. Nett, J. Pursley, M. d'Errico, S.P. Griso, D. Lucchesi, A. Robson, and R. St.Denis. Updated search for $h \to ww$ production using likelihood-based electron selection. CDF/PHYS/EXOTIC/CDFR/9863, 2009.

[17] Florencia Canelli, Bruno Casal Larana, Craig Group, Eric James, Jonathon Lewis, and Tom. Wright. Muon trigger studies: Focusing on the gaps. CDF/DOC/JET/PUBLIC/9106, 2007.

[18] CDF and D0 Collaborations. Combined cdf and d0 upper limits on standard model higgs boson production with up to 5.4 fb^{-1} of data. *Phys. Rev. Lett.*, 104, 2010. arXiv:0911.3930v1 [hep-ex].

[19] CDF Collaboration. Cdf central outer tracker. CDF/PUB/TRACKING/PUBLIC/6267, 2001.

[20] CDF Collaboration. *CDF Run II Technical Design Report*, 2003. CDF/DOC/CDF/PUBLIC/6261.

[21] David Dummit and Richard Foote. *Abstract Algebra, 3rd. ed.* John Wiley & Sons, Inc., 2004.

[22] Michael Feindt. A neural bayesian estimator for conditional probability densities. *arXiv:physics/0402093v1 [physics.data-an]*, February 2004. IEKP-KA/04-05.

[23] R. D. Field, Y. Kanev, M. Tayebnejad, and P. A. Griffin. Using neural networks to enhance the higgs boson signal at hadron colliders. *Physical Review D*, 53(5):2296–2308, March 1996. The American Physical Society.

[24] Joel Goldstein, Tim Nelson, and Rick. Snider. Silicon tracking for plug electrons. /CDF/DOC/TRACKING/CDFR/5970, 2002.

[25] Francis Halzen and Alan Martin. *Quarks and Leptons: An Introductory Course in Modern Particle Physics*. John Wiley & Sons, Inc., 1984.

[26] Matthew Herndon. Tracking at cdf. Website, March 2003. www.slac.stanford.edu/econf/C0303241/proc/pres/360.PS.

[27] Thomas Junk. Confidence level computation for combining searches with small statistics. *arXiv:hep-ex/9902006v1*, February 1999. CARLETON/OPAL PHYS 99-01.

[28] Richard J. Larsen and Morris L. Marx. *An Introduction to Mathematical Statistics and Its Applications (3rd ed.)*. Prentice Hall, 2001.

[29] Richard J. Larsen and Morris L. Marx. *An Introduction to Mathematical Statistics and Its Applications (3rd ed.)*. Prentice Hall, 2001.

[30] Richard J. Larsen and Morris L. Marx. *An Introduction to Mathematical Statistics and Its Applications (3rd ed.)*. Prentice Hall, 2001.

[31] M. McFarlane, H. Bachacou, J. Nielson, and W. Yao. Study of high p_T lepton identification efficiency factor and related cuts and parameters in 5.3.3. CDF/ANAL/TOP/CDFR/7682, 2005.

[32] Donald H. Perkins. *Introduction to High Energy Physics, 3rd ed.* Addison-Wesley Publishing Company, Inc., 1987.

[33] Michael E. Peskin and Daniel V. Schroeder. *An Introduction to Quantum Field Theory*. Addison-Wesley Publishing Company, Inc., 1995.

[34] J. J. Sakurai. *Modern Quantum Mechanics (Revised Edition)*. Addison-Wesley Publishing Company, 1994.

[35] Phil Schlabach. The cdf muon detectors. Website, July 2004. http://www.phy.duke.edu/ kotwal/detectorLectures/detector_lectures_Phil_Schlabach_1_muondetectors.pdf.

[36] R.G. Wagner. Electron identification for run ii: Understanding and using lshr. CDF/DOC/ELECTRON/CDFR/6249, 2003.

[37] W.M. Yao and K. Bloom. "outside-in" silicon tracking at cdf. CDF/TRACKING/DOC/CDFR/5991, 2002.